INFORMATION TO USERS

This manuscript has been reproduced from the microfilm master. UMI films the text directly from the original or copy submitted. Thus, some thesis and dissertation copies are in typewriter face, while others may be from any type of computer printer.

The quality of this reproduction is dependent upon the quality of the copy submitted. Broken or indistinct print, colored or poor quality illustrations and photographs, print bleedthrough, substandard margins, and improper alignment can adversely affect reproduction.

In the unlikely event that the author did not send UMI a complete manuscript and there are missing pages, these will be noted. Also, if unauthorized copyright material had to be removed, a note will indicate the deletion.

Oversize materials (e.g., maps, drawings, charts) are reproduced by sectioning the original, beginning at the upper left-hand corner and continuing from left to right in equal sections with small overlaps. Each original is also photographed in one exposure and is included in reduced form at the back of the book.

Photographs included in the original manuscript have been reproduced xerographically in this copy. Higher quality 6" x 9" black and white photographic prints are available for any photographs or illustrations appearing in this copy for an additional charge. Contact UMI directly to order.

UMI

A Bell & Howell Information Company
300 North Zeeb Road, Ann Arbor MI 48106-1346 USA
313/761-4700 800/521-0600

Université d'Ottawa · University of Ottawa

Acknowledgements

I wish to thank Tito Scaiano for everything that he has done for me. Tito's generosity with his time and funding was greatly appreciated. Mostly, I would like to thank Tito for his patience. Students must struggle in order to grow, but sometimes it must be painful to watch.

I could not have completed this thesis without the love and support of my wife. Thank you Sophie for your encouragement and understanding. This was our project.

My parents may not have agreed with everything I have done and every decision I have made, but they always believed in me and supported me. I believe in myself today because they have believed in me all my life. It is about time that I put into words what I have felt for so long. I thank them for sacrificing so much energy and time to make me a better person. Thanks Mom and Dad, I love you.

Je veux remercier Lionel et Céline pour leur amour et leur soutien. Si vous ne le savez pas encore, je veux vous dire que je me sens comme votre fils. Je suis tellement fier de dire que vous êtes mes beaux-parents. I hope that I can make you proud of me as well.

Last, but not least, there are many people in and out of the lab who have helped me along the way. I wish to thank André Simard and Alain Berinstain for all their help with the laser system. The system is user-friendly today because André and Alain have put a tremendous amount of work into it. I appreciate their efforts. Gracias to Monica Barra for being a wonderful teacher as well as a friend. I am indebted to Roger Sinta for synthesizing the compound that started it all. Thanks Roger! Thanks to Jeff Banks for always dropping what he was doing in order to help get me back on track and thanks for letting me win at cribbage. I owe a special thank you to Nadereh Mohtat for being a great friend and for doing some long distance paper-work. Thank you to Mike Whittlesey,

Simon Belt, Fran Cozens, and Ron Boch for getting me started in the early days of my studies.

I am grateful to all members of Tito's group, past and present, that have crossed my path. We have all learned from each other and have become friends in the process.

Table of Contents

Acknowledgements ii

Table of Contents iv

List of Schemes vii

List of Figures ix

List of Tables xiv

List of Abbreviations xvi

List of *vicinal* dibromides xviii

Abstract xxi

1. Introduction 1

1.1 Applications For *Vicinal*-Debrominations 2
(i) Alkene Purification 2
(ii) Alkene Protection/Deprotection 3
(iii) Synthetic Applications 3
(iv) Photoinitiated, Acid-Catalyzed, Polymer Cross-linking 5

1.2 Photochemical Debrominations 7
(i) The Photodebromination of 1,2-Dibromoethane 8
(ii) The Photodebromination of Aryl-Substituted Vicinal Dibromides 10

1.3 Other Methods For *Vicinal*-Debrominations 12
(i) Reductions of Vicinal-Dibromides By Two-Electron Nucleophiles 12
(ii) Reductions of vicinal-Dibromides By One-Electron Reductants 15

1.4 β-Bromo Radicals 18
(i) The Rate-Enhancing (Anchimeric) Effect of Bromine Substituents in Radical Reactions 19
(ii) The Stereoelectronic Factors For The Anchimeric Effect 21
(iii) The Nature of the Bromine Bridged Radical 23

1.5 Chapter 1 References 27

2. Laser Flash Photolysis (LFP) 30

2.1 Introduction 31

2.2 Nanosecond Absorption LFP 34
2.3 Sample Holder and Sample Cells 38
2.4 LFP Solutions 41
2.5 Chapter 2 References 43

3. Bromine Atom/Halide Ion Complexes (BrX^-) 44
3.1 Introduction: The Dibromide Radical Anion (Br_2^-) 45
3.2 Other Dihalide and Di-pseudo-halide Radical Anions (X_2^-) 47
3.3 Mixed Radical Anion Complexes (XY^-) 55
(i) BrI^- 55
(ii) $BrCl^-$ and BrF^- 61
(iii) BrX^- Extinction Coefficients 67
(iv) $BrOH^-$ 72
(v) Halo-thiocyanate Radical Anions ($XSCN^-$) 73
3.4 Equilibria of the Bromine Atom/Halide Complexes (BrX^-) 77
(i) Decay of the Radical Anions 78
3.5 Temperature Effects on the Radical Anions 90
3.6 Chapter 3 References 93

4. The LFP Generation of ß-bromoradicals From *Vicinal* Dibromides 95
4.1 The LFP Search for the β-bromo Radical 96
4.2 The Kinetics of the Photochemical Debromination of *Vicinal* Dibromides in the Presence of a Halide Trap/Probe 103
(i) The 1st Equivalent, BrX^- (1) 104
(ii) The 2nd Equivalent, BrX^- (2) 106
(iii) The Combined Equation 107
4.3 The Decay of RBr• in the Presence of Halide 110
(i) Low [X^-] Regime 111
(ii) High [X^-] Regime (see Table 4-B) 111
4.4 Halide Reduction of β-bromo Radicals 115
(i) Fluoride Reduction of β-bromo Radicals 115
(ii) Reduction of β-bromo Radicals by the Halide Series 120
4.5 The Stability and Reactivity of β-Bromo Radicals in the Presence of Halides 127
(i) The β-Bromoethyl Radical 127
(ii) The Effect of Fluorination 129
(iii) The Effect of Alkyl Substitution 130
(iv) The Effect of a Silyl Group on the β-Bromo Radical 132
(v) The Effect of Ring Size on the β-Bromo Radical 132
(vi) The Effect of a β-Silyl Group on the β-Bromo Radical 134
4.6 Temperature Effects on the β-Bromo Radicals 134
(i) Temperature Effects of the Halide Reduction of the β-Bromo Radicals 136

(ii) The Temperature Dependence of the β-Bromo Radical Lifetimes 136

4.7 Conclusion 137

4.8 Chapter 4 References 139

5. Bromine Atom/Organic Complexes 141

5.1 Introduction 142

5.2 Bromine Atom/Organic Complexes 144

(i) The Jump 150

(ii) The Growth 157

5.3 The Nature of the Bromine Atom/Organic Complex 166

5.4 Conclusions 167

5.5 Chapter 5 References 169

6. Claims to Original Research 171

List of Schemes

Scheme 1-1 Representation of the reduction of a *vicinal* dibromoalkane to an alkene..... 2

Scheme 1-2 Representation of the reduction of a *vicinal* dibromoalkene to an alkyne. 2

Scheme 1-3 Solo's synthesis of 3–β-acetoxy-20-keto-5,14,16-pregnatriene..... 3

Scheme 1-4 Allred's synthesis of tetracyclo[5.3.0,$0^{2,10}$.$0^{3,6}$]deca-4,8-diene..... 4

Scheme 1-5 Allred's synthesis of bicyclo[4.2.0]octa-2,7-diene..... 4

Scheme 1-6 Schematic of photoresist functions..... 5

Scheme 1-7 The light initiated, acid catalyzed, cross-linking of a phenol based polymer resist. 7

Scheme 1-8 The relationship between the E1cB, E2, and E1 elimination mechanisms for debromination of a *vicinal* dibromide by a two electron nucleophile..... 13

Scheme 1-9 The iodide catalyzed formation of the iodine/ethene bridged complex. 14

Scheme 1-10 The interconversion between bridged intermediates for the deiodination of 1,2-diiodoethane as proposed by Miller *et al*..... 14

Scheme 1-11 The reduction of *meso*-2,3-dibromobutane to *trans*-2-butene by iodide..... 15

Scheme 1-12 The stepwise two-electron reduction of a *vicinal* dibromide by a one-electron reductant..... 16

Scheme 1-13 The possible fates of the β-bromo radical in the presence of a one-electron reductant..... 17

Scheme 1-14 The equilibrium between the two geometric isomers of a bromine-bridged radical..... 17

Scheme 1-15 The radical bromination of *trans*-(1-bromomethyl)-4-methylcyclohexane. 21

Scheme 1-16 A comparison of the radical brominations of *cis*- and *trans*-1-bromo-4-*t*-butylcyclohexane..... 22

Scheme 1-17 The photobromination of (+)-1-bromo-2-methylbutane.....23

Scheme 1-18 A qualitative representation of the distance between the chlorine atom and the α and β carbons for radicals with 0, 1, and 2 methyl groups on the α-carbon.....25

Scheme 3-1 The pulse radiolytic production of $Br_2^{\bullet}$ from an aqueous solution of bromide.....46

Scheme 3-2 The photochemical dissociation and subsequent recombination of the pulse radiolytically produced $X_2^{\bullet}$ radical anions.....48

Scheme 3-3 The consecutive first-order growth and decay of the $Br_2^{\bullet}$ ion.....52

Scheme 3-4 The formation of $BrSCN^{\bullet}$ from the pulse radiolysis of a 20 mM bromide solution in the presence of 100 μM SCN^-.[22].....74

Scheme 3-5 The formation of $ISCN^{\bullet}$ from the pulse radiolysis of a thiocyanate solution in the presence of iodide.[21].....76

Scheme 3-6 The main modes of decay of halo-bromo radical anions in the presence of excess halide.....82

Scheme 3-7 The kinetic mechanism for the partial, fast, pseudo-first-order decay of the $Br_2^{\bullet}$ radical anion.....83

Scheme 3-8 The mechanistic implications of the fast growth and decay kinetics of the $BrX^{\bullet}$ complex.....86

Scheme 4-1 The kinetic scheme of the photochemical debromination of $Si(DBE)_4$ in the presence of halide probe (X^-).....104

Scheme 5-1 Bromine atom production and complexation from the pulse radiolysis of bromoalkanes.....144

Scheme 5-2 The equilibria of the bromine atom complexes in $CHCl_3$ containing 10 mM 1,2-dibromoethane and 0.16 mM bromide.....157

List of Figures

Figure 1-1 The Potential Energy Profile for the S_o and S_1 states of a typical bromoalkane..... 8

Figure 2-1 Simple schematic representation of a laser flash photolysis set-up.....32

Figure 2-2 Layout of the laser lab at the University of Ottawa.....33

Figure 2-3 The sequence of timed events in an LFP experiment.....35

Figure 2-4 The Cell Holder.....39

Figure 2-5 An LFP static cell.....40

Figure 2-6 An LFP flow cell. 40

Figure 2-7 Percent Transmission of the incident laser light versus Path Length as the laser passes through solutions of different optical densities.....42

Figure 3-1 The spectra of $Cl_2^{\bullet}$, $Br_2^{\bullet}$, $I_2^{\bullet}$, and $(SCN)_2^{\bullet}$ in water.[4] 47

Figure 3-2 $Br_2^{\bullet}$ spectrum in MeCN at 296 K. *trans*-1,2-Dibromocycloheptane was irradiated with a pulse from a 266 nm laser in the presence of 11.2 mM of Bu_4NBr. The solution was purged with nitrogen and the experiment was run under flow conditions. 50

Figure 3-3 The growth and partial decay of the $Br_2^{\bullet}$ absorption generated from the LFP of 2,3-dibromobutane in MeCN at 296 K. The signal was monitored at 360 nm . The solution contained 0.36 mM of Bu_4NBr.....53

Figure 3-4 Bromide concentration dependence of the growth of $Br_2^{\bullet}$ for $Si(DBE)_4$ in acetonitrile at 23°C. 54

Figure 3-5 Comparative ground state spectra of *trans*-10,11-dibromo-dibenzosuberone in MeCN in the presence and absence of tetrabutyl ammonium iodide. Spectra before and after LFP. 56

Figure 3-6 Spectra of the products formed from the thermal debromination and the photochemical debromination of *trans*-10,11-dibromo-dibenzosuberone in the presence of 20 mM iodide. The spectra were obtained by subtracting the spectrum from that of the parent dibromide.....57

Figure 3-7 Ground state absorption spectra for a solution of 1,2-dibromoethyl-benzene in the presence of 20 mM Bu_4NI before and after LFP.....58

Figure 3-8 The 266 nm LFP of 1,2-dibromoethyl-benzene in MeCN. The solutions were purged with either nitrogen or oxygen. The experiment was run under flow conditions with no added halide.....59

Figure 3-9 The dependence of the observed growth rate constant, k_{obs}, of the BrI^- complex versus the concentration of iodide. 1,2-Dibromoethyl-benzene was photolyzed in MeCN. The traces were monitored at 370 nm.....60

Figure 3-10 Chloride and fluoride quenching of bromine atoms produced from the 266 nm photolysis of 1,2-dibromo-1,1-difluoroethane in MeCN.....62

Figure 3-11 The $BrCl^-$ spectrum in MeCN at 296 K. The bromine atoms were produced via the photolysis of $Si(DBE)_4$ and trapped using Bu_4NCl.....63

Figure 3-12 The BrF^- spectrum recorded in MeCN. The bromine atoms were produced via the 266 nm photolysis of 1,2-dibromopropane. The bromine atoms were trapped with 7.5 mM Bu_4NF.....64

Figure 3-13 The 520 nm decay and the 360 nm growth signals taken from the BrF^-/1,2-dibromopropane spectrum of Figure 3-12. Both the original 520 nm trace and a normalized trace are shown in comparison to the 360 nm trace. The traces were recorded in flowing MeCN with 7.5 mM Bu_4NF.....65

Figure 3-14 The jump and growth of the 360 nm signal after the photolysis of $Si(DBE)_4$ in MeCN.....69

Figure 3-15 The BrF^- signal monitored at 360 nm in MeCN at 296 K. The complex was produced by the LFP of 1,2-dibromopropane in the presence of 2.72 mM Bu_4NF.....78

Figure 3-16 The second order decay of the Br_2^- complex monitored at 360 nm in 5% aqueous MeCN. LFP of *trans*-1,2-dibromocyclopentane in the presence of 5 mM KBr.....79

Figure 3-17 The dependence of the Br_2^- decay with $[Br^-]$. Results from a compilation of the LFP of many vicinal dibromides.....84

Figure 3-18 The iodide dependence of the fast decay component of the BrI^- complex. The complex was generated from the photolysis of 1,2-dibromoethyl-benzene in the presence of Bu_4NI. The rate constants were measured in MeCN at 296 K and monitored at 370 nm.....87

Figure 3–19 Chlorine quenching of the $BrCl^{\bullet-}$ radical ion and fluoride quenching of the $BrF^{\bullet-}$ radical anion. The bromine atoms were produced via the 266 nm photolysis of $Si(DBE)_4$ and 1,2-dibromo-1,1-difluoroethane respectively in MeCN. 88

Figure 3-20 The dependence of the bromine atom probe rate constant (k_{BrX^-}) in MeCN versus the radii of the halide ion (r_X) traps. The iodide values are not included in the fit of the line because of the large error. 90

Figure 3-21 Bromine atom quenching plots at various temperatures in MeCN. Bromine atoms were produced from the LFP of *trans*-1,2-dibromocyclopentane and trapped with Bu_4NBr. 91

Figure 3-22 An Arrhenius plot for the temperature dependence of the trapping of bromine atoms by bromide. The log of the rate constants were plotted against the inverse of the temperature for the LFP of *trans*-1,2-dibromocyclopentane in MeCN. 92

Figure 4-1 The expected jump and growth kinetics expected for the photodebromination of 1,2-dibromoethane. 97

Figure 4-2 The observed kinetics of the photodebromination of 1,2-dibromoethane. Both bromine atoms are lost instantaneously in the presence of 10 mM bromide. 97

Figure 4-3 The normalized growths observed for the LFP of (●) 1,2-dibromoethane and (○) $Si(DBE)_4$ at 360 nm in MeCN in the presence of 6 mM Bu_4NBr.[19] 100

Figure 4-4 The expected plateau of the bromide dependence of the $Br_2^{\bullet-}$ growth for $Si(DBE)_4$. 101

Figure 4-5 The observed bromide dependence of the $Br_2^{\bullet-}$ growth at 360 nm in MeCN for the LFP of $Si(DBE)_4$. 102

Figure 4-6 The jump, growth, and decay signal of the $Br_2^{\bullet-}$ complex generated from the 2.06 mM fluoride trapping of the LFP of 1,2-dibromopropane in MeCN. The line represents the fit by Equation 4.15 to the points. 109

Figure 4-7 The dependence of the elimination rate constant for the second bromine atom ($k_{RBr^\bullet}$) versus fluoride concentration for the LFP of $Si(DBE)_4$ in MeCN. 116

Figure 4-8 The fluoride dependence of $k_{RBr^\bullet}$ for the LFP of 1,2-dibromoethane in MeCN at 296 K. The traces were monitored at 360 nm. 117

Figure 4-9 The fluoride dependence of $k_{RBr^\bullet}$ for the LFP of *trans*-1,2-dibromocycloheptane in MeCN. 119

Figure 4-10 The fluoride dependence of the rate constant of the elimination of the bromine atom from the 2-bromo-1,1-difluoroethyl radical ($k_{RBr^{\bullet}}$) in MeCN..... 120

Figure 4-11 A theoretical comparison of the β-bromo radical quenching plots for the halides. 121

Figure 4-12 The halide dependence of $k_{RBr^{\bullet}}$ for $Si(DBE)_4$ in MeCN at 296K. The bromide and chloride linear fits have been forced through the 9.5 μs^{-1} intercept of the fluoride line. 123

Figure 4-13 The halide dependence of $k_{RBr^{\bullet}}$ for $Si(DBE)_4$ in MeCN at 296K. The bromide and chloride linear fits have NOT been forced through the 9.5 μs^{-1} intercept of the fluoride line. 123

Figure 4-14 Two-centred, three-electron bonding between a bromoalkane and a radical centre..... 129

Figure 4-15 The dipolar character of the intramolecular two-centred, three-electron bridged β-bromoethyl radical 130

Figure 4-16 The temperature dependence of the unimolecular decay ($k_o^{RBr^{\bullet}}$, s^{-1}) and the halide reduction (k_{red}, $M^{-1} s^{-1}$) of the β-bromo radicals from the photolysis of 1,2-dibromoethane (Dibromide II, ○) and *trans*-1,2-dibromocyclopentane (Dibromide IX, ●). The 1,2-dibromoethane was studied in the presence of fluoride and *trans*-1,2-dibromocyclopentane was studied in the presence of bromide. The MeCN solutions were excited with 266 nm light..... 135

Figure 5-1 The instantaneous jump followed by the growth of the 360 nm transient after the photolysis of $Si(DBE)_4$ in MeCN in the absence of halide probe..... 143

Figure 5-2 Normalized bromine atom/bromoalkane spectra ($RBr_n^{\bullet}Br$) in cyclohexane. The spectra were produced from the PR of the bromoalkanes in cyclohexane solution. $[CBr_4]$ = 0.05M, $[CHBr_3]$ = 0.23 M, $[CH_2Br_2]$ = 0.29 M, and $[CH_3CH_2Br]$ = 0.54 M.[6] 145

Figure 5-3 (Upper) The spectrum of the complex between bromoethane and a bromine atom in cyclohexane.[6] 146

Figure 5-4 (Lower) The LFP spectrum of Si(DBE)4 in acetonitrile..... 146

Figure 5-5 Expansion of Figure 5-4. The spectrum gradually shifts with time from a maximum of 380 nm (after 280 ns) to 370 nm (after 7280 ns). $Si(DBE)_4$ in MeCN..... 148

Figure 5-6 The time evolution of the LFP spectra of 1,2-dibromo-2-methylpropane in MeCN..... 149

Figure 5-7 $CHCl_3$•Br (λ_{max} = 310 nm) and $Br_2^{\bullet-}$ (λ_{max} = 350 nm) complexes produced by the 337 nm LFP of α-bromoacetophenone in an oxygen purged $CHCl_3$ solution containing 10mM TBAB 153

Figure 5-8 $CHCl_3$•Br second-order decay recorded at 360 nm. The complex was produced by the LFP of 1,2-dibromoethane in an oxygen purged $CHCl_3$ solution containing no TBAB 154

Figure 5-9 360 nm decay traces in oxygen purged $CHCl_3$: (●) [Br-] = 0.0 mM and (○) [Br-] = 10 mM. From the LFP of 1,2-dibromoethane..... 155

Figure 5-10 360 nm decay traces in oxygen purged $CHCl_3$: (●) [Br-] = 0.0 mM and (○) [Br-] = 0.16 mM. From the LFP of 1,2-dibromoethane..... 156

Figure 5-11 The quenching of bromine atoms by the $Si(DBE)_4$ precursor. The observed growth rate constant, k_{obs} of the $Si(DBE)_4$•Br complex is plotted against the concentration of the $Si(DBE)_4$. 160

Figure 5-12 The (●) 360 nm growth and the (○) 460 nm decay traces recorded after the 266 nm LFP of *trans*-1,2-dibromocyclopentane in MeCN..... 163

List of Tables

Table 1-A Thaler's product distribution of the radical bromination of bromocyclohexane.[29] 20

Table 3-A Literature probe rate constants (k_{X2^-}), absorption maxima (λ_{max}), and extinction coefficients (ε) for the dihalide radical ions (X_2^-) and $(SCN)_2^-$. 48

Table 3-B The relative extinction coefficients of the BrX^- radical anion complexes in MeCN at 298 K. 71

Table 3-C The equilibrium reactions of the halide ions with the dithiocyanate radical anion, $(SCN)_2^-$ and the mixed radical anion, $XSCN^-$.[21-23] 76

Table 3-D A comparison of rate and equilibrium constants for the various halide complexes of bromine atoms. 89

Table 4-A The Kaleidagraph output values for the fitting of Equation 4.15 to the points in Figure 4-6. The trace was generated by the 2.06 mM fluoride trapping of the bromine atoms produced by the LFP of 1,2-dibromopropane in MeCN. k_{probe} was fixed at 21 μs^{-1} (2.06×10^{-3} M^- * 10×10^9 M^{-1} s^{-1}) 110

Table 4-B Simulations of the three high-halide kinetic cases. 114

Table 4-C A comparison of the high-halide data for the LFP of $Si(DBE)_4$ in MeCN when the intercepts are fixed at the fluoride intercept versus when they are not fixed. 124

Table 4-D A compilation of β-bromo radical lifetimes and their rates of reduction by fluoride, chloride, and bromide. An entry of "case 1" refers to the fact that the particular experiment never altered from the probe rate constant, therefore no lifetime could be determined. 125

Table 4-E A compilation of β-bromo radical lifetimes and their rates of reduction by fluoride, chloride, and bromide for the cyclic *vicinal* dibromides. The dihedral angle between the bromine atoms has been included in the table. The dihedrals were calculated using MM2 optimized geometries. 133

Table 4-F The Arrhenius parameters for the fluoride probed photolysis of 1,2-dibromoethane and the bromide probed photolysis of *trans*-1,2-dibromocyclopentane in MeCN. 136

Table 5-A A compilation of absorption maxima and ionization potentials for various bromine atom complexes (R•Br) with bromoalkanes, chloroalkanes, and alkanes. LFP = Laser Flash Photolysis; PR = Pulse Radiolysis.[7] 147

Table 5-B RBr_2•Br Complexes of *vicinal* dibromides in MeCN. The spectra were recorded by the 266 nm LFP of the respective *vicinal* dibromides in MeCN. 161

Table 5-C The absorption maxima of the *vicinal* dibromide•Br complexes in MeCN and the vertical ionization potentials (I_D) of some of the *vicinal* dibromides studied. 164

Table 5-D The possible three-electron bonds for the charge-transfer complexes (CTC) of a bromine atom with bromoethane, dimethyl sulfoxide (DMSO), acetonitrile (MeCN), and $Si(DBE)_4$ 166

List of Abbreviations

A/D	Analogue/Digital
Abs	Absorbance
Bu_4NBr	Tetrabutylammonium Bromide
Bu_4NCl	Tetrabutylammonium Chloride
Bu_4NF	Tetrabutylammonium Fluoride
Bu_4NI	Tetrabutylammonium Iodide
CIDNP	Chemically Induced Dynamic Nuclear Polarization
CTC	Charge Transfer Complex
DBE	1,2-Dibromoethane
DMSO	Dimethylsulfoxide
ESR	Electron Spin Resonance
I	Intensity
I_D	Ionization Potential
LFP	Laser Flash Photolysis
MeCN	Acetonitrile
NIST	National Institute of Standards and Technology
O.D.	Optical Density

Obs	Observed
PAG	Photoacid Generator
PMT	Photomultiplier Tube
PR	Pulse Radiolysis
$Si(DBE)_4$	Tetrakis(1,2-dibromoethyl)-silane
TBAB	Tetrabutylammonium Bromide
TBAB	Tetrabutylammonium Fluoride
TBAC	Tetrabutylammonium Chloride
TBAI	Tetrabutylammonium Iodide
TTL	Transistor-Transistor Linked

List of *vicinal* dibromides

Vicinal Dibromide	Structure
Dibromide I: 1,2-dibromo-1,1-difluoroethane	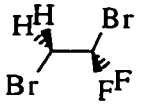
Dibromide II: 1,2-dibromoethane	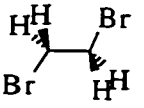
Dibromide III: 1,2-dibromopropane	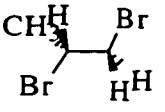
Dibromide IV: 1,2-dibromobutane	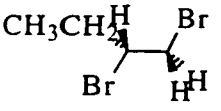
Dibromide V: 1,2-dibromo-3,3-dimethylbutane	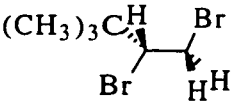
Dibromide VI: 2,3-dibromobutane	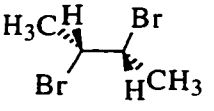
Dibromide VII: 1,2-dibromo-2-methylpropane	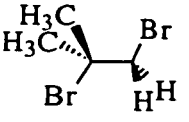

Vicinal Dibromide	Structure
Dibromide VIII: tris(2,3-dibromopropyl) isocyanurate	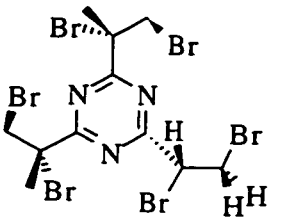
Dibromide IX: trans-1,2-dibromocyclopentane	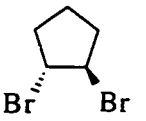
Dibromide X: trans-1,2-dibromocyclohexane	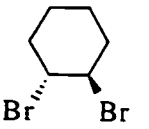
Dibromide XI: trans-1,2-dibromocycloheptane	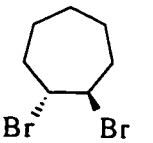
Dibromide XII: trans-10,11-dibromodibenzosuberone	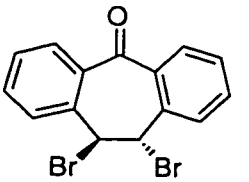
Dibromide XIII: Tetrakis(1,2-dibromoethyl)-silane **Si(DBE)4**	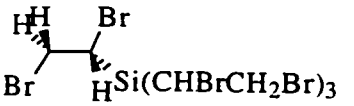
Dibromide XIV: 1,2-dibromoethyl-diethylmethylsilane	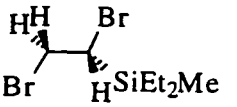

Vicinal Dibromide	Structure
Dibromide XV: 2,3-dibromopropyl-trimethylsilane	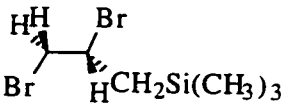
Dibromide XVI: 2-(1,2-Dibromoethyl)-naphthalene	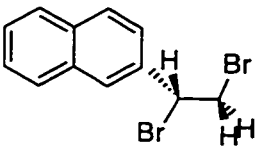
Dibromide XVII: 2-Bromo-9-(1,2-dibromoethyl)-anthracene	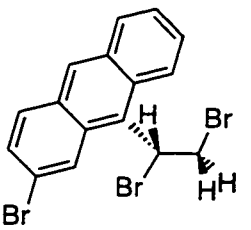
Dibromide XVIII: 1,2-Dibromoethyl-benzene	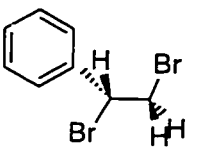

Abstract

The photolysis of *vicinal* dibromoalkanes in acetonitrile produces bromine atoms and β-bromoalkyl radicals. Bromine atoms react with halide ions to produce easily detectable and long-lived radical anions ($BrX^{\cdot-}$). The reaction of photolytically produced bromine atoms with iodide, bromide, chloride, and fluoride occurs with rate constants of $(1.4 \pm 0.8) \times 10^{10}$ M^{-1} s^{-1}, $(1.6 \pm 0.3) \times 10^{10}$ M^{-1} s^{-1}, $(1.4 \pm 0.1) \times 10^{10}$ M^{-1} s^{-1}, and $(1.0 \pm 0.1) \times 10^{10}$ M^{-1} s^{-1}, respectively in acetonitrile. The formation of the $Br_2^{\cdot-}$ radical anion was found to have an activation energy of 1.9 ± 0.4 kcal/mol and a logA factor of 11.6 ± 0.3. These radical anions have extinction coefficients of $(13 \pm 1) \times 10^3$ M^{-1} cm^{-1} ($BrI^{\cdot-}$), $(9 \pm 1) \times 10^3$ M^{-1} cm^{-1} ($BrCl^{\cdot-}$), and $(6.9 \pm 0.7) \times 10^3$ M^{-1} cm^{-1} ($BrF^{\cdot-}$) at 360 nm in MeCN.

The formation of the $BrX^{\cdot-}$ radical anions can be used to probe the dynamics of the decays of β-bromoalkyl radicals. For example, the lifetimes of the β-bromoethyl and β-bromocyclopentyl radicals were determined to be 145 ns and 100 ns, respectively

The halides were found to reduce the β-bromoalkyl radicals with rate constants in the 10^9 M^{-1} s^{-1} regime. For example, the bromide, chloride, and fluoride reduction rate constants were determined for the reaction with the β-bromocyclopentyl radical to be $(3.2 \pm 0.3) \times 10^9$ M^{-1} s^{-1}, $(2.0 \pm 0.2) \times 10^9$ M^{-1} s^{-1}, and $(1.3 \pm 0.1) \times 10^9$ M^{-1} s^{-1}, respectively. The activation energies and log(A) factors were determined for the temperature dependence of the bromide reduction of the β-bromocyclopentyl radical to be 3.3 ± 0.5 kcal/mol and 11.8 ± 0.5 and for the fluoride reduction of the β-bromoethyl radical to be 4.0 ± 0.5 kcal/mol and 12.2 ± 0.5.

1. Introduction

1.1 Applications For *Vicinal*-Debrominations **2**
(i) Alkene Purification 2
(ii) Alkene Protection/Deprotection 3
(iii) Synthetic Applications 3
(iv) Photoinitiated, Acid-Catalyzed, Polymer Cross-linking 5

1.2 Photochemical Debrominations **7**
(i) The Photodebromination of 1,2-Dibromoethane 8
(ii) The Photodebromination of Aryl-Substituted Vicinal Dibromides 10

1.3 Other Methods For *Vicinal*-Debrominations **12**
(i) Reductions of Vicinal-Dibromides By Two-Electron Nucleophiles 12
(ii) Reductions of vicinal-Dibromides By One-Electron Reductants 15

1.4 β-Bromo Radicals **18**
(i) The Rate-Enhancing (Anchimeric) Effect of Bromine Substituents in Radical Reactions 19
(ii) The Stereoelectronic Factors For The Anchimeric Effect 21
(iii) The Nature of the Bromine Bridged Radical 23

1.5 Chapter 1 References **27**

Vicinal Dehalogenations are a special class of β–eliminations in which two halogen atoms are eliminated from *vicinal* dihaloalkanes or dihaloalkenes to produce the corresponding alkenes or alkynes.[1] The processes are overall reductions of the *vicinal* dihalides and can be represented by Scheme 1-1 and Scheme 1-2.

Scheme 1-1 Representation of the reduction of a *vicinal* dibromoalkane to an alkene.

Scheme 1-2 Representation of the reduction of a *vicinal* dibromoalkene to an alkyne.

Vicinal Debrominations are the sub-class of *vicinal* dehalogenations of concern in this report. Throughout the text, constant references and comparisons will be made to the rest of the *vicinal* dehalogenation classes where appropriate examples exist.

1.1 Applications For *Vicinal*-Debrominations

There are several uses for *vicinal* debrominations, but of all the uses, only the photodebromination of *vicinal* dibromides has flourished recently. The microlithographic industry uses *vicinal* dibromides as photochemical sources of hydrobromic acid to image the patterns into their resists.

(i) Alkene Purification

The debromination of *vicinal* dibromides has traditionally enjoyed a very limited role in organic chemistry. They have been used for many years as a means to purify alkenes.[2] Bromination of an alkene leads to the high boiling *vicinal* dibromide, which can

then be easily purified by distillation or recrystalization. Subsequent debromination leads to the pure olefin.

(ii) Alkene Protection/Deprotection

Scheme 1-3 illustrates the use of the bromination-debromination procedure to protect double bonds that would have otherwise been altered during a particular synthetic step. Solo and Singh add Br_2 to protect the 5,6 double bond during an allylic bromination step en route to the target 3-β-acetoxy-20-keto-5,14,16-pregnatriene.[3] The final conversion to the target triene is accomplished using sodium iodide. Under these conditions, both the *vicinal* dibromide as well as the allylic bromine sites are converted to double bonds (see Scheme 1-3).

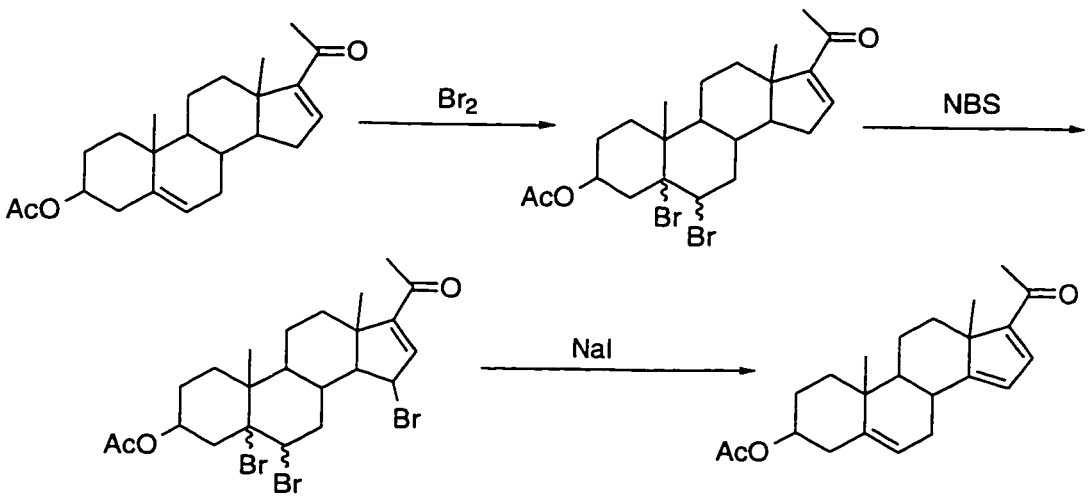

Scheme 1-3 Solo's synthesis of 3–β-acetoxy-20-keto-5,14,16-pregnatriene.

(iii) Synthetic Applications

Other than the above-mentioned purification and protecting uses of *vicinal* debrominations, the synthetic utility of *vicinal* dibromides has been said to be scarce since they are generally prepared from alkenes and alkynes. There are, however, examples such as those investigated by Allred *et al.*, where the starting materials are not the dihalides of the resulting alkenes.[4] Scheme 1-4 and Scheme 1-5 depict such examples. In Scheme 1-4

Allred *et al.* synthesize tetracyclo[5.3.0.$0^{2,10}$.$0^{3,6}$]deca-4,8-diene from benzene and 3,4-dichloro-cyclobutadiene. Scheme 1-5 represents Allred's synthesis of bicyclo[4.2.0]octa-2,7-diene from cyclooctatetraene and chlorine gas. It is obvious from these two examples that the dehalogenation of *vicinal* dihalides can be a very effective synthetic tool to introduce structurally significant double bonds.

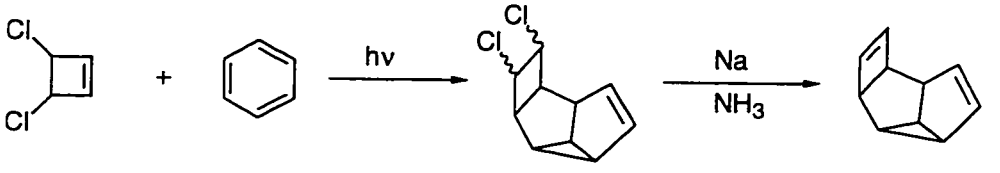

Scheme 1-4 Allred's synthesis of tetracyclo[5.3.0,$0^{2,10}$.$0^{3,6}$]deca-4,8-diene.

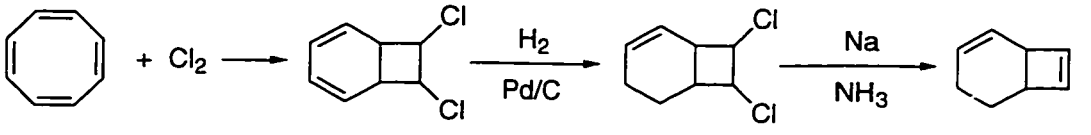

Scheme 1-5 Allred's synthesis of bicyclo[4.2.0]octa-2,7-diene.

Similar dehalogenations have been used as simple and effective routes to the previously unattainable, anti-Bredt, highly strained, adamantene.[5-7]

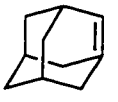

Adamantene

In all three cases, the adamantene was prepared from either 1,2-dibromo or 1,2 diiodo adamantane. None of the groups were able to isolate the adamantene. Its existence was inferred from the isolation and characterization of either the dimer of adamantene or the dienic trapped products.

(iv) Photoinitiated, Acid-Catalyzed, Polymer Cross-linking

Imaging in the photoresist and photolithographic industries depends on the directed production of acid to catalyze polymer cross-linking (negative resists) or to enhance solubilization in base (positive resist) during the development stage.

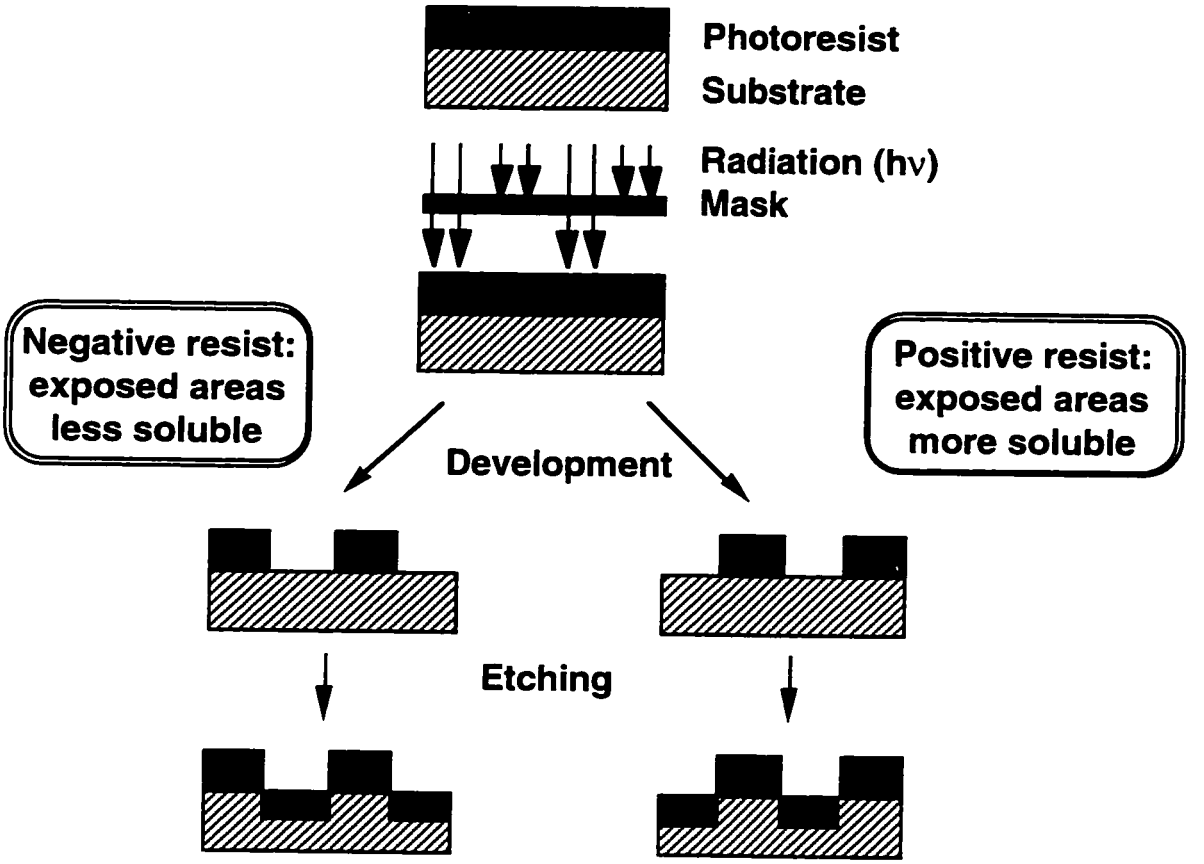

Scheme 1-6 Schematic of photoresist functions.

This directed production of acid is accomplished photolytically. Scheme 1-6 is a representation of the photoresist functions. The photoresist serves to protect certain areas of a substrate which is to be etched. The desired pattern is sculpted into the photoresist via irradiation and development. The photoresist is irradiated through a radiation mask or template containing a pattern. In a negative resist, the exposed areas become less soluble and remain after development. The resulting pattern etched into the substrate is a negative image of the radiation mask. In a positive resist, the exposed areas become more soluble

and are removed after development. The resulting image etched into the substrate is a positive image of the radiation mask.

Commonly, photoacid generators (PAGs) have been diazonaphthoquinones, and aryl diazonium, iodonium, and sulfonium salts with complex metal halide anions.[8] The main disadvantage to these four PAGs is their inconvenient absorption properties. The lack of any significant visible or near UV absorption of these types of molecules requires the use of deep UV irradiation where the polymeric bulk of the resist also absorbs the light. The advantages to using *vicinal* dibromides are their tunable absorption characteristics, high thermal stability, and high acid quantum yield (namely HBr).

Barra *et al.* show in Scheme 1-7 how light initiates a chain of events to cross-link, and thus render insoluble, the phenolic polymer backbone of a typical negative photoresist.[9] In Equation 1.1, the PAG (a *vicinal* dibromide) is debrominated photochemically to produce HBr. The HBr then acid catalyzes the elimination of methanol from the cross-linking agent, hexamethoxymethylmelamine in this case (Equation 1.2). Equation 1.3 shows the reaction of the cationic intermediate of the cross-linker to the phenolic moiety of the polymer backbone of the resist.

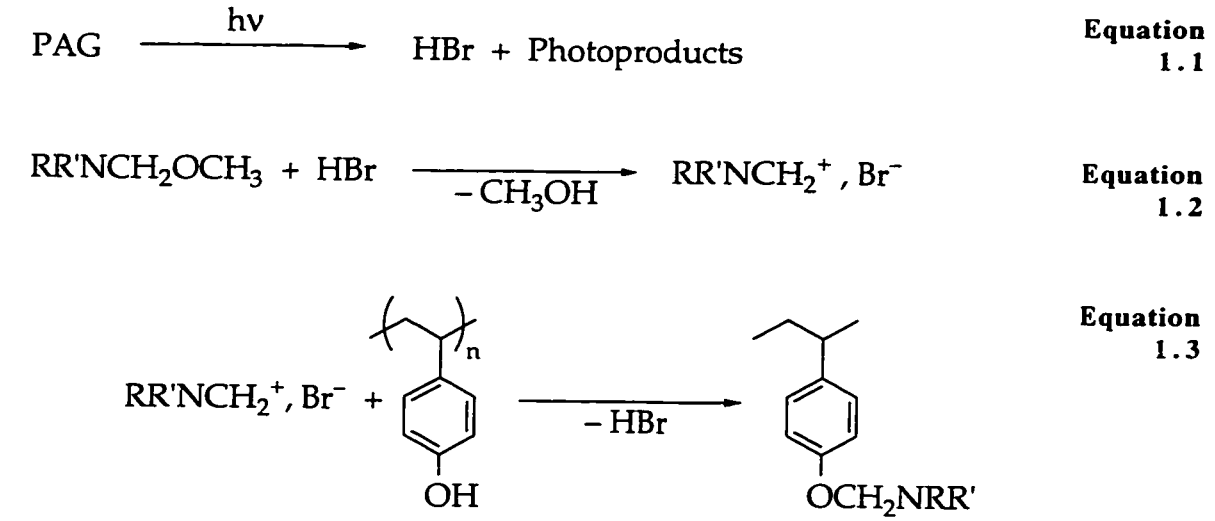

Scheme 1-7 The light initiated, acid catalyzed, cross-linking of a phenol based polymer resist.

The production of HBr in Equation 1.1 is a two-step process. Photolysis of the *vicinal* dibromides produces bromine atoms, which in turn, abstract hydrogen atoms from the environment to produce the HBr. Since the environment includes phenols, the process is a very effective one. There are presently several studies to deduce the detailed mechanisms of both the bromine atom production, and the hydrogen abstraction.

1.2 Photochemical Debrominations

Based on the absence of any observed triplets in *vicinal* dibromide photochemistry, it is assumed that the dissociation occurs from the singlet manifold. Figure 1-1 shows a representation of the ground state and first excited singlet states of a typical carbon-bromine bond in a bromoalkane. The excited singlet state (S*) is meant to portray a dissociative σ^* state of the molecule.

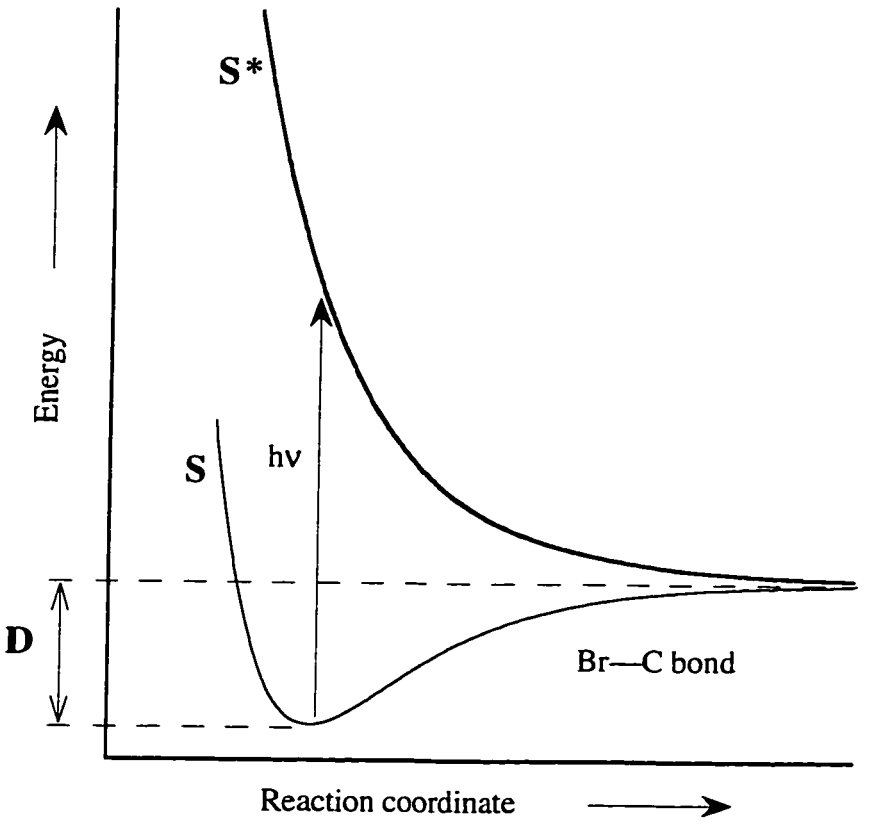

Figure 1-1 The Potential Energy Profile for the S_0 and S_1 states of a typical bromoalkane

(i) The Photodebromination of 1,2-Dibromoethane

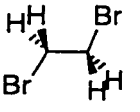

Dibromide II

1,2-Dibromoethane

In 1992, Scaiano *et al.* studied the photochemistry of 1,2-dibromoethane (Dibromide **II**) as a model for the generation of HBr.[10] While 1,2-dibromoethane suffers from the same poor absorption characteristics as the aforementioned salts, it is, however, the simplest *vicinal* dibromide.

The study of this simple system was undertaken with the desire that the results would lend some valuable insights into the production of HBr from more complicated systems with more appropriate absorption properties. Using laser flash photolysis techniques, Scaiano *et al.* determined that the first bromine atom is expelled from the molecule upon absorption of a photon from the 266 nm YAG laser (Equation 1.4). Under the experimental conditions employed, Scaiano's group also determined that the β-bromo radical thermally cleaves to produce the second bromine atom and ethylene (Equation 1.5). Because neither the β-bromo radical, nor the bromine atom produced after the initial photolysis absorb in the region normally accessible to the laser flash photolysis technique (250 nm to 800 nm), bromide was added to probe the system. It is known that bromide (Br^-) forms a highly absorbing complex, $Br_2^{\bullet-}$, with bromine atoms ($\varepsilon = 9900\ dm^3\ mol^{-1}\ cm^{-1}$)[11] with $\lambda_{max} \sim 360$ nm[12] (Equation 1.6). Thus, the detection of the $Br_2^{\bullet-}$ complex serves as a direct indication of the presence of bromine atoms.

Equation 1.4

$$CH_2Br-CH_2Br \xrightarrow{266nm} CH_2Br-CH_2\bullet + Br\bullet$$

Equation 1.5

$$CH_2Br-CH_2\bullet \xrightarrow{fast} CH_2=CH_2 + Br\bullet$$

Equation 1.6

$$Br\bullet + Br^- \rightleftharpoons Br_2^{\bullet-}$$

Scaiano *et al.* measured the rate constant for the formation of the $Br_2^{\bullet-}$ complex (Equation 1.6) to be $1.6 \times 10^{10}\ M^{-1}s^{-1}$ in acetonitrile at room temperature. This value agrees well with those obtained in water by Treinin and Hayon ($1.1 \times 10^{10}\ M^{-1}s^{-1}$)[13] and by Nagarajan and Fessenden ($9 \times 10^9\ M^{-1}s^{-1}$).[14] This rather rapid rate of formation of the complex, coupled with its rather slow decay (several microseconds) means that at sufficiently high bromide concentrations (>10mM), the complex formation will only be limited by the rate of bromine atom production. Thus, the kinetics of the $Br_2^{\bullet-}$ complex

formation at high concentrations of bromide should represent the kinetics of the bromine atoms themselves as they are eliminated from the *vicinal* dibromide.

Under these high bromide concentrations, >10 mM, the formation of the $Br_2^{\bullet}$ complex was observed to be complete within the duration of the laser pulse (~6ns). Therefore, it was concluded that Equation 1.5 must be very fast, making the lifetime of the β-bromo radical less than 20 ns (the detection limit of the system).

In addition, Scaiano's group determined the quantum yield of bromine atom production to be 2.3 ± 0.5. The quantum yield of bromine atom production was determined using benzophenone as an actinometer. The benzophenone triplet is produced with a quantum yield of 1.0, and has a well known extinction coefficient in acetonitrile of 7800 M^{-1} cm^{-1} at 535 nm.[15] In conclusion, within experimental error, 1,2-dibromoethane (as well as other aliphatic *vicinal* dibromides) released two atoms of bromine per photon absorbed.

(ii) The Photodebromination of Aryl-Substituted Vicinal Dibromides

Gannon and McGimpsey confirmed and added to the results obtained by Scaiano's group using *trans*-10,11-dibromodibenzosuberone (Dibromide **XII**).[16] Unlike 1,2-dibromoethane, *trans*-10,11-dibromodibenzosuberone has a ground state absorption spectrum that extends into the near UV. Gannon and McGimpsey employed Br^-, as well as benzene, as probes for the bromine atoms in the laser flash photolysis studies. Benzene, like $Br_2^{\bullet}$, also forms a strongly absorbing complex with bromine atoms.[17] They determined the yield of bromine atom from *trans*-10,11-dibromodibenzosuberone to be 2.4 ± 0.6 also using benzophenone as an actinometer. This is in strong agreement with the value of 2.3 ± 0.5 obtained for 1,2-dibromoethane.[10] Gannon and McGimpsey confirmed their results by titrating their samples with base to determine the amount of HBr produced. Their titrations confirmed a quantum yield of 2 for HBr within the errors of the experiments.

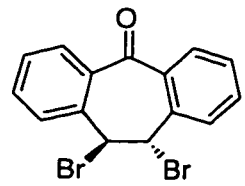

Dibromide XII

***trans*-10,11-dibromodibenzosuberone**

As in Scaiano's studies, Gannon and McGimpsey saw no sign of a delayed elimination of the second bromine atom, thus also concluding that the β-bromo radical must have a very short lifetime (<20 ns). In the following year, McGimpsey's group pursued other red-shifted *vicinal* dibromides as potential PAGs and published an article on 1,2-dibromoethyl arenes.[8]

Their results showed for the first time that not all *vicinal* dibromides have quantum yields of 2. In their search for other *vicinal* dibromides with desirable ground state absorptions such as that of *trans*-10,11-dibromodibenzosuberone, McGimpsey's group indirectly sacrificed the quantum yield of acid production. It was determined that $\Phi(Br\bullet)$ was 0.87 ± 0.10 for 2-(1,2-dibromoethyl)-naphthalene (Dibromide **XVI**) and 0.45 ± 0.10 for 2-bromo-9-(1,2-dibromoethyl)-anthracene (Dibromide **XVII**). Apparently these aryl substituted dibromoethanes have stabilized the β-bromo radical to the extent that the second bromine atom is not expelled within the timescale of the experiment. In the case of *trans*-10,11-dibromodibenzosuberone, also an aryl substituted dibromoethane, the conjugation of the two phenyl rings is probably the driving force behind the rapid thermal debromination, giving it $\Phi(Br\bullet) \sim 2$. Thus, these long-lived β-bromo radicals are in complete contrast to the radicals derived from 1,2-dibromoethane and *trans*-10,11-dibromodibenzosuberone which seem to thermally cleave instantaneously.

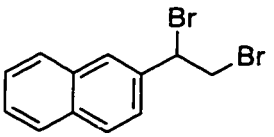

Dibromide XVI

2-(1,2-Dibromoethyl)-naphthalene

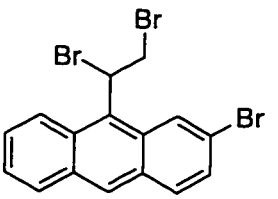

Dibromide XVII

2-Bromo-9-(1,2-dibromoethyl)-anthracene

1.3 Other Methods For *Vicinal*-Debrominations

There are several reagents that will accomplish the reduction of *vicinal* dibromides: nucleophiles, metal ions, and metals. *Vicinal* dibromides can also be reduced electrochemically, with high energy radiation, thermally, and, as we saw, photochemically. Of the other methods, only the nucleophilic reactions will be treated in detail in this thesis. The nucleophilic reductions show similarities with the photochemical debrominations of concern in this work (especially the one-electron reductions).

(i) Reductions of Vicinal-Dibromides By Two-Electron Nucleophiles

A wide variety of two electron nucleophiles have been used to reduce *vicinal* dibromides to alkenes. These include the halides (except fluoride), nucleophiles of sulfur, phosphorous, nitrogen, and oxygen, organometalic compounds, pseudo-halides, and many more. Iodide has been the most prevalent nucleophile to reduce *vicinal* dibromides (Equation 1.7).

Equation 1.7

There have been two main mechanisms put forward for these two electron reductions. The first one is the E2hal mechanism which is based on the E2 dehydrohalogenation reaction, and the second is based on the halonium type ion of the

reverse reaction (halogenation of an alkene). Despite the reaction conditions and the arguments for each mechanism, one thing remains constant: the nucleophile attacks one of the two bromine atoms. While the attacked bromine atom acts as the electrophilic center, the other acts as the leaving group.

The E2hal reaction, as applied to Equation 1.7, would imply that the iodide attacks one of the bromine atoms, removing it as the second bromine atom leaves simultaneously (Equation 1.8).

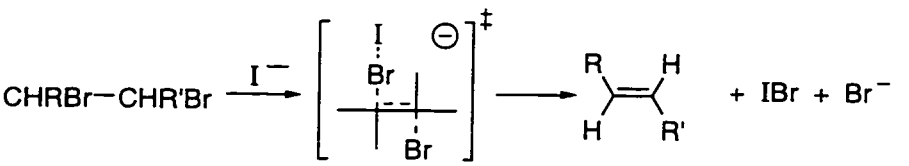

Equation 1.8

Of course, as in the respective dehydrobromination, the degree of concertedness of the elimination depends upon the reaction conditions employed. Depending on the solvent, the nucleophile, and the *vicinal* dibromide, the transition state of the reaction may lean towards either an E1 or an E1cB type transition state.

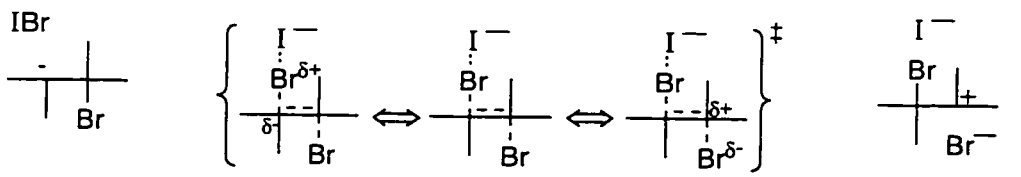

Scheme 1-8 **The relationship between the E1cB, E2, and E1 elimination mechanisms for debromination of a *vicinal* dibromide by a two electron nucleophile.**

The halonium ion interpretation stems from the principle of microscopic reversibility. Hine and Braider suggested that the reduction of 1,2-diodoethane by iodide must proceed through a transition state resembling that of the reverse reaction of iodine with ethene (Scheme 1-9).[18]

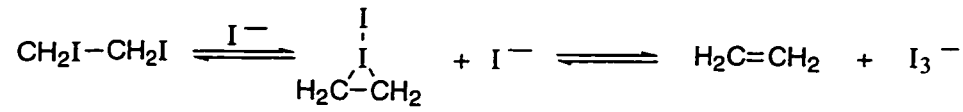

Scheme 1-9 The iodide catalyzed formation of the iodine/ethene bridged complex.

Miller and co-workers extended the mechanism to formally include the iodonium ion, as well as an open carbonium ion (Scheme 1-10).[19]

Both mechanisms adequately explain the results of various reactions under a multitude of conditions. It has been suggested that the E2hal mechanism operates under normal conditions and the halonium ion mechanism only takes over when the latter becomes difficult under the particular conditions.

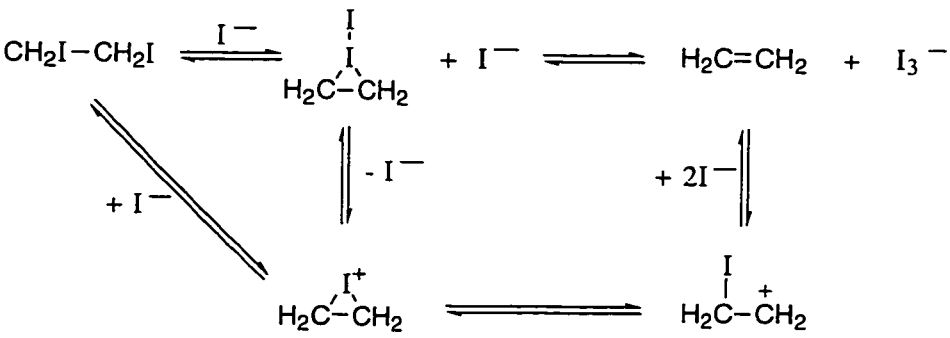

Scheme 1-10 The interconversion between bridged intermediates for the deiodination of 1,2-diiodoethane as proposed by Miller *et al.*.

Regardless of which mechanism prevails, the important aspect of these debrominations is that there is a definite stereoelectronic preference for an *anti*-elimination. Both the E2hal and the bridged halonium ion mechanisms would account for the observed stereochemical control.

There are numerous examples in the literature of two-electron-nucleophilic reductions of *vicinal* dibromides that give predominantly (or even exclusively) the

geometric isomer due to an *anti*-elimination. The two electron reduction of *meso*-2,3-dibromobutane gives a greater than 90% yield of *trans*-2-butene (Scheme 1-11).[20]

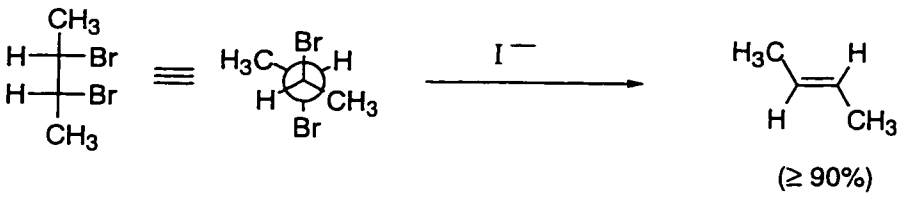

Scheme 1-11 The reduction of *meso*-2,3-dibromobutane to *trans*-2-butene by iodide.

trans-Stilbene is the exclusive product from the debromination of meso-1,2-dibromo-1,2-diphenylethane by iodide, bromide and chloride.[21] In fact, the requirements for proper *anti* alignment can be so important that certain eliminations can be shut off if the bromine atoms are fixed in a low dihedral angle. The reduction of 5α,6β-dibromocholestan-3β-yl benzoate by iodide in acetone proceeds at a rather rapid rate, whereas there is no elimination from the 5β-6α isomer under the same conditions.[22] In a simpler system, *trans*-1,2-dibromocyclohexane has been shown to react 11 times faster with iodide than *cis*-1,2-dibromocyclohexane.[23]

(ii) Reductions of vicinal-Dibromides By One-Electron Reductants

Like the previous two-electron reductants, the one-electron reductants also transfer 2 electrons to the *vicinal* dibromides. The difference is that the one-electron reductants do so by a stepwise mechanism, one electron at a time.

Equation 1.9

Equation 1.10

Scheme 1-12 The stepwise two-electron reduction of a *vicinal* dibromide by a one-electron reductant.

In Equation 1.9, the one-electron reductant transfers one electron to the *vicinal* dibromide causing the elimination of a bromide ion leaving behind a β-bromo radical. In the second step, Equation 1.10, a second equivalent of the one-electron reductant transfers an electron to the β-bromo radical causing it to also eliminate a bromide ion, thus producing the resultant alkene. The combined reactions of Equation 1.9 and Equation 1.10 in Scheme 1-12 lead to the same overall reduction as that of Scheme 1-1.

The list of one-electron reductants includes radical anions, carbanions, free or complexed metal ions, and radicals. Because the one-electron reduction of *vicinal* dibromides requires two equivalents of reductant, and the reaction proceeds via an intermediate β-bromo radical, the overall reaction is more susceptible to the reaction conditions.

The β-bromo radical, once formed has two options for further reaction. Path (a), Scheme 1-13; It may eliminate a bromine atom thermally, as is the case for the photodebromination of 1,2-dibromoethane.[10] Or, path (b), Scheme 1-13; the β-bromo radical may receive an electron from a second equivalent of reductant to produce a β-bromo anion which then loses a bromide ion to produce the final olefin. For non-stabilized *vicinal* dibromides, path (a) appears to be the dominant pathway.[1]

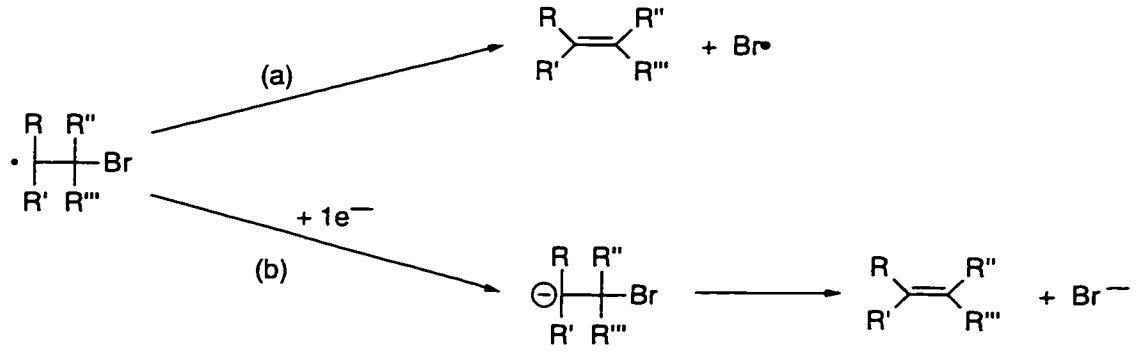

Scheme 1-13 The possible fates of the β-bromo radical in the presence of a one-electron reductant.

The stereochemical results for the one-electron reductions of *vicinal* dibromides show an even more complicated mechanism at work. The reduction of 3,4-dibromohexane by the diphenyl-cyanomethyl anion, $[Ph_2CCN]^-$, gives exclusively *trans*-3-hexene, regardless of whether the *meso* or the D,L diasteriomer was used for the reaction.[24] On the other hand, when sodium naphthalenide is used to reduce 2,3-dibromo-3-methylpentane in dimethoxyethane, each diasteriomer gives only its respective *anti*-elimination product.[25] These, and other less extreme examples, are thought to be controlled by numerous factors including that of bromine-bridging. The rotameric relaxation of β-bromo radicals should be retarded by bromine-bridging (Scheme 1-14).

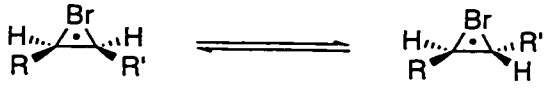

Scheme 1-14 The equilibrium between the two geometric isomers of a bromine-bridged radical.

The stereochemical results of one-electron reductions of *vicinal* dibromides are said to be controlled by the partitioning of the mechanism between paths (a) and (b) of Scheme 1-13, as well as by the equilibrium between the two possible isomers of the bridged radical.

Bridging is proposed to preserve the stereochemical memory of the β-bromo radical in the case of the exclusive *anti*-eliminations from the two isomers of 2,3-dibromo-3-methylpentane. In the case of the 3,4-dibromohexanes, it is assumed that the β-bromo radical has time to equilibrate to the more stable *trans* isomer before elimination of the bromine atom.

As for the intervention of path (b), it is of course, dependent on the concentration of the reductant. In studies with chromium(II)-promoted debrominations of *meso* and D,L-2,3-dibromobutanes, the highest *anti*-elimination results are obtained at high chromium(II) concentrations.[26] Under these high chromium concentrations, the bromine-bridge does not have as much time to equilibrate, therefore the *anti*-elimination is obtained.

1.4 β-Bromo Radicals

Although the review is somewhat dated, the observations and conclusions reached by Skell and Shea in their chapter on bridged free radicals is as pertinent today as the day it was written.[27] The authors report that based on the multitude of product information from both the debrominations of *vicinal* dibromides and the radical reactions of alkyl bromides, a bromine bridged radical intermediate must be invoked to explain the results.

The bridged bromine radical is analogous to the bridged, three-membered bromonium ion formed during the electrophilic addition of Br_2 to olefins. In either case, the bromine is placed between the two adjacent carbon centers. Bridging in these intermediates results in the stabilization of the reactive center as well as the restriction of rotation about the two carbon centers involved.

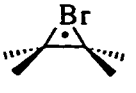

Bromine Bridged Radical

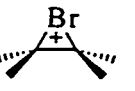

Bromonium Ion

As yet, there does not exist any conclusive spectral proof of the existence of bromine bridging. The overwhelming evidence from product studies, however, will be reviewed in order to establish the basis for the assignment of the bridged β-bromo radicals. Also, comparison with other β-halo radicals will be made when appropriate examples exist. Other than the β-bromo radicals, the majority of other examples are those of β-chloro radicals. β-Chloro radicals have the advantage of being easily observed in the ESR timescale. Unfortunately for comparison, the β-Chloro-effect is not nearly as dramatic as the β-bromo-effect. The corresponding β-iodo and β-bromo radicals are presumably too unstable (even at -120°C) to be observed by ESR. The β-fluoro radicals do not show the β-effect at all. In fact, β-fluoro radicals behave simply as radicals with electron withdrawing groups.

(i) The Rate-Enhancing (Anchimeric) Effect of Bromine Substituents in Radical Reactions

A compound containing a halogen (or any other electronegative substituent) should inductively deactivate proximal positions to radical halogenation.[28] This means, that in the case of alkyl bromides, the more remote positions should be favored in radical brominations. The results obtained are in complete opposition to this trend. Instead, it is found that the position *vicinal* to the bromine substituent is preferentially brominated, sometimes exclusively.

In 1963, both Thaler[29] and Skell's group[30] reported this unusual directing ability of a bromo-substituent. Thaler reported that 94% of the radical bromination of bromocyclohexane produced *trans*-1,2-dibromocyclohexane (Table 1-A).

Similar reactions with bromocyclopentane and 1-bromobutane gave yields of 90% and 84.5% respectively of the *trans*-1,2-dibromides. Thaler concluded that bromine invokes a rather strong neighboring group effect in radical brominations despite its electronegativity. Thaler also postulated that, in order to stabilize the transition state of the abstraction, the bromine may form a three-membered ring with the two adjacent carbons.

Table 1-A **Thaler's product distribution of the radical bromination of bromocyclohexane.[29]**

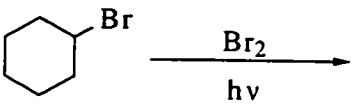

Dibromocyclohexane	% of total Dibromide
trans-1,2-	94.0
trans-1,3-	0.92
trans-1,4-	0.50
1,1- and/or cis-1,2-	3.53
cis-1,3-	0.52
cis-1,4-	0.53

Many subsequent studies have further demonstrated the effects of directing and accelerating radical brominations of alkylbromides. In the case of 1-bromobutane, Shea, Lewis, and Skell determined that the C-2 position was 22.5 times more reactive than the C-3 position for radical bromination in both the gas and condensed phases.[31] More dramatically, the bromination of *trans*-1-(bromomethyl)-4-methylcyclohexane occurs solely at the C-1 carbon (Scheme 1-15).[32]

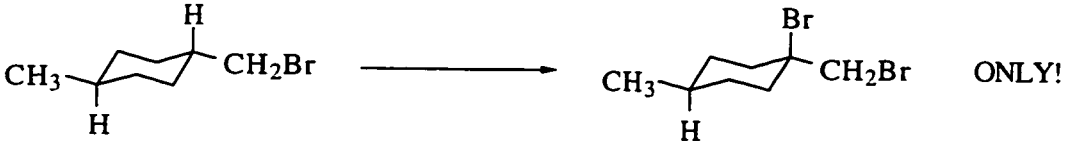

Scheme 1-15 The radical bromination of *trans*-(1-bromomethyl)-4-methylcyclohexane.

(ii) The Stereoelectronic Factors For The Anchimeric Effect

There are numerous examples in the literature that show that the anchimeric effect is greatly dependent on the neighboring group's ability to be periplanar with the developing radical center. For radical brominations of alkylbromides, the *anti* addition predominates. Concurrently, the products from an *anti* alignment of the two bromine atoms in a debromination are preferred. The products from these favorable alignments are preferred, but are not necessarily exclusive. For many reactions, the accompanying *syn*-additions or eliminations are also present. The ratio of *syn* to *anti* products depends on whether the molecules in question are capable of obtaining the preferred anti-alignment. When the molecules cannot attain the preferred anti-alignment, the *syn* reactions become increasingly important and may surpass the *anti* reactions. One thing remains constant, when the *anti* eliminations or additions are possible, they are usually several orders of magnitude faster than the respective *syn* reactions. The *syn* reactions must proceed via the traditional radical transition states.

As seen above,[30] the radical brominations of bromocyclohexane and bromocyclopentane give over 90% yields of the *trans*-1,2-dibromocycloalkanes. Not only is the β-position activated relative to the unsubstituted cycloalkanes, but more specifically the hydrogen *anti* to the bromine atom is preferentially removed. In a more rigid case, where the equilibrium between conformations is hindered, the selectivity is even greater. *Trans*-1-bromo-4-*tert*-butylcyclohexane shows normal radical substitution behavior, i.e. a second bromine atom is substituted at various positions on the ring, all at relatively slow reaction rates. The *cis* isomer, on the other hand, shows an accelerated rate and exclusive formation of the *trans*-1,2-dibromo product (Scheme 1-16).[33]

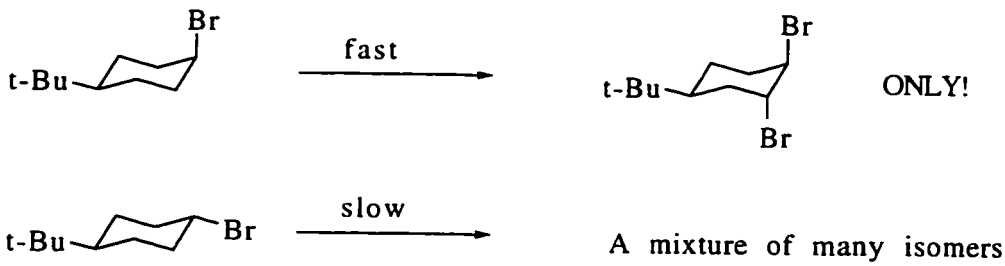

Scheme 1-16 A comparison of the radical brominations of *cis*- and *trans*-1-bromo-4-*t*-butylcyclohexane.

In a direct competition between a mixture of the two isomers, it was conservatively estimated that the *cis*-1-bromo-4-*tert*-butylcyclohexane was ≥15 times more reactive than the *trans* isomer.[33] Compared to the parent *t*-butylcyclohexane, the *cis*-1-bromo-4-*tert*-butylcyclohexane is 115 times more reactive per hydrogen.[34] Taking into account the fact the bromine atom should be deactivating by a factor of 0.14 (based on its electronegativity), this translates to an acceleration of 10^3 times what would have been expected when neglecting the neighboring group effect. Skell estimates that this rate enhancement corresponds to a net 3.4 kcal/mol stabilization by the neighboring bromine atom when it is periplanar to the developing radical center.[34]

Eliminations of *vicinal* dibromides also show this dependence on dihedral angle between the two bromine atoms, as seen in sections 1.3 (i) and 1.3 (ii) for both 2 and 1 electron reductions of *vicinal* dibromides. Electrochemical studies have shown that there is a direct correlation between the dihedral angle of the two carbon-bromine bonds and the reduction potential of the *vicinal* dibromide.[35]

Furthermore Skell's group showed that, unlike other radical intermediates, stereogenic β-bromo radicals preserve their asymmetry. It was shown that radical bromination of (+)-1-bromo-2-methylbutane yields (-)-1,2-dibromo-2-methylbutane of high optical purity (Scheme 1-17).[30] This was previously unheard of in radical chemistry where the radical center should be free to rotate and thus produce a final racemic mixture.

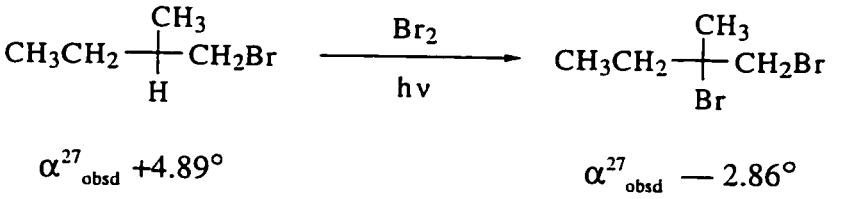

Scheme 1-17 The photobromination of (+)-1-bromo-2-methylbutane.

Based on this stereochemical control, Skell concluded that the bromine atom must be bridging between the two carbon centers thus preventing bond rotation and preserving the asymmetry of the molecule. The possibility of bridging, as well as the intramolecular rate-enhancing (anchimeric) effect, of the bromine atom in β-bromo radicals was first postulated in 1952.[36] These effects have previously been well established in bromonium ion chemistry.

(iii) The Nature of the Bromine Bridged Radical

There appears to be plenty of product data to feel confident concluding that a bromine atom is capable of forming a three-membered, bridged, radical intermediate. There have been no other mechanisms put forward that could account for the observed results. The potential to form a bridged radical intermediate would serve to activate the positions adjacent to the bromine atom, thus explaining the enhanced reactivities of these sites. Once formed, this bridged radical would restrict the rotation of the radical itself, thus preserving any stereochemistry.

What is not answered by these product studies is the nature of the bridged radical. A major concern is the symmetry of the bridged intermediate. Is it symmetrical i.e. is the bromine atom equidistant from both carbon centers? Or, is it unsymmetrical i.e. is the bromine atom closer to one of the carbons than the other? If the bridged radical is unsymmetrical, does the bromine atom retain any memory of it's original position? Questions also exist about the lifetime of the bridged form. Is it in equilibrium with the open, classical radical form? If so, how fast is this equilibrium?

Classical (Unbridged) **Symmetrically Bridged** **Unsymmetrically Bridged with shuttling of Br•**

The answer, as with many such systems, is probably a combination of all of the above. The radicals most likely interconvert between all of the forms. The relative time spent in each form being directly related to the stability of the forms. In a symmetrically substituted molecule with little or no stabilizing groups (other than the remaining bromine atom), one would expect the radical to be symmetrically bridged. There will probably be a certain amount of shifting of the bromine atom from one carbon to the other. Although this interconversion can be considered as moving from one unsymmetrical form to the other, the average structure will be that of the symmetrically bridged form.

A truly unsymmetrical bridged β-bromo radical will most likely have unsymmetrical substitution. There may also be cases in ring systems where ring twisting produces an unsymmetrical environment for the bridging bromine atom that can lead to unsymmetrical bridging. The most prevalent cases will be those of unsymmetrical substitution, whether in open chain or ring systems. If a *vicinal* dibromide is unsymmetrically substituted with groups capable of stabilizing a radical center, then the need for bromine bridging is lessened. In such cases, the bromine atom will lean closer to the carbon center that needs it more, i.e. the unstabilized one. The greater the stabilizing effect of the substituents, the more unsymmetrical the radical. Ultimately, with extremely stabilizing substituents, the radical becomes closer to being a classical, open radical.

In the case of substituted β-chloroethyl radicals, Kochi's group showed that the chlorine atom is closer to the less substituted carbon.[37] Kochi also demonstrated that the distance between the β-carbon and the chlorine atom increases as methyl groups are added

to the β-carbon, i.e. the amount of bridging decreases as the β–carbon becomes more substituted (Scheme 1-18).

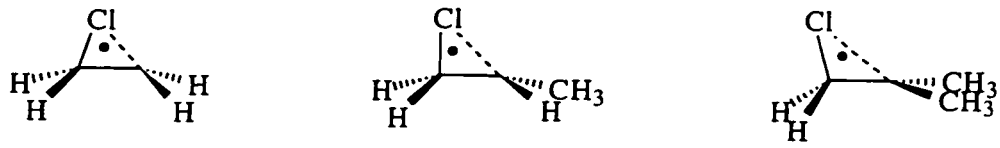

Scheme 1-18 **A qualitative representation of the distance between the chlorine atom and the α and β carbons for radicals with 0, 1, and 2 methyl groups on the α-carbon.**

The classical, open radical will most likely have more complicated circumstances than simply having highly stabilizing substituents. The 3.4 kcal/mol of stabilization offered by a β-bromine atom is quite formidable.[34] As long as the stereoelectronic and strain factors are favourable for bromine bridging, the stabilization offered by the bromine bridging is additive. Therefore, there should be very few circumstances where the bromine atom cannot help, or is not needed to help stabilize both carbon centers. As was seen with the arene radicals studied by McGimpsey's group[8], the arenes produce β-bromo radicals that are stable on the microsecond timescale. These pseudo-stable β-bromo radicals generated from the respective 1,2-dibromoethyl substituted naphthalene and anthracene moieties were shown not to lose the second bromine atom during the timescale of the experiment. Having established the reasonable stability of these β-bromo "benzyl-like" radicals, they were then shown not to react with oxygen. The reactivities of the respective unbrominated arene radicals with oxygen have pseudo-first-order rate constants in the 10^8 s^{-1} region.[38] The unreactivity of these "stable" β-bromo radicals was explained using bromine-bridging as a shield against attack by the incoming oxygen.

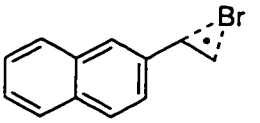

Bridged radical from 2-(1,2-Dibromoethyl)-naphthalene

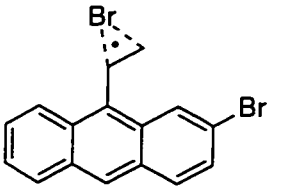

Bridged radical from 2-Bromo-9-(1,2-dibromoethyl)-anthracene

Despite being well stabilized by aromatic substitution, these β-bromo radicals do not behave as classical radicals. Therefore, there must still be a contribution from bromine bridging. The radicals are most likely unsymmetrically bridged, but bridged nonetheless.

1.5 Chapter 1 References

(1) Baciocchi, E. In *Supplement D: the chemistry of halides, pseudohalides, and azides*; S. Patai and Z. Rappoport, Eds.; John Wiley & Sons Ltd.: Chichester, 1983; Vol. 1; pp 161.

(2) Soday, F. J.; Boord, C. E. *J. Am. Chem. Soc.* **1933**, *55*, 3293. As cited in Bachiocchi;*1*.

(3) Solo, A. J.; Singh, B. *J. Org. Chem.* **1965**, *30*, 1658.

(4) Allred, E. L.; Beck, B. R.; Voorhees, K. J. *J. Org. Chem.* **1974**, *39*, 1426.

(5) Burns, W.; Grant, D.; McKervey, M. A.; Step, G. *J. Chem. Soc., Perkin Trans. I* **1976**, 234.

(6) Gillespie, D. G.; Walker, B. J. *Tetrahedron Lett.* **1977**, 1673.

(7) Cadogan, J. I. G.; Leardini, R. *J. Chem. Soc., Chem. Commun.* **1979**, 783.

(8) Zhang, B.; Pandit, C. R.; McGimpsey, W. G. *J. Phys. Chem.* **1994**, *98*, 7022.

(9) Barra, M.; Scaiano, J. C.; Calabrese, G. S.; Sinta, R.; Thackeray, J. *Chem. Mater.* **1994**, *6*, 724.

(10) Scaiano, J. C.; Barra, M.; Calabrese, G.; Sinta, R. *J. Chem. Soc., Chem. Commun.* **1992**, 1418.

(11) Hug, G. L. *Optical Spectra of Nonmetallic Inorganic Transient Species in Aqueous Solution*; National Bureau of Standards: Washington, 1981; Vol. NSRDS-NBS 69, pp 160.

(12) Zehavi, D.; Rabani, J. *J. Phys. Chem.* **1972**, *76*, 312.

(13) Treinin, A.; Hayon, E. *J. Am. Chem. Soc.* **1975**, *87*, 1716.

(14) Nagarajan, V.; Fessenden, R. W. *J. Phys. Chem.* **1985**, *89*, 2330.

(15) Wintgens, V.; Johnston, L. J.; Scaiano, J. C. *J. Am. Chem. Soc.* **1988**, *110*, 511.

(16) Gannon, T.; McGimpsey, W. *J. Org. Chem.* **1993**, *58*, 913.

(17) McGimpsey, W. G.; Scaiano, J. C. *Can. J. Chem.* **1988**, *66*, 1474.

(18) Hine, J.; Brader, W. H. *J. Am. Chem. Soc.* **1955**, *77*, 361.

(19) Tsai Lee, C. S.; Mathai, I. M.; Miller, S. I. *J. Am. Chem. Soc.* **1970**, *92*, 4602.

(20) Winstein, S.; Pressman, D.; Yound, W. G. *J. Am. Chem. Soc.* **1939**, *61*, 1645.

(21) Baciocchi, E.; Schiroli, A. *J. Chem. Soc. B* **1969**, 554.

(22) Barton, D. H. R.; Miller, E. *J. Am. Chem. Soc.* **1950**, *72*, 1066.

(23) Goering, H. L.; Espy, H. H. *J. Am. Chem. Soc.* **1955**, *77*, 5023.

(24) Korzan, D. G.; Chen, F.; Ainsworth, C. *J. Chem. Soc., Chem. Commun.* **1971**, 1053.

(25) Adam, W.; Arce, J. *J. Org. Chem.* **1972**, *37*, 507.

(26) Kochi, J. K.; Singleton, D. M. *J. Am. Chem. Soc.* **1968**, *90*, 1582.

(27) Skell, P. S.; Shea, K. J. In *Free Radicals*; J. K. Kochi, Ed.; Wiley: New York, 1973; pp 809.

(28) Tedder, J. M. *Tetrahedron* **1982**, 313.

(29) Thaler, W. *J. Am. Chem. Soc.* **1963**, *85*, 2607.

(30) Skell, P. S.; Tuleen, D. L.; Readio, P. D. *J. Am. Chem. Soc.* **1963**, *85*, 2849.

(31) Shea, K. J.; Lewis, D. C.; Skell, P. S. *J. Am. Chem. Soc.* **1973**, *95*, 7768.

(32) Traynham, J. G.; Hines, W. G. *J. Am. Chem. Soc.* **1968**, *90*, 5208.

(33) Skell, P. S.; Readio, P. D. *J. Am. Chem. Soc.* **1964**, *86*, 3334.

(34) Skell, P. S.; Traynham, J. G. *Acc. Chem. Res.* **1984**, *17*, 160.

(35) O'Connell, K. M.; Evans, D. H. *J. Am. Chem. Soc.* **1983**, *105*, 1473.

(36) Goering, H. L.; Abell, P. I.; Aycock, B. F. *J. Am. Chem. Soc.* **1952**, *74*, 3588.

(37) Chen, K. S.; Elson, I. H.; Kochi, J. K. *J. Am. Chem. Soc.* **1973**, *95*, 5341.

(38) Maillard, B.; Ingold, K. U.; Scaiano, J. C. *J. Am. Chem. Soc.* **1983**, *105*, 5095.

2. Laser Flash Photolysis (LFP)

2.1. Introduction 31
2.2. Nanosecond Absorption LFP 34
2.3. Sample Holder and Sample Cells 38
2.4. LFP Solutions 41
2.5. Chapter 2 References 43

2.1 Introduction

Observing short-lived transients requires that they can be generated and detected faster than they decay. Transient species can be effectively generated using pulsed lasers. Fast and ultra-fast pulsed lasers have been developed with pulse durations in the nano-, pico-, and femtosecond ranges. The transient species, once generated, can be monitored by measuring the change in optical density (absorbance) of the solution. Changes in light absorption are instantaneous and can be monitored on short timescales. The absorption spectrum of a given species is characteristic for that species and is proportional to its concentration.

Kosonocky, in 1965[1], and Lindqvist, in 1966[2], were the first to report the use of laser excitation to produce transient species. The majority of present day laser flash photolysis (LFP) systems more closely resemble the system developed by Lindqvist. Lindqvist was the first researcher to take full advantage of the short timescales (~100 ns) made available due to the short laser excitation pulses. Since that time, many groups have independently and simultaneously expanded on the concept of LFP. Porter described a laser flash photolysis (LFP) system at the Nobel symposium in 1967.[3] His first detailed report followed in 1970.[4]

In its simplest form, a LFP system is a fast spectrophotometer with a laser excitation source (Figure 2-1). The spectrophotometric aspect (the horizontal array in Figure 2-1) of the system monitors changes in optical density (absorption, ΔOD) with time. The laser is used to rapidly generate the transient species within a sample whose optical density is simultaneously being monitored.

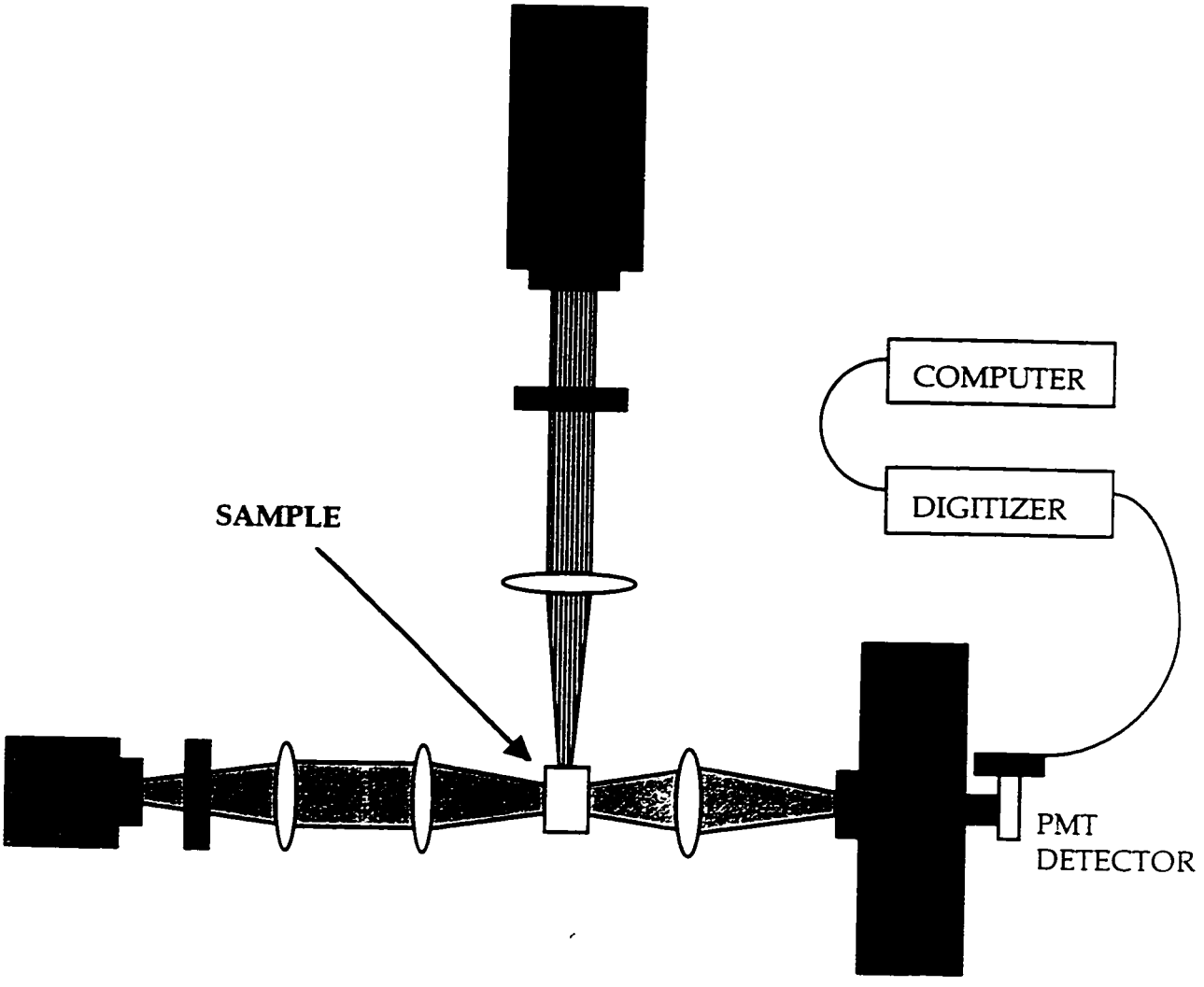

Figure 2-1 Simple schematic representation of a laser flash photolysis set-up.

The laser lab at the University of Ottawa has both nanosecond and picosecond LFP capabilities. Of the two systems, only the nanosecond system was used for the experiments described within this thesis. There exist two side-by-side nanosecond systems in our laser lab designated as TABLE 1 and TABLE 2 in Figure 2-2.

The laser lab is divided into three sections: the lasers, a redirectional table, and the monitoring tables. A variety of lasers are available for use. There are two Lumonics lasers: an EX530 and an EX510. These are presently filled with a Xe/HCl mixture (Ne buffer, 308 nm, < 150 mJ/pulse) and a Kr/F_2 mixture (He buffer, 248 nm, < 100 mJ/pulse), respectively. There is also a nitrogen laser (337 nm, < 5 mJ/pulse) and a dye

laser (dye-dependent wavelength, <20 mJ/pulse) which must be pumped with the 308 nm laser. Finally, there are two Nd:YAG Surelite lasers (1064 nm). The frequency of both Surelites can be doubled, tripled, or quadrupled to give 532 nm (< 200 mJ/pulse), 355 nm (< 50 mJ/pulse), or 266 nm (< 20 mJ/pulse) outputs, respectively. For convenience, one Surelite is fixed at 266 nm output, while the other is fixed at 355 nm output.

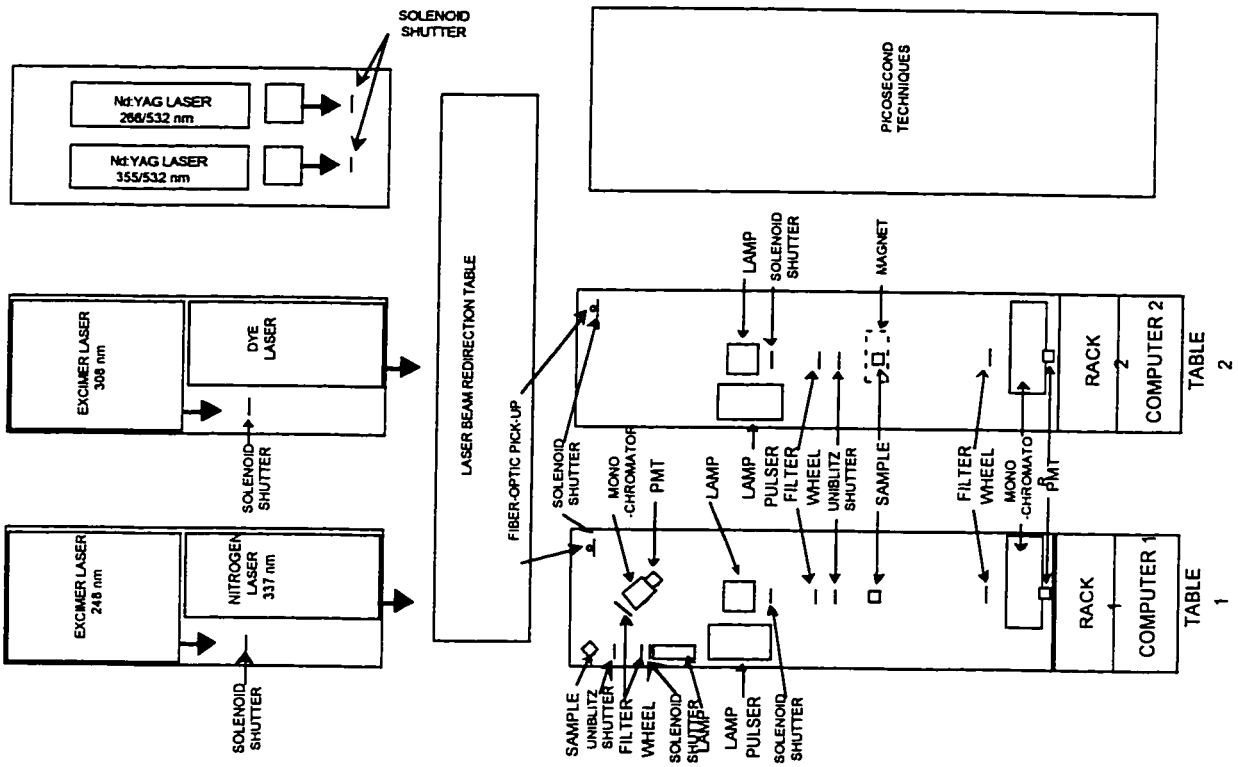

Figure 2-2 Layout of the laser lab at the University of Ottawa.

Due to the poor near-UV absorption characteristics of *vicinal*-dibromoalkanes, the quadrupled output (266 nm) of one of the Nd:YAG Surelite lasers was used for the LFP experiments. On occasion, when working with aryl-substituted *vicinal*-dibromides, there was sufficient ground state absorption in the near-UV to use the 308 nm output from the Xe/HCl Excimer.

The redirectional table contains a series of prisms that can be used to redirect any laser to any monitoring table. The two monitoring tables, TABLE 1 and TABLE 2, have unique variations of the nanosecond LFP technique, but both are capable of standard transmission experiments. TABLE 1 has a time-resolved Diffuse Reflectance[5] set-up that can measure the changes in reflectance of a solid sample or an opaque solution. TABLE 2 has an electro-magnet with a variable power supply for monitoring magnetic field effects on transients.

Diffuse reflectance and magnetic field effects are the most common variations on the standard LFP technique used in our laboratory. When needed, however, either table can be adapted to measure temperature dependence, singlet oxygen emission[6], photoacoustic calorimetry[7], two-laser two colour LFP[8-11], and time-resolved conductance.[12]

2.2 Nanosecond Absorption LFP

The monitoring/detection system consists of a pulsed 150 Watt xenon lamp, a high intensity monochromator and a photomultiplier tube (PMT) detector operating on five or six dynodes. The monitoring lamp is pulsed so that the intensity of the beam is increased by a factor of 5 - 20 during a few milliseconds. This enhances the signal-to-noise ratio which is especially important for small or short-lived (<100 ns) signals. The monitoring beam is concentrated, but not focused, through the sample and into a monochromator which selects the wavelength of light to be monitored. The selected wavelengths of light are detected by the PMT detector which yields a current terminated into an appropriate load resistor (typically 93 Ohms) giving a voltage signal. The voltage signal changes with time and is captured by a Tektronix 2440 digital storage oscilloscope equipped with pre-trigger capabilities which is interfaced with Macintosh computers controlled by LabVIEW software. A line synchronizer co-ordinates the various components of the LFP system including the lasers, lamp pulser and shutters. The line synchronizer uses a series of transistor-transistor linked (TTL) pulses that originate at the same point on a 60 Hz AC sine wave so that proper time sequences of events are maintained.

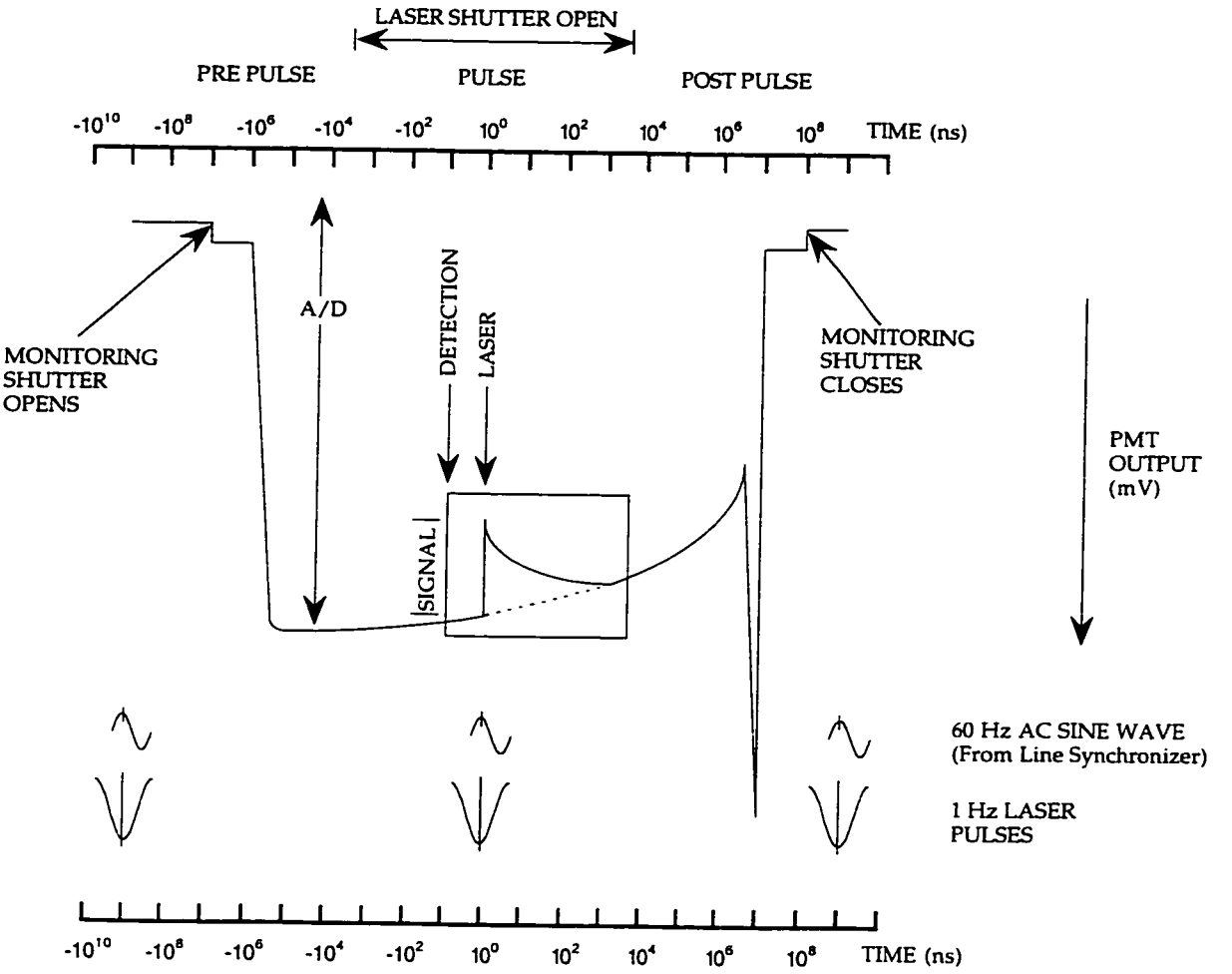

Figure 2-3 The sequence of timed events in an LFP experiment.

Figure 2-3 shows a semi-log plot of PMT output versus time for a period from one second before (- 10^9 ns) to one second after (10^9 ns) a particular laser pulse. For convenience, time zero is when the laser fires. Negative time refers to the time before the laser pulse, and positive time refers to the time after the laser pulse. Note that the time-axis is logarithmic. At the start of the experiment (-10^9 ns), a voltage is applied to the PMT (the initial plateau in the figure). There is a small step in the PMT voltage at -10^7 ns when the monitoring shutter is opened and light is allowed into the PMT. The sharp increase in the PMT voltage at -10^6 ns occurs when the lamp is pulsed. The laser then fires and subsequently strikes a fiberoptic cable which triggers the transient digitizer to start saving data points (time zero). The signal that results is shown in the small box in Figure 2-3.

The box extends into negative time due to the pre-trigger capability of the scope which saves a pre-set number of channels from before it had been triggered.

The PMT OUTPUT axis is inverted so as to put the absorption signal right-side-up. All signals are relative to the initial intensity of the monitoring beam. An absorption detracts from the monitoring beam and would therefore appear as a negative (up) signal. Chemiluminescence or fluorescence adds to the monitoring beam and would therefore appear as positive (down) signal.

At 10^7 ns the lamp-pulser is suddenly shut off producing the spike in the light intensity and PMT voltage. The PMT voltage returns to the voltage induced by the steady illumination of the 150 W lamp. At 10^8 ns, the monitoring shutter closes, and the PMT voltage returns to normal. There are two important features to note about the effect of pulsed-lamp-monitoring. Firstly, the pulsed intensity of the lamp is not stable. Between -10^6 ns and 10^6 ns the intensity of the light decays until the pulser finally shuts off. This effect manifests itself as a baseline drift. Secondly, the size of the detection box is determined by the timescale of the scope. Therefore, for pulsed experiments, the timescales available must fit within the few milliseconds of the lamp pulse. Methods of compensation exist for both of these problems. The baseline drift can be corrected for by running the experiment without allowing the laser to strike the sample. This way, the lamp profile can be observed without the transient signal. The second problem is solved by not choosing a timescale beyond the duration of the lamp pulse. If timescales beyond the duration of the lamp pulse are desired, then the experiment can be run without pulsing the lamp. All experiments in this research were done on short timescales (between 200 ns and 10 μs) where the lamp profile is reasonably flat, therefore no baseline correction was needed.

The change in optical density (ΔOD) of the solution due to the production of a transient is equal to the negative log of the ratio of the transmitted light intensity before (I_o) and after laser irradiation (I) according to Lambert's Law (Equation 2.1).

$$\Delta OD = -\log\left(\frac{I}{I_o}\right)$$ **Equation 2.1**

Because the LFP system can be considered as a single-beam spectrophotometer, the initial intensity (I_o) of transmitted light must be recorded prior to recording the intensity of light transmitted through the sample containing the transient. In the above described LFP system, the I_o is taken as the intensity of the pulsed monitoring beam before the laser strikes the sample, i.e. the PMT voltage recorded during the pre-trigger section of the detection box in Figure 2-1. This I_o can then be compared to the time-resolved light intensities picked up by the PMT after the laser pulse (I's). Using Equation 2.1, the above data can be converted into a time-resolved ΔOD trace of the transient.

Theoretically, that is all that is needed to obtain a time-resolved ΔOD trace of a transient. In practice, however, a little manipulation of the PMT signal is required for better precision. When measuring a transient signal, the change in voltage measured is usually small compared to the large change in voltage caused by the lamp pulsing. A typical change in signal due to a transient can be on the order of 10 to 50 mV. This small change is superimposed on a large voltage change of ~280 mV due to the lamp pulse. If this signal were taken as is, the voltage resolution of the oscilloscope would be based on the large overall voltage of the signal. Therefore, the small superimposed changes of interest would be poorly resolved. In order to get the maximum resolution of the digitizer, the small changes of interest have to be separated from the total PMT voltage.

A high-pass filter at the input of the digitizer is used to separate the signals. The pre-laser-flash baseline acts as a low-frequency signal (which is filtered out) and the transient signal is the only signal allowed to pass through the filter and this is input into channel 1 of the scope. This pre-laser-flash baseline of the transient signal appears at ground so we are able to use a small vertical amplitude in order to get maximum digitizing

resolution of the transient's trace. In order to obtain the actual pre-laser-flash baseline, which in fact is the I_o, the untreated PMT signal is fed into the second channel of the digitizer (at a different and much higher vertical amplitude) and acquired simultaneously. Therefore, the signal acquired in channel 1 is not the intensity of transmitted light (I), but rather the difference between the I_o and the transmitted light intensity (Equation 2.2).

$$\text{Signal} = I_o - I \qquad \textbf{Equation 2.2}$$

Therefore,

$$I = I_o - \text{Signal} \qquad \textbf{Equation 2.3}$$

Inserting this into Equation 2.1 gives,

$$\Delta OD = -\log\left(1 - \frac{\text{Signal}}{I_o}\right) \qquad \textbf{Equation 2.4}$$

Equation 2.4 is used to prepare ΔOD vs. time plots of the transient data.

2.3 Sample Holder and Sample Cells

The sample holder is a square brass tube with an internal diameter of 9 x 9 mm^2. The cell holder on TABLE 1 is fitted with a thermocouple which is interfaced with the computer. The cell holder is placed between the monitoring lamp and the monochromator. There are two holes on opposite faces of the cell holder that permit the passage of light from the monitoring beam, through the sample, and to the monochromator. The hole on the side of monitoring beam is 1/16 of an inch in diameter. The hole on the opposite side has a much larger diameter (1/4 inch) for the exit of the monitoring beam. The sides of the cell holder perpendicular to the monitoring beam are for the laser excitation. The side for the laser light entrance into the sample has a 7 x 4 mm^2 rectangle at the same height as the monitoring holes. The laser exit face of the cell holder is completely removed except for

two vertical slats. The slats are on opposing sides of the cell holder to prevent the cell from moving (Figure 2-4).

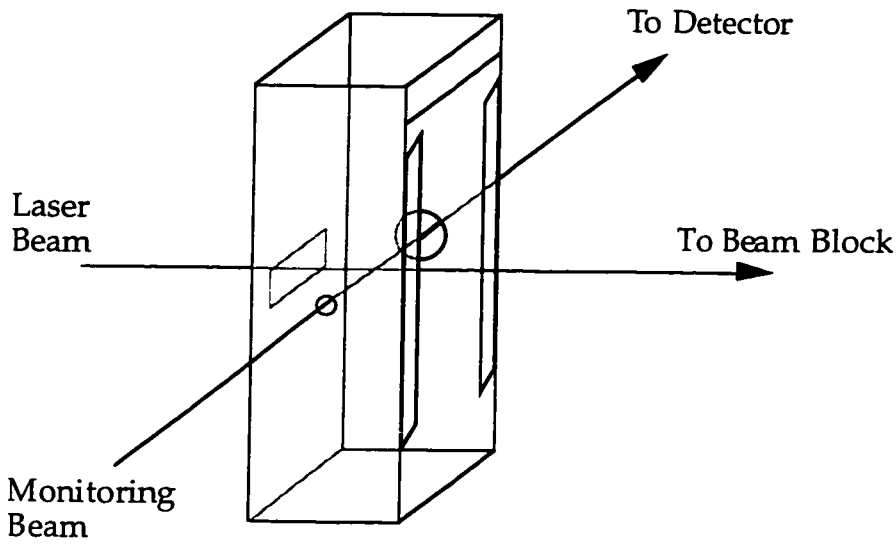

Figure 2-4 The Cell Holder.

Experiments were either performed in a "Static Cell" (Figure 2-5) or a "Flow Cell" (Figure 2-6). Both cells are made from Suprasil quartz. The irradiation chamber of each is made from 7 x 7 mm^2 square Suprasil quartz tubing from either Friedrich and Dimmock (NJ, USA), or Vitro Dynamics. The cells were prepared by the University of Ottawa glassblower.

Static cells are made up from 5 cm of the square tubing and 7 cm of round quartz tubing (7 mm internal diameter). The interface between the two types of tubing is blown out to create a reservoir. The finished cell can hold approximately 5 ml of solution. The flow cell uses slightly less of the square tubing (4 cm). Luer tips are then joined to both ends of the flow cell. The bottom luer tip (the inlet) is bent 90°. The flow cell can be inserted into the cell holder with the inlet luer tip sliding between the slats.

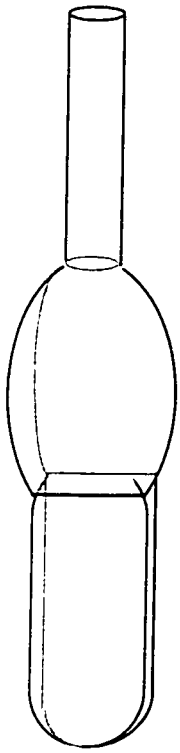

Figure 2-5 An LFP static cell.

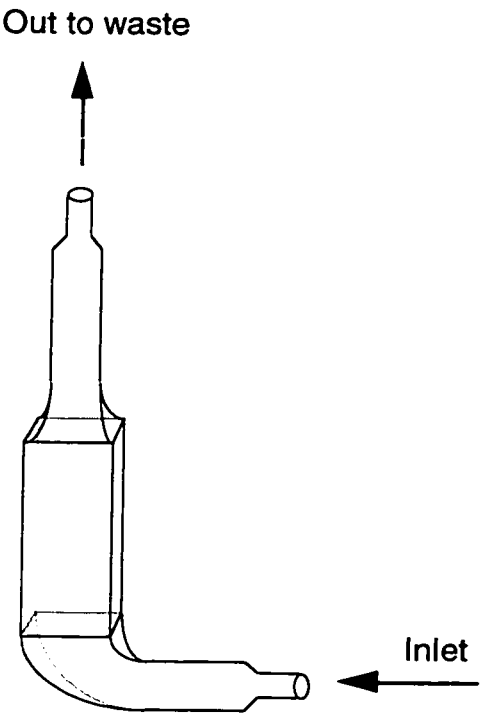

Figure 2-6 An LFP flow cell.

Flow cells are used when, during the course of a LFP experiment, the photolysis produces a net chemical reaction that will interfere with the remaining acquisitions. The flow set-up ensures that a fresh portion of solution is irradiated with each laser shot. The solution is supplied to the flow cell via a reservoir (usually 100 ml tank). The "Flow Tank" is also equipped with a luer tip outlet. The flow tank outlet is connected to the inlet of the flow cell with Teflon tubing fitted with syringe needle connectors. The flow of the solution out of the tank is controlled with a stop-cock. The waste from the cell is also removed using Teflon tubing fitted with a syringe connector.

2.4 LFP Solutions

The gas content of a solution in either type of cell can be altered by bubbling with the desired gas. For a flow system, the gas is bubbled into the reservoir tank. The tank is equipped with a fritted gas inlet tube. The top of the tank is covered with a white rubber septum. The septum is pierced with an outlet needle so that the gases may escape. A 100 ml flow tank should be bubbled with the appropriate gas for about 30 minutes. For transient lifetimes in the microsecond range, static cells should be bubbled with the desired gas for about 10 minutes (less if the cell is not full). The gas in a static cell is also exchanged through a white rubber septum. In this case, however, both the gas inlet and escape are through syringes that are pierced through the septum. The white rubber septa were purchased from Aldrich and soaked twice in benzene prior to use in order to extract contaminants, particularly polymer stabilizers.

All samples were prepared in concentrations such that the absorbance at the laser wavelength ($Abs_{\lambda exc}$) was between 0.3 and 0.5. Lower concentrations may not give enough transient to be detected. Also, at low precursor concentrations, there exists the possibility of sample depletion. Making samples more concentrated leads to a risk of shock wave production when the laser strikes the sample. Shock waves, create ripples in the solution, thus creating a refringent pattern in the light that reaches the PMT. This appears on the scope as intermittent spikes on the traces. Samples of high optical density at the laser wavelength also lead to concentration gradients within the detection area. Figure 2-7 is a plot of the Percent Transmission versus Path Length of a laser as it passes through a series of solutions of different optical densities at the laser wavelength. The plot can be viewed as a cross section of the 7 x 7 mm^2 sample. The dark band represents the monitoring beam. For simplicity, the beam width was chosen to be 1 mm wide.

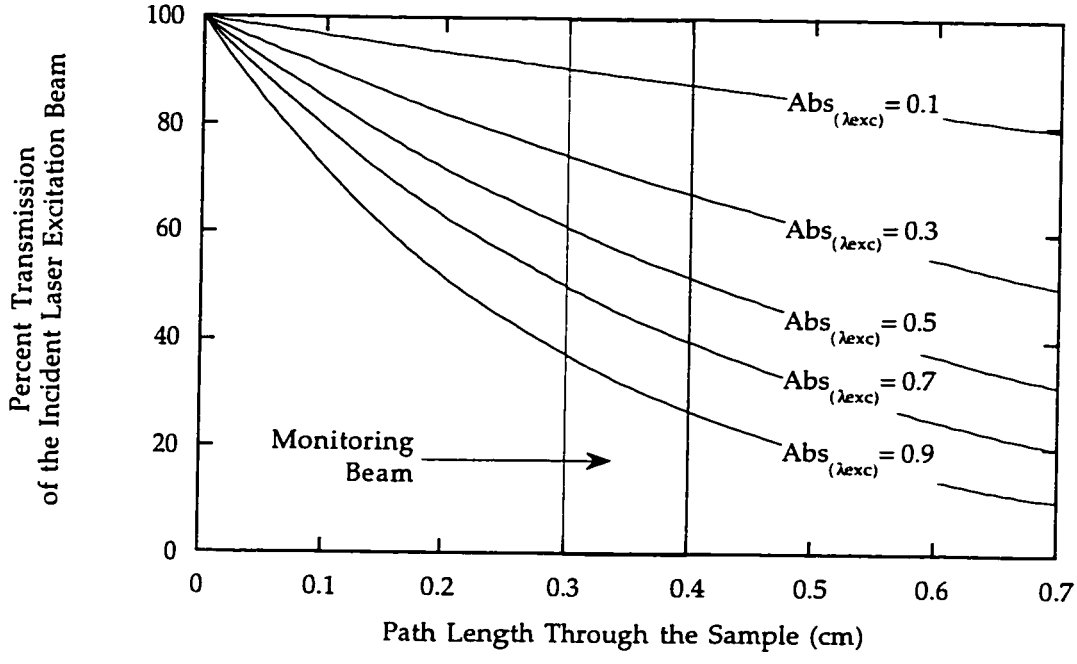

Figure 2-7 **Percent Transmission of the incident laser light versus Path Length as the laser passes through solutions of different optical densities.**

As can be seen, the laser must pass through ~3 mm of solution before reaching the area being monitored. The concentration of transients produced is a factor of both the laser intensity and the precursor concentration. As the precursor concentration is increased, the potential for transient concentration also increases, but the amount of laser light that reaches the monitoring beam decreases. So, as the precursor concentration is increased, the concentration of transient will increase to a maximum value, and then start to decrease. It is not always desirable to have a high transient concentration, anyway. The higher the transient concentration, the more likely it becomes to have transient/transient reactions (i.e.. triplet-triplet annihilation[13]). Figure 2-7 also shows the potential for concentration gradients of the transient. As the optical density (thus the concentration) of the solution is increased, the disparity between the percent laser intensity at the beginning of the monitoring beam (0.3 cm) and the end of the monitoring beam (0.4 cm) also increases.

2.5 Chapter 2 References

(1) Kosonocky, W. F.; Harrison, S. E.; Stander, R. *J. Chem. Phys.* **1965**, *43*, 831.

(2) Lindqvist, L. *Hebd. Seances Acad. Sci., Ser. C* **1966**, *263*, 852.

(3) Porter, G. In *Fast Reactions and Primary Processes in Chemical Kinetics*; S. Claesson, Ed.; Almqvist and Wiksell: Stockholm, 1967; pp 141.

(4) Porter, G.; Topp, M. R. *Proc. Roy. Soc. Lond. A* **1970**, *315*, 163.

(5) Wilkinson, F.; Willsher, C. J.; Casal, H. L.; Johnston, L. J.; Scaiano, J. C. *Can. J. Chem.* **1986**, *64*, 539.

(6) Arnason, J. T.; Guèrin, B.; Kraml, M. M.; Mehta, B.; Redmond, R. W.; Scaiano, J. C. *Photochem. Photobiol.* **1992**, *55*, 35.

(7) Belt, S. T.; Scaiano, J. C.; Whittlesey, M. K. *J. Am. Chem. Soc.* **1993**, *115*, 1921.

(8) Scaiano, J. C.; Johnston, L. J. In *Organic Photochemistry*; A. Padwa, Ed.; Marcel Dekker, Inc.: New York, 1989; Vol. 10; pp 309.

(9) Scaiano, J. C.; Johnston, L. J. *Pure Appl. Chem.* **1986**, *58*, 1273.

(10) Scaiano, J. C.; Tanner, M.; Weir, D. *J. Am. Chem. Soc.* **1985**, *107*, 4396.

(11) Scaiano, J. C.; Johnston, L. J.; McGimpsey, W. G.; Weir, D. *Acc. Chem. Res.* **1988**, *21*, 22.

(12) Asmus, K. D.; Janata, E. In *The Study od Fast Processes and Transient Species by Electron Pulse Radiolysis*; J. Basendale and F. Busi, Eds.; Reidel Publishing: 1982; pp 91.

(13) Turro, N. J. In *Modern Molecular Photochemistry*; University Science Books: Mill Valley, 1991; pp 343.

3. Bromine Atom/Halide Ion Complexes ($BrX^{\bullet-}$)

3.1 Introduction: The Dibromide Radical Anion ($Br_2^{\bullet-}$) 45

3.2 Other Dihalide and Di-pseudo-halide Radical Anions ($X_2^{\bullet-}$) 47

3.3 Mixed Radical Anion Complexes ($XY^{\bullet-}$) 55

(i) $BrI^{\bullet-}$ 55

(ii) $BrCl^{\bullet-}$ and $BrF^{\bullet-}$ 61

(iii) $BrX^{\bullet-}$ Extinction Coefficients 67

(iv) $BrOH^{\bullet-}$ 72

(v) Halo-thiocyanate Radical Anions ($XSCN^{\bullet-}$) 73

3.4 Equilibria of the Bromine Atom/Halide Complexes ($BrX^{\bullet-}$) 77

(i) Decay of the Radical Anions 78

3.5 Temperature Effects on the Radical Anions 90

3.6 Chapter 3 References 93

3.1 Introduction: The Dibromide Radical Anion ($Br_2^{\bullet-}$)

In section 1.2 (i), Scaiano *et al.* took advantage of the bromine atom's affinity for forming complexes. The spectrally invisible bromine atoms were rendered visible by complexing them with bromide ions (Equation 1.6). The forward reaction was shown to proceed with an almost diffusion controlled rate of 1.6×10^{10} M^{-1} s^{-1} in MeCN. The resulting, rapidly-formed, $Br_2^{\bullet-}$ complex has a relatively high extinction coefficient of 9900 $M^{-1}cm^{-1}$ at 360 nm and was ideal for monitoring the evolution of bromine atoms into solution. The complexation of bromine atoms with a halide anion (bromide in this case) to form the $BrX^{\bullet-}$ radical anion is central to the work in this thesis and will generally be referred to as the "probe reaction" (Equation 3.1). The term probe refers to the fact that bromine atoms are made "visible" by probing them with halide ions to form absorbing species ($BrX^{\bullet-}$).

The Bromine Atom "Probe" Reaction

$$Br^{\bullet} + X^{-} \xrightarrow{k_{BrX^{\bullet-}}} BrX^{\bullet-}$$

Equation 3.1 (probe reaction)

Grossweiner and Matheson were the first to attribute an absorption band around 350 nm to the $Br_2^{\bullet-}$ ion.[1] The authors observed this absorption band after the photolysis of a Br^- solution. Since then, the $Br_2^{\bullet-}$ ion has been extensively studied in both radiolysis and photolysis experiments. The majority of the data on this ionic complex comes from aqueous pulse radiolysis studies.

The net chemical reaction of the pulse radiolysis of an aqueous solution of bromide ions is a simple electron exchange. The net reaction (shown in Equation 3.2) is the transfer of an electron from the bromide ion to the radiolytically produced hydroxyl radical (OH•). The detailed mechanism, however, is not so simple and involves several intermediary ions

including $Br_2^{\bullet-}$ (Scheme 3-1). Initially, the two species (Br^- and OH•) form a short-lived intermediate ($BrOH^{\bullet-}$, $\tau \sim 100$ ns, Equation 3.3)[2] which subsequently disproportionates into a bromine atom and a hydroxide ion (Equation 3.4). The bromine atoms produced are then probed by bromide ions to produce the $Br_2^{\bullet-}$ radical anion (Equation 3.5). Conversely, Equation 3.6 represents the reverse of the probe reaction to reform the bromine atom and bromide ion.

$Br^- + OH\bullet \longrightarrow Br\bullet + OH^-$	**Equation 3.2**
$Br^- + OH\bullet \longrightarrow BrOH^{\bullet-}$	**Equation 3.3**
$BrOH^{\bullet-} \longrightarrow Br\bullet + OH^-$	**Equation 3.4**
$Br\bullet + Br^- \xrightarrow{k_{Br_2^{\bullet-}}} Br_2^{\bullet-}$	**Equation 3.5 ($Br_2^{\bullet-}$ Probe)**
$Br_2^{\bullet-} \xrightarrow{k_{-Br_2^{\bullet-}}} Br\bullet + Br^-$	**Equation 3.6**

Scheme 3-1 The pulse radiolytic production of $Br_2^{\bullet-}$ from an aqueous solution of bromide.

The absorption spectrum of the $Br_2^{\bullet-}$ ion in water was shown to have a maximum band at 360 nm ($\varepsilon = 9900\ M^{-1}\ cm^{-1}$)[3] and a smaller band at 700 nm. The bromine atom probe reaction (Equation 3.5) was determined to have a pseudo-first-order rate constant, $k_{Br_2^{\bullet-}}$, of $1.1 \times 10^{10}\ M^{-1}\ s^{-1}$ in water (Figure 3-1). Because of the multiple steps required to obtain the desired $Br_2^{\bullet-}$ product, the overall kinetics of the reaction can become complicated.

3.2 Other Dihalide and Di-pseudo-halide Radical Anions ($X_2^{\bullet-}$)

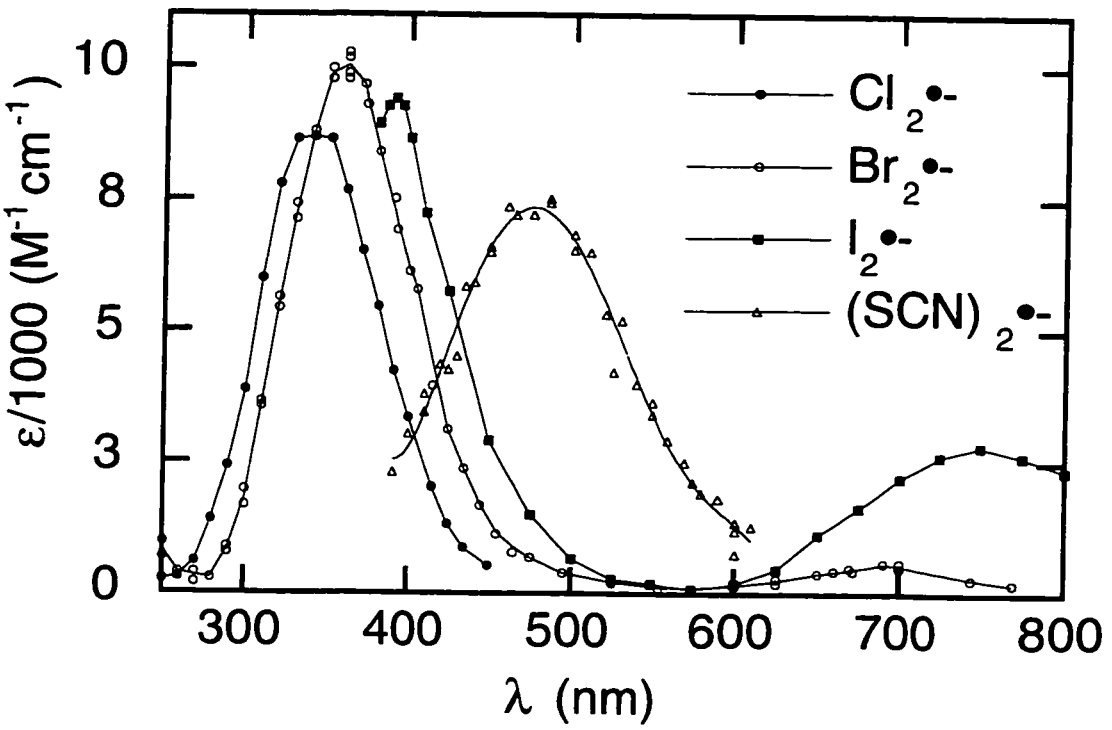

Figure 3-1 The spectra of $Cl_2^{\bullet-}$, $Br_2^{\bullet-}$, $I_2^{\bullet-}$, and $(SCN)_2^{\bullet-}$ in water.[4]

Radical anion complexes are also known for iodine[4] {$I_2^{\bullet-}$}, chlorine[4] {$Cl_2^{\bullet-}$}, and for some pseudo-halides[4-7] {$N_6^{\bullet-}$, $(SH)_2^{\bullet-}$, and $(SCN)_2^{\bullet-}$}. The halide complexes are all very similar to one another. Both the $Cl_2^{\bullet-}$ and the $I_2^{\bullet-}$ have strong absorptions in the 340 to 380 nm area, as well as a weaker band > 700 nm in water (Figure 3-1).[4] Both are rapidly produced from a combination of the halogen atom and the halide ion as in the probe reaction of $Br_2^{\bullet-}$ (Equation 3.5).

Table 3-A summarizes the literature data for the $Br_2^{\bullet-}$, $Cl_2^{\bullet-}$, $I_2^{\bullet-}$, and $(SCN)_2^{\bullet-}$ complexes in water.[8] All of the ions were generated via pulse radiolysis except for the $I_2^{\bullet-}$ ion. In the case of $I_2^{\bullet-}$, direct photolysis of iodide (I^-) produces the source of iodine atoms for complexation.

Table 3-A **Literature probe rate constants ($k_{X_2^{\bullet-}}$), absorption maxima (λ_{max}), and extinction coefficients (ε) for the dihalide radical ions ($X_2^{\bullet-}$) and $(SCN)_2^{\bullet-}$.**

$$X\bullet + X^- \xrightarrow{k_{X_2^{\bullet-}}} X_2^{\bullet-}$$

Species	(M^{-1} s^{-1}, in water)[8]	λ_{max} (nm)[4]	ε (M^{-1} s^{-1})[4]
$Cl_2^{\bullet-}$	8×10^9	340	8800
$Br_2^{\bullet-}$	9×10^9	360	9900
$I_2^{\bullet-}$	11×10^9	380	9400
$(SCN)_2^{\bullet-}$	9×10^9	475	7600

As mentioned, the kinetics of the initial formation of $Br_2^{\bullet-}$ from pulse radiolysis (PR) can be complicated. The rate constant data obtained in Table 3-A was measured by monitoring the recombination of the two precursor fragments and not the initial formation of the complex.[8] Nagarajan and Fessenden produced the initial ionic complexes via PR $\{Br_2^{\bullet-}, Cl_2^{\bullet-}, (SCN)_2^{\bullet-}\}$ or direct photolysis $\{I_2^{\bullet-}\}$, and then they photolysed the resulting complexes, thus regenerating the fragments (Scheme 3-2).

$$2X^- + OH^\bullet \xrightarrow{PR} X_2^{\bullet-} + OH^- \qquad \textbf{(Scheme 3-1)}$$

$$X_2^{\bullet-} \xrightarrow{h\nu} X^\bullet + X^- \xrightarrow{k_{X_2^{\bullet-}}} X_2^{\bullet-}$$

Scheme 3-2 **The photochemical dissociation and subsequent recombination of the pulse radiolytically produced $X_2^{\bullet-}$ radical anions.**

By observing the recombination kinetics of the complexes, Nagarajan and Fessenden eliminated any errors that may have been associated with the initial pulse radiolytic formation of the complexes. All four of the recombination reactions in Table 3-A have rate constants ~ 10^{10} M^{-1} s^{-1} in water.

Laser flash photolysis (LFP) can produce bromine atoms directly from a number of brominated precursors: molecular bromine,[9-12] bromobenzene,[9] α-bromo-acetophenone,[13] and *vicinal* dibromides.[14-18] By adding bromide to the solution to trap the bromine atoms, LFP offers a more direct approach to produce the $Br_2^{\bullet-}$ ions. LFP also offers the advantage of making it possible to perform studies in non-aqueous solvents. Effectively, Equation 3.2 to Equation 3.4 of Scheme 3-1 are skipped, thus simplifying the system. Figure 3-2 shows the spectrum measured for $Br_2^{\bullet-}$ in MeCN at room temperature (296 K).

Trans-1,2-Dibromocycloheptane (Dibromide **XI**) was photolysed with a pulse from a 266 nm laser to produce bromine atoms. The MeCN contained 11.2 mM of tetrabutyl ammonium bromide, Bu_4NBr, as a bromide ion source. Under these conditions, the bromine atoms were instantaneously converted to $Br_2^{\bullet-}$ ions.

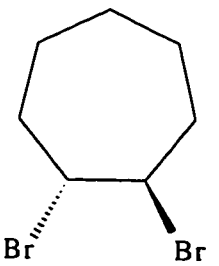

Dibromide XI

***trans*-1,2-dibromocycloheptane**

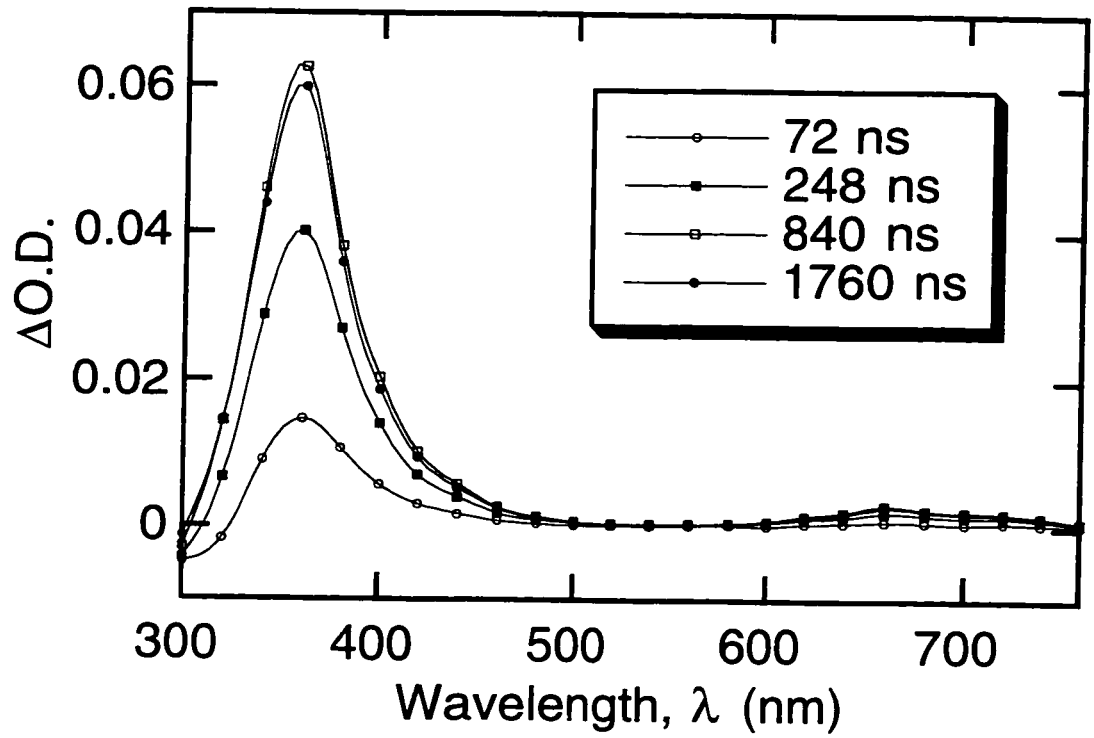

Figure 3-2 **$Br_2^{\cdot}$ spectrum in MeCN at 296 K. *trans*-1,2-Dibromocycloheptane was irradiated with a pulse from a 266 nm laser in the presence of 11.2 mM of Bu_4NBr. The solution was purged with nitrogen and the experiment was run under flow conditions.**

As can be seen, the spectrum of the $Br_2^{\cdot}$ has the same maximum at 360 nm in MeCN as in water. The spectrum also consists of the weaker, red band. However, the band has shifted from 700 nm in water to 660 nm in MeCN. The spectra were similar enough for Scaiano *et al.* to assume that the maximum would have roughly the same extinction coefficient as in water ($\varepsilon = 9900\ M^{-1}\ cm^{-1}$) so as to determine the quantum yield of bromine atom production from 1,2-dibromoethane.[17] If the MeCN extinction coefficient is not equal to the aqueous value, then the quantum yield determinations would be wrong. The kinetics are independent of the value of the extinction coefficient.

From the photolysis of a series of *vicinal* dibromides in acetonitrile, the average rate constant for Equation 3.5 was determined to be $(1.5 \pm 0.3) \times 10^{10}\ M^{-1}\ s^{-1}$ at 23°C (296 K). This value is in excellent agreement with the initial value of $1.6 \times 10^{10}\ M^{-1}\ s^{-1}$ reported in acetonitrile.[17]

In the presence of low concentrations of bromide (< 1 mM), the growth of the $Br_2^{\bullet}$ signal at 360 nm can be monitored. Despite being in low concentrations, the bromide is still several orders of magnitude more concentrated than the transient bromine atoms produced from the photolysis of the *vicinal* dibromide (< 0.01 mM). Under these conditions, the $Br_2^{\bullet}$ appears as a pseudo-first-order growth.

At these low bromide concentrations, the growth of the $Br_2^{\bullet}$ signal is only about ten times faster than its decay, therefore the time-resolved trace must be fitted with a consecutive growth and decay mechanism (Scheme 3-3). The growth is pseudo-first-order, while the decay of the $Br_2^{\bullet}$ is mainly second order. For reasons that will be discussed in section 3.4 (i), the decay component is also fitted with a monoexponential expression. The decay component occurs to a minor degree in the timescale of interest and serves only to make a small correction to the larger growth component. The growth rate constants calculated by the fitting routine were nearly identical when either a first or second order decay was included in the expression. It made little difference to the growth value whether the decay was treated as first or second order, but there was a large difference if no decay component was accounted for. Perhaps this insensitivity to decay treatment reflects the fact that the $Br_2^{\bullet}$ radical anion was shown to react with countless substrates, thereby giving it a decay of mixed order. The treatment of the mechanism (Scheme 3-3) leads to a standard kinetic expression for two consecutive first-order processes (Equation 3.9).[19]

The expression of Equation 3.9 contains a correction factor, "C", introduced to account for a small persistent jump in the signal. This jump in the signal may be due to the instantaneous complexation of the bromine atoms produced by other complexing agents in solution. This point will be discussed in chapter 5. The other complexing agents may include the solvent, the parent dibromide, residual HBr, or impurities.

$$Br\bullet + Br^- \xrightarrow{k_{Br_2^{\bullet-}}} Br_2^{\bullet-} \xrightarrow{k_{1°decay}} \text{Products}$$

$$\frac{d[Br_2^{\bullet-}]}{dt} = k_{Br_2^{\bullet-}}[Br\bullet][Br^-] - k_{1°decay}[Br_2^{\bullet-}] \qquad \textbf{Equation 3.7}$$

At constant bromide concentration...

$$\frac{d[Br_2^{\bullet-}]}{dt} = k_{probe}[Br\bullet] - k_{1°decay}[Br_2^{\bullet-}] \qquad \textbf{Equation 3.8}$$

$$[Br_2^{\bullet-}]_t = C + \frac{[Br\bullet]_o k_{probe}}{k_{1°decay} - k_{probe}}\left(e^{-k_{probe}t} - e^{-k_{1°decay}t}\right) \qquad \textbf{Equation 3.9}$$

Scheme 3-3 The consecutive first-order growth and decay of the $Br_2^{\bullet-}$ ion.

Figure 3-3 below is a sample trace of the $Br_2^{\bullet-}$ growth monitored at 360 nm in MeCN. The signal was produced by the LFP of 2,3-dibromobutane (Dibromide **VI**) in the presence of 0.36 mM Bu_4NBr. As can be seen, the growth is much faster than the decay. The curve represents the fit of the points to the expression in Equation 3.9. Values of 6.73 x 10^6 s^{-1} for k_{probe} and 0.53 x 10^6 s^{-1} for $k_{1°decay}$ were determined for the trace shown under these conditions.

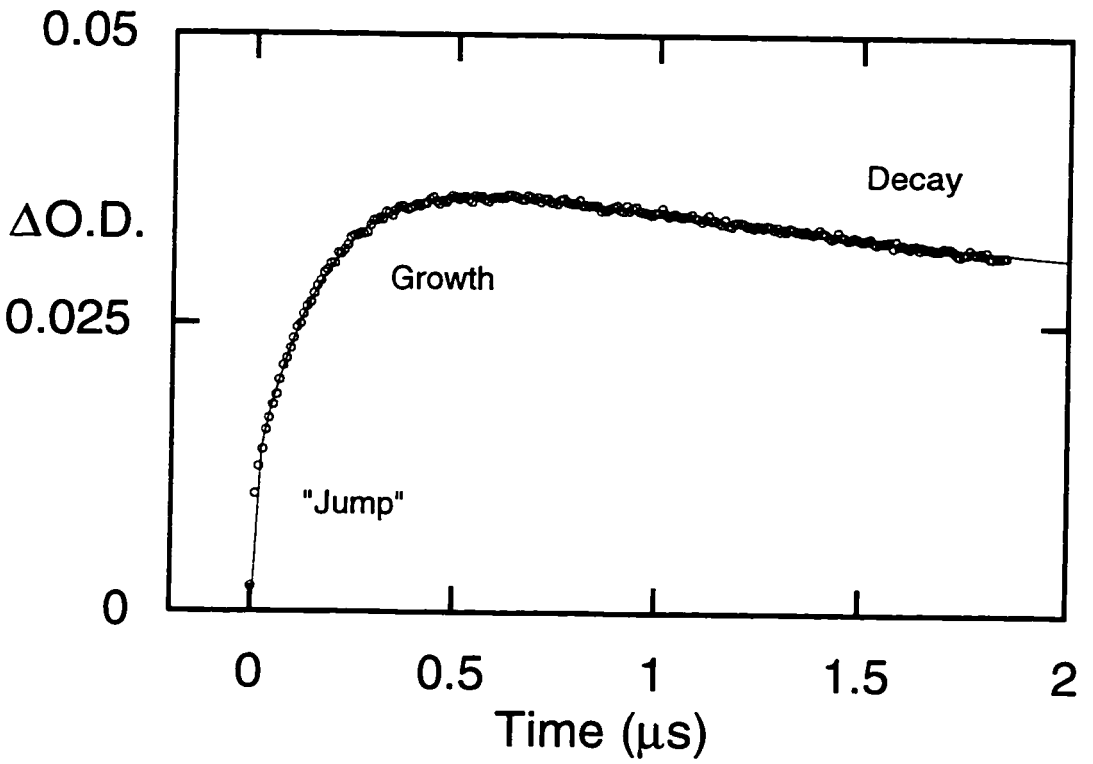

Figure 3-3 **The growth and partial decay of the $Br_2^{\bullet-}$ absorption generated from the LFP of 2,3-dibromobutane in MeCN at 296 K. The signal was monitored at 360 nm . The solution contained 0.36 mM of Bu_4NBr.**

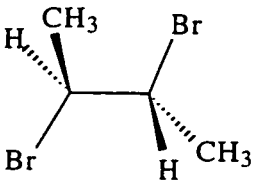

Dibromide VI

2,3-dibromobutane

Under these pseudo-first-order conditions the growth rate constant, k_{probe}, extracted by Equation 3.9, depends linearly on the concentration of bromide in solution according to Equation 3.10.

$$k_{probe} = k_o^{Br\bullet} + k_{Br_2^{\bullet-}}[Br^-] \qquad \textbf{Equation 3.10}$$

A plot of k_{probe} versus the concentration of bromide should give a straight line with a slope equal to the bimolecular rate constant, $k_{Br_2^{\bullet-}}$. The intercept of the plot, $k_o^{Br\bullet}$, is non-zero and should represent the finite lifetime of the bromine atoms in the absence of added quencher. Figure 3-4 is a quenching plot for the dependence of the observed growth rate constant, k_{probe}, versus bromide concentration for the reaction of bromide ions with bromine atoms generated from the LFP of tetrakis(1,2-dibromoethyl)-silane ($Si(DBE)_4$, Dibromide **XIII**) in MeCN. The plot gives a straight line with a slope of (1.55 ± 0.06) x 10^{10} M^{-1} s^{-1} for $k_{Br_2^{\bullet-}}$.[14]

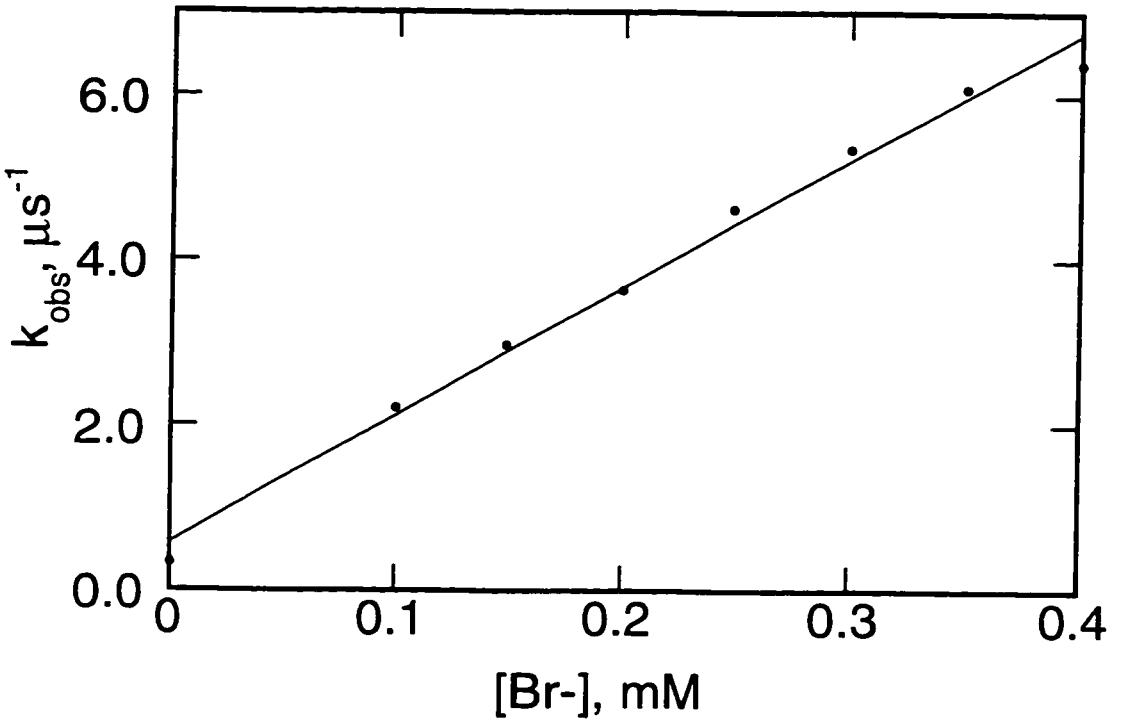

Figure 3-4 **Bromide concentration dependence of the growth of $Br_2^{\bullet-}$ for $Si(DBE)_4$ in acetonitrile at 23°C.**

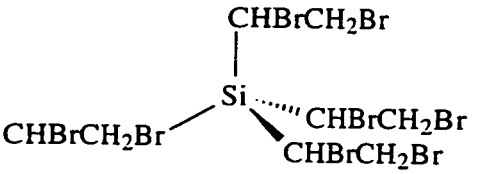

Dibromide XIII

Tetrakis(1,2-dibromoethyl)-silane ($Si(DBE)_4$)

3.3 Mixed Radical Anion Complexes ($XY^{\cdot}$)

The photolysis of *vicinal* dibromides is an excellent method for preparing mixed radical anions of bromine. The bromine atoms produced from the photolysis can be trapped by the addition of the appropriate halide or pseudo-halide into the solution.

As seen for the homo-nuclear radical anions ($X_2^{\cdot}$)[4], the probe processes are all extremely fast in water ($k_{X_2^{\cdot}} \sim 10^{10}$ M^{-1} s^{-1}, Table 3-A), therefore the production of the mixed $BrX^{\cdot}$ radicals should also be accomplished within 10 ns in the presence of > 10 mM of X^-.

Using various *vicinal* dibromides as bromine atom precursors, the mixed bromohalide ($BrX^{\cdot}$) radical anions were prepared for I^-, Cl^-, and F^-. The treatment of the halide dependent kinetic traces were performed in the same manner as those for the bromine dependence (Scheme 3-2). Both the first-order growth and decay components were extracted from the data.

(i) $BrI^{\cdot}$

The $BrI^{\cdot}$ complex proved to be challenging. I^- strongly absorbs the 266 nm light used to photolyze *vicinal* dibromo-alkanes. This required the use of *vicinal* dibromides with absorption spectra shifted further into the near-UV region. With a shifted absorption spectrum, the *vicinal* dibromides could be photolyzed with 308 nm or 355 nm light where the I^- does not absorb. The preparation of $BrI^{\cdot}$ was further complicated due to the strong

nucleophilicity of the iodide. The majority of *vicinal* dibromides were thermally debrominated upon the addition of tetrabutyl ammonium iodide (Bu_4NI) to the MeCN solution (re Section 1.3 (i)). Figure 3-5 shows the effect of adding Bu_4NI to an MeCN solution of *trans*-10,11-dibromodibenzosuberone (Dibromide **XII**). After the addition of Bu_4NI, a new band grows in at 365 nm. Irradiation of the sample causes a further increase of the 365 nm band. A second, and more intense band at 295 nm emerges from the near-UV absorption shoulder of *trans*-10,11-dibromodibenzosuberone.

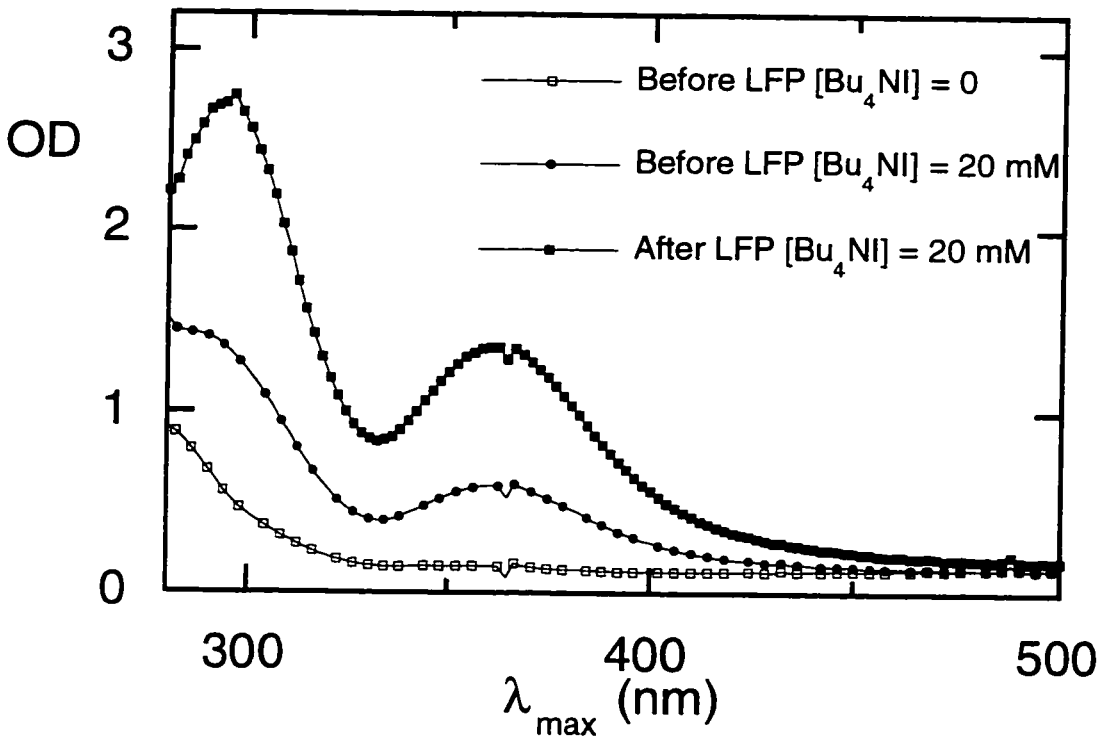

Figure 3-5 **Comparative ground state spectra of *trans*-10,11-dibromo-dibenzosuberone in MeCN in the presence and absence of tetrabutyl ammonium iodide. Spectra before and after LFP.**

This new absorption is not likely to be the absorption due to the $BrI^{\cdot}$ radical anion. The absorption could be the BrI_2^{2-} radical dianion formed from the combination of the $BrI^{\cdot}$ radical anion with a second iodide ion. However, on this long timescale, the absorption is more likely to be Br_2I^- (re. I_3^-) formed from the ultimate Br_2 production and the excess I^- in

solution. The product of the thermal reaction is the same as the product from the laser irradiation reaction from the LFP experiment.

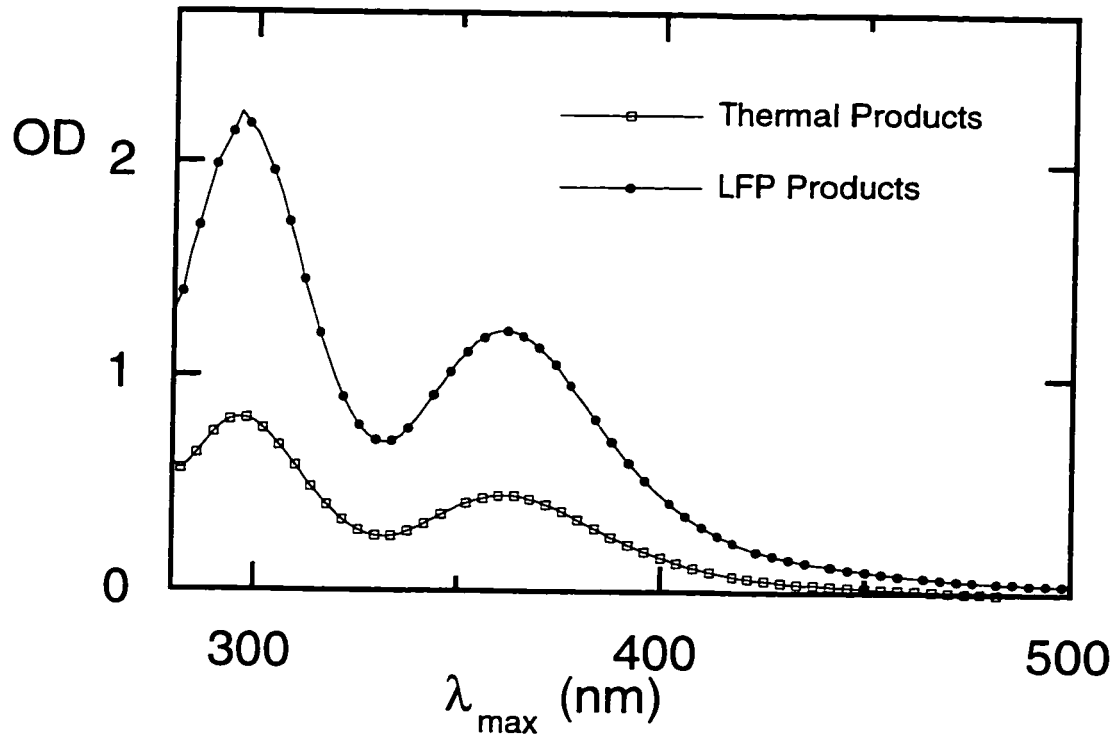

Figure 3-6 **Spectra of the products formed from the thermal debromination and the photochemical debromination of *trans*-10,11-dibromo-dibenzosuberone in the presence of 20 mM iodide. The spectra were obtained by subtracting the spectrum from that of the parent dibromide.**

Figure 3-6 shows the differential spectra of the two spectra containing 20 mM Bu_4NI. The spectrum from the *trans*-10,11-dibromodibenzosuberone without any Bu_4NI was subtracted from each of the spectra from Figure 3-5. The dibenzosuberenone produced from the debromination was ruled out as being responsible for the observed absorbance because the same spectrum was produced after the LFP of 1,2-dibromoethyl-benzene (Figure 3-7).

1,2-Dibromoethyl-benzene (Dibromide **XVIII**) proved to have suitable absorption characteristics and resistance to elimination to perform LFP at 308 nm in the presence of I^-.

Figure 3-7 shows the spectra for a solution of 1,2-dibromoethyl-benzene in MeCN with 20 mM Bu_4NI before and after LFP. As can be seen by the lack of the 365 nm band before LFP, the 1,2-dibromoethyl-benzene did not react thermally within the time-frame of the experiment. After photolysis, the spectrum takes on the same profile as the products from *trans*-10,11-dibromodibenzosuberone.

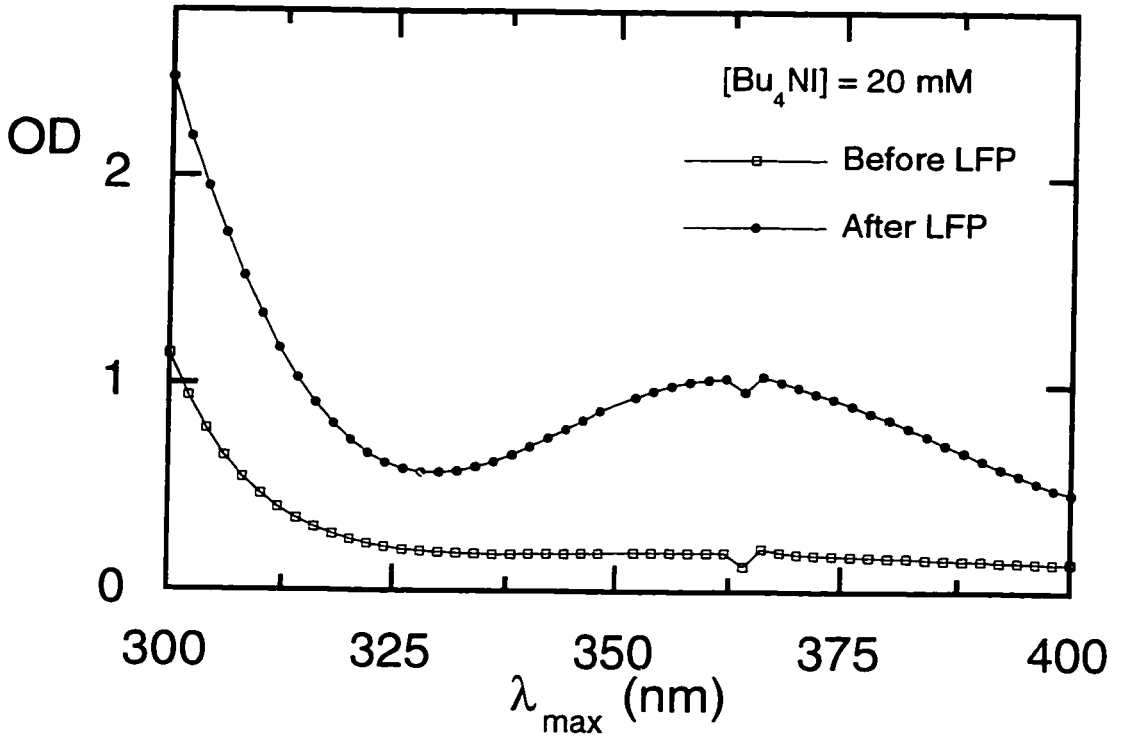

Figure 3-7 **Ground state absorption spectra for a solution of 1,2-dibromoethyl-benzene in the presence of 20 mM Bu_4NI before and after LFP.**

The drawback to using a conjugated *vicinal* dibromide such as 1,2-dibromoethyl-benzene is that the LFP becomes more complicated. The intermediates of *vicinal* dibromo-alkanes are invisible, therefore the spectrum is quite simple. The photolysis of a conjugated *vicinal* dibromide may produce visible intermediates. Conjugation of a vicinal dibromide increases the chances for the molecule to produce a triplet state, a radical, a

product, or all of the above that absorb in the area of interest. This is the case for 1,2-dibromoethyl-benzene which forms a benzylic-like radical upon irradiation and absorbs strongly at 310 nm (Figure 3-8). For this reason a reliable spectrum for the $BrI^{\bullet}$ radical anion could not be obtained from the photolysis of this precursor.

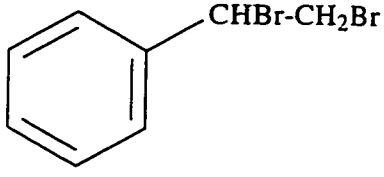

Dibromide XVIII

1,2-Dibromoethyl-benzene

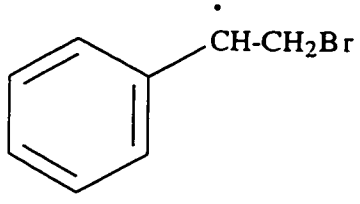

2-Bromo-1-phenyl ethyl radical

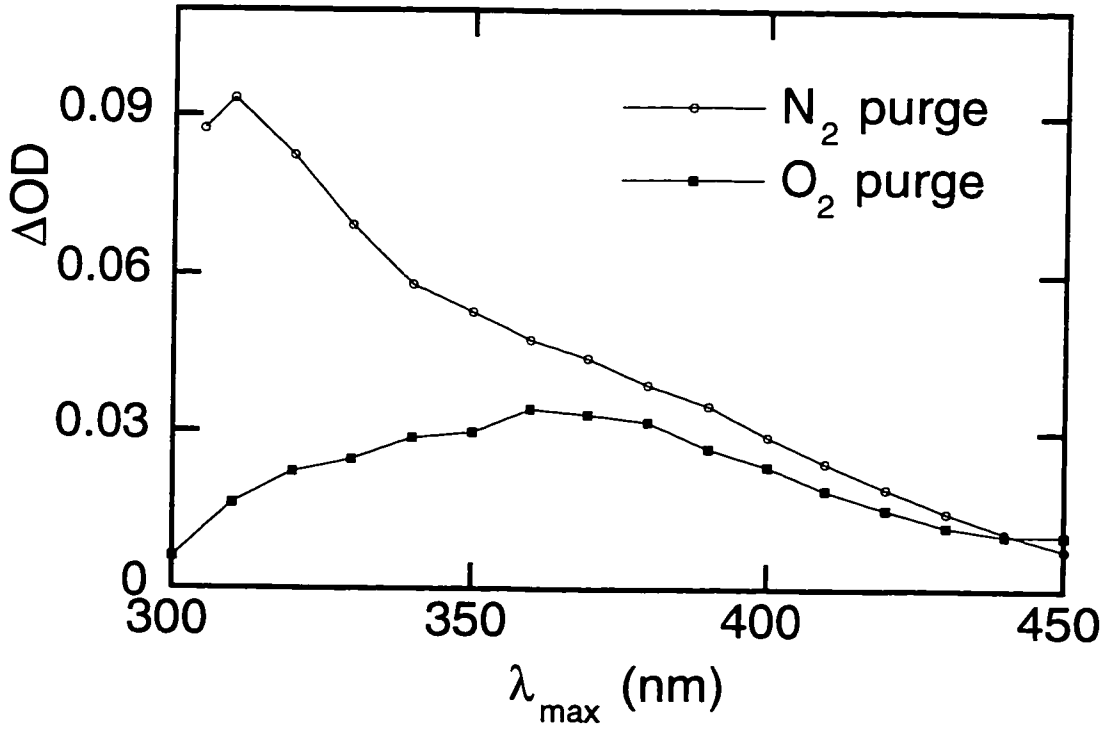

Figure 3-8 **The 266 nm LFP of 1,2-dibromoethyl-benzene in MeCN. The solutions were purged with either nitrogen or oxygen. The experiment was run under flow conditions with no added halide.**

Under a nitrogen atmosphere and in the absence of added I^-, the absorption of the 2-bromo-1-phenyl ethyl radical can be observed at 310 nm (Figure 3-8). Under oxygen, the radical is quenched and only the absorption due to the species that causes the jump can be observed at 360 nm. To clarify the absorptions for the kinetics of the formation of the $BrI^{\cdot-}$ complex, the solutions were purged with oxygen so as to eliminate the unwanted interference from the benzylic-radical absorption.

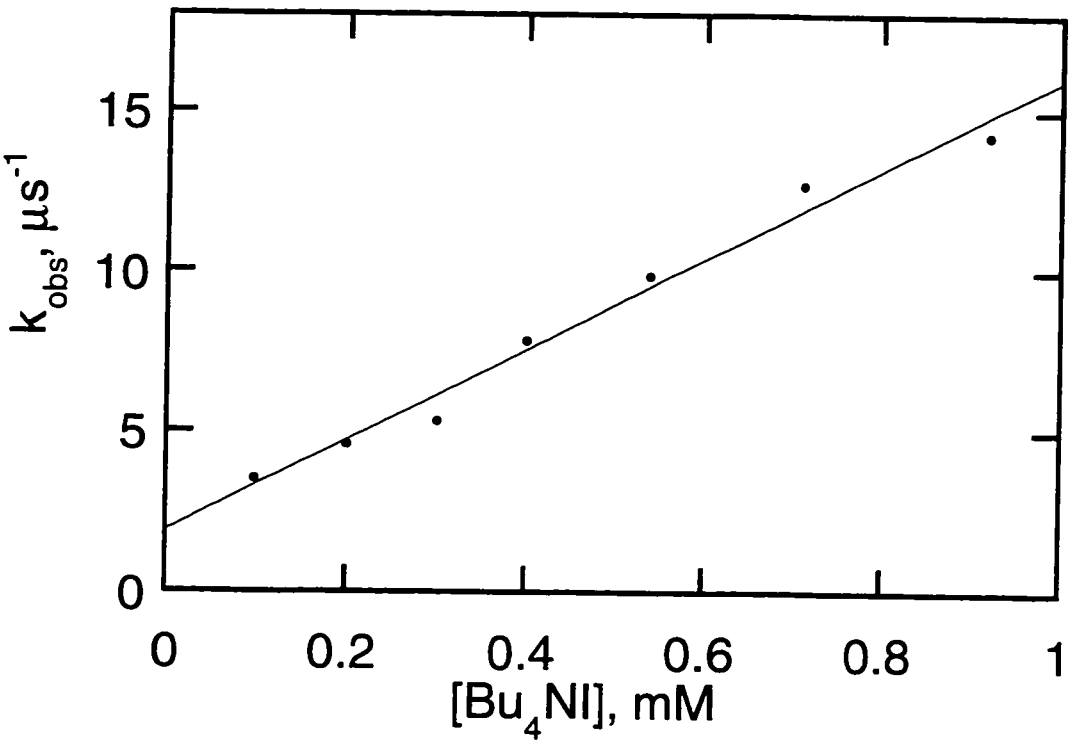

Figure 3-9 **The dependence of the observed growth rate constant, k_{obs}, of the $BrI^{\cdot-}$ complex versus the concentration of iodide. 1,2-Dibromoethyl-benzene was photolyzed in MeCN. The traces were monitored at 370 nm.**

Figure 3-9 displays the quenching of bromine atoms with iodide. From the plot, the rate constant for the $BrI^{\cdot-}$ ion formation was determined to be $(1.4 \pm 0.8) \times 10^{10}$ M^{-1} s^{-1}. Within experimental error, this value is the same as the one determined for $Br_2^{\cdot-}$ complexation in MeCN.

(ii) $BrCl^{\cdot-}$ and $BrF^{\cdot-}$

The $BrCl^{\cdot-}$ and $BrF^{\cdot-}$ complexes were a little easier to produce and to monitor than the $BrI^{\cdot-}$ complex. Chlorine and fluorine participated in much the same manner as bromine. Neither of these two tetrabutylammonium halide salts had near-UV absorption bands that would interfere with the photolysis of the *vicinal* dibromides. Also, neither of these two halides appeared to thermally reduce the bromine atom precursors. Because the chlorine and fluorine bromine-atom-trapping experiments could be accomplished using *vicinal* dibromoalkanes, there was much less spectral interference from the products.

Figure 3-10 shows examples of bromine atom quenching plots for chlorine and fluorine. Both of the $BrX^{\cdot-}$ complexes grow in with rate constants in the same, close to diffusion controlled, magnitude as the $Br_2^{\cdot-}$ and $BrI^{\cdot-}$ radical anions. Using 1,2-dibromo-1,1-difluoroethane (Dibromide **I**) as a bromine atom source, the trapping of bromine atoms with chlorine was determined from the slope of the plot to have a rate constant of $(1.3 \pm 0.1) \times 10^{10}\ M^{-1}\ s^{-1}$. Fluorine trapping with the same *vicinal* dibromide had a slightly lower rate constant of $(1.1 \pm 0.1) \times 10^{10}\ M^{-1}\ s^{-1}$.

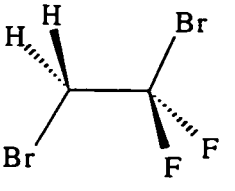

Dibromide I

1,2-dibromo-1,1-difluoroethane

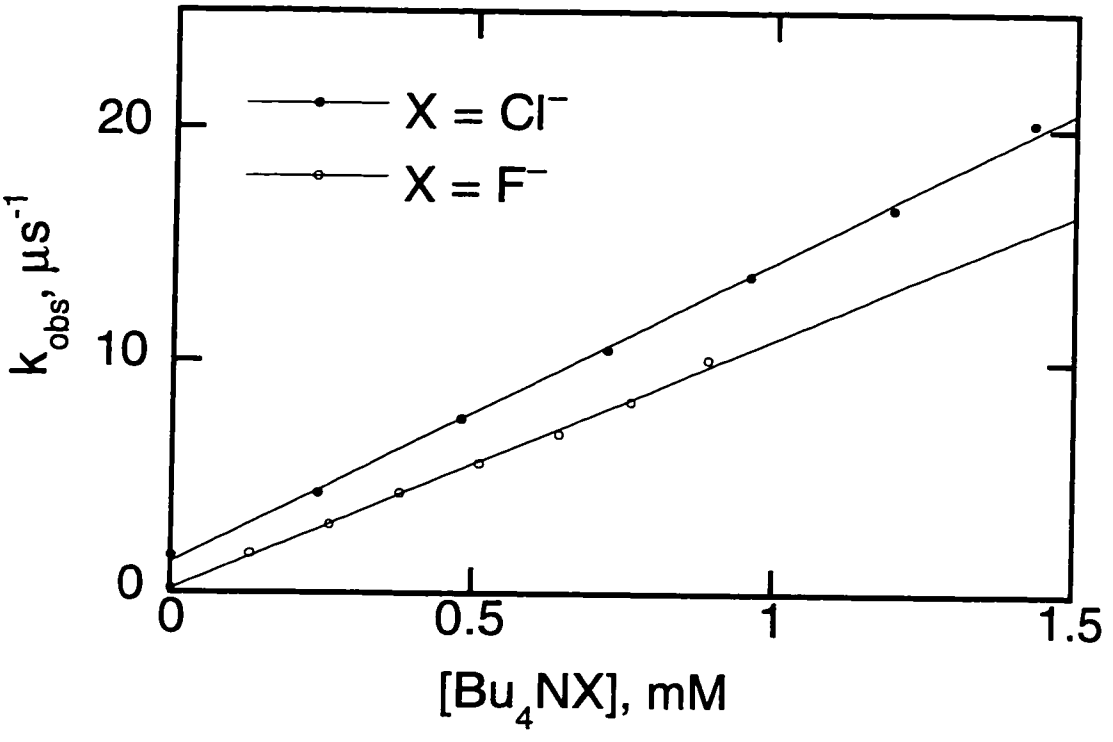

Figure 3-10 Chloride and fluoride quenching of bromine atoms produced from the 266 nm photolysis of 1,2-dibromo-1,1-difluoroethane in MeCN.

Over the course of many quenching plots, using many different *vicinal* dibromides, average values of (1.4 ± 0.1) x 10^{10} M^{-1} s^{-1} and (1.0 ± 0.1) x 10^{10} M^{-1} s^{-1} were determined for the formation of the $BrCl^{\bullet-}$ and $BrF^{\bullet-}$ complexes, respectively.

The spectrum for the $BrCl^{\bullet-}$ radical anion (Figure 3-11) was very similar to the spectrum for $Br_2^{\bullet-}$. $BrCl^{\bullet-}$ has a maximum absorbance at 360 nm and a smaller absorption band at 680 nm.

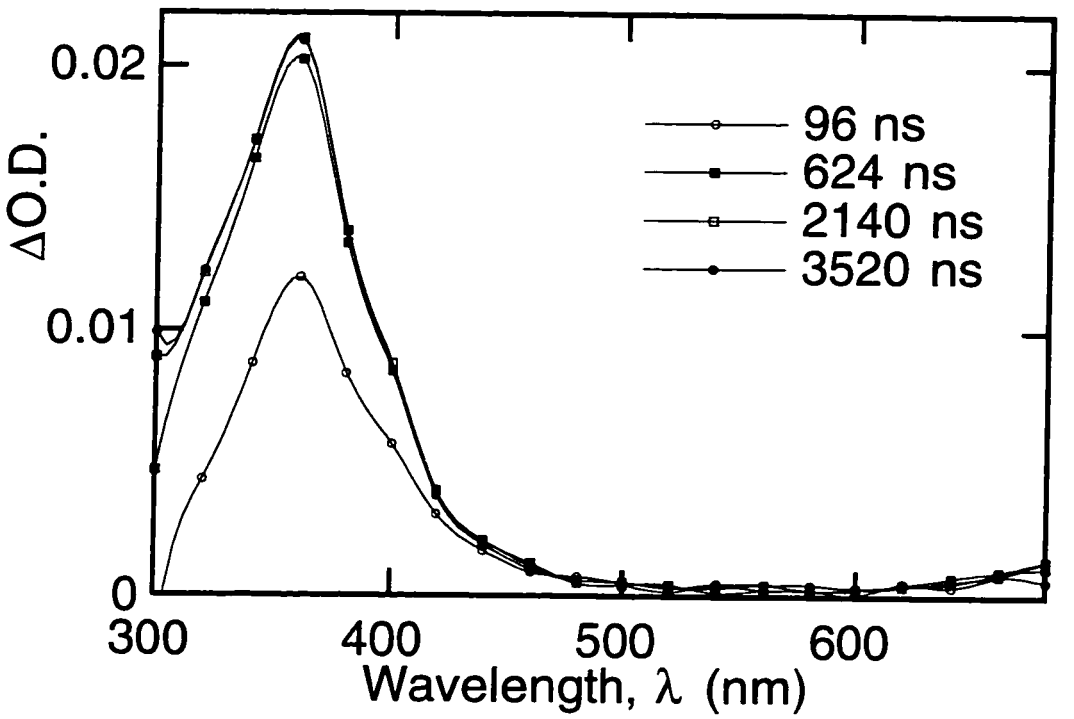

Figure 3-11 The $BrCl^-$ spectrum in MeCN at 296 K. The bromine atoms were produced via the photolysis of $Si(DBE)_4$ and trapped using Bu_4NCl.

The spectrum of the BrF^- complex also had similar features to the Br_2^- and $BrCl^-$ spectra: a maximum at 360 nm and a small absorption band out in the 700 nm region (Figure 3-12). This BrF^- spectrum was recorded by trapping the bromine atoms released from the photolysis of 1,2-dibromopropane (Dibromide **III**) with 7.5 mM Bu_4NF. The spectrum of the BrF^- complex also had a feature that has not been observed in any of the other complexes thus far. At 520 nm, there is a band that decays with a first-order rate constant of $3.78 \times 10^6\ s^{-1}$ ($\tau = 265$ ns) under these conditions.

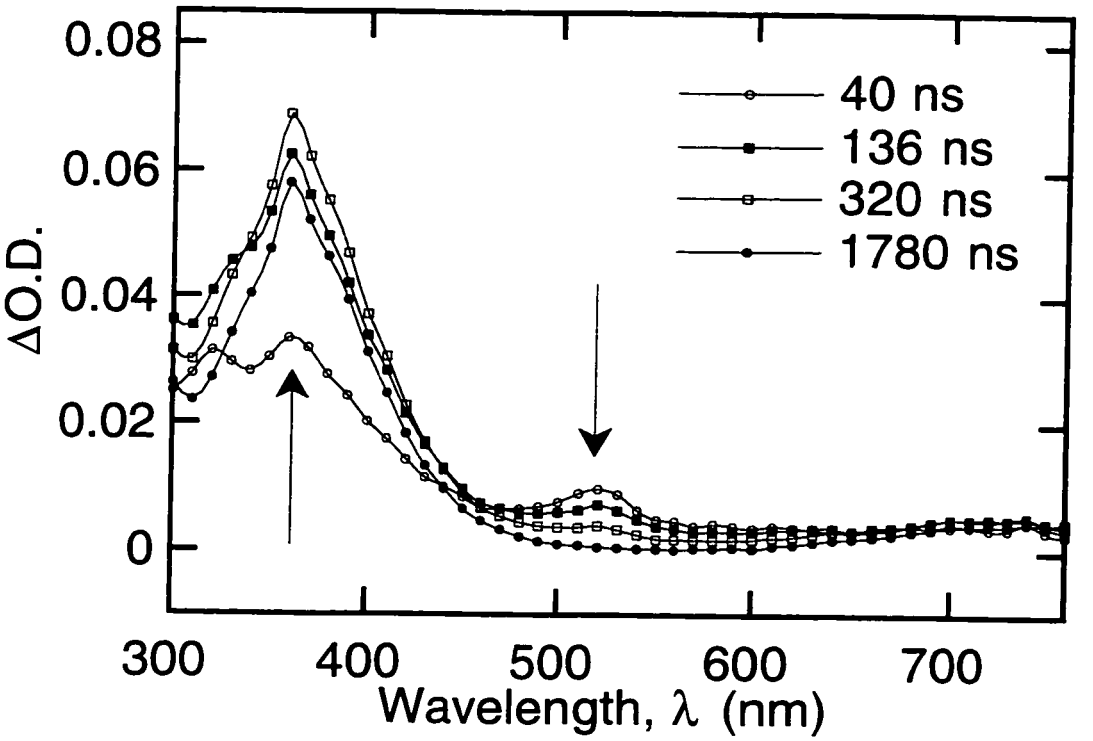

Figure 3-12 **The BrF_2^- spectrum recorded in MeCN. The bromine atoms were produced via the 266 nm photolysis of 1,2-dibromopropane. The bromine atoms were trapped with 7.5 mM Bu_4NF.**

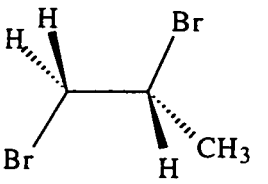

Dibromide III

1,2-dibromopropane

The fluoride concentration dependence at 520 nm was not studied, therefore there is no way of saying whether the absorption signal is fluoride dependent. From the data that is available, we are able to conclude that the decay of the 520 nm transient is not concurrent with the growth of the 360 nm transient, therefore the 520 nm transient cannot be a precursor to the BrF_2^- radical anion. In Figure 3-12, the spectrum shows that the growth of the BrF_2^- complex at 360 nm has a rate constant of 10.6 μs^{-1}, while the decay of the 520 nm

transient has a rate constant of 3.78 μs^{-1}. The decay of the 520 nm transient is slower than the 360 nm's growth, and faster than the 360 nm's decay (Figure 3-13). Therefore, the 520 nm transient cannot be the same transient that causes the 360 nm absorption.

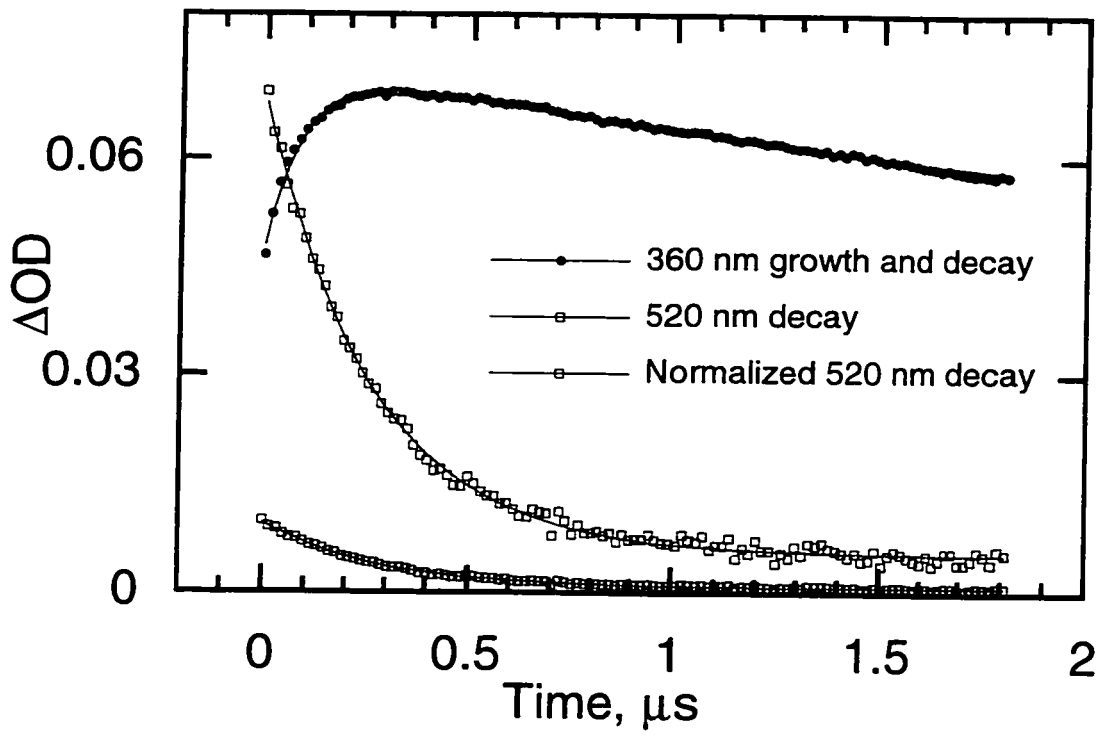

Figure 3-13 **The 520 nm decay and the 360 nm growth signals taken from the BrF_2^-/1,2-dibromopropane spectrum of Figure 3-12. Both the original 520 nm trace and a normalized trace are shown in comparison to the 360 nm trace. The traces were recorded in flowing MeCN with 7.5 mM Bu_4NF.**

Clearly, the 520 nm transient is not an absorption band due to any of the species that have been proposed so far in the general mechanism for the halide complexes of bromine. The 520 nm transient is also not something unique to 1,2-dibromopropane. An identical spectrum was obtained when 1,2-dibromo-3,3-dimethylbutane was used as the bromine atom source. The 520 nm transient requires the participation of the fluoride in one way or another. This decay signal is not present when either 1,2-dibromopropane or 1,2-dibromo-3,3-dimethylbutane are photolysed in the absence of fluoride. This transient

cannot be the product of fluoride trapping. When only a small concentration of fluoride is present (0.341 mM), the 520 nm signal appears instantaneously. This concentration of fluoride is too low to instantaneously trap bromine atoms. To be instantaneous on this system, the observed rate constant would have to be greater than 143 μs^{-1} (τ = 6.9 ns, the rise-time of the LFP system). At a fluoride concentration of 0.341 mM the bromine/fluoride probe rate constant would have to be at least 4.2 x 10^{11} M^{-1} s^{-1} to give an instantaneous signal. The only possible processes that might explain the results are electron transfer or static quenching.

If electron transfer were to occur, it would have to be between the photolytically produced bromine atom and a dissolved fluoride ion. The resulting fluorine atom would then have to be trapped instantaneously. Fluorine atoms were shown to react with a rate constant of diffusion an order of magnitude greater than the rate constant of diffusion for an average sized organic molecule.[20]

The reaction of a fluorine atom with a fluoride ion to produce the $F_2^{\bullet-}$ radical anion might be instantaneous under these conditions. The assignment of the 520 nm transient as the difluoride radical anion is unlikely. The absorption at 520 nm and the 265 ns lifetime are uncharacteristic for the rest of the dihalide species (Table 3-A). This could be verified by producing the $F_2^{\bullet-}$ species independently to compare with the present results. Bucher and Scaiano have shown that fluorine atoms can be generated via the photolysis of xenon difluoride.[20] The authors studied the fluorine atoms in freon-113 because this solvent forms a loose, but visible complex with the fluorine atoms. Fluorine atoms should also be trapped by added fluoride to produce the $F_2^{\bullet-}$ complex.

A fluorine atom, if produced through electron transfer, may also react with the parent dibromide or the solvent. The parent *vicinal* dibromides are usually present in ~ 10 mM concentrations. This concentration is sufficient to instantaneously react with a fluorine atom at normal diffusion limits. The abstraction of a bromine atom from the *vicinal* dibromide would produce the BrF species. Br_2 is known to have an absorption in

the 500 nm region. Based on the relatively invariant spectra of the hetero-nuclear radical anions of bromine ($BrX^{\bullet-}$), the spectra of the neutral hetero-nuclear dihalides (BrX) may also have similar spectra to one another. The reaction with the MeCN solvent would certainly be instantaneous, but Bucher and Scaiano showed that the production of fluorine atoms in MeCN gave no observable transient.[20]

There is not enough evidence to make a positive identification of the species responsible for the 520 nm transient. Spectroscopically, we would lean towards the BrF neutral molecule, but its instantaneous production would preclude more than one step. The need for having several consecutive instantaneous steps reduces the probability that this is the species. The mechanism would be easier to explain if the fluorine atoms could be produced from direct 266 nm irradiation of the Bu_4NF.

(iii) $BrX^{\bullet-}$ Extinction Coefficients

The extinction coefficients for the $BrI^{\bullet-}$, $BrCl^{\bullet-}$, and $BrF^{\bullet-}$ complexes were determined relative to the $Br_2^{\bullet-}$ complex. Under identical LFP conditions, the ratio of the optical densities of the transient complexes is equal to the ratio of the extinction coefficients (Equation 3.11). By measuring the maximum optical densities (TopOD) of the $BrX^{\bullet-}$ and $Br_2^{\bullet-}$ radical ions, the extinction coefficient of the $BrX^{\bullet-}$ complexes can be calculated, knowing the extinction coefficient of the $Br_2^{\bullet-}$ complex (9900 $M^{-1}cm^{-1}$).

$$\frac{\varepsilon_{BrX^{\bullet-}}}{\varepsilon_{Br_2^{\bullet-}}} = \frac{TopOD_{BrX^{\bullet-}}}{TopOD_{Br_2^{\bullet-}}}$$ **Equation 3.11**

Normally, in order to perform LFP actinometry, the samples should be matched in every possible way. The samples should contain the same *vicinal* dibromide precursor with identical absorbances at the excitation wavelength. The samples should also contain the same concentration of trapping halides. The concentration of the halide should also be

as high as possible in order to instantaneously trap all bromine atoms. Irradiation should be accomplished with the same laser intensity and power. These steps should ensure that the same amount of bromine atoms were produced and trapped in all the samples.

Experimental conditions for trapping bromine atoms with chloride and fluoride can easily be matched to the the conditions used for bromide trapping. Working with iodide is not as straightforward, therefore a way to normalize the data was necessary. When bromine atoms are produced in acetonitrile, in the absence of trapping halide, a weak instantaneous absorption band at 360 nm is observed. This is the band that we have referred to as the jump. The time-resolved traces at 360 nm either look like a jump and a growth, or simply like a jump (Figure 3-14). In both cases, the signals eventually decay away slowly.

It will be shown in chapter 5 that the jump is caused by an instantaneous complexation of the bromine atoms with the acetonitrile solvent. The growth component (if it exists) is due to bromine atom complexation with the parent *vicinal* dibromide. This complex grows in because the parent *vicinal* dibromide is usually in low concentration (~ 10 mM). The weak growth can be absent if the parent *vicinal* dibromide is too low in concentration or if the bromine atom/*vicinal* dibromide complex has a low extinction coefficient.

The presence of these absorptions gives the experiments an internal standard. Within a given solvent, acetonitrile in this case, the experimental conditions (laser power, excitation/monitoring beam overlap, *vicinal* dibromide concentration, etc.) can be normalized relative to the magnitude of the jump observed. The signal due to the solvent complex jump (and not the *vicinal* dibromide/Br• growth) must be used since the *vicinal* dibromides irradiated may be different or in different concentrations. The MeCN•Br jump is a relative measure of the amount of bromine atoms produced under those particular experimental conditions.

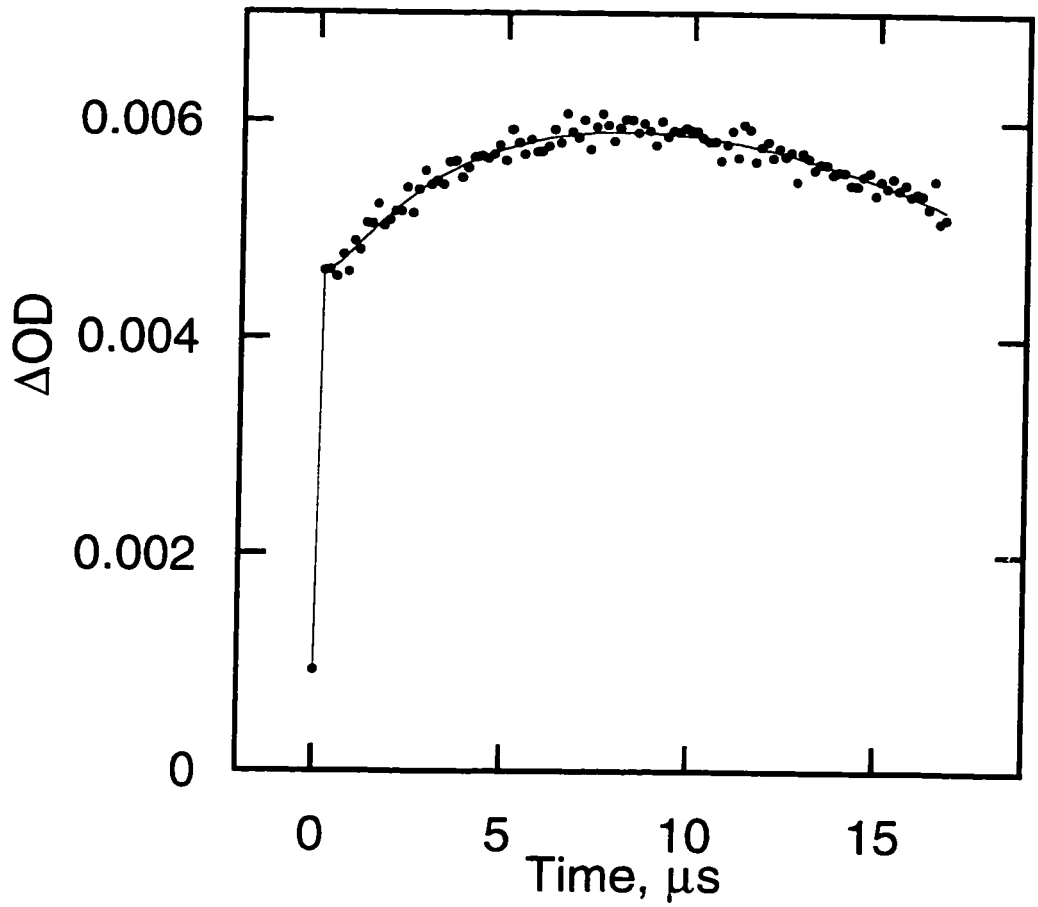

Figure 3-14 The jump and growth of the 360 nm signal after the photolysis of $Si(DBE)_4$ in MeCN.

In Figure 3-14, the jump is obvious in the absence of added halide and can easily be obtained from the trace. Once the halides are added, the jump becomes somewhat obscured by the stronger $BrX^{\bullet-}$ signal as in Figure 3-3. Despite the strong $Br_2^{\bullet-}$ signal in Figure 3-3, we can still see that there exists a short jump in the beginning of the trace. The magnitude of this jump is calculated via the fitting iterations of Equation 3.9 and is represented by the constant, C. The total yield of $BrX^{\bullet-}$ for each trace is given by the factor $[Br^{\bullet}]_o$ also determined by Equation 3.9. $[Br^{\bullet}]_o$ represents the $BrX^{\bullet-}$ signal that would be achieved if all the initially produced bromine atoms were immediately trapped by halide. This value is equivalent to the maximum absorbance possible for a given *vicinal* dibromide/halide trace. If there were no $BrX^{\bullet-}$ decay component, $[Br^{\bullet}]_o$ would be equal to the $BrX^{\bullet-}$ optical density at infinite time. We generally refer to this maximal transient optical density as the TopOD.

Dividing all $BrX^{\bullet}$ TopOD's by their respective jumps (C) effectively normalizes all traces (Equation 3.12) that have been fit by Equation 3.9.

$$\frac{\varepsilon_{BrX^{\bullet}}}{\varepsilon_{Br_2^{\bullet}}} = \frac{TopOD_{BrX^{\bullet}} / C_{BrX^{\bullet}}}{TopOD_{Br_2^{\bullet}} / C_{Br_2^{\bullet}}}$$

Equation 3.12

Table 3-B shows a comparison of the relative TopOD's and the resulting extinction coefficients of the $BrX^{\bullet}$ complexes. The complexes of bromide, chloride, and fluoride were measured from the LFP of $Si(DBE)_4$ in the presence of 1.0 mM halide in MeCN. The iodide values were determined via the LFP of 1,2-dibromoethyl-benzene in the presence of 1.0 mM iodide in MeCN. The extinction coefficients of the bromine atom complexes increase down the halide series. In hindsight, the use of 1,2-dibromoethyl-benzene was not the wisest choice for the $BrI^{\bullet}$ determination because there may be some uncertainty with respect to the quantum yield of the complex. In theory, the quantum yield of the debromination of the *vicinal* dibromide should be corrected for by dividing by the TopOD of the MeCN•Br complex. This assumption only holds if the addition of the iodide does not alter the quantum yield of the process. Iodide is known to reduce many *vicinal* dibromides, it may also be possible for iodide to reduce the intermediate β-bromo radical. Other than the expected pseudo-first-order dependence, there was no observable deviation in the kinetics of the $BrI^{\bullet}$ growth as the iodide concentration was gradually increased. If the iodide was reducing the intermediate 2-bromoethyl-benzyl radical, it would also form $BrI^{\bullet}$ as a product (Equation 3.13).

$$PhCHCH_2Br + I^- \not\rightarrow PhCH{=}CH_2 + BrI^{\bullet}$$

Equation 3.13

The formation of the $BrI^{\bullet-}$ from the reduction of 2-bromoethyl-benzyl radical would not have the same rate as the formation of the $BrI^{\bullet-}$ from the trapping of bromine atoms released due to photolysis. Therefore, if iodide was reducing the β-bromo radical, then we would expect the kinetics of the growth signal to reflect this second source of $BrI^{\bullet-}$. This was not observed, therefore we assumed that the iodide was not artificially raising the quantum yield. The experiment was run under oxygen saturation conditions in order to remove the unwanted signals of the 2-bromoethyl-benzyl radical. Perhaps the iodide was unable to compete with the oxygen quenching of the radical.

Table 3-B **The relative extinction coefficients of the $BrX^{\bullet-}$ radical anion complexes in MeCN at 298 K.**

Radical Anion	$TopOD_{BrX^{\bullet-}}/C_{BrX^{\bullet-}}$	$\varepsilon_{360}/10^3\ M^{-1}cm^{-1}$
$BrI^{\bullet-}$	5.1 ± 0.1	13 ± 1
$Br_2^{\bullet-}$	4.0 ± 0.1	9.9 ± 0.6[4]
$BrCl^{\bullet-}$	3.6 ± 0.2	9 ± 1
$BrF^{\bullet-}$	2.8 ± 0.1	6.9 ± 0.7

The temperature effects on the extinction coefficients of the $BrX^{\bullet-}$ complexes were not studied. The kinetics measured by LFP are independent of the extinction coefficient of the species. This is best exemplified by the fact that the entire spectrum of a given species follows the same kinetics regardless of the monitored wavelength.

The magnitude of the absorbance of a species is directly proportional to its extinction coefficient according to the Beer-Lambert law (Equation 4.14). For this reason, quantum yield determinations would be greatly affected by any variations in the extinction

coefficients. There were no quantum yield studies performed in this thesis that were not at room temperature.

(iv) $BrOH^{\bullet}$

The $BrOH^{\bullet}$ radical anion was introduced as an intermediate in the pulse radiolysis of bromine solutions (Scheme 3-1).[2] Although very little is known about the species, there are a few noteworthy comparisons to the $BrX^{\bullet}$ series. The reaction of a bromide ion with a hydroxyl radical (Equation 3.3) is very similar to the reaction of a bromide ion with a bromine atom (Equation 3.5). Zehavi and Rabani determined the rate constant for the formation of the $BrOH^{\bullet}$ radical anion to be 1.1×10^{10} M^{-1} s^{-1} in water.[3] This value is the same order of magnitude as all of the bromine atom trapping experiments discussed so far. The authors attributed an absorption at 360 nm to the $BrOH^{\bullet}$ complex. Again, this is comparable to the $BrX^{\bullet}$ complexes. From their experiments, Zehavi and Rabani measured the back-reaction to be about 100 times faster than the estimates for the $BrX^{\bullet}$ back-reactions {~ 10^5 M^{-1} s^{-1}, section 3.4 (i)}. The $BrOH^{\bullet}$ back-reaction was determined to be 3.3×10^7 M^{-1} s^{-1}, for an equilibrium constant of 333 M^{-1}. This back-reaction is not quite analogous to the $BrX^{\bullet}$ back-reactions since the $BrOH^{\bullet}$ back-reaction produces a hydroxyl radical and not a bromine atom.

In a more appropriate comparison to the $BrX^{\bullet}$ back-reactions, Zehavi and Rabani determined that the $BrOH^{\bullet}$ complex also disproportionated into a bromine atom and a hydroxide ion (Equation 3.14). This back-reaction is a closer comparison to the $BrX^{\bullet}$ back-reactions which disproportionate to give a bromine atom and a halide ion (Equation 3.6).

$$BrOH^{\bullet} \xrightarrow{k_{-BrOH^{\bullet}}} Br\bullet + OH^{-} \qquad \textbf{Equation 3.14}$$

The rate constant for Equation 3.14 was determined to be 4.2 x 10^6 $M^{-1}s^{-1}$.[3] This value is still faster than the back-reactions of the $BrX^{\bullet 2-}$ radical anions, but it is an order of magnitude closer than the value for the production of the hydroxyl radical from the back-reaction of Equation 3.3.

The $BrOH^{\bullet 2-}$ radical was also shown to react with a second equivalent of bromide. The reaction was an ion exchange reaction. The second bromide ion displaced a hydroxyl anion to produce the $Br_2^{\bullet 2-}$ complex (Equation 3.15) with a rate constant of 1.9 x 10^8 M^{-1} s^{-1}.[3]

$$BrOH^{\bullet 2-} + Br^- \xrightarrow{k_{IE}} Br_2^{\bullet 2-} + OH^- \qquad \textbf{Equation 3.15}$$

This final reaction may be generalized to the $BrX^{\bullet 2-}$ case. Perhaps all of the $BrX^{\bullet 2-}$ radical ions have an ion exchange equilibrium (Equation 3.16).

$$BrX^{\bullet 2-} + X^- \xrightarrow{k_{IE}} X_2^{\bullet 2-} + Br^- \qquad \textbf{Equation 3.16}$$

(v) Halo-thiocyanate Radical Anions ($XSCN^{\bullet 2-}$)

The only semi-analogous series to the mixed halo-bromide radical anions that have been studied are the halo-thiocyanate radical anions. The mixed halide complexes of thiocyanate ($XSCN^{\bullet 2-}$) have been measured for chlorine, bromine, and iodine by Schoeneshoefer.[21-23] The spectra of these complexes have absorption maxima at 390 nm (ε = 4700 M^{-1} cm^{-1}), 400 nm (ε = 7300 M^{-1} cm^{-1}), and 420 nm (ε = 9200 M^{-1} cm^{-1}) respectively.

The spectra were obtained via the pulse radiolysis of solutions containing thiocyanate (SCN^-) and halide (X^-). The presence of thiocyanate allowed for an ion-

exchange equilibrium between $XSCN^{\cdot 2-}$ and $(SCN)_2^{\cdot -}$ to be established (Equation 3.17). In each case the spectra were corrected for the absorption due to $(SCN)_2^{\cdot -}$.

$$(SCN)_2^{\bullet -} + X^- \rightleftharpoons XSCN^{\bullet 2-} + SCN^- \qquad \textbf{Equation 3.17}$$

For the chlorine[23] and bromine[22] experiments, the concentration of the halide was far greater than the thiocyanate, therefore the pulse radiolysis (PR) sequence initially produced the dihalide ion as in Scheme 3-1. Scheme 3-4 shows the sequence of reactions for $Br_2^{\cdot -}$ with SCN^-.

$$Br^- \xrightarrow{PR} Br_2^{\bullet -} \qquad \textbf{Scheme 3-1 (page 46)}$$

$$Br_2^{\bullet -} + SCN^- \longrightarrow 2Br^- + SCN^{\bullet} \qquad \textbf{Equation 3.18}$$

$$SCN^{\bullet} + SCN^- \rightleftharpoons (SCN)_2^{\bullet -} \qquad \textbf{Equation 3.19}$$

$$(SCN)_2^{\bullet -} + Br^- \rightleftharpoons SCN^- + BrSCN^{\bullet -} \qquad \textbf{Equation 3.20}$$

Scheme 3-4 The formation of $BrSCN^{\cdot 2-}$ from the pulse radiolysis of a 20 mM bromide solution in the presence of 100 μM SCN^-.[22]

Once formed, the $Br_2^{\cdot -}$ ion undergoes an electron transfer with the SCN^- to produce the thiocyanate radical (SCN•) (Equation 3.18). The SCN• radical then reacts with SCN^- to produce $(SCN)_2^{\cdot -}$ (Equation 3.19). Finally, the $(SCN)_2^{\cdot -}$ reacts with the excess halide in an ion exchange reaction to produce the $XSCN^{\cdot 2-}$ ion (Equation 3.20).

In the case of the reaction of $Br_2^{\bullet-}$ with SCN^-, two other equilibria were observed, Equation 3.21 and Equation 3.22.[22] Equation 3.21 is an ion exchange reaction similar to Equation 3.20, but this time the reaction involves the $Br_2^{\bullet-}$ complex and SCN^-. In both ion exchange reactions, $BrSCN^{\bullet-}$ is generated. Equation 3.22 is the trapping of the SCN• radical with the excess Br^-. Equation 3.22 also produces $BrSCN^{\bullet-}$.

$$Br_2^{\bullet-} + SCN^- \rightleftharpoons BrSCN^{\bullet-} + Br^- \qquad \textbf{Equation 3.21}$$

$$SCN^{\bullet} + Br^- \rightleftharpoons BrSCN^{\bullet-} \qquad \textbf{Equation 3.22}$$

For both the $Br_2^{\bullet-}$ and the $Cl_2^{\bullet-}$ reactions with SCN^-, the final spectra were combinations of $XSCN^{\bullet-}$ and $(SCN)_2^{\bullet-}$. In neither case, under the conditions employed, was there any appreciable $X_2^{\bullet-}$ remaining .[22,23]

For the iodine equilibrium,[21] it was the thiocyanate that was in far greater concentration than the iodine, therefore the $(SCN)_2^{\bullet-}$ ion was generated via the pulse radiolytic sequence of Scheme 3-1. The $(SCN)_2^{\bullet-}$ and the iodide then established an equilibrium with $ISCN^{\bullet-}$ and $I_2^{\bullet-}$ (Equation 3.23 and Equation 3.24).

$$SCN^- \xrightarrow{PR} (SCN)_2^{\bullet-}$$

$$(SCN)_2^{\bullet-} + I^- \rightleftharpoons SCN^- + ISCN^{\bullet-} \qquad \textbf{Equation 3.23}$$

$$ISCN^{\bullet -} + I^- \rightleftharpoons I_2^{\bullet -} + SCN^-$$ **Equation 3.24**

Scheme 3-5 **The formation of $ISCN^{\bullet -}$ from the pulse radiolysis of a thiocyanate solution in the presence of iodide.[21]**

As in the bromide case,[22] I^- is also capable of displacing the thiocyanate ion of the mixed radical anion in order to form the diiodide radical anion (Equation 3.24).

Table 3-C **The equilibrium reactions of the halide ions with the dithiocyanate radical anion, $(SCN)_2^{\bullet -}$ and the mixed radical anion, $XSCN^{\bullet -}$.[21-23]**

(X^-)	$(SCN)_2^{\bullet -} + X^- \Leftrightarrow XSCN^{\bullet -} + SCN^-$	$XSCN^{\bullet -} + X^- \Leftrightarrow X_2^{\bullet -} + SCN^-$
Halide	$K((SCN)_2^{\bullet -}/XSCN^{\bullet -})$	$K(XSCN^{\bullet -}/X_2^{\bullet -})$
Cl^-	0.0033	–
Br^-	0.0091	0.001
I^-	400	55

The equilibria of Table 3-C reflect the relative nucleophilicity of the halides with respect to thiocyanate.

$$Cl^- < Br^- < SCN^- < I^-$$

Because of the "messy" pulse radiolytic formation of the complexes, the rates of complexation for the two elementary units of the mixed halothiocyanate radical anions were not measured.

$$X^- + SCN^\bullet \rightleftharpoons XSCN^{\bullet-}$$ **Equation 3.25**

$$X^\bullet + SCN^- \rightleftharpoons XSCN^{\bullet-}$$ **Equation 3.26**

For the halo-thiocyanate complexes, Nagarajan and Fessenden's method[8] of photolysing the desired complexes after their pulse radiolytic formation would not work due to the spectral interference of the omnipresent $(SCN)_2^{\bullet-}$ complexes in all of the solutions. Neither the complexation of X^- and $SCN^\bullet$ (Equation 3.25), nor the complexation of $X^\bullet$ and SCN^- (Equation 3.26) were possible in these solutions.

Again, LFP offers a route to the direct formation of the complex via Equation 3.26. Halogen atoms can be produced via the photolysis of the appropriate precursors in solutions containing SCN^-.

3.4 Equilibria of the Bromine Atom/Halide Complexes ($BrX^{\bullet-}$)

The equilibria for most of the homo-nuclear radical anions and the mixed thiocyanate radical anions have been measured. During our studies of bromine atoms, we have been able to produce, and observe, the hetero-nuclear halide complexes of bromine ($BrX^{\bullet-}$). These observations appear to be the first reports and measurements of such bromo-halo-species in solution other that $Br_2^{\bullet-}$ itself. In order to further compare our data with the species that have already been characterized, we shall attempt to extract equilibrium constants from our data. The calculation of equilibrium constants for the $BrX^{\bullet-}$ radical anions requires the measurement of the reverse process of the bromine atom probe reactions (Equation 3.27).

$$BrX^{\bullet}_{2}^{-} \xrightarrow{k_{-BrX^{\bullet}_{2}^{-}}} Br^{\bullet} + X^{-}$$ **Equation 3.27**

(i) Decay of the Radical Anions

Since the growth of the $BrX^{\bullet}_{2}^{-}$ complexes was more closely related to the main area of research for this thesis, the kinetic traces were monitored at fast timescales. Figure 3-15 is typical of the high halide concentration traces recorded during this investigation. The trace of Figure 3-15 was produced via the LFP of 1,2-dibromopropane (Dibromide **III**) in the presence of 2.72 mM Bu_4NF in MeCN.

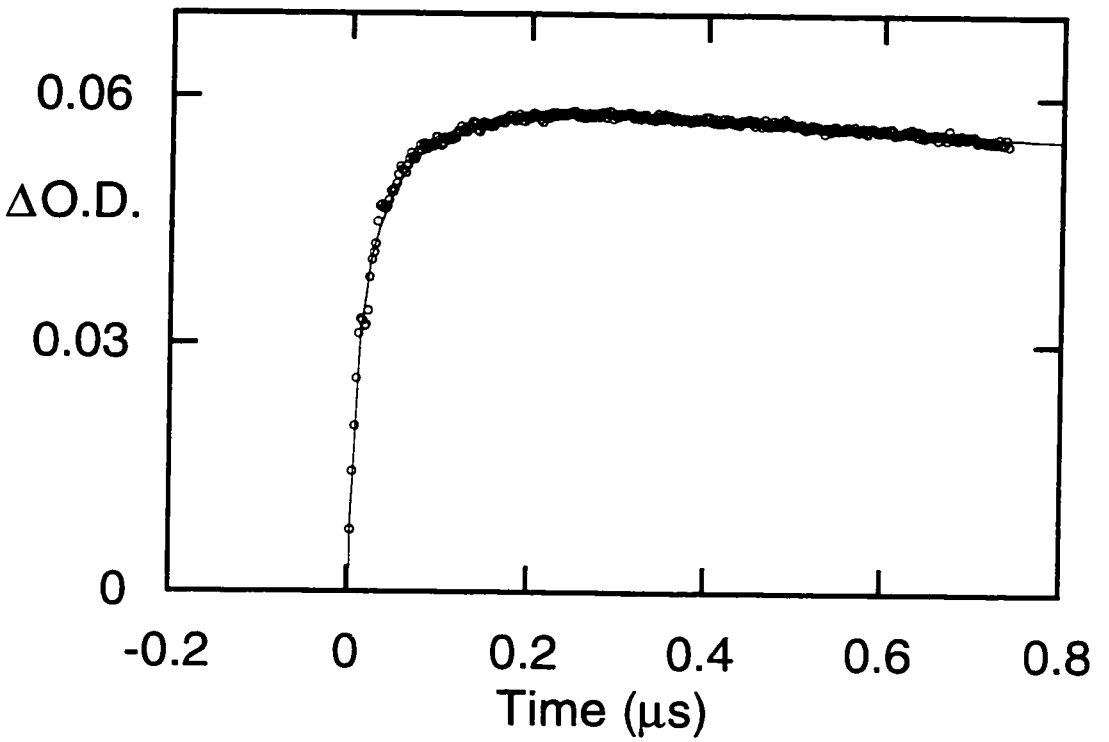

Figure 3-15 **The $BrF^{\bullet}_{2}^{-}$ signal monitored at 360 nm in MeCN at 296 K. The complex was produced by the LFP of 1,2-dibromopropane in the presence of 2.72 mM Bu_4NF.**

The growth of the signal contains the relevant information about the production of bromine atoms that was to be the focus of the research. For this reason, the time resolution of the LFP was optimized for the growth, thus sacrificing the decay information. Very few

traces were recorded on long enough timescales to observe the decay to completion. Of course, there were some traces that were monitored specifically to see the entire decay, i.e. Figure 3-16, but that was only done for characterization, not for detailed study. Nevertheless, a few observations can be made about the lifetime and the mode of decay of the $BrX^{\cdot}$ complexes.

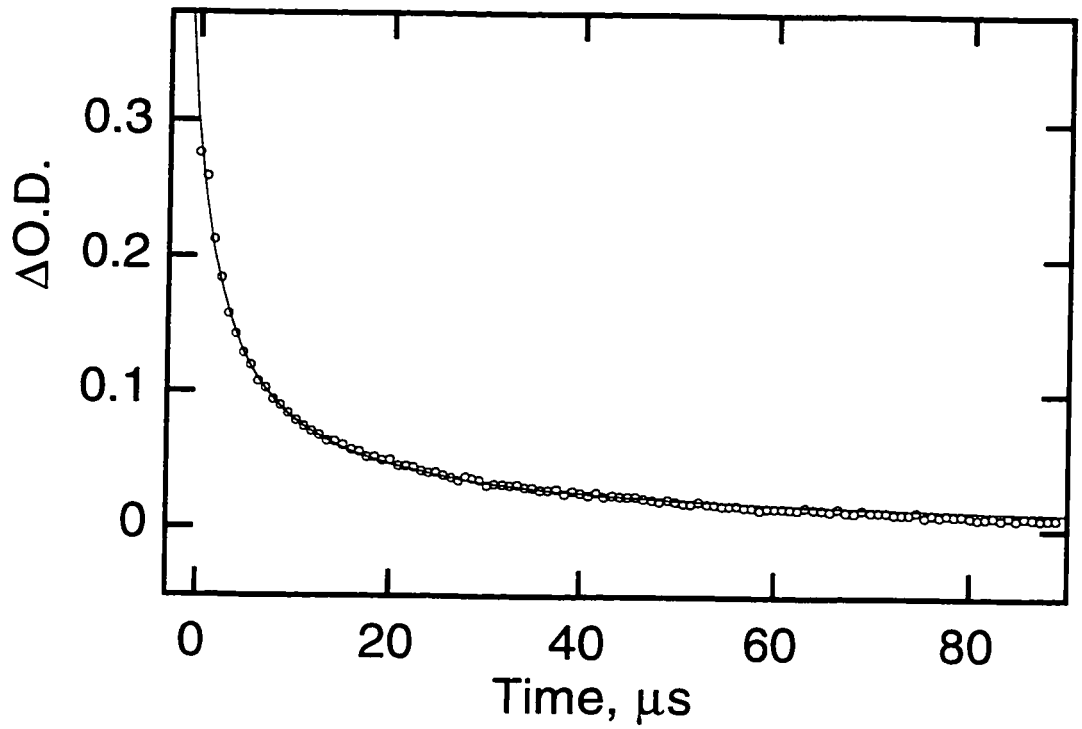

Figure 3-16 **The second order decay of the $Br_2^{\cdot}$ complex monitored at 360 nm in 5% aqueous MeCN. LFP of *trans*-1,2-dibromocyclopentane in the presence of 5 mM KBr.**

Figure 3-16 shows the decay of the $Br_2^{\cdot}$ complex at 360 nm for the LFP of *trans*-1,2-dibromocyclopentane (Dibromide **IX**) in 5% aqueous MeCN. Five percent water was added in order to solubilize the KBr added as the bromide ion source. The decay of the $Br_2^{\cdot}$ complex on this long timescale is mainly second order. The majority of the $Br_2^{\cdot}$ ions decay via the combination of two equivalents of the radical ions to produce Br_2 and two bromide ions (Equation 3.28).

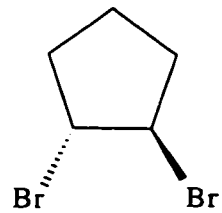

Dibromide IX:

***trans*-1,2-dibromocyclopentane**

$$Br_2^{\bullet -} + Br_2^{\bullet -} \xrightarrow{k_{2^\circ decay}} 2Br^- + Br_2$$

Equation 3.28

Despite not recording the decays of the $BrX^{\bullet -}$ complexes to completion, there was usually enough of the decays for the data analysis to extract values from the growth traces. In all quenching experiments, the trapping process of the probe reactions (Equation 3.1) increased as expected with increasing halide ion concentration. However, so too did the rate of decay of the complexes with each increase in halide concentration. This effect was also observed in one of the original pulse radiolysis studies of the $Br_2^{\bullet -}$ complex by Zehavi and Rabani.[3] The authors attributed this effect to the reaction of the $Br_2^{\bullet -}$ ion with bromide to produce a tribromide ion, $Br_3^{2-\bullet}$ (Equation 3.29).

$$Br_2^{\bullet -} + Br^- \xrightarrow{k_{Br3^{2-\bullet}}} Br_3^{2-\bullet}$$

Equation 3.29 (Tribromide dianion)

The formation of the tribromide species is reversible (Equation 3.30). Knowing both the forward and reverse reactions for the tribromide dianion leads to the equilibrium expression of Equation 3.31.[3]

$$Br_3^{2-\bullet} \xrightarrow{k_{-Br3^{2-\bullet}}} Br_2^{-\bullet} + Br^- \qquad \textbf{Equation 3.30}$$

$$K_{Br_3^{2-\bullet}} = \frac{[Br_3^{2-\bullet}]}{[Br_2^{-\bullet}][Br^-]} = \frac{k_{Br_3^{2-\bullet}}}{k_{-Br_3^{2-\bullet}}} \qquad \textbf{Equation 3.31}$$

The decay trace shown in Figure 3-16 is clearly not first-order or pseudo-first-order despite being on the high end of bromide concentrations for our study (5 mM). Zehavi and Rabani used concentrations at least 20 to 200 times greater than the highest concentrations used in the present investigation.[3] The concentrations of bromide in their pulse radiolysis experiments reached 1.0 M! Under the conditions of Figure 3-16, the $Br_2^{-\bullet}$ complex still predominantly decays via the bimolecular self-reaction of Equation 3.28. At the comparatively low bromide concentration of 5 mM, $k_{2^{\circ}decay}[Br_2^{-\bullet}]^2 >> k_{Br3^{2-\bullet}}[Br_2^{-\bullet}][Br^-]$. In fact, Zehavi and Rabani did not see a complete decay of the $Br_2^{-\bullet}$ complex in their PR experiments either. What they reported was a partial first-order decay of the transient.[3] In other words, what they saw was a fast, pseudo-first-order, partial decay followed by the usual slow second order decay. What they implied from their study was that the equilibrium of Equation 3.31 lay very much on the side of the $Br_2^{-\bullet}$ complex even at 1M bromide. Therefore, the fast, pseudo-first-order, partial decay they observed represented the establishment of the tribromide equilibrium (Equation 3.31).

In our case, if all of the $BrX^{-\bullet}$ radical anions are assumed to follow the same mechanism for decay as the $Br_2^{-\bullet}$ complex, then we can single out three main modes of decay for the radical anions (Scheme 3-6). The first mode of decay for the $BrX^{-\bullet}$ complexes is the slow bimolecular reaction of two transient anions to produce molecular bromine and to regenerate two halide ions (Equation 3.32). The second mode is the disproportionation of the radical anions back to their original fragments (Equation 3.33). The third mode is

the pseudo-first-order reaction of the complexes with a second halide ion (Equation 3.34) to produce the trihalide radical dianions.

$$2\,BrX^{\bullet 2-} \xrightarrow[\text{SLOW}]{k_{2^{\circ}BrX}} Br_2 + 2\,X^- \qquad \textbf{Equation 3.32}$$

$$BrX^{\bullet 2-} \xrightarrow[\text{SLOW}]{k_{-BrX}} Br^{\bullet} + X^- \qquad \textbf{Equation 3.33}$$

$$BrX^{\bullet 2-} + X^- \xrightarrow[\text{FAST}]{k_{BrX2}} BrX_2^{2\bullet 2-} \qquad \textbf{Equation 3.34 (Trihalide dianion)}$$

Scheme 3-6 The main modes of decay of halo-bromo radical anions in the presence of excess halide.

Over long timescales, the $BrX^{\bullet 2-}$ complexes decay mainly by the second order kinetics of Equation 3.32, but certainly not cleanly (Figure 3-16). The decay is obviously quite complicated. On the fast timescales that the probe reactions are studied (100 ns to 2000 ns) we would not expect any appreciable decay of the complex. Nonetheless, we do see some decay of the complex and the decay component is dependent on the halide concentration. Based on this observation, and on Nagarajan and Fessenden's Br_3^{2-} equilibrium,[3] we concluded that we were seeing the same fast equilibrium being established with our $BrX^{\bullet 2-}$ species.

If the slow bimolecular decay (Equation 3.32) is assumed to be several orders of magnitude slower that the pseudo-first-order reaction with a second halide ion, then, on the fast timescales, the decay can be treated as a first-order decay.

Scheme 3-7 shows the development of the kinetic mechanism for the pseudo-first-order decay of the $BrX^{\bullet 2-}$ radical anions. The scheme incorporates the first-order decay of Equation 3.33 and the pseudo-first-order decay of Equation 3.34.

$$\frac{-d[BrX^{\bullet 2-}]}{dt}(\text{fast}) = k_{-BrX^{\bullet 2-}}[BrX^{\bullet 2-}] + k_{BrX_2^{\bullet 2-}}[BrX^{\bullet 2-}][X^-] \qquad \textbf{Equation 3.35}$$

$$\frac{-d[BrX^{\bullet 2-}]}{dt}(\text{fast}) = \left(k_{-BrX^{\bullet 2-}} + k_{BrX_2^{\bullet 2-}}[X^-]\right)[BrX^{\bullet 2-}] \qquad \textbf{Equation 3.36}$$

$$\frac{-d[BrX^{\bullet 2-}]}{dt}(\text{fast}) = k_{1°decay}[BrX^{\bullet 2-}] \qquad \textbf{Equation 3.37}$$

$$k_{1°decay} = k_{-BrX^{\bullet 2-}} + k_{BrX_2^{\bullet 2-}}[X-] \qquad \textbf{Equation 3.38}$$

Scheme 3-7 The kinetic mechanism for the partial, fast, pseudo-first-order decay of the $Br_2^{\bullet -}$ radical anion.

By taking the first-order decay rate constants, $k_{1°decay}$, extracted from the kinetic traces of the LFP of several dibromides, a quenching plot was constructed (Figure 3-17). The quenching plot shows the dependence of the decay rate constant of the $Br_2^{\bullet -}$ complex with added bromide. As can be expected, the plot is quite scattered. As explained earlier, the decay rate constants were extracted from traces that were predominantly growths, therefore they cannot be expected to be very precise. Equation 3.38 predicts that a plot of the observed fast decay rate constant, $k_{1°decay}$, versus halide concentration should give a straight line. The slope of this $Br_2^{\bullet -}$ quenching plot is equal to the rate constant for the reaction of the $Br_2^{\bullet -}$ complex with a second equivalent of bromide, k_{Br3}^{2-} (Equation 3.29). The intercept of this plot, when the bromide concentration is zero, is equal to the rate constant for the reverse probe reaction, $k_{-Br2}^{\bullet -}$ (Equation 3.6).

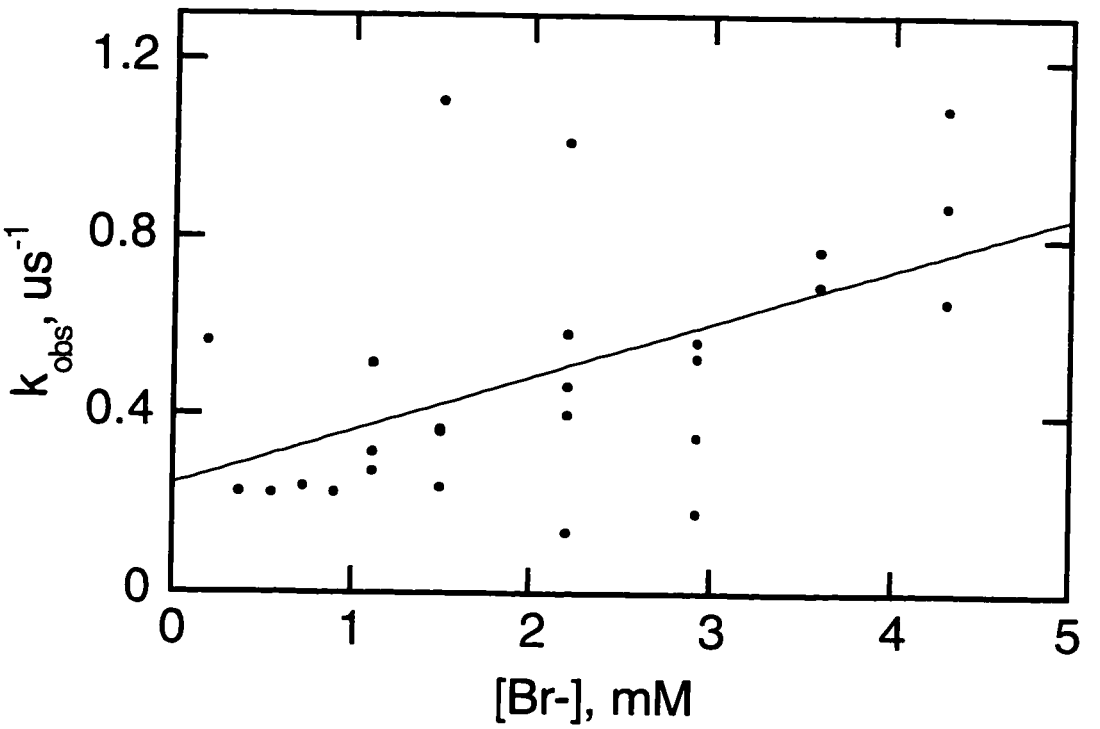

Figure 3-17 The dependence of the $Br_2^{\bullet-}$ decay with [Br^-]. Results from a compilation of the LFP of many vicinal dibromides.

From Figure 3-17, the rate constant for tribromide formation was determined from the slope to be $(1.2 \pm 0.7) \times 10^8$ M^{-1} s^{-1} in MeCN at room temperature. At zero bromide concentration, the intercept of Figure 3-17 was determined to be $(2 \pm 1) \times 10^5$ s^{-1} for a lifetime of 5 ± 3 μs.

From the growth and decay results in MeCN, the equilibrium constant for the probe reaction can be calculated.

$$Br\bullet + Br^- \underset{k_{-Br_2^{\bullet-}}}{\overset{k_{Br_2^{\bullet-}}}{\rightleftharpoons}} Br_2^{\bullet-}$$

Equation 3.5 and Equation 3.6 (Page 46)

$$K_{Br_2^{\bullet-}} = \frac{k_{Br_2^{\bullet-}}}{k_{-Br_2^{\bullet-}}} = \frac{(1.5 \pm 0.3) \times 10^{10}}{(2 \pm 1) \times 10^{5}}$$

$$K_{Br_2^{\bullet-}} = (8 \pm 6) \times 10^{4}\ M^{-1}$$

The value of $(8 \pm 6) \times 10^4\ M^{-1}$ for the probe equilibrium in MeCN is in excellent agreement with the value of $10^5\ M^{-1}$ estimated in water by Nagarajan and Fessenden.[8]

In summary, the rapid pseudo-first-order formation of the $BrX^{\bullet-}$ radical anions followed by the fast pseudo-first-order decay of the complexes can be expressed by the general mechanism of Scheme 3-8. This mechanism was used to fit the kinetic traces of the $BrX^{\bullet-}$ signals such as in Figure 3-15.

Equation 3.39 was used in the computer fitting routine. Once the growth and decay rate constants are extracted from the traces, the halide dependence of the two components can be evaluated using Equation 3.40 and Equation 3.38. Quenching plots of halide concentration versus k_{probe} lead to the determination of the probe rate constants ($k_{BrX^{\bullet-}}$) and the lifetime of the bromine atoms in solution in the absence of probe ($k_o^{Br^{\bullet}}$). Quenching plots of halide concentration versus $k_{1^{\circ}decay}$ lead to the determination of the trihalide rate constants ($k_{BrX_2^{2-}}$) and the reverse probe rate constants ($k_{-BrX^{\bullet-}}$). Knowing $k_{BrX^{\bullet-}}$ and $k_{-BrX^{\bullet-}}$, the equilibrium constants for the probe reactions ($K_{BrX^{\bullet-}}$) can be calculated.

$$Br\bullet + X^- \underset{k_{-BrX^{\bullet 2-}}}{\overset{k_{BrX^{\bullet 2-}}}{\rightleftharpoons}} BrX^{\bullet 2-} + X^- \xrightarrow{k_{BrX_2^{2\bullet 2-}}} BrX_2^{2\bullet 2-}$$

$$[BrX^{\bullet 2-}]_t = C + \frac{[Br\bullet]_o k_{probe}}{k_{1°decay} - k_{probe}}\left(e^{-k_{probe}t} - e^{-k_{1°decay}t}\right) \qquad \textbf{Equation 3.39}$$

$$k_{probe} = k_o^{Br\bullet} + k_{BrX^{\bullet 2-}}[Br-] \qquad \textbf{Equation 3.40}$$

$$k_{1°decay} = k_{-BrX^{\bullet 2-}} + k_{BrX_2^{2\bullet 2-}}[Br-] \qquad \textbf{Equation 3.38 from Scheme 3-7}$$

Scheme 3-8 The mechanistic implications of the fast growth and decay kinetics of the $BrX^{\bullet 2-}$ complex.

The rate constant for the formation of the $BrI_2^{\bullet 2-}$ radical dianion was determined from the slope of its decay quenching plot (Figure 3-18) to be $(1.5 \pm 0.8) \times 10^8\ M^{-1}\ s^{-1}$. The unimolecular decay rate constant of the $BrI^{\bullet 2-}$ complex was determined from the intercept of the plot to be $(5 \pm 2) \times 10^4\ s^{-1}$.

From the values of $k_{BrI}^{\bullet 2-}$ and $k_{-BrI}^{\bullet 2-}$ from the $BrI^{\bullet 2-}$'s growth and decay quenching plots, the equilibrium constant for the $BrI^{\bullet 2-}$ radical ion was determined to be $(3 \pm 3) \times 10^5\ M^{-1}$.

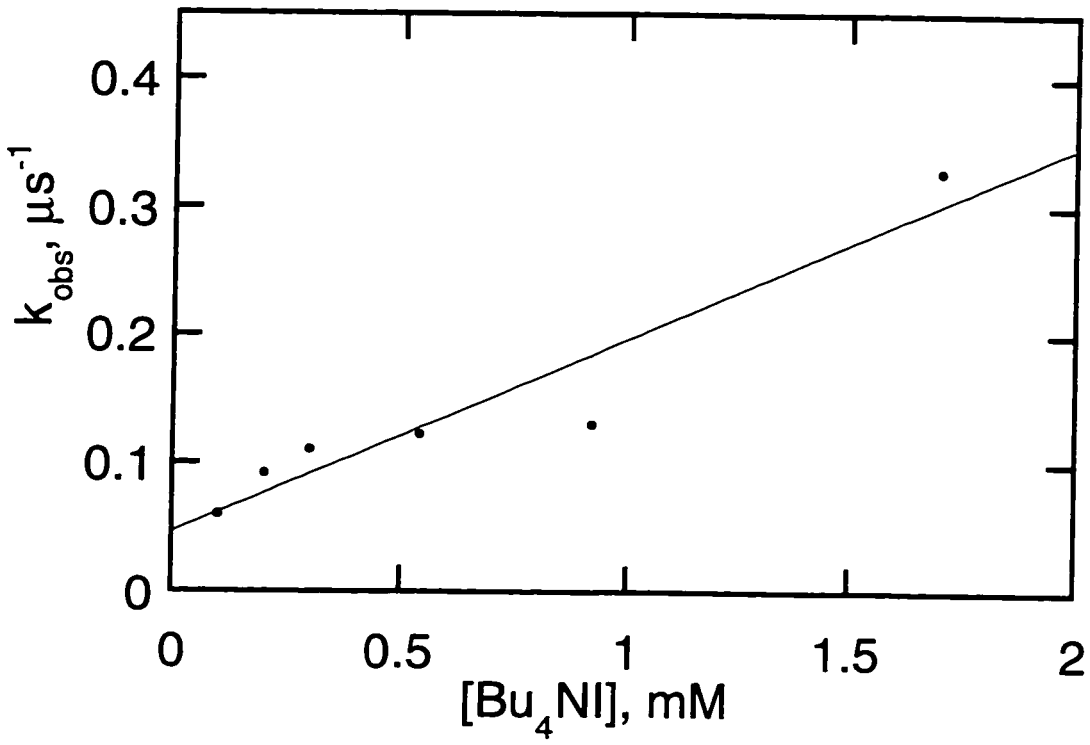

Figure 3-18 **The iodide dependence of the fast decay component of the $BrI^{\cdot}$ complex. The complex was generated from the photolysis of 1,2-dibromoethylbenzene in the presence of Bu_4NI. The rate constants were measured in MeCN at 296 K and monitored at 370 nm.**

Figure 3–19 represents the $BrX_2^{\cdot}$ decay quenching plots for chlorine and fluorine. The rate constants for the formation of the trihalide species, $BrCl_2^{2-}$ and BrF_2^{2-}, were determined from the slopes to be (1.0 ± 0.5) x 10^8 M^{-1} s^{-1} and (1.4 ± 0.7) x 10^8 M^{-1} s^{-1} respectively. Extrapolation of the quenching plots to zero halide concentration gives the rate constants for the disproportionation of the two $BrX^{\cdot}$ complexes. The disproportionation rate constant for the bromochloride complex, $k_{-BrCl}^{\cdot}$, was determined as (1.4 ± 0.7) x 10^5 s^{-1}. Combining this value with the forward rate constant ($k_{BrCl}^{\cdot}$ = (1.4 ± 0.1) x 10^{10} M^{-1} s^{-1}) gives an equilibrium constant for the $BrCl^{\cdot}$ complex as (1.0 ± 0.5) x 10^5 M^{-1}. The intercept from the $BrF^{\cdot}$ complex was (3 ± 1) x 10^4 s^{-1} for an equilibrium constant of (4 ± 2) x 10^5 M^{-1}.

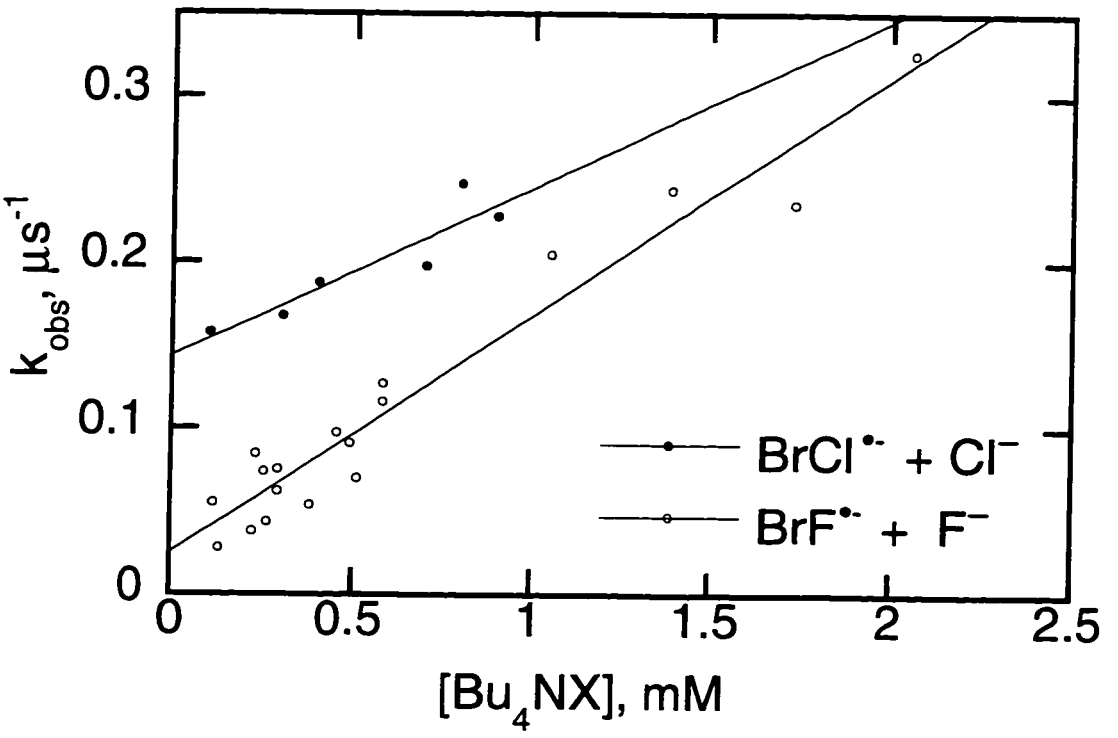

Figure 3–19 **Chlorine quenching of the $BrCl^{\bullet-}$ radical ion and fluoride quenching of the $BrF^{\bullet-}$ radical anion. The bromine atoms were produced via the 266 nm photolysis of $Si(DBE)_4$ and 1,2-dibromo-1,1-difluoroethane respectively in MeCN.**

Table 3-D represents a summary of the average values obtained for the $BrX^{\bullet-}$ radical anions obtained from the LFP of *vicinal* dibromides in the presence of the respective halides. For each of the sets of rate constants and the set of equilibrium constants, the values fall within the same order of magnitude for all of the halides. The values of $k_{-BrX}^{\bullet-}$, $K_{BrX}^{\bullet-}$, and $k_{BrX_2}^{2\bullet-}$, all depend on the accuracy of the extraction of the decay information from the growth traces, therefore they can be expected to have large errors. It is sufficient to conclude that these values agree amongst themselves and with the literature data that is available.

Table 3-D **A comparison of rate and equilibrium constants for the various halide complexes of bromine atoms.**

X^-	$k_{BrX}^{\cdot}/10^{10}$, $M^{-1}s^{-1}$	$k_{-BrX}^{\cdot}/10^{5}$, s^{-1}	$K_{BrX}^{\cdot}/10^{5}$, M^{-1}	$k_{BrX_2}^{2\cdot}/10^{8}$, $M^{-1}s^{-1}$
I^-	14 ± 8	0.5 ± 0.2	3 ± 3	1.5 ± 0.8
Br^-	15 ± 3	2 ± 1	0.8 ± 0.6	1.2 ± 0.7
Cl^-	14 ± 1	1.4 ± 0.7	1.0 ± 0.5	1.0 ± 0.5
F^-	10 ± 1	0.3 ± 0.1	4 ± 2	1.4 ± 0.7

The rate constants for the probe reactions, $k_{BrX}^{\cdot}$, are the results of many experiments (except for $BrI^{\cdot}$) and are reasonably accurate. In general, the rate constants increase with increasing size of the halide ion according to the Smoluchowski equation.[24]

$$k_{diff} = 4\pi N_A r_{BrX} D_{BrX} \qquad \textbf{Equation 3.41}$$

At the diffusion controlled limit, the rate of reaction is linearly proportional to the sum of the radii of the reacting species (r_{BrX}). For the halide trapping experiments, the bromine atom is a constant in all of the reactions, therefore the rate constants are linearly dependent on the radius of the trapping halide. The sum of the diffusion coefficients, D_{BrX}, will not change very much. Atoms and ions diffuse extremely rapidly. The variation in radii of the halide ions will not significantly alter the diffusion coefficients.

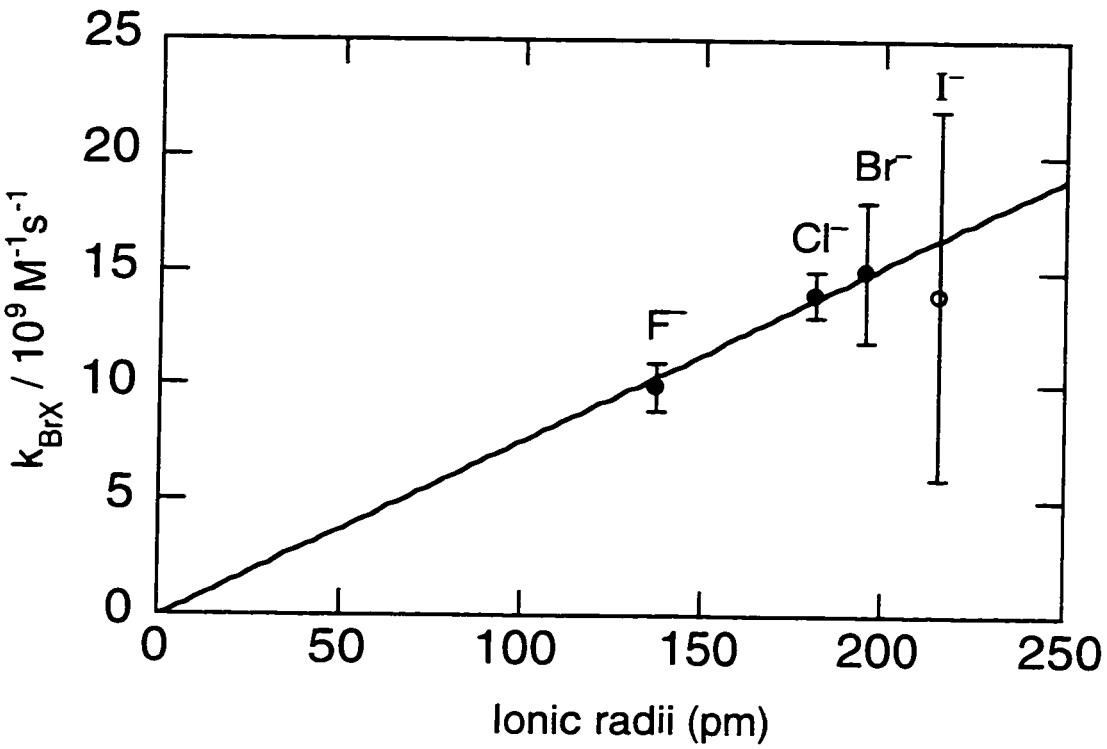

Figure 3-20 **The dependence of the bromine atom probe rate constant (k_{BrX^-}) in MeCN versus the radii of the halide ion (r_X) traps. The iodide values are not included in the fit of the line because of the large error.**

Figure 3-20 shows a tentative linear relationship between the measured probe rate constants versus the ionic radii of the halides. Iodide is included in the plot, but the iodide value is not included in the fit of the line because of the large uncertainty associated with this value.

3.5 Temperature Effects on the Radical Anions

The formation of the $Br_2^{\bullet-}$ complex (Equation 3.5) was monitored over the temperature range from 233 K to 321 K. *Trans*-1,2-dibromocyclopentane was photolyzed in MeCN at various temperatures. At each temperature, a complete quenching plot (re Figure 3-4) of the observed rate constant of the growth of the $Br_2^{\bullet-}$ radical anion versus the concentration of bromide was constructed. In Figure 3-21, all of the quenching plots are displayed together on one graph.

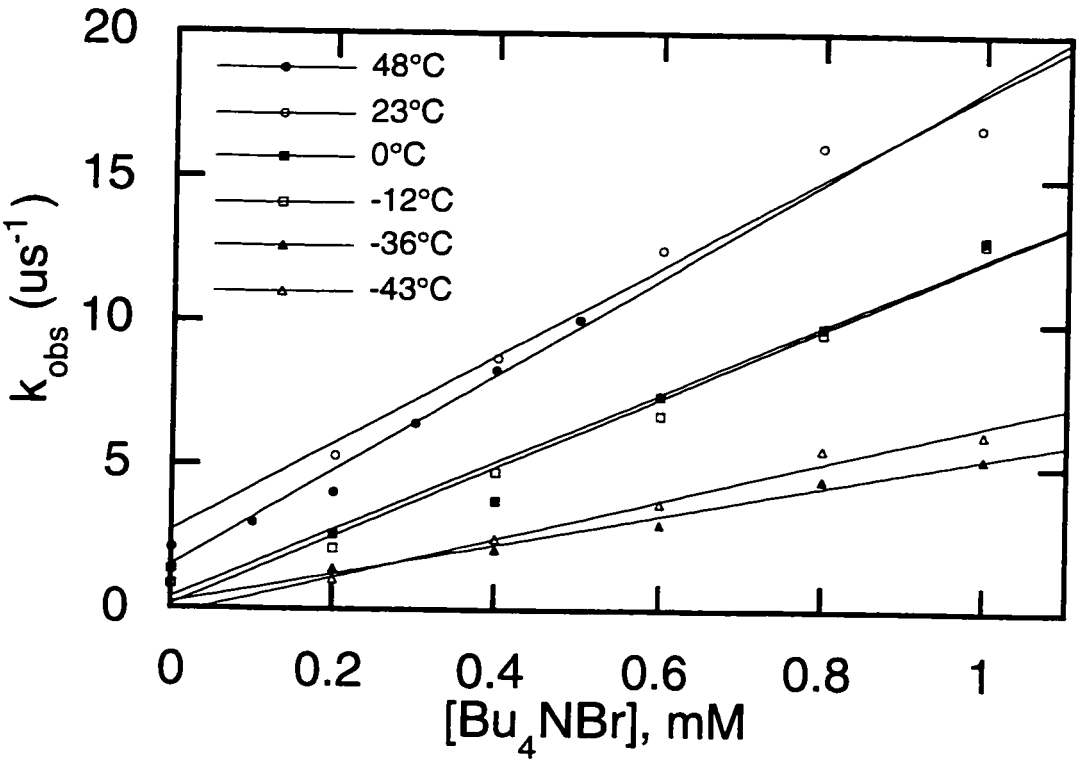

Figure 3-21 **Bromine atom quenching plots at various temperatures in MeCN. Bromine atoms were produced from the LFP of *trans*-1,2-dibromocyclopentane and trapped with Bu_4NBr.**

From the rate constants calculated from the slopes of the plots at the different temperatures, an Arrhenius relationship was obtained. Figure 3-22 represents the log of the rate constants versus the inverse of the temperature. From the plot, the Arrhenius dependence was determined.

$$\log\left(k_{Br_2^{\bullet-}}\right) = (11.6 \pm 0.3) - \frac{(1.9 \pm 0.4 \text{ kcal/mol})}{2.3R}\left(\frac{1000 \text{ cal/kcal}}{T}\right)$$

The activation energy of 1.9 ± 0.4 kcal/mol for the reaction of the atom and the ion of bromine is slightly lower than the activation energy for diffusion in MeCN. For comparison, Chin and Wine measured the activation energy of the formation of $(SCN)_2^{\bullet-}$ to

be 0.5 ± 0.7 kcal/mol in water.[25] The logA factor measured for the $Br_2^{\cdot}$ formation is higher than the logA factor of 10.2 reported for the $(SCN)_2^{\cdot}$ radical anion in water.

Chin and Wine also determined the enthalpy change for the formation of the $(SCN)_2^{\cdot}$ to be exothermic by 8.8 ± 2.8 kcal/mol. In a similar experiment, Kosanic determined the formation of the $Br_2^{\cdot}$ complex to be exothermic by 7 kcal/mol in water.[26]

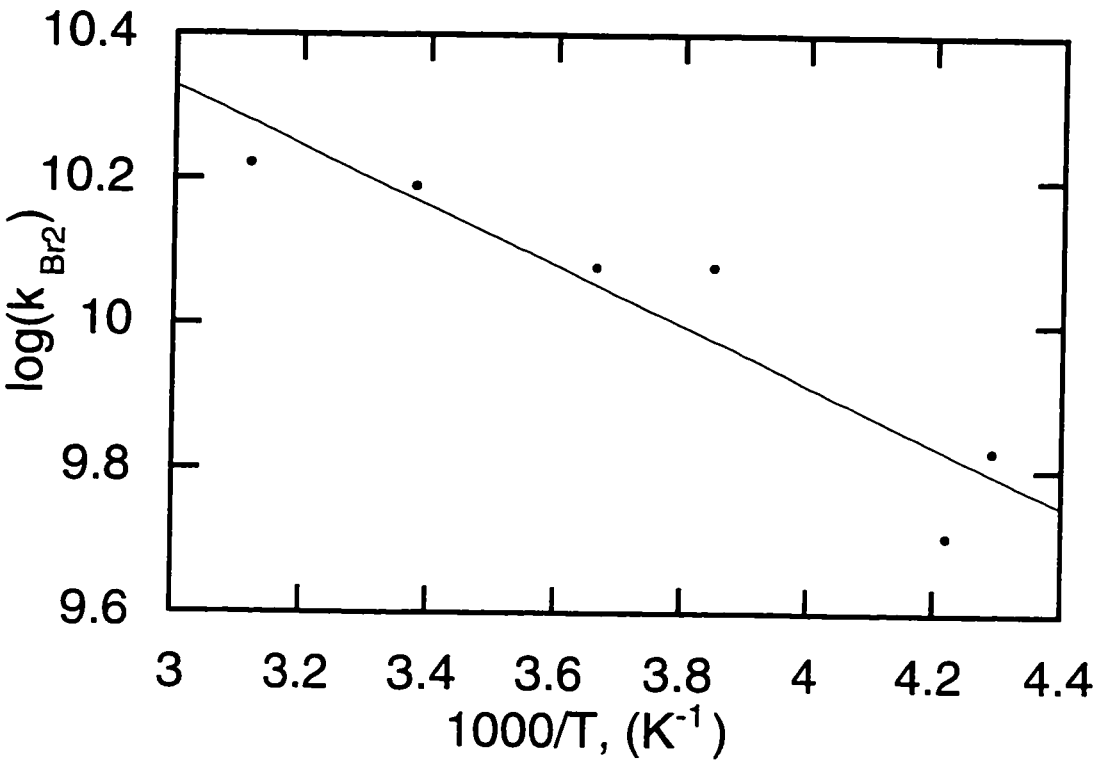

Figure 3-22 **An Arrhenius plot for the temperature dependence of the trapping of bromine atoms by bromide. The log of the rate constants were plotted against the inverse of the temperature for the LFP of *trans*-1,2-dibromocyclopentane in MeCN.**

3.6 Chapter 3 References

(1) Grossweiner, L. I.; Matheson, M. S. *J. Phys. Chem.* **1957**, *61*, 1089.

(2) Matheson, M. S.; Mulac, W. A.; Weeks, J. L.; Rabani, J. *J. Phys. Chem.* **1966**, *70*, 2092.

(3) Zehavi, D.; Rabani, J. *J. Phys. Chem.* **1972**, *76*, 312.

(4) Hug, G. L. *Optical Spectra of Nonmetallic Inorganic Transient Species in Aqueous Solution*; National Bureau of Standards: Washington, 1981; Vol. NSRDS-NBS 69, pp 160.

(5) Workentin, M. S.; Wagner, B. D.; Negri, F.; Zgierski, M. Z.; Lusztyk, J.; Siebrand, W.; Wayner, D. M. *J. Phys. Chem.* **1995**, *99*, 94.

(6) Workentin, M. S.; Wagner, B. D.; Lusztyk, J.; Wayner, D. M. *J. Am. Chem. Soc.* **1995**, *117*, 119.

(7) Neta, P.; Huie, R. E.; Ross, A. B. *J. Phys. Chem. Ref. Data* **1988**, *17*, 1027.

(8) Nagarajan, V.; Fessenden, R. W. *J. Phys. Chem.* **1985**, *89*, 2330.

(9) Treinin, A.; Hayon, E. *J. Am. Chem. Soc.* **1975**, *87*, 1716.

(10) Alfassi, Z. B.; Huie, R. E.; Mittal, J. P.; Neta, P.; Shoute, L. C. T. *J. Phys. Chem.* **1993**, *97*, 9120.

(11) Shoute, L. C. T.; Neta, P. *J. Phys. Chem.* **1990**, *94*, 2447.

(12) Shoute, L. C. T.; Neta, P. *J. Phys. Chem.* **1990**, *94*, 7181.

(13) McGimpsey, W. G.; Scaiano, J. C. *Can. J. Chem.* **1988**, *66*, 1474.

(14) Weldon, D.; Barra, M.; Sinta, R.; Scaiano, J. C. *J. Org. Chem.* **1995**, *60*, 3921.

(15) Zhang, B.; Pandit, C. R.; McGimpsey, W. G. *J. Phys. Chem.* **1994**, *98*, 7022.

(16) Scaiano, J. C.; Barra, M.; Krzywinski, M.; Sinta, R.; Calabrese, G. *J. Am. Chem. Soc.* **1993**, *115*, 8340.

(17) Scaiano, J. C.; Barra, M.; Calabrese, G.; Sinta, R. *J. Chem. Soc., Chem. Commun.* **1992**, 1418.

(18) Gannon, T.; McGimpsey, W. *J. Org. Chem.* **1993**, *58*, 913.

(19) Laidler, K. J. In *Chemical Kinetics*; Third ed. ed.; Harper & Row: New York, 1987; pp 278.

(20) Bucher, G.; Scaiano, J. C. *J. Am. Chem. Soc.* **1994**, *116*, 10076.

(21) Schoeneshoefer, M.; Henglein, A. *Ber. Bunsenges. Phys. Chem.* **1970**, *74*, 393.

(22) Schoeneshoefer, M.; Henglein, A. *Ber. Bunsenges. Phys. Chem.* **1969**, *73*, 289.

(23) Schoeneshoefer, M. *Int. J. Radiat. Phys. Chem.* **1969**, *1*, 505.

(24) Gilbert, A.; Baggot, J. *Essentials of Molecular Photochemistry*; Blackwell Science: Oxford, 1991, pp 538.

(25) Chin, M.; Wine, P. H. *J. Photochem. Photobiol. A: Chem.* **1992**, *69*, 17.

(26) Kosanic, M. M. *J. Serb. Chem. Soc.* **1995**, *58*, 55.

4. The LFP Generation of ß-bromoradicals From *Vicinal* Dibromides

4.1 The LFP Search for the β-bromo Radical 96

4.2 The Kinetics of the Photochemical Debromination of *Vicinal* Dibromides in the Presence of a Halide Trap/Probe 103
(i) The 1st Equivalent, BrX^- (1) 104
(ii) The 2nd Equivalent, BrX^- (2) 106
(iii) The Combined Equation 107

4.3 The Decay of RBr• in the Presence of Halide 110
(i) Low [X^-] Regime 111
(ii) High [X^-] Regime (see Table 4-B) 111

4.4 Halide Reduction of β-bromo Radicals 115
(i) Fluoride Reduction of β-bromo Radicals 115
(ii) Reduction of β-bromo Radicals by the Halide Series 120

4.5 The Stability and Reactivity of β-Bromo Radicals in the Presence of Halides 127
(i) The β-Bromoethyl Radical 127
(ii) The Effect of Fluorination 129
(iii) The Effect of Alkyl Substitution 130
(iv) The Effect of a Silyl Group on the β-Bromo Radical 132
(v) The Effect of Ring Size on the β-Bromo Radical 132
(vi) The Effect of a β-Silyl Group on the β-Bromo Radical 134

4.6 Temperature Effects on the β-Bromo Radicals 134
(i) Temperature Effects of the Halide Reduction of the β-Bromo Radicals 136
(ii) The Temperature Dependence of the β-Bromo Radical Lifetimes 136

4.7 Conclusion 137

4.8 Chapter 4 References 139

4.1 The LFP Search for the β-bromo Radical

The detection of β-bromo radicals has eluded ESR even at low temperatures (-120°C).[1] ESR would be an ideal method to detect and to characterize β-bromo radicals, but unfortunately the radicals appear to be too unstable on the ESR timescale. Nanosecond laser flash photolysis (LFP) has the advantage over conventional ESR of having a much faster time resolution by at least two orders of magnitude. Nanosecond LFP can measure transients with lifetimes as short as 20 ns. The disadvantage of LFP is that neither the β-bromo-alkyl radicals nor the bromine atoms produced after photolysis are "visible" in the 250 - 800 nm region normally accessible to LFP. In order to monitor the photochemical debromination of *vicinal* dibromides in the LFP system, a probe (Chapter 3) is added to the solution. Halides (Br^-, Cl^-, F^-, and on occasion I^-) are added to form the highly visible complexes, $BrX^{\cdot-}$ with bromine atoms released after photolysis (section 3.3(iii)). The rates of complexation were all determined to be $\geq 10^{10}$ M^{-1} s^{-1}. At high enough halide concentrations ($\geq$ 10 mM), the pseudo-first-order trapping of bromine atoms is greater than 10^8 s^{-1} and is observed as instantaneous on the LFP timescale. Thus, at halide concentrations > 10 mM, the kinetics of the $BrX^{\cdot-}$ complexes represent the kinetic evolution of bromine atoms into solution.

One of the original expectations of the study of 1,2-dibromoethane[2] was to observe the β-bromoethyl radical (albeit indirectly through the $Br_2^{\cdot-}$ complex). It was expected that at high bromide concentrations, when the trapping of bromine atoms is instantaneous, the growth of the $Br_2^{\cdot-}$ signal would be due to the rate-limiting debromination of the β-bromoethyl radical, thereby making it possible to observe and quantify the lifetime of the radical. Under these conditions, it was expected that the growth of $Br_2^{\cdot-}$ would appear in two stages: a jump followed by a growth (Figure 4-1).

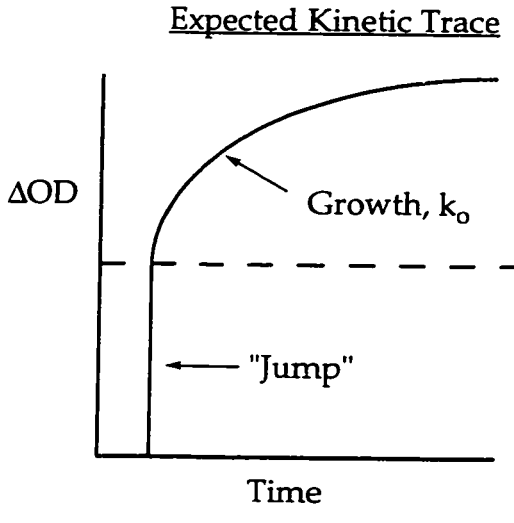

Figure 4-1 The expected jump and growth kinetics expected for the photodebromination of 1,2-dibromoethane.

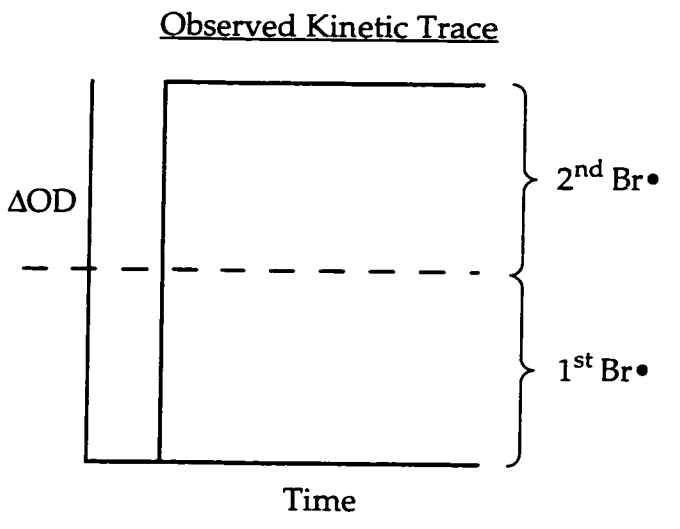

Figure 4-2 The observed kinetics of the photodebromination of 1,2-dibromoethane. Both bromine atoms are lost instantaneously in the presence of 10 mM bromide.

A jump and growth mechanism, in the absence of added halide, was introduced in chapter 3. Remember that the jump was due to an instantaneous complexation of the bromine atoms by the solvent, whereas the growth that followed was due to the transfer of the bromine atom from the instantaneous solvent-complex to the parent *vicinal* dibromide. This will be discussed in greater detail in chapter 5.

The jump and growth expected now, in the presence of high concentrations of halide, would appear because of a similar kinetic mismatch between two stages of a reaction. In the absence of halide, the bromine atoms were produced instantaneously on the timescale of the experiment, but the trapping by the *vicinal* dibromide solute was rate-limiting. In the high halide concentration case, the reverse is expected. In the presence of high concentrations of halide, the trapping of bromine atoms is instantaneous, therefore any growth observed would be due to a rate-limiting production of bromine atoms.

It was expected that, upon photolysis in the presence of 10 mM bromide, 1,2-dibromoethane would lose the first bromine atom immediately, thus producing the jump in the signal. The observation of the second bromine atom was expected to be limited by the unimolecular decay of the β-bromoethyl radical (Equation 4.1).

$$CH_2Br—CH_2^{\bullet} \xrightarrow{k_o^{RBr\bullet}} CH_2=CH_2 + Br^{\bullet}$$ **Equation 4.1**

The expected growth would represent the rate of the β-bromoethyl radical decay. A jump and growth was not observed. Instead, only a jump was observed (Figure 4-2). Through quantum yield studies, this jump was determined to represent two bromine atoms. Therefore, Scaiano *et al.* concluded that both bromine atoms were being eliminated within the < 20 ns resolution of the LFP system.[2]

While the β-cleavage leading to loss of bromine in 1,2-dibromoethane and related systems proved too fast for nanosecond techniques, we reasoned that the reaction could be slowed down if β-cleavage involved a somewhat stabilized radical. In the extreme case, McGimpsey *et al.*[3] have shown that aryl-substituted β-bromoethyl radicals are stabilized to the point that they do not undergo β-bromine elimination in the timescale of their experiments (section 1.2(ii)). What was needed was a compound with a stability somewhere between these two extremes.

Neighboring group participation in the formation of radicals has received considerable attention.[1,4-9] Stabilization of radicals has been observed for compounds having for example, a β-silyl,[10-12] a β-bromo[13-16], or a β-chloro[1,17,18] group. Apparently, the β-stabilizing effect of the bromine atom in 1,2-dibromoethane is not sufficient to observe the radical in the LFP system. If a second β-stabilizing group can be introduced into the molecule, and the stabilizing effects of two β-groups are additive, then the radical may be encouraged to live long enough to be observed.

The use of more halogens in any given *vicinal* dibromide would most likely complicate matters. Silicon turned out to be a practical choice for the second β-stabilizing group. Silicon should not participate in the photochemistry of the molecule. Also, there are a number of commercially available alkyl-vinyl silanes that can be easily brominated to produce the desired alkyl-1,2-dibromo silanes. Roger Sinta of Shipley Company graciously prepared tetrakis(1,2-dibromoethyl)silane {$Si(DBE)_4$, Dibromide **XIII**} from tetra-vinyl silane for this study (Equation 4.2).[19] The addition of the silyl group will hopefully add the needed stability to the radical.

$$Si(CH{=}CH_2)_4 + Br_2 \xrightarrow[0°C,\ 3\ hrs]{CH_2Cl_2} Si(CHBrCH_2Br)_4 \qquad \textbf{Equation 4.2}$$

The LFP of $Si(DBE)_4$ in MeCN behaved as all other *vicinal* dibromides at low bromide concentrations. Below 1 mM bromide, the probe reaction with the bromine atoms to produce the visible $Br_2^{\bullet-}$ complex was rate-limiting (see Figure 3-4). At higher bromide concentrations, the kinetics of the $Br_2^{\bullet-}$ signal did not follow the usual results obtained for all other *vicinal* dibromides. At 6 mM bromide, a jump and growth was observed for the LFP of $Si(DBE)_4$ in MeCN (Figure 4-3).

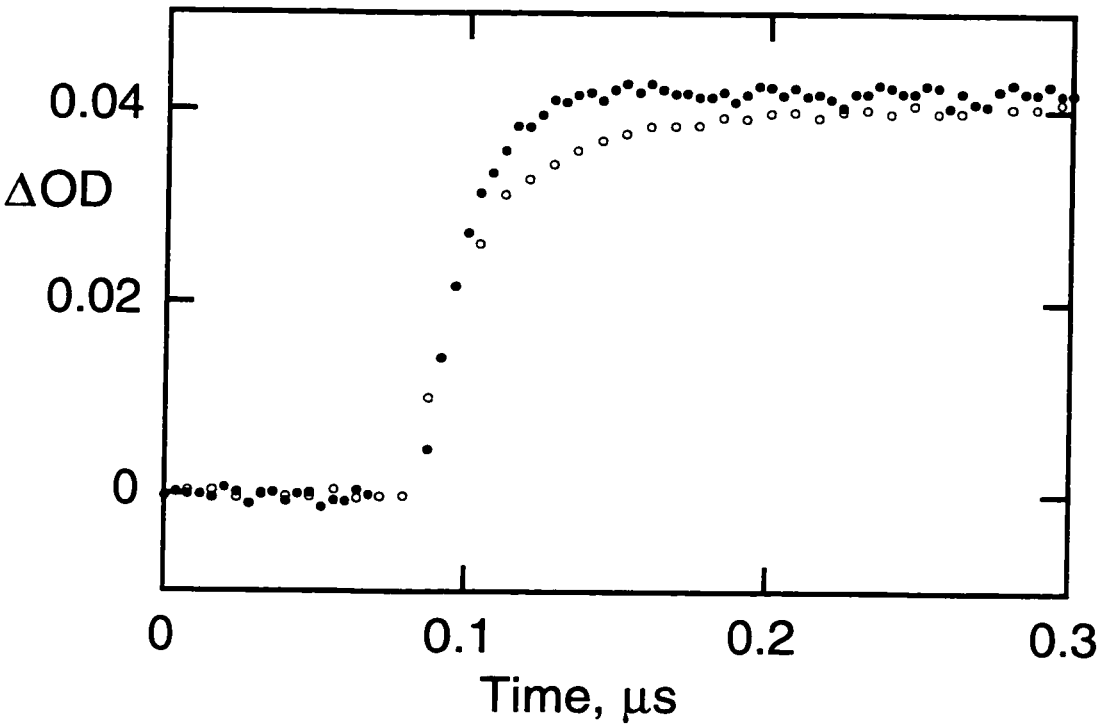

Figure 4-3 **The normalized growths observed for the LFP of (●) 1,2-dibromoethane and (○) Si(DBE)$_4$ at 360 nm in MeCN in the presence of 6 mM Bu$_4$NBr.[19]**

The bromide quenching of Si(DBE)$_4$ was done in parallel with 1,2-dibromoethane so as to compare the results against a known standard. Up to this point, 1,2-dibromoethane has been determined to instantaneously eliminate two bromine atoms after LFP in the presence of > 5 mM bromide. A concentration of 6 mM bromide should provide a bromine atom trapping rate of 9.6 x 10^7 M^{-1} s^{-1} for a lifetime of 10.4 ns. This 10.4 ns rise represents the expected jump. The growth component of the 1,2-dibromoethane trace in Figure 4-3 was calculated to have a lifetime of 10.3 ns. The trace for the Si(DBE)$_4$, however, had a growth lifetime of 43 ns. Initially, this lifetime was attributed to the decay of the β-bromo radical of Si(DBE)$_4$ (Equation 4.3).[19]

$$(DBE)_3SiCHBrCH_2^{\bullet} \xrightarrow{k_o^{RBr\bullet}} (DBE)_3SiCH{=}CH_2 + Br^{\bullet}$$ **Equation 4.3**

Having finally observed a β-bromo radical, we assumed that further additions of bromide would not affect the rate of Equation 4.3, therefore, at high bromide concentrations, the observed rate constant would plateau at the rate constant limited by Equation 4.3 (Figure 4-4).

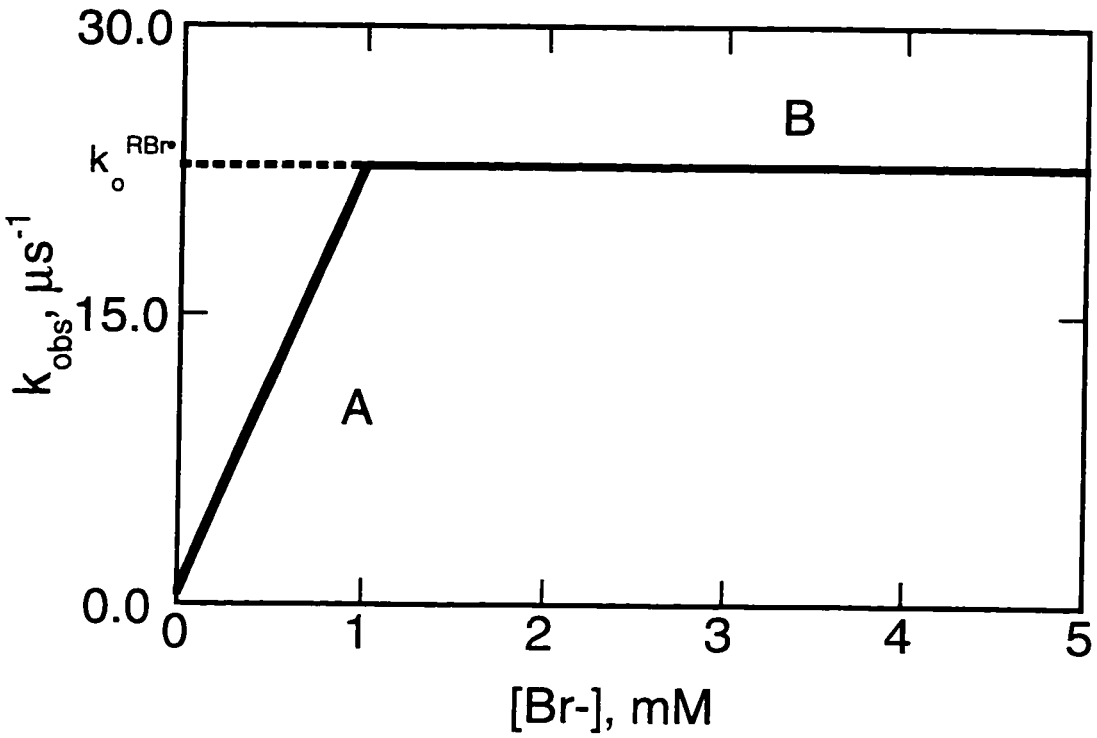

Figure 4-4 **The expected plateau of the bromide dependence of the $Br_2^{\bullet-}$ growth for $Si(DBE)_4$.**

Region A of Figure 4-4 represents the stage of the reaction whereby the bromide concentration is low enough such that the probe reaction is still rate determining. In region B of the theoretical plot, the observed rate constant was expected to plateau at the rate for the second bromine atom to be spontaneously eliminated from the β-bromo radical. In the case of the 6 mM $Si(DBE)_4$ trace of Figure 4-3, we expected the quenching plot to plateau at 22.7 μs^{-1} (τ = 43 ns).

Experimentally, we observed a drastic reduction in the slope of the quenching plot, but not a plateau. The second segment (region B, at high bromide) yields a slope of 5.3 x

10^9 M^{-1} s^{-1} and an intercept of 8.1 x 10^6 s^{-1}. While k_{obs} changes with bromide concentration in this range, the total $Br_2^{\bullet-}$ yield remains essentially constant. The results are consistent with β-cleavage occurring by two mechanisms: the unimolecular elimination of Equation 4.3 *and* the "assisted" reduction of Equation 4.4.

$$(DBE)_3SiCHBrCH_2^{\bullet} + Br^- \xrightarrow{k_{red}} (DBE)_3SiCH{=}CH_2 + Br_2^{\bullet-} \qquad \textbf{Equation 4.4}$$

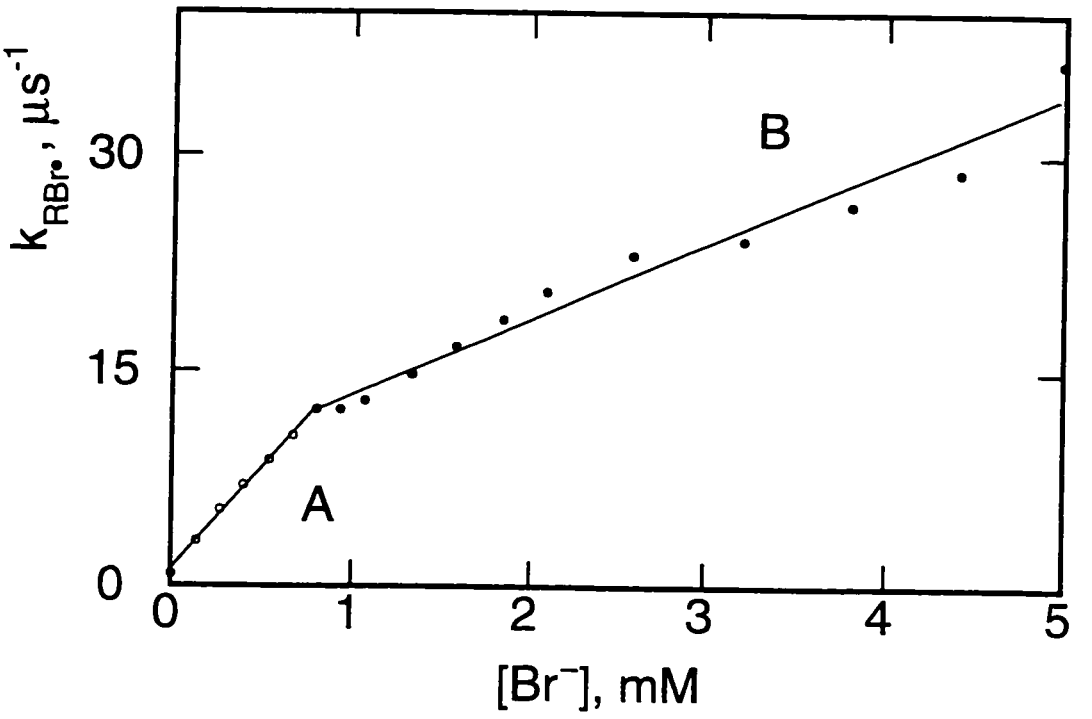

Figure 4-5 **The observed bromide dependence of the $Br_2^{\bullet-}$ growth at 360 nm in MeCN for the LFP of $Si(DBE)_4$.**

In retrospect, the bromide assisted elimination of the second bromine atom from the β-bromo radical should not have been totally unexpected. We saw in section 1.3(i) that halides are quite capable of thermally reducing *vicinal* dibromides. The halide reduction of a transient radical must be that much more facile than the dibromo-precursor. Fortunately for our studies in MeCN, only iodide gave us thermal reduction problems of the *vicinal* dibromides (section 3.3(i)).

The realization that bromide can reduce our transient β-bromo radicals brought two points instantly to mind: one, the reducing ability of the halides parallels their trend in nucleophilicity, and two, the concentrations of bromide in the 1,2-dibromoethane study[2] may have reduced the β-bromoethyl radical, thus preventing its observation.

The first point could lead to some flexibility and increased resolution in our studies. If we can trap the bromine atoms with the less-nucleophilic chloride or fluoride ions to form visible $BrX^{\cdot-}$ radical anions, then we may limit the halides involvement in the chemistry. Recall that "a probe" should not participate in the chemistry. Note from chapter 3 that these trapping reactions are possible, but, at the time of the $Si(DBE)_4$ experiment , we had not studied the $BrX^{\cdot-}$ complexes. It was the observation of the bromide dependence of the reduction of the β-bromo radical from $Si(DBE)_4$ that spawned all of the research in this thesis.

The second point that came to mind was that, if bromide is reducing the β-bromo radical, then it is conceivable that the β-bromoethyl radical with a significant lifetime does exist, but it was reduced by the excess bromide in solution before it could be seen. Using the less nucleophilic halides should increase our chances of observing the β-bromoethyl radical.

4.2 The Kinetics of the Photochemical Debromination of *Vicinal* Dibromides in the Presence of a Halide Trap/Probe

Before we continue, we should evaluate the kinetic scheme that was eventually used to fit all of the halide quenching data obtained.

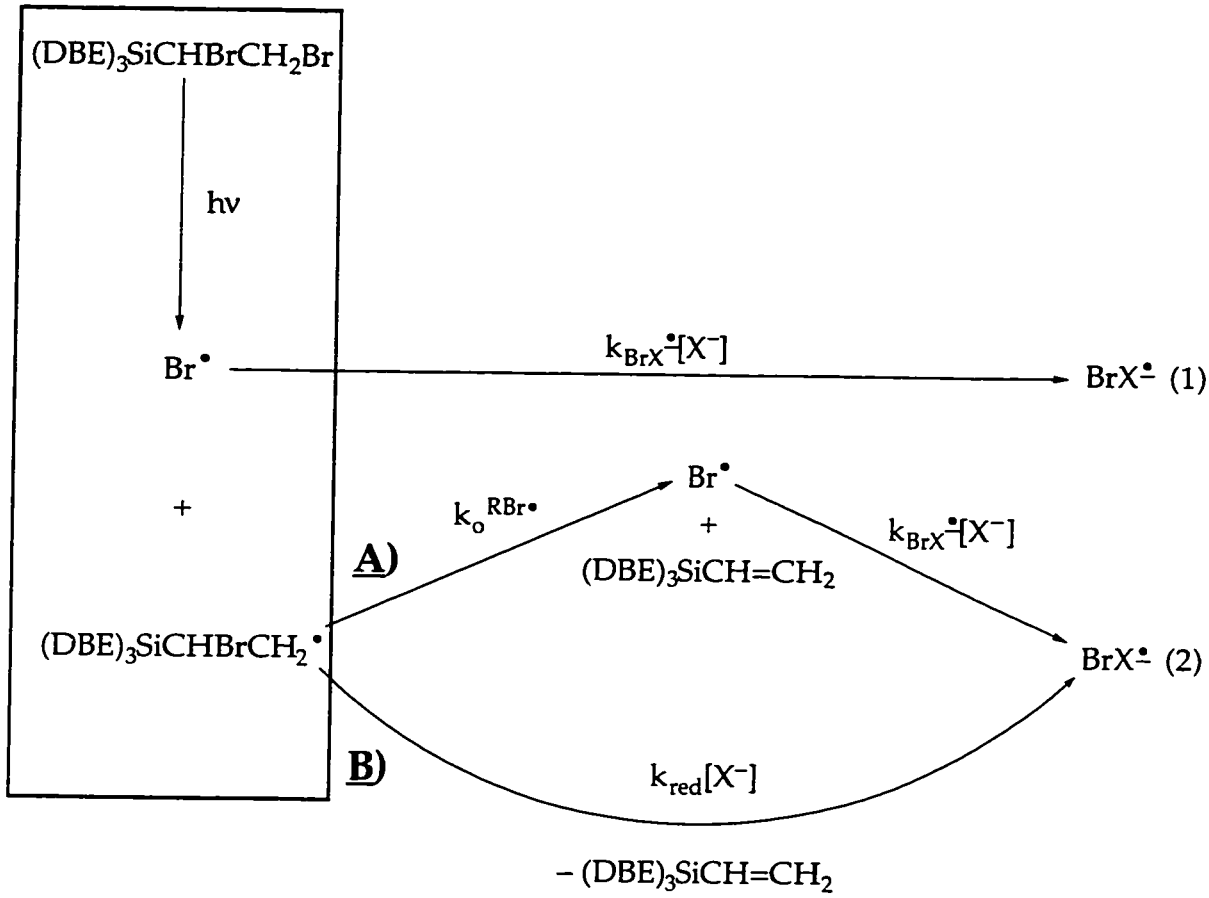

Scheme 4-1 The kinetic scheme of the photochemical debromination of $Si(DBE)_4$ in the presence of halide probe (X^-).

Scheme 4-1 shows the pathways accessible to the photoproducts of the irradiation of $Si(DBE)_4$ in the presence of halide. The scheme shown is for $Si(DBE)_4$, but it can be applied to any *vicinal* dibromide. After photolysis, two equivalents of $BrX^{\bullet}$ are ultimately produced. The first $BrX^{\bullet}$ equivalent comes from the direct trapping of the bromine atom. The second $BrX^{\bullet}$ equivalent comes from the decay of the β-bromo radical.

(i) The 1st Equivalent, $BrX^{\bullet}$ (1)

The first equivalent of $BrX^{\bullet}$ comes from the $Br^{\bullet}$ produced directly by photolysis of the $Si(DBE)_4$. This equivalent of $BrX^{\bullet}$ is produced at the rate of halide trapping and decays initially by a first-order decay. Equation 3.39 is the expression for a consecutive growth

and decay mechanism derived in chapter 3. At all halide concentrations that the $BrX^{\bullet}$ complexes are detectable, $k_{probe} >> k_{1^{\circ}decay}$, therefore the pre-exponential factor reduces simply to $-[Br^{\bullet}]_o$ and the equation rearranges to that of Equation 4.5.

$$[BrX^{\bullet}]_t^{(1)} = \frac{[Br^{\bullet}]_o k_{probe}}{k_{1^{\circ}decay} - k_{probe}}\left(e^{-k_{probe}t} - e^{-k_{1^{\circ}decay}t}\right) \qquad \textbf{Equation 3.39}$$

$$[BrX^{\bullet}]_t^{(1)} = [Br^{\bullet}]_o\left(e^{-k_{1^{\circ}decay}t} - e^{-k_{probe}t}\right) \qquad \textbf{Equation 4.5}$$

If all the photolytically produced bromine atoms were converted to $BrX^{\bullet}$ radical anions, then the concentration of $BrX^{\bullet}$ at infinite time would be equal to the initial concentration of bromine atoms immediately after photolysis (Equation 4.6). The expression of Equation 4.7 gives us the concentration of $BrX^{\bullet}$ (1) at a given time, t.

$$[Br^{\bullet}]_o = [BrX^{\bullet}]_{\infty}^{(1)} \qquad \textbf{Equation 4.6}$$

$$[BrX^{\bullet}]_t^{(1)} = [BrX^{\bullet}]_{\infty}^{(1)}\left(e^{-k_{1^{\circ}decay}t} - e^{-k_{probe}t}\right) \qquad \textbf{Equation 4.7}$$

Recall from Equation 3.10 that the pseudo-first-order rate constant, k_{probe}, is equal to the sum of the intrinsic rate constant of decay of the bromine atom in the solvent ($k_o^{Br\bullet}$) plus the probe rate constant ($k_{BrX^{\bullet}}$) multiplied by the halide concentration.

$$k_{probe} = k_o^{Br\bullet} + k_{BrX^{\bullet}}[X^-] \qquad \textbf{Equation 3.10}$$

(ii) The 2nd Equivalent, $BrX^{\bullet}$ (2)

The second equivalent of $BrX^{\bullet}$ comes from the decay of the β-bromo radical. The β-bromo radical decays via two pathways, A and B, of Scheme 4-1. Pathway A is a two stage process. The first stage of pathway A is the unimolecular decay of the radical to produce a bromine atom and the olefin. The second stage of pathway A is the trapping of the bromine atom by halide to produce the resulting $BrX^{\bullet}$ radical anion. Pathway B represents the newly discovered halide reduction pathway.[19] The production and subsequent decay of the second equivalent of $BrX^{\bullet}$ can also be expressed by a similar equation to Equation 3.39. Note that in Equation 4.8, k_{probe}, has been replaced by $k_{RBr\bullet}$. The rate constant for the <u>total decay</u> of the β-bromo radical is $k_{RBr\bullet}$ and is equal to the sum of the rate constants for pathways A and B (Equation 4.9). This time, the rates of these modes of $BrX^{\bullet}$ production are not necessarily much greater than the rate of decay, therefore no approximation is made in this case.

$$[BrX^{\bullet}]_t^{(2)} = \frac{[RBr^{\bullet}]_o k_{RBr\bullet}}{k_{1^\circ decay} - k_{RBr\bullet}}\left(e^{-k_{RBr\bullet}t} - e^{-k_{1^\circ decay}t}\right) \qquad \textbf{Equation 4.8}$$

$$k_{RBr\bullet} = k_A + k_B \qquad \textbf{Equation 4.9}$$

At time-zero, as the photon is absorbed, the $Si(DBE)_4$ splits into the two initial fragments. At this time, $[Br^{\bullet}]_o$ is equal to $[RBr^{\bullet}]_o$. We have already shown that $[Br^{\bullet}]_o$ was equal to the concentration of $BrX^{\bullet}$ (1) at infinite time, therefore we can replace the $[RBr^{\bullet}]_o$ term in Equation 4.8 with $[BrX^{\bullet}]_\infty^{(1)}$. Equation 4.10 represents the concentration of the second equivalent of $BrX^{\bullet}$ at any time, t.

$$[BrX^{\bullet}]_t^{(2)} = \frac{[BrX^{\bullet}]_\infty^{(1)} k_{RBr\bullet}}{k_{1^\circ decay} - k_{RBr\bullet}}\left(e^{-k_{RBr\bullet}t} - e^{-k_{1^\circ decay}t}\right) \qquad \textbf{Equation 4.10}$$

(iii) The Combined Equation

Naturally, the observed signal is a combination of the time-resolved production of both equivalents of $BrX^{\bullet}$. The addition of Equation 4.5 and Equation 4.10 leads to the overall expression Equation 4.12.

$$[BrX^{\bullet}]_t^{total} = [BrX^{\bullet}]_t^{(1)} + [BrX^{\bullet}]_t^{(2)} \qquad \textbf{Equation 4.11}$$

$$[BrX^{\bullet}]_t^{total} = C + [BrX^{\bullet}]_{\infty}^{(1)}\left(e^{-k_{1°decay}t} - e^{-k_{probe}t}\right) + \frac{[BrX^{\bullet}]_{\infty}^{(1)} k_{RBr\bullet}}{k_{1°decay} - k_{RBr\bullet}}\left(e^{-k_{RBr\bullet}t} - e^{-k_{1°decay}t}\right) \qquad \textbf{Equation 4.12}$$

The constant, C, has been added to account for the non-$BrX^{\bullet}$ related spontaneous jump that is observed. On very short time-scales, the constant, C, has to be given a time-dependent exponential factor to account for the finite rise-time of the LFP system. To determine the rise-time of the system, an instantaneous signal was recorded at the highest resolution of the system. The LFP of 1,2-dibromoethane in the presence of 100 mM bromide was recorded at 360 nm in MeCN. The growth rate constant of the subsequent "instantaneous" trace was determined to be 144 μs^{-1}. Using this system-dependent rise-time constant (k_{sys}), the constant C was modified according to Equation 4.13.

$$C = C' - C'e^{-144t} \qquad \textbf{Equation 4.13}$$

The change in optical density (ΔO.D.) produced by the $BrX^{\bullet}$ radical anions is proportional to the concentration of the radical anions according to the Beer-Lambert Law[20] (Equation 4.14).

$$\Delta O.D. = \varepsilon[BrX^{\bullet-}]l \qquad \textbf{Equation 4.14}$$

Because the ΔO.D. and $[BrX^-]$ are directly proportional, the ΔO.D. can be substituted into Equation 4.12. Equation 4.15 is the final form of the expression.

$$\Delta O.D._t^{total} = C' - C'e^{-144t} + \Delta O.D._\infty^{(1)}\left(e^{-k_{1°decay}t} - e^{-k_{probe}t}\right) + \frac{\Delta O.D._\infty^{(1)} k_{RBr\bullet}}{k_{1°decay} - k_{RBr\bullet}}\left(e^{-k_{RBr\bullet}t} - e^{-k_{1°decay}t}\right) \qquad \textbf{Equation 4.15}$$

At each concentration of halide, the pseudo-first-order value of k_{probe} could be calculated according to Equation 3.10. This value was then input into the fitting equation for that particular halide concentration. The concentration of fluoride in the bromine atom probing experiment of Figure 4-6 was 2.06 mM, therefore the value of k_{probe} was fixed at 21 μs^{-1} during the fitting iterations.

$$k_{probe} = 1 \times 10^{-5} s^{-1} + \left(1.0 \times 10^{10}\ M^{-1}s^{-1}\right)\left(2.06 \times 10^{-3}\ M\right)$$
$$= 2.07 \times 10^{7}\ s^{-1}$$
$$= 21\ \mu s^{-1}$$

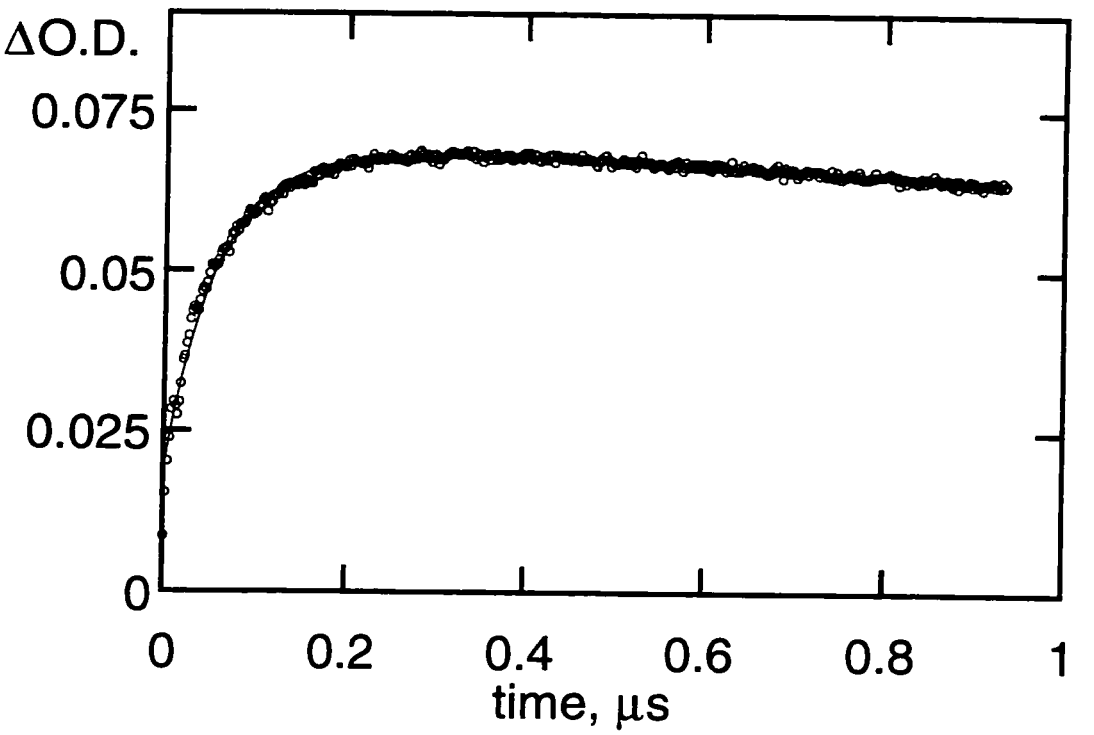

Figure 4-6 **The jump, growth, and decay signal of the $Br_2^{\cdot-}$ complex generated from the 2.06 mM fluoride trapping of the LFP of 1,2-dibromopropane in MeCN. The line represents the fit by Equation 4.15 to the points.**

Note that the data obtained from the LFP system is in units of microseconds (μs), therefore any rate constants input into the fitting routine or determined by the routine will be in inverse microseconds (μs^{-1}).

The calculated line fits very well to the experimental points. Table 4-A shows the values calculated for Figure 4-6 by Kaleidagraph[21] according to Equation 4.15. A value of 13.9 ± 0.3 μs^{-1} was calculated for $k_{RBr\cdot}$. This value is 33% slower than the 21 μs^{-1} trapping of bromine atoms in the presence of 2.06 mM fluoride. Notice that $k_{RBr\cdot}$ is also two orders of magnitude greater than the value of 0.14 μs^{-1} determined for $k_{1^{\circ}decay\cdot}$.

Table 4-A **The Kaleidagraph output values for the fitting of Equation 4.15 to the points in Figure 4-6. The trace was generated by the 2.06 mM fluoride trapping of the bromine atoms produced by the LFP of 1,2-dibromopropane in MeCN. k_{probe} was fixed at 21 μs^{-1} (2.06 x 10^{-3} M^{-} * 10 x 10^{9} M^{-1} s^{-1}).**

	Value	Error
C'	0.019068	0.00032051
$k_{RBr\bullet}$	13.862 μs^{-1}	0.34261 μs^{-1}
$\Delta O.D._{\infty}^{(1)}$	0.02553	0.0001601
$k_{1^{\circ}decay}$	0.13765 μs^{-1}	0.0060951 μs^{-1}
χ^2	0.00039789	NA
R	0.9928	NA

4.3 The Decay of RBr• in the Presence of Halide

The fitting routine effectively separates the rate of production of the first bromine atom (k_{probe}) from the second ($k_{RBr\bullet}$). With the rates of the second bromine atom's evolution into solution, we can now start to characterize the two pathways of interest, (A) and (B) of Scheme 4-1. Depending on the β-bromo radical, the halide, and the halide concentration, there are three possible outcomes for the growth rate constant, $k_{RBr\bullet}$. In all three cases, the results of the k_{probe} are invariable.

It is useful to separate the quenching plots of the rate constants determined from the kinetic traces into two regimes: the low halide concentration regime (Low [X^-]) and the high halide concentration regime (High [X^-]). Generally, the intersection of the low and high regimes occurs at ~1 mM. The three possible cases for the $k_{RBr\bullet}$ occur in the high halide regime.

(i) Low [X^-] Regime

When the halide concentration is low, the rate of unimolecular decay of the β-bromo radical is much faster than the reduction pathway, therefore all of the β-bromo radicals decay via pathway A of Scheme 4-1. At these low halide concentrations, the rate of unimolecular decay of the β-bromo radicals is also much faster than the trapping of bromine atoms by halide, therefore pathway A is limited by, and equal to the probe rate constant.

$$k_o^{RBr\bullet} >> k_{red}[X^-]$$

$$\therefore k_{RBr\bullet} = k_A$$

$$k_o^{RBr\bullet} >> k_{probe}$$

$$\therefore k_A = k_{probe}$$

$$k_{RBr\bullet} = k_{probe}$$

At low halide concentrations, the rates of $BrX^{\bullet-}$ production for both equivalents are always equal to k_{probe}.

(ii) High [X^-] Regime (see Table 4-B)

(a) Case 1: $k_o^{RBr\bullet} > k_{red}[X^-]$ AND $k_o^{RBr\bullet} > k_{probe}$

When the rate of unimolecular decay of the β-bromo radical is faster that its pseudo-first-order reduction by halide ($k_o^{RBr\bullet} > k_{red}[X^-]$), then the rate of decay of the β-bromo radical will be determined by pathway A of Scheme 4-1. If the unimolecular decay of the β-bromo radical is also faster than the pseudo-first-order trapping of bromine atoms at high halide concentrations ($k_o^{RBr\bullet} > k_{probe}$), then the rate of pathway A will be limited by the trapping process.

$$k_{RBr\bullet} = k_{probe}$$

Under these circumstances, the rate of $BrX^{\bullet-}$ production at high halide concentrations is indistinguishable from the rate at low halide concentrations and is equal to the probe rate (Table 4-B, case 1).

(b) Case 2: $k_o^{RBr\bullet} > k_{red}[X^-]$ AND $k_{probe} > k_o^{RBr\bullet}$

As in case 1, the rate of decay of the β-bromo radical is determined solely by pathway A of Scheme 4-1. This time, however, the rate of bromine atom trapping is faster than the rate of unimolecular decay of the β-bromo radical ($k_{probe} > k_o^{RBr\bullet}$). The rate of β-bromo radical decay is limited by, and equal to the rate the β-bromo radical's unimolecular decay.

$$k_o^{RBr\bullet} >> k_{red}[X^-]$$

$$\therefore k_{RBr\bullet} = k_A$$

$$k_{probe} > k_o^{RBr\bullet}$$

$$\therefore k_A = k_o^{RBr\bullet}$$

$$k_{RBr\bullet} = k_o^{RBr\bullet}$$

The rate of unimolecular decay of the β-bromo radical is not halide dependent, therefore the plot of $k_{RBr\bullet}$ versus halide concentration plateaus (Table 4-B, case 2). The plateau occurs when the halide concentration reaches a level such that the product of $k_{BrX^{\bullet-}}$ times $[X^-]$ is equal to $k_o^{RBr\bullet}$.

(c) Case 3: $(k_o^{RBr\bullet} \sim k_{red}[X^-]) < k_{probe}$

If the rates of the β-bromo radical pathways A and B of Scheme 4-1 are of comparable magnitudes and are less than the probe rate, then the overall rate of decay of the β-bromo radical is equal to the sum of both of the pathways.

$$k_{RBr\bullet} = k_o^{RBr\bullet} + k_{red}[X^-]$$

The simulated quenching plot of Table 4-B (case 3) shows a bend in the line at 1 mM when $k_{RBr\bullet}$ becomes rate-limiting. The slope of the line in the high halide region is equal to k_{red} and the intercept is equal to $k_o^{RBr\bullet}$.

(d) Case 4: ?

One could argue that there is a fourth case to be considered, but it does not turn out to be relevant. The fourth case would have the same equality of paths A and B as case 3 $(k_o^{RBr\bullet} \sim k_{red}[X^-])$, but this time the two rates would be greater than the probe rate. This is not relevant because k_{probe} is diffusion controlled, therefore the pseudo-first-order, bimolecular reduction of the β-bromo radical can never be greater than k_{probe}. Of course, the unimolecular decay is not constrained by diffusion, but case 3 defines the unimolecular decay as being within the same order of magnitude as the pseudo-first-order reduction.

Table 4-B Simulations of the three high-halide kinetic cases

Case 1: $k_o^{RBr\bullet} > k_{red}[X^-]$ **AND** $k_o^{RBr\bullet} > k_{probe}$

Low Regime

$k_{RBr\bullet} = k_{probe}$

High Regime

$k_{RBr\bullet} = k_{probe}$

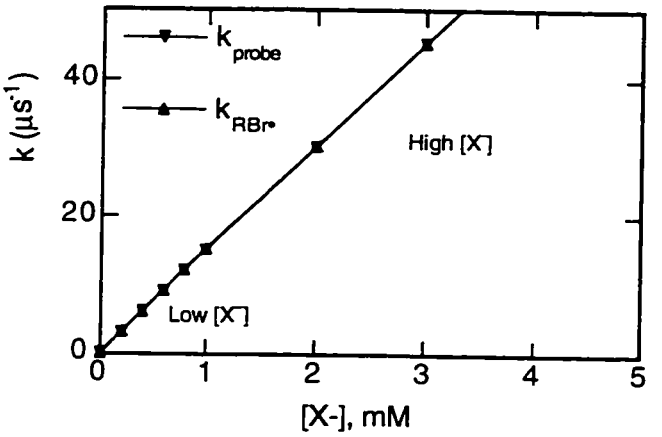

Case 2: $k_o^{RBr\bullet} > k_{red}[X^-]$ **AND** $k_{probe} > k_o^{RBr\bullet}$

Low Regime

$k_{RBr\bullet} = k_{probe}$

High Regime

$k_{RBr\bullet} = k_o^{RBr\bullet}$

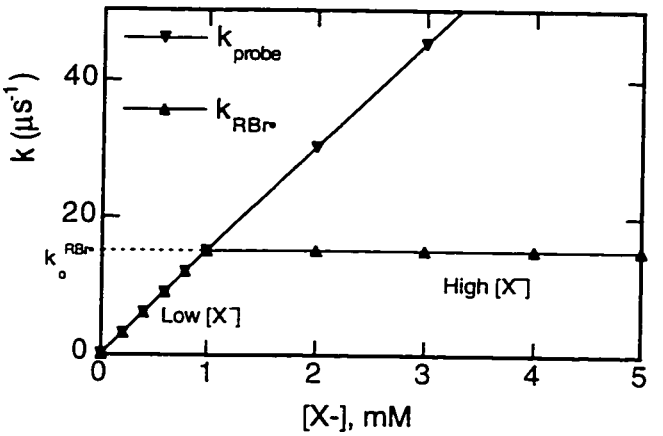

Case 3: $(k_o^{RBr\bullet} \sim k_{red}[X^-]) < k_{probe}$

Low Regime

$k_{RBr\bullet} = k_{probe}$

High Regime

$k_{RBr\bullet} = k_o^{RBr\bullet} + k_{red}[X^-]$

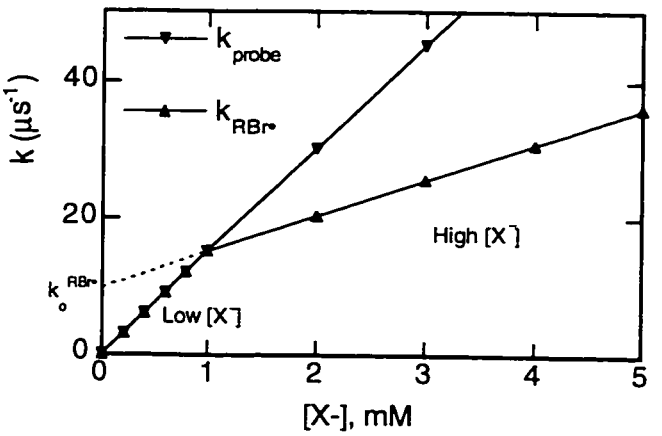

4.4 Halide Reduction of β-bromo Radicals

We saw in section 1.3(i), that the halides (except fluoride) were capable of reducing *vicinal* dibromides to olefins. We have now shown[19] in Figure 4-5 that the β-bromo radical of $Si(DBE)_4$ is also subject to reduction by bromide. The reduction of the $(DBE)_3SiCHBrCH_2^{\bullet}$ radical by bromide proceeded with a rapid, but less than diffusion-controlled rate constant of 5.3×10^9 M^{-1} s^{-1} in MeCN. We reasoned that the use of the less nucleophilic fluoride ion may not reduce the β-bromo radical, therefore making it easier to determine the lifetime of the β-bromo radical.

(i) Fluoride Reduction of β-bromo Radicals

(a) Fluoride Probing of the LFP of $Si(DBE)_4$

$Si(DBE)_4$ was subject to LFP in MeCN in the presence of varying amounts of Bu_4NF. The fluoride complexed with the bromine atoms produced as discussed in chapter 3 to form the $BrF^{\bullet-}$ complex ($\varepsilon_{360} = 6900$ M^{-1} cm^{-1}, $k_{BrF^{\bullet-}} = 1.0 \times 10^{10}$ M^{-1} s^{-1}). Each kinetic trace measured was fit with the expression of Equation 4.15. The values of k_{probe} for each trace were fixed at the appropriate rate constants according to the concentration of fluoride used.

From the values of $k_{RBr^{\bullet-}}$ extracted from each trace, a quenching plot of $k_{RBr^{\bullet-}}$ versus the fluoride concentration was constructed (Figure 4-7). Figure 4-7 shows that the elimination of the bromine atom from the $(DBE)_3SiCHBrCH_2^{\bullet}$ radical in the presence of fluoride follows the kinetics of a case 3 situation much in the same way that it did in the presence of bromide. It is not until higher fluoride concentrations that the mechanism changes to reflect the new rate-limiting steps of unimolecular decay and fluoride reduction of the β-bromo radical. The second region of the fluoride quenching of the second bromine atom from $Si(DBE)_4$ was determined to have a slope of 1.1×10^9 M^{-1} s^{-1} and an intercept of 9.5×10^6 s^{-1} representing the rate of fluoride reduction (k_{red}) and the unimolecular decay of the $(DBE)_3SiCHBrCH_2^{\bullet}$ radical ($k_o^{RBr^{\bullet-}}$), respectively.

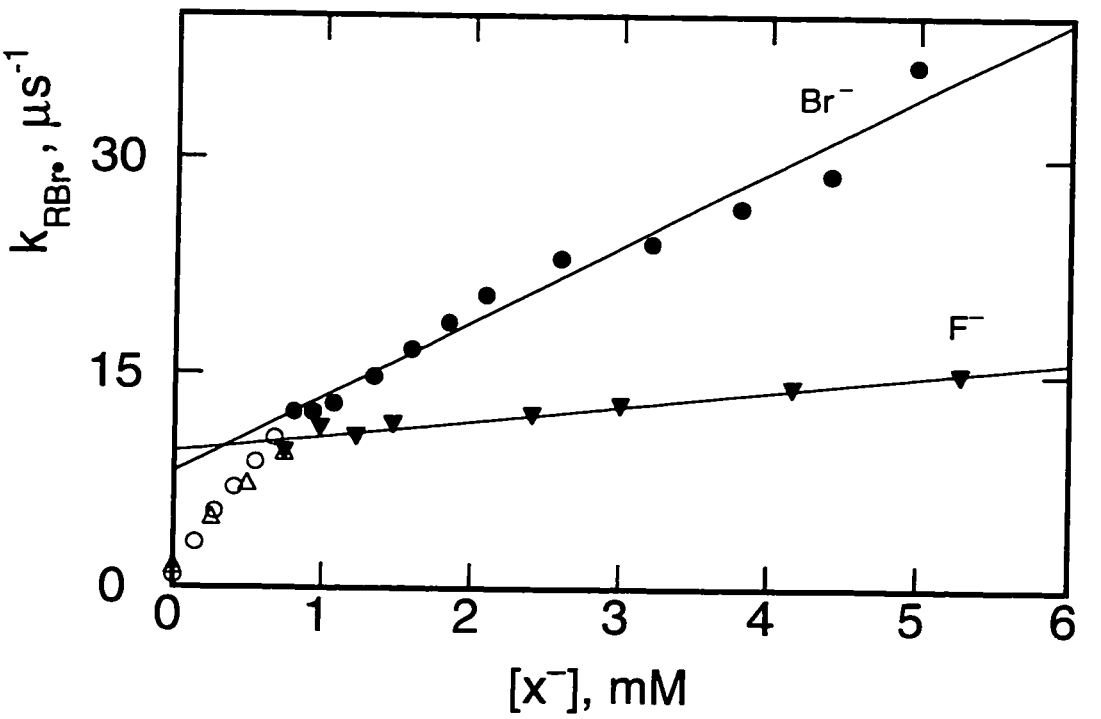

Figure 4-7 **The dependence of the elimination rate constant for the second bromine atom ($k_{RBr\bullet}$) versus fluoride concentration for the LFP of $Si(DBE)_4$ in MeCN.**

The lifetime of the $(DBE)_3SiCHBrCH_2^{\bullet}$ radical as determined by the inverse of the intercept is 105 ns. Recall that the intercept of the analogous bromide plot had an intercept of $8.1 \times 10^6\ s^{-1}$ for a lifetime of 125 ns. Both these numbers represent the lifetime of the same radical, in the same solvent, in the absence of halide and should therefore be identical. The difference between these two numbers reflects the large errors associated with the intercepts of such plots.

Probing the photochemical debromination of *vicinal* dibromides with fluoride has the advantage of a potentially slower β-bromo radical reduction step. The disadvantage of using fluoride is that its tetrabutylammonium salt is much more hygroscopic than the other halide salts and the extinction coefficient of the BrF^- complex is the lowest of the halides. These two minor inconveniences are far outweighed by the advantage of slowing down the β-bromo radical reduction step. Fluoride can now be used to screen the photochemical debrominations of *vicinal* dibromides.

(b) Fluoride Probing of the LFP of 1,2-Dibromoethane

Does the β-bromoethyl radical have a measurable lifetime? The LFP of 1,2-dibromoethane in MeCN showed case 3 kinetics when the system was probed with Bu_4NF (Figure 4-8). The rate constant for the β-bromoethyl radical reduction by fluoride (k_{red}) was determined from the slope of the high-halide region to be 3.5 x 10^9 M^{-1} s^{-1}. According to the intercept of the high-halide plot, the β-bromoethyl radical has a unimolecular rate constant of decay of 6.9 x 10^6 s^{-1} for a lifetime of 145 ns in MeCN.

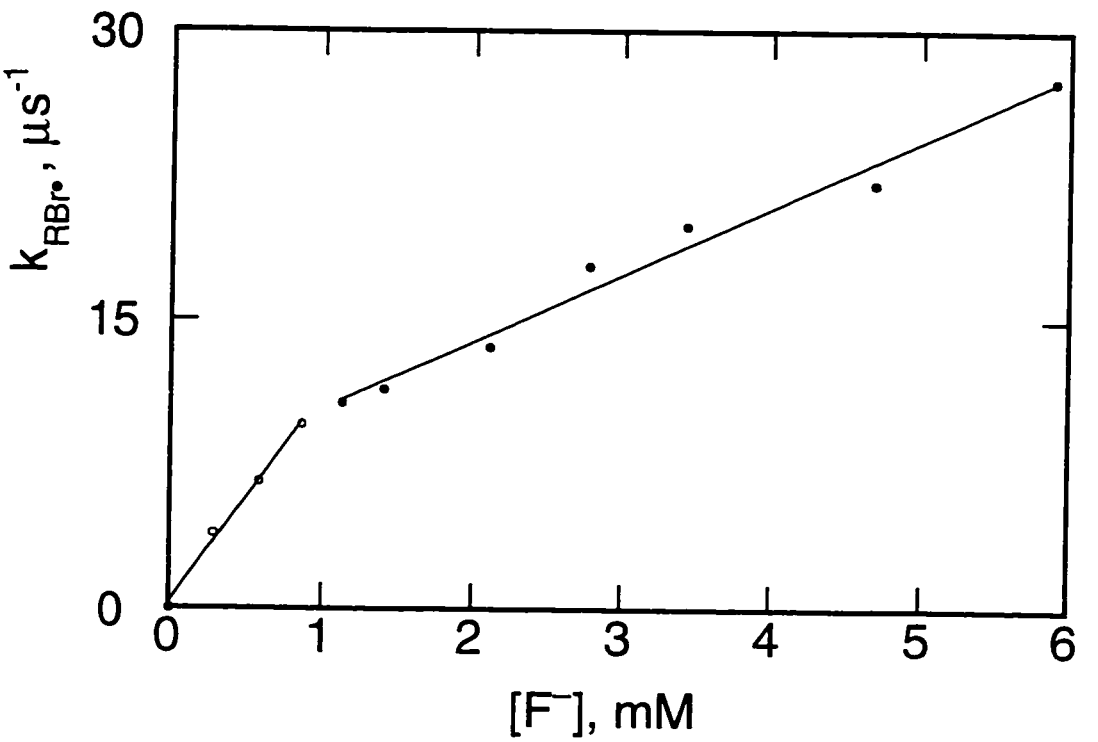

Figure 4-8 **The fluoride dependence of $k_{RBr\bullet}$ for the LFP of 1,2-dibromoethane in MeCN at 296 K. The traces were monitored at 360 nm.**

In the original report, Scaiano *et al.* unfortunately used case 1 conditions in order to look for the β-bromoethyl radical.[2] Within the detection limits of our LFP system, there is no concentration of bromide that makes $k_o^{RBr\bullet} + k_{red}[Br^-]$ less than k_{probe}, therefore the β-bromoethyl radical will always have case 1 kinetics in the presence of bromide. Chloride

was also determined to have a case 1 kinetic effect on the β-bromoethyl radical. Only fluoride showed kinetics other than case 1.

(c) The Three Kinetic Cases of Fluoride

Fluoride is the only halide so far that has allowed us to see examples of all three kinetic cases from the *vicinal* dibromides studied. We have already seen two fluoride case 3 examples for $Si(DBE)_4$ in Figure 4-7 and 1,2-dibromoethane in Figure 4-8.

A case 2 plateau was observed for *trans*-1,2-dibromocycloheptane (Dibromide **XI**). The fluoride dependence of the k_{RBr^-} for *trans*-1,2-dibromocycloheptane plateaus at 10.2 μs^{-1}. Figure 4-9 shows the rate constant of elimination of the bromine atom from the β-bromocycloheptyl radical becoming rate-limiting at ~0.8 mM fluoride. At this concentration of fluoride, the rate of BrF^- growth is equal to the rate of unimolecular decay of the radical. Of the compounds studied, this is the only one to show a plateau under any conditions. When bromide is used, the β-bromocycloheptyl radical is reduced with a rate constant (k_{red}) of $1.9 \times 10^9\ M^{-1}s^{-1}$.

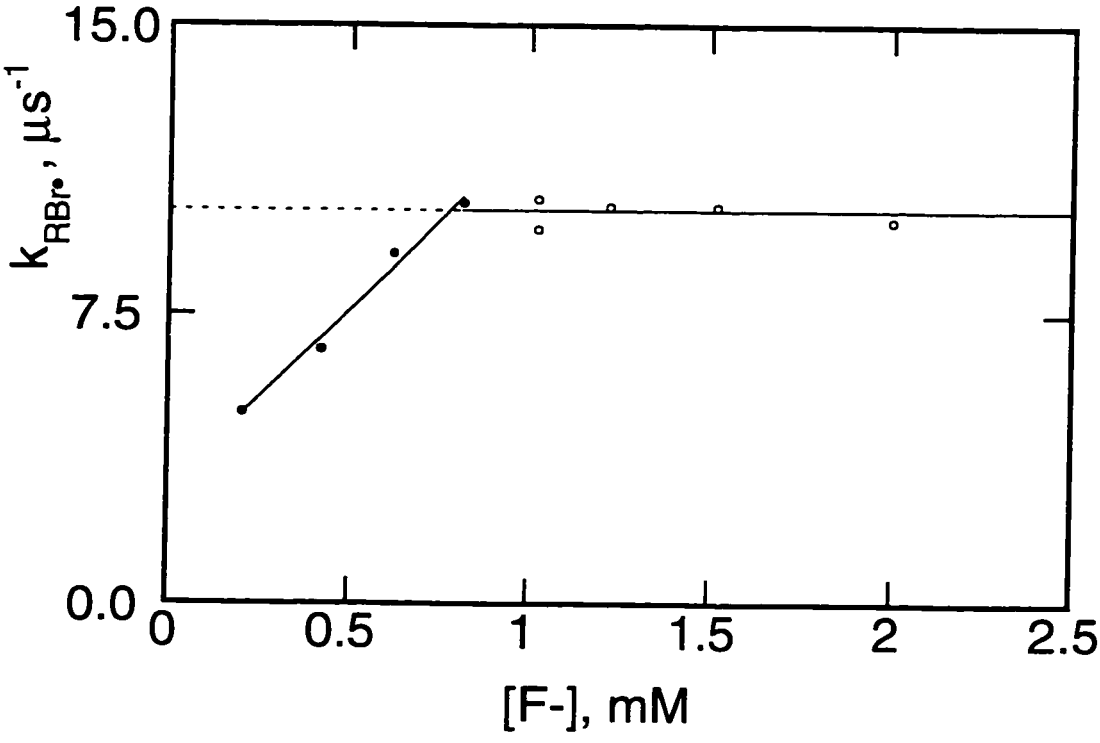

Figure 4-9 **The fluoride dependence of $k_{RBr\bullet}$ for the LFP of *trans*-1,2-dibromocycloheptane in MeCN.**

Fluoride proved to be an excellent probe. Only a single case 1 example was observed for the *vicinal* dibromides studied. Only the photolysis of 1,2-dibromo-1,1-difluoroethane (Dibromide **I**) failed to show a reduction of the $k_{RBr\bullet}$ rate constant at high fluoride concentrations. For this *vicinal* dibromide $k_{RBr\bullet}$ was equal to k_{probe} for all fluoride concentrations up to the detection limit of the system (Figure 4-10).

1,2-dibromo-1,1-difluoroethane became our new kinetic standard. Under all halide conditions in MeCN, 1,2-dibromo-1,1-difluoroethane always shows case 1 kinetics. For all intents and purposes, the photolysis of 1,2-dibromo-1,1-difluoroethane is an instantaneous source of two equivalents of $BrX^{\bullet}$.

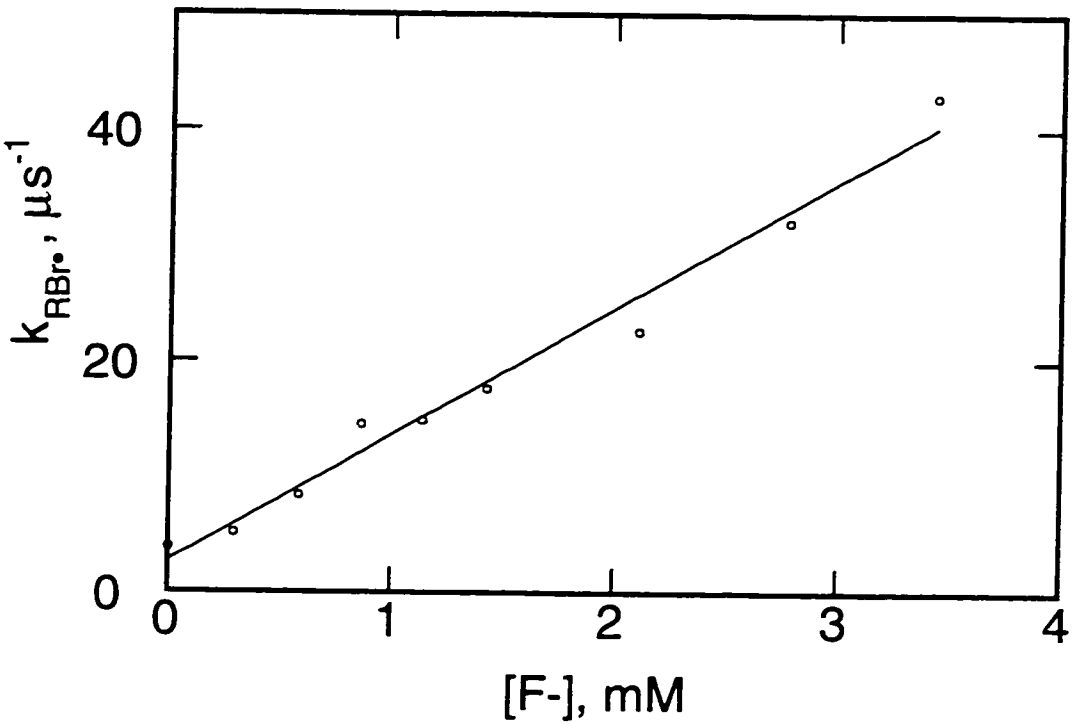

Figure 4-10 **The fluoride dependence of the rate constant of the elimination of the bromine atom from the 2-bromo-1,1-difluoroethyl radical ($k_{RBr\bullet}$) in MeCN.**

(ii) Reduction of β-bromo Radicals by the Halide Series

Figure 4-11 is a theoretical representation of what we would expect for a typical β-bromo radical/halide series quenching plot. Figure 4-11 is a plot of the total decay of the β-bromo radical ($k_{RBr\bullet}$) versus halide concentration for all the halides. In this theoretical plot, the bromide, chloride, and fluoride quenchings are presented as high-halide case 3 examples. The iodide quenching of the β-bromo radical is presented as a high-halide case 1 example.

The thick gray line represents the combined average probe rate constants for all the halides ($k_{BrX}^{\ddagger} \sim 10^{10}\ M^{-1}\ s^{-1}$). Any one halide experiment is initially limited by the trapping process (the gray line) until the total decay of the β-bromo radical becomes rate-limiting at the intersection of the halide lines with the trapping line. The thick dashed line represents the detection limit of our LFP system.

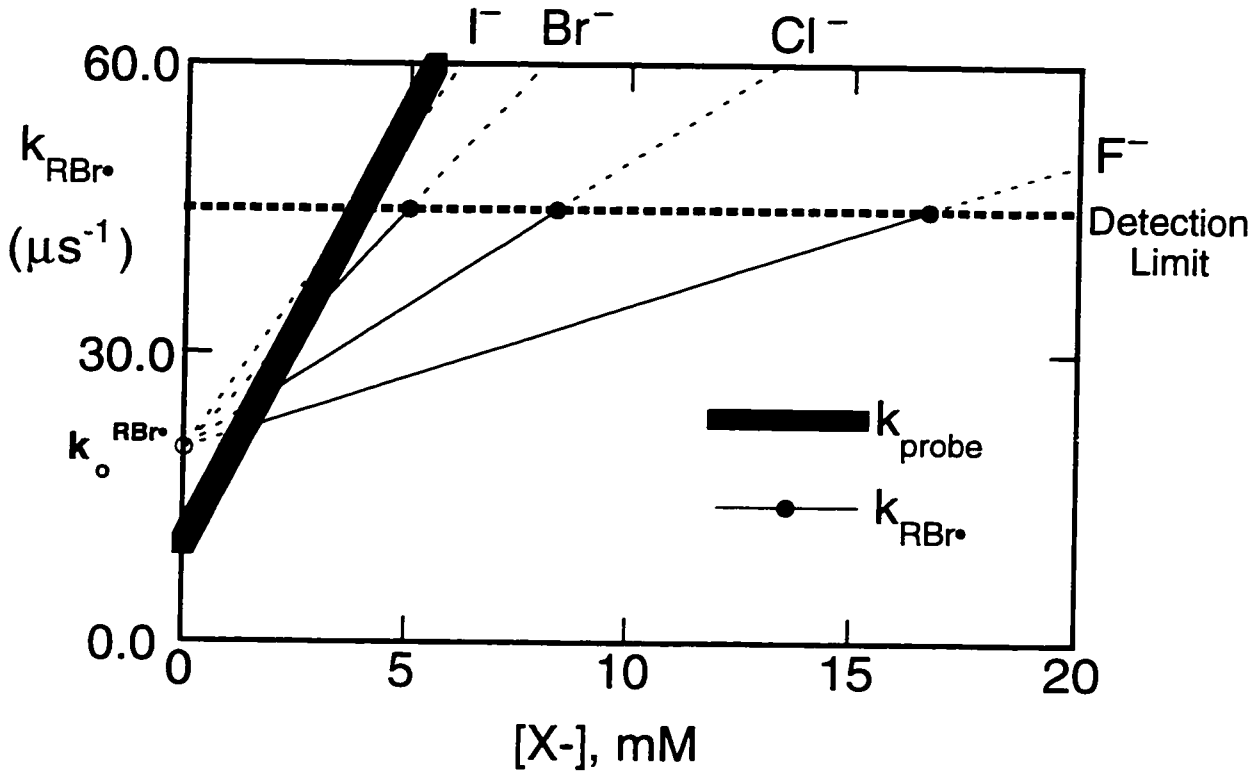

Figure 4-11 **A theoretical comparison of the β-bromo radical quenching plots for the halides.**

We can see in Figure 4-11 that the theoretical $k_{RBr•}$ plot for iodide does not intersect the k_{probe} plot until it is at (or close to) the detection limit of the system. As it is shown, one could argue that the iodide dependence is case 1 up to the detection limit, but case 3 above the detection limit. For obvious reasons, we are only concerned with classifying the cases up to the detection limit of the LFP system.

We expect the halide reduction rates to parallel the nucleophilic trend, i.e. the rate of β-bromo radical reduction should increase from fluoride to iodide. All of the β-bromo radical/halide quenching plots should converge at the same intercept. The common intercept represents the rate of halide-independent unimolecular decay of the β-bromo radical ($k_o^{RBr•}$).

The key point to emphasize with Figure 4-11 is that all the information related to the β-bromo radicals ($k_{RBr\bullet}$), for a particular halide experiment, is contained in the region where the trapping process is no longer rate-limiting and is below the detection limit. This useful region of each high-halide plot is demonstrated with a solid line terminated with black dots (●—●).

Note that the $k_{RBr\bullet}$ regions get smaller and steeper as the rates of β-bromo radical reduction get faster going from fluoride to bromide. In the bromide case, there is a very small and steep range to obtain data, therefore any errors in measurement would lead to very large errors in the slope and the intercept. For this reason, the fluoride reduction plots are considered to be the most reliable sources of the intercept for a given β-bromo radical.

Typically, once the fluoride dependence has been established, the intrinsic β-bromo radical decay rate constant ($k_o^{RBr\bullet}$) determined is then used as the intercept for the other halide $k_{RBr\bullet}$ plots. In other words, the plots of the other halides are forced through the fluoride plot's intercept.

Figure 4-12 is an example of the bromide and chloride plots of $Si(DBE)_4$ being forced through the fluoride intercept. Figure 4-13, on the other hand, is the same three halide plots of $Si(DBE)_4$ when their intercepts are not fixed. In either plot, the slopes (k_{red}) increase from fluoride to bromide.

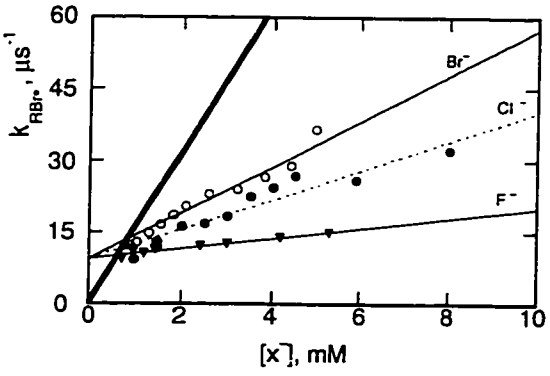

Figure 4-12 The halide dependence of $k_{RBr^{\bullet}}$ for $Si(DBE)_4$ in MeCN at 296K. The bromide and chloride linear fits have been forced through the 9.5 μs^{-1} intercept of the fluoride line.

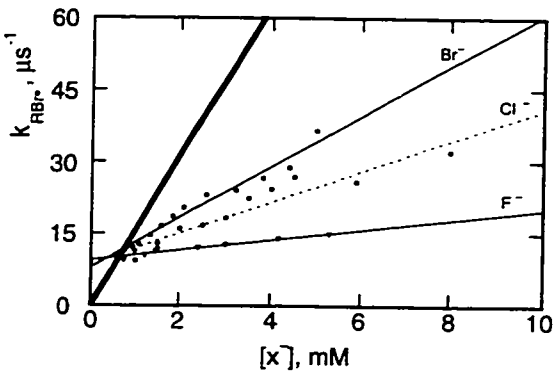

Figure 4-13 The halide dependence of $k_{RBr^{\bullet}}$ for $Si(DBE)_4$ in MeCN at 296K. The bromide and chloride linear fits have NOT been forced through the 9.5 μs^{-1} intercept of the fluoride line.

Table 4-C shows a comparison of the data obtained when the bromide and chloride linear regressions are forced through the fluoride intercept (Figure 4-12) versus when their intercepts are not fixed (Figure 4-13). The rate constants can vary within 10%, but the big difference occurs in the lifetime of the radical obtained. Notice that the lifetime ranges from 125 ns to 105 ns based on the intercepts predicted by the bromide and fluoride plots respectively. In almost all *vicinal* dibromide cases, when the halide plots are not forced through the fluoride intercept, the radical lifetimes predicted (τ_o) by bromide and chloride plots are usually underestimates of the real radical lifetimes.

Table 4-C **A comparison of the high-halide data for the LFP of Si(DBE)$_4$ in MeCN when the intercepts are fixed at the fluoride intercept versus when they are not fixed.**

		F^-	Cl^-	Br^-
$k_o^{RBr\bullet}$ fixed at 6.2 μs^{-1}	$k_{red}/10^9$ M^{-1} s^{-1}	1.1	3.1	4.8
$k_o^{RBr\bullet}$ NOT fixed	$k_{red}/10^9$ M^{-1} s^{-1}	1.1	3.2	5.3
	τ_o (ns)	105	92	125

Table 4-D is a compilation of the β-bromo radical lifetimes (τ_o) and halide reduction rates (k_{red}) determined to date. Several compounds only have entries for bromide quenching. These compounds were studied before the general mechanism was determined. At the time when they were studied, the kinetic traces were fit with a single exponential. A plot of the rate constants determined versus bromide concentration showed slight deviations from the probe quenching line, but the deviations were not very drastic and were attributed to experimental error. Once the mechanism for halide reduction of β-bromo radicals was determined, the kinetic traces of these compounds were re-fit with Equation 4.15. The kinetic traces fit much better to Equation 4.15 than the previous single exponential. The rate constants for the total β-bromo radical decay ($k_{RBr\bullet}$) determined from Equation 4.15 showed the expected bent plot (case 3) as the β-bromo radical decay becomes rate-limiting.

Table 4-D **A compilation of β-bromo radical lifetimes and their rates of reduction by fluoride, chloride, and bromide. An entry of "case 1" refers to the fact that the particular experiment never altered from the probe rate constant, therefore no lifetime could be determined.**

	vicinal dibromide $\xrightarrow{h\nu}$ β-bromo radical	$k_{red}/10^9\ M^{-1}s^{-1}$			$\tau_o^{RBr\bullet}$ (ns)		
		F^-	Cl^-	Br^-	F^-	Cl^-	Br^-
I	1,2-dibromo-1,1-difluoroethane 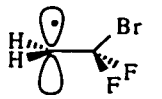	> 10	> 14	> 16	case 1	case 1	case 1
II	1,2-dibromoethane 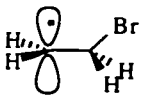	3.5	> 14	>16	145	case 1	case 1
III	1,2-dibromopropane 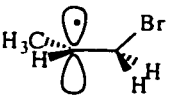	4.0		7.4 (7.0)	208		138
IV	1,2-dibromobutane 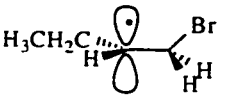			7.4			117
V	1,2-dibromo-3,3-dimethylbutane 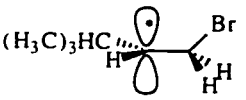	1.6		> 16	192		case 1
VI	2,3-dibromobutane 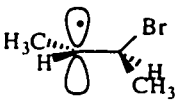			8.1			138
VII	1,2-dibromo-2-methylpropane 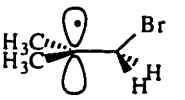	3.9	7.9 (7.5)	9.6 (8.0)	155	108	128

	vicinal dibromide $\xrightarrow{h\nu}$ β-bromo radical	k_{red} /10^9 $M^{-1}s^{-1}$			$\tau_o^{RBr\bullet}$ (ns)		
		F^-	Cl^-	Br^-	F^-	Cl^-	Br^-
VIII	Gyro 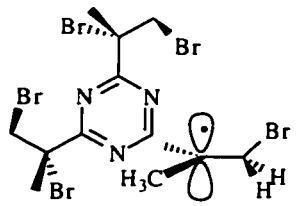	3.91			235		
IX	*trans*-1,2-dibromocyclopentane 	1.3	2.0 (1.8)	3.2 (2.0)	100	65	60
X	*trans*-1,2-dibromocyclohexane 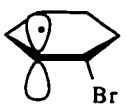	1.0	5.11 (4.5)	5.0 (3.9)	117	85	70
XI	*trans*-1,2-dibromocycloheptane 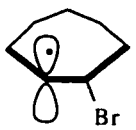	< 0.5	1.5 (0.9)	1.9 (1.0)	98	42	30
XII	*trans*-10,11-dibromodibenzosuberone 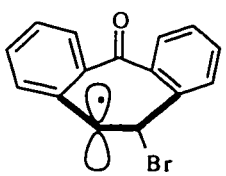			8.0			146
XIII	$Si(DBE)_4$ 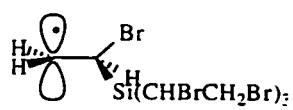	1.1	3.6 (3.1)	5.3 (4.8)	105	92	125
XIV	1,2-dibromoethyl-diethylmethylsilane 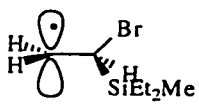			3.3			85
XV	2,3-dibromopropyl-trimethylsilane 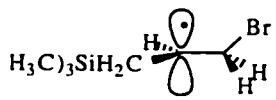			8.3			149

4.5 The Stability and Reactivity of β-Bromo Radicals in the Presence of Halides

It is difficult to discuss the stability and reactivity of β-bromo radicals separately because they are both influenced by many of the same parameters. In addition to the effects of hyperconjugation, steric hindrance, as well as inductive and resonance stabilization/destabilization caused by substitution, β-bromo radicals are stabilized by bromine atom bridging. Bromine atom bridging has not been directly observed in the present LFP study, but the results obtained join the long list of indirect proof of the bridge's existence.

The present study surpasses the previous indirect studies because the LFP/halide trapping is capable of directly monitoring the evolution of the β-bromo radicals. The present study offers for the first time conclusive proof and quantification of the transient lifetimes of a series of β-bromo radicals. While this technique has not been able to directly observe the bromine atom bridge, so far, the LFP/halide trapping has brought the field one step closer. The discovery that halides will reduce the β-bromo radicals makes it possible to study the effects of substituents on the β-bromo radicals.

(i) The β-Bromoethyl Radical

We have seen through a series of product studies that most β-bromoalkyl radicals must have short, but measurable lifetimes. Table 4-D confirms that the lifetimes of β-bromoalkyl radical appear to be in the 100 to 200 ns range. This would explain why the detection of the β-bromo radicals have eluded low time resolution techniques such as ESR and CIDNP. The lack of LFP detection of β-bromo radicals before this work was due to an unfortunate choice of reaction probe, namely bromide.

In 1994, Merényi and Lind monitored the pulse radiolysis of 1,2-dibromoethane in water (Equation 4.16).[22] The decay of the β-bromoethyl radical produced (Equation 4.17) was monitored by probing the production of bromine atoms using promethazine (Equation 4.18). The authors determined a limiting rate constant of $3.8 \pm 0.3\ \mu s^{-1}$ for the formation

of the promethazinium radical cation. This rate constant represents the limiting β-bromoethyl radical decay and is equal to a lifetime of 263 ns in water.

$$e^-_{aq} + BrCH_2CH_2Br \longrightarrow BrCH_2CH_2^{\bullet} + Br^- \qquad \textbf{Equation 4.16}$$

$$BrCH_2CH_2^{\bullet} \xrightarrow{k_o^{RBr^{\bullet}}} CH_2CH_2 + Br^{\bullet} \qquad \textbf{Equation 4.17}$$

$$Br^{\bullet} + \text{Promethazine} \longrightarrow Br^- + \text{Promethazine}^{+\bullet} \qquad \textbf{Equation 4.18}$$

We determined the lifetime of the β-bromoethyl radical to be 145 ns in MeCN using fluoride as a probe. The longer aqueous lifetime may reflect a partial dipole in the intermediate radical. Classical radicals are rather solvent independent due to their electronic neutrality. The bromine-bridged radicals, however, may have an unusual dipolar character. If the bromine atom were bridged to two carbon atoms, one would expect a stronger dipole for an asymmetrically, rather than a symmetrically, bridged radical. Many groups suggest that halide-bridged radicals are indeed asymmetrical.[13,14,17,18,23,24]

An asymmetrical bridge is easy to imagine for an asymmetrically substituted radical, but there seems to be evidence that β-chloroethyl[17] and β-bromoethyl[23] radicals are also asymmetrically bridged. Asymmetrical bridging in a symmetrical radical suggests that the two bonds in the bridge are not equivalent. This would occur if the stabilization to the radical center offered by the bromine atom was in the form of a lone pair. This would create a two-centered, three-electron bond between the bromine atom and the carbon-centered radical.

Shoute and Neta have suggested such two-centered, three-electron bonds for the charge transfer complexes of bromine atoms with bromoalkanes.[25] In the case of β-bromo radicals, the two-centered, three-electron bond would be an intramolecular equivalent of

Shoute and Neta's charge transfer complexes. The intramolecular complexation would cause rehybridization at both carbon centers, but not to the same extent.

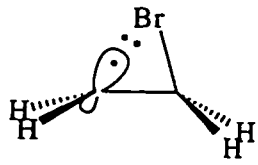

Intramolecular 2c3e bond

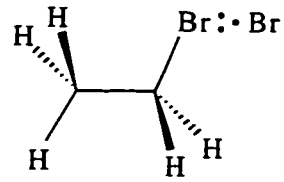

Intermolecular 2c3e bond

Figure 4-14 Two-centred, three-electron bonding between a bromoalkane and a radical centre.

This proposed two-centered, three-electron bond would satisfy the observed non-equivalence, while still maintaining the stereochemical control offered by a bridged radical. The structure of other substituted β-bromo radicals would range from the asymmetrical intramolecular complex to that of a more classical open-radical depending on the effect of the various substituents.

(ii) The Effect of Fluorination

Dibromide **I** and Dibromide **II** of Table 4-D show that the presence of fluorine substituents either destabilize the β-bromo radical or increase the radical's reactivity to the halides relative to the β-bromoethyl radical. 1,2-dibromo-1,1-difluoroethane shows case 1 kinetics for all three of the halide probes. With case 1 kinetics there is no way to tell whether both or either k_o^{RBr} or $k_{red}[X^-]$ is greater than $k_{BrX}^{\cdot}[X^-]$.

Since the 2-bromo-2,2-difluoroethyl radical is the only radical studied to show case 1 kinetics with fluoride, we would suggest that the high decay rate constant reflects a very short radical lifetime rather than a rapid fluoride reduction. Electron-withdrawing groups like fluorine are capable of resonance stabilizing a radical center, but it is the inductive destabilizing effect of electron-withdrawing groups that seem to have the most influence on radical chemistry. This inductive destabilization stems from the partial polar characteristic

of the transition state for radical formation, but how does this induction affect an already formed β-bromo radical?

If β-bromo radicals are asymmetrically bridged due to a two-centered, three-electron bond (Figure 4-14), then there would be more dipolar character to the radicals than would normally be expected. The presence of fluorine substituents would serve to further destabilize the dipole of the β-bromo radical (Figure 4-15).

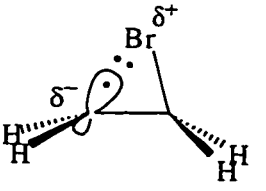

Figure 4-15 The dipolar character of the intramolecular two-centred, three-electron bridged β-bromoethyl radical

(iii) The Effect of Alkyl Substitution

Alkyl substitution can lengthen a β-bromo radical's lifetime in two ways. The first way is to increase the natural lifetime of the β-bromo radical via hyperconjugation. This is observed by an increase in $\tau_o^{RBr\bullet}$. The addition of an α-methyl group increased the β-bromo radical lifetime from 145 ns for the β-bromoethyl radical (II, Table 4-D), to 208 ns for the 1-bromo-2-propyl radical (III, Table 4-C).

The second way alkyl substitution can increase a radical's lifetime is to sterically hinder reactions of the radical. Steric hindrance was shown to extend the lifetime of **Triarylmethyl Radical II** indefinitely even in the solid state.[26] The analogous radical, **Triarylmethyl Radical I**, has increased resonance stabilization over **Triarylmethyl Radical II** due to its planar structure, yet the planar radical exists primarily as a dimer in solution.

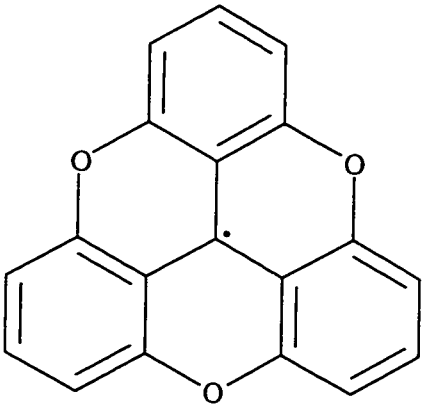

Triarylmethyl Radical I

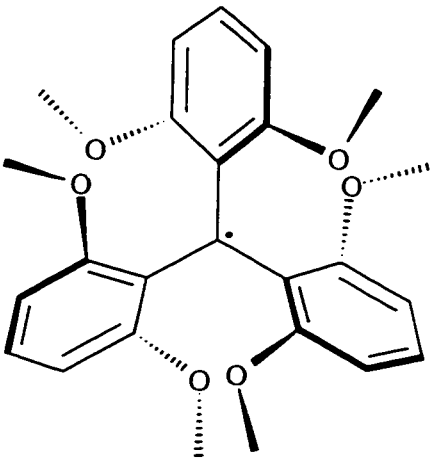

Triarylmethyl Radical II

The β-bromo radicals produced in the present LFP study are too unstable and too low in concentration to be affected by dimerization. They are, however, subject to the bimolecular reduction by the halide probe anions in solution. The β-bromoethyl radical reacts with bromide at the diffusion limit, while all of the alkyl substituted β-bromoethyl radicals have measurable bromide reduction rates except for the bromo-t-butylethyl radical (V, Table 4-D). The bromo-t-butylethyl radical does have the slowest fluoride reduction rate of the alkylethyl radicals.

The apparent anomolously fast bromide reduction of the bromo-t-butylethyl radical may reflect a trade-off. The t-butyl group hyperconjugatively stabilizes the radical center therefore opening up the bromine bridge and exposing the bromine atom to bromide attack. The other bromo-alkylethyl radicals cause the same opening of the bridge, but it is the t-butyl group's bulk that forces the bridge open more than the other groups.

The more the bromine atom bridges to the radical center, the more pyramidal the radical center becomes. Conversely, the more the alkyl groups stabilize the radical center, the less bromine-bridging, and therefore the more planar the radical center. The bromo-t-butylethyl radical is a primary radical like most of the rest of the alkyl series, therefore its hyperconjugative stabilization should be no more than the rest. It is the bulk of the t-butyl

group that forces the radical closer into planarity thus further opening the bromide-bridge and exposing the bromine atom to bromide attack. The low fluoride reduction of the bromo-t-butylethyl radical reflects the lower nucleophilicity of the fluoride anion. Under the less reactive fluoride conditions, the bulk of the t-butyl group becomes the dominant factor.

This trade-off is observed for most of the more stable radicals. Groups that stabilize the radical increase its innate lifetime ($\tau_o^{RBr\bullet}$), but also increase its reduction rate (k_{red}). If the substituent is bulky, then it may serve to hinder the reduction. There is a rather delicate balance. Gyro (VII, Table 4-D) has the longest radical lifetime measured under fluoride conditions and *trans*-10,11-dibromodibenzosuberone (XII, Table 4-D) and 2,3-dibromopropyl-trimethylsilane (XV, Table 4-D) have two of the longest radical lifetimes measured under bromide conditions. These three molecules have the fastest reduction rate constants measured under their respective conditions.

(iv) The Effect of a Silyl Group on the β-Bromo Radical

The effect of a second neighboring group was of interest during the study of $Si(DBE)_4$. It was rationalized that two β-groups on the same side of the radical center could not simultaneously eclipse the radical center. To test if the β-bromo radical could be further stabilized by a second neighboring group, 2,3-dibromopropyl-trimethylsilane was photolyzed. It was postulated that the bromine atom in the 2-position would be lost during photolysis thus leaving behind a radical center flanked by two β-stabilizing groups; the remaining bromine atom and the silyl group. As it turns out, the β-bromo radical from 2,3-dibromopropyl-trimethylsilane did indeed have the longest lifetime of 149 ns under bromide conditions.

(v) The Effect of Ring Size on the β-Bromo Radical

All three of the dibromocycloalkanes studied had among the shortest β-bromo radical lifetimes and slowest reduction rate constants measured. It is difficult to see why

the ring compounds would have the slowest reduction rate constants. The short lifetimes can be a reflection of the strain involved in creating a bicyclic ring system to accommodate the bromine atom bridge. The lifetimes of the three β-bromo-cycloalkyl radicals are short but they follow the trend in dihedral angle between the two bromine atoms in the parent *vicinal* dibromide.

Table 4-E is an out-take of the *trans*-dibromocycloalkanes from Table 4-D. In Table 4-E the MM2 calculated dihedral angles have been included. The lifetimes appear to get shorter as the two bromine atoms in the parent *vicinal* dibromide get farther from being parallel. The longest lifetime is for the *trans*-1,2-dibromocyclohexane which is only 21° from having periplanar bromine atoms. It was shown in chapter 1 that radical formation is accelerated by a neighboring bromine atom that is in a position to overlap the developing radical center.

Table 4-E **A compilation of β-bromo radical lifetimes and their rates of reduction by fluoride, chloride, and bromide for the cyclic *vicinal* dibromides. The dihedral angle between the bromine atoms has been included in the table. The dihedrals were calculated using MM2 optimized geometries.**

	vicinal dibromide $\xrightarrow{h\nu}$ β-bromo radical	k_{red} /10^9 $M^{-1}s^{-1}$			$\tau_o^{RBr\bullet}$ (ns)		
		F^-	Cl^-	Br^-	F^-	Cl^-	Br^-
IX	*trans*-1,2-dibromocyclopentane  BrCCBr = 139° (MM2)	1.3	2.0 (1.8)	3.2 (2.0)	100	65	60
X	*trans*-1,2-dibromocyclohexane 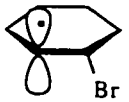 BrCCBr = 158° (MM2)	1.0	5.11 (4.5)	5.0 (3.9)	117	85	70
XI	*trans*-1,2-dibromocycloheptane 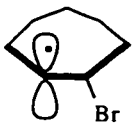 BrCCBr = 56° (MM2)	< 0.5	1.5 (0.9)	1.9 (1.0)	98	42	30

An interesting, but difficult, experiment would be to compare the *trans*-dibromocycloalkanes to their respective *cis* isomers. If the lifetime of the photogenerated β-bromo-cycloalkyl radicals are truly dependent on the dihedral angle between the remaining bromine atom and the developing radical center. This experiment would be difficult in the sense that there would probably be only 10's of nanoseconds separating the lifetimes of the *cis/trans* pairs.

(vi) The Effect of a β-Silyl Group on the β-Bromo Radical

The two β-bromo-β-silyl radicals (Dibromide **XIII** and Dibromide **XIV**) have similarly moderate lifetimes and reduction rate constants to the halides. A significant difference occurs when the silyl group is moved to the opposite side of the radical center from the bromine atom. 2,3-dibromopropyl-trimethylsilane (Dibromide **XV**) has one bromine atom that is flanked by the second bromine atom and the silyl group. This arrangement allows for more cooperation of the two neighboring groups. The β-bromo-β'-silyl radical has a significantly longer lifetime (149 ns, bromide conditions) and a larger bromide reduction rate constant ($8.3 \times 10^9\ M^{-1}\ s^{-1}$) than the two β-bromo-β-silyl radicals. Again, complete overlap of both neighboring groups is not possible, but the β,β'-arrangement allows for a more flexible and better overlap than the two β,β-radicals.

4.6 Temperature Effects on the β-Bromo Radicals

The effect of temperature on β-bromo radicals can be studied by performing complete quenching experiments at a variety of temperatures. A complete quenching study at each temperature is necessary in order to get the full range of the k_{RBr} dependence from which the k_{red} and k_o^{RBr} values can be extrapolated. Figure 4-16 represents an Arrhenius plot of log(k) versus 1000/T (Equation 4.19) for the rate constants obtained for the photolysis of 1,2-dibromoethane and *trans*-1,2-dibromocyclopentane in MeCN.

$$\log(k) = \log A - \frac{E_a}{2.3RT}$$ **Equation 4.19**

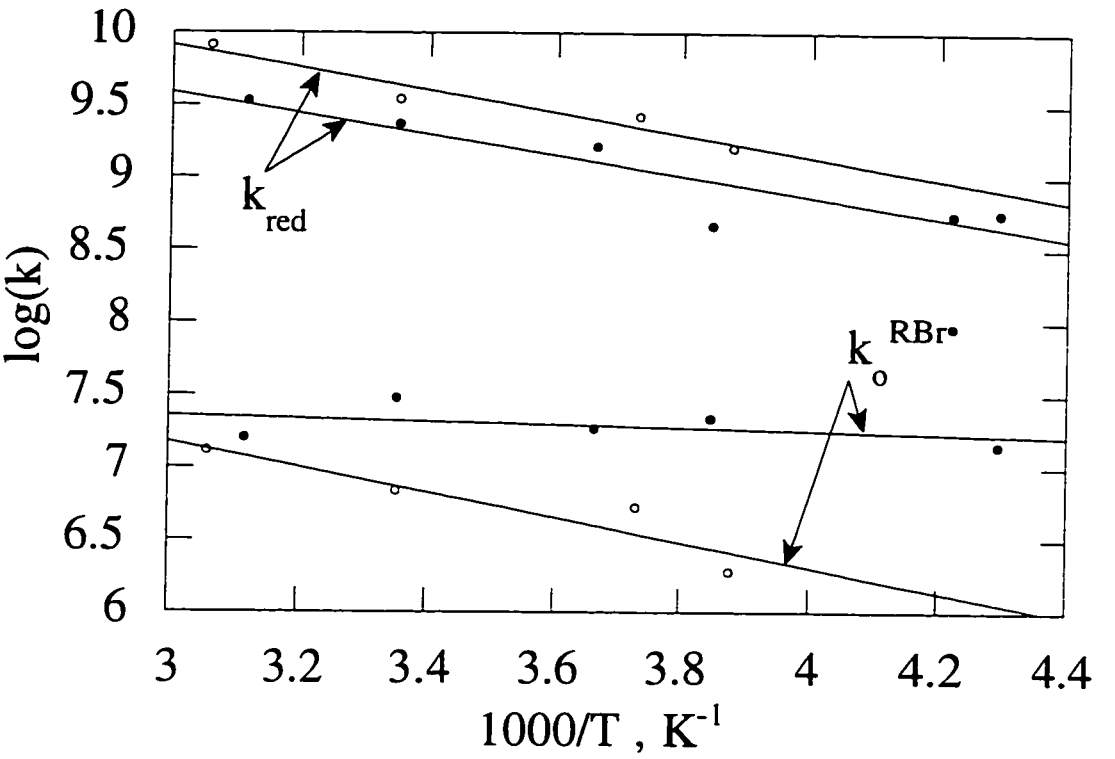

Figure 4-16 **The temperature dependence of the unimolecular decay ($k_o^{RBr\bullet}$, s^{-1}) and the halide reduction (k_{red}, $M^{-1}\ s^{-1}$) of the β-bromo radicals from the photolysis of 1,2-dibromoethane (Dibromide II, ○) and *trans*-1,2-dibromocyclopentane (Dibromide IX, ●). The 1,2-dibromoethane was studied in the presence of fluoride and *trans*-1,2-dibromocyclopentane was studied in the presence of bromide. The MeCN solutions were excited with 266 nm light.**

Table 4-F **The Arrhenius parameters for the fluoride probed photolysis of 1,2-dibromoethane and the bromide probed photolysis of *trans*-1,2-dibromocyclopentane in MeCN.**

		logA	E_a (kcal/mol)
1,2-dibromoethane	$k_o^{RBr\bullet}$	9.8	3.5
	k_{red}	12.2	4.0
trans-1,2-dibromocyclopentane	$k_o^{RBr\bullet}$	7.7	0.5
	k_{red}	11.8	3.3

The 1,2-dibromoethane data was measured using fluoride as a probe, while the *trans*-1,2-dibromocyclopentane data was measured using bromide as a probe. A summary of the Arrhenius parameters determined from Figure 4-16 and Equation 4.19 is presented in Table 4-F.

(i) Temperature Effects of the Halide Reduction of the β-Bromo Radicals

The activation energies and log(A) factors for the halide reductions of both radicals were similar to one another. Values of 4.0 kcal/mol and 12.2 were obtained for E_a and log(A) for the fluoride reduction of the β-bromoethyl radical. Values of 3.3 kcal/mol and 11.8 were obtained for the bromide reduction of β-bromocyclopentane.

The low activation barriers and close to diffusion-controlled rates contribute to the high log(A) factors. The activation energies and log(A) factors are what one would expect for a diffusion controlled process.

(ii) The Temperature Dependence of the β-Bromo Radical Lifetimes

The data for the unimolecular decay of the β-bromoalkyl radicals were also included in the Arrhenius plot of Figure 4-16, but the parameters extracted are relatively useless. The values of $k_o^{RBr\bullet}$ extracted from the intercepts of the quenching plots at each temperature

are already extremely error-prone. The inaccuracy of this poor data is then compounded by the large errors associated with 4- and 5-point Arrhenius plots over a narrow temperature range (230 K to 320 K).

The activation energies for the unimolecular fragmentation of the β-bromoethyl and β-bromocyclopentyl radicals were determined to be 3.5 and 0.5 kcal/mol, respectively. The logA factors were determined to be 9.8 and 7.7, respectively. The activation energies are low, as would be expected, and could be explained, but there is no explanation for the logA factors other than experimental error.

The logA factors are usually between 11 and 15 for unimolecular decays. Both of our values are much lower than this normal range. If our two values were at least self-consistent, we may argue that they reflect something of fundamental importance. These low logA factors are probably a reflection of the fact that the β-bromoradicals do not undergo a true unimolecular decay. Instead, the β-bromoradicals most likely react directly with the solvent to produce the MeCN•Br complex. The low logA factors occur because of the entropic losses associated with forming the solvent complex.

The fact that the two logA factors are very different from each other only confirms the imprecise nature of their determination. The difference between the two values can be accounted for by experimental error, but experimental error cannot account for the drop from the expected values of ~13 to the observed values of 7.7 and 9.8.

4.7 Conclusion

It has long been inferred from indirect studies that β-bromo radicals must exist in bridged form long enough to influence the stereochemical outcome of many reactions. So far, there has been no direct proof of the bridge nor of the lifetimes of the β-bromo radicals.

The halide probing of the LFP debromination of *vicinal* dibromides in this present study demonstrates what product studies have been telling us all along, but which

spectroscopic techniques have failed to capture. The results of the present study confirms that most β-bromo-alkyl radicals have measurable lifetimes in the 100 to 200 ns range.

Halides are valuable probes for the LFP debrominations of *vicinal* dibromides. Under the right conditions, a halide can both probe the kinetics of a β-bromo radical decay and give us some clues to the radical's reactivity and stability. It was shown that β-bromo-alkyl radicals are reduced by halides in MeCN at rates in the 10^9 $M^{-1}s^{-1}$ range.

4.8 Chapter 4 References

(1) Kochi, J. K.; Krusic, P. J. In *Essays on Free Radical Chemistry, Special Publication No. 24*; R. O. C. Norman, Ed.; The Chemical Society: London, 1970; Vol. 24; pp 147.

(2) Scaiano, J. C.; Barra, M.; Calabrese, G.; Sinta, R. *J. Chem. Soc., Chem. Commun.* **1992**, 1418.

(3) Zhang, B.; Pandit, C. R.; McGimpsey, W. G. *J. Phys. Chem.* **1994**, *98*, 7022.

(4) Tanner, D. D.; Darwish, D.; Mosher, M. W.; Bunce, N. J. *J. Am. Chem. Soc.* **1969**, *91*, 7398.

(5) Lyons, A. R.; Symons, M. C. R. *J. Chem. Soc., Faraday Trans. 2* **1972**, *68*, 622.

(6) Krusic, P. J.; Kochi, J. K. *J. Am. Chem. Soc.* **1971**, *93*, 846.

(7) Griller, D.; Ingold, K. U. *J. Am. Chem. Soc.* **1973**, *95*, 6459.

(8) Norman, R. O. C.; Storey, P. M. *J. Chem. Soc. B* **1971**, 1009.

(9) Cooper, J.; Hudson, A.; Jackson, R. A. *Tetrahedron Lett.* **1973**, 831.

(10) Auner, N.; Walsh, R.; Westrup, J. *J. Chem. Soc., Chem. Commun.* **1986**, 207.

(11) Jackson, R. A.; Ingold, K. U.; Griller, D.; Nazran, A. S. *J. Am. Chem. Soc.* **1985**, *107*, 208.

(12) Walsh, R. *Pure & Appl. Chem.* **1987**, *59*, 69.

(13) Skell, P. S.; Traynham, J. G. *Acc. Chem. Res.* **1984**, *17*, 160.

(14) Symons, M. C. R.; Smith, I. G. *J. Chem. Soc., Perkin Trans. 2* **1979**, 1362.

(15) Skell, P. S.; Tuleen, D. L.; Readio, P. D. *J. Am. Chem. Soc.* **1963**, *85*, 2849.

(16) Thaler, W. *J. Am. Chem. Soc.* **1963**, *85*, 2607.

(17) Chen, K. S.; Elson, I. H.; Kochi, J. K. *J. Am. Chem. Soc.* **1973**, *95*, 5341.

(18) Edge, D. J.; Kochi, J. K. *J. Am. Chem. Soc.* **1972**, *94*, 6485.

(19) Weldon, D.; Barra, M.; Sinta, R.; Scaiano, J. C. *J. Org. Chem.* **1995**, *60*, 3921.

(20) Gilbert, A.; Baggot, J. *Essentials of Molecular Photochemistry*; Blackwell Science: Oxford, 1991, pp 538.

(21) "Kaleidagraph" Abelbeck Software: 1994 version 3.0.4.

(22) Merényi, G.; Lind, J. *J. Am. Chem. Soc.* **1994**, *116*, 7872.

(23) Hargis, J. H.; Shevlin, P. B. *J. Chem. Soc., Chem. Commun.* **1973**, 179.

(24) Skell, P. S.; Shea, K. J. In *Free Radicals*; J. K. Kochi, Ed.; Wiley: New York, 1973; pp 809.

(25) Shoute, L. C. T.; Neta, P. *J. Phys. Chem.* **1990**, *94*, 2447.

(26) Sabacky; Johnson; Smith; Gutowski; Martin *J. Am. Chem. Soc.* **1967**, *89*, 2054.

5. Bromine Atom/Organic Complexes

5.1. Introduction **142**

5.2. Bromine Atom/Organic Complexes **144**

(i) The Jump 150

(ii) The Growth 157

5.3. The Nature of the Bromine Atom/Organic Complex **166**

5.4. Conclusions **167**

5.5. Chapter 5 References **169**

5.1 Introduction

Through our LFP studies of the photodebromination of *vicinal* dibromides, we have observed absorptions in the absence of added probe. These absorptions took the form of a weak jump and growth, or simply a weak growth. These weak absorptions were observed either to not interfere with our probe experiments or to be reproducible and arithmetically accountable. The reasons for these absorptions are not perfectly clear, but they deserve some comment.

The purpose of the probe reactions of chapters 3 and 4 was to monitor bromine atoms. For the photochemical debromination of *vicinal* dibromides, it was not only necessary to observe the bromine atoms, but also to elucidate their kinetic evolution into solution. As with any indirect analysis, there is always the question of what happens in the absence of probe. In the absence of complexing halide (X^-), the photochemical debromination of *vicinal* dibromides invariably produced a transient signal at 360 nm in our studies. The signal always consisted of a small instantaneous rise that we usually refer to as a jump in the signal. Instantaneous with our system means anything that occurs with a rate constant of greater than 143 μs^{-1} ($\tau < 7$ ns). More often than not, the jump is followed by a weak growth. Figure 5-1 is the same trace as Figure 3-14 which displays both the weak jump and the weak growth of the 360 nm transient in MeCN.

This phenomenon has been observed in whole, or in part, by several other groups. Because the spectrum of the unprobed solutions have very similar characteristics to the known spectrum of the $Br_2^{\bullet}$ complex, most groups so far have attributed this weak signal to the $Br_2^{\bullet}$ species. The formation of the $Br_2^{\bullet}$ complex has been attributed to either traces of bromide[1-3] in solution, or to the direct formation of $Br_2^{\bullet}$ from the precursor reactions.[3,4]

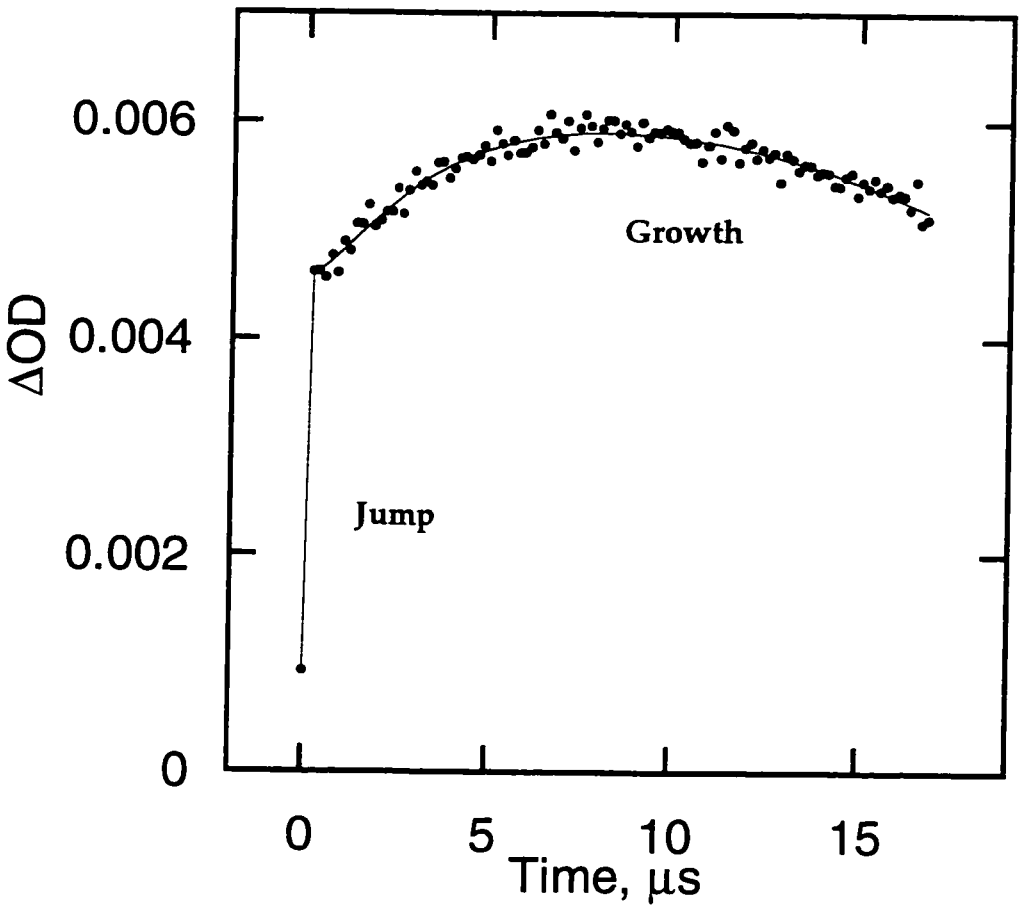

Figure 5-1 **The instantaneous jump followed by the growth of the 360 nm transient after the photolysis of $Si(DBE)_4$ in MeCN in the absence of halide probe.**

$$Br^{\bullet} + S \underset{k_{-S\bullet Br}}{\overset{k_{S\bullet Br}}{\rightleftharpoons}} S \bullet Br$$

Equation 5.1 (Solvent/Br• complex)

$$S \bullet Br + RBr_n \underset{k_{-RBr\bullet Br}}{\overset{k_{RBr\bullet Br}}{\rightleftharpoons}} RBr_n \bullet Br + S$$

Equation 5.2 (RBr_n/Br• complex)

It will be shown in this chapter that the jump observed in Figure 5-1 is due to the immediate complexation of the bromine atom with the solvent (Equation 5.1). The

subsequent slow growth will be attributed to the reaction of the bromine atom/solvent complex (S•Br) with the bromine atom's precursor (usually present in mM amounts) to form a $Br•RBr_n$ complex (Equation 5.2).

5.2 Bromine Atom/Organic Complexes

The UV absorption spectra of chlorine atoms in some chlorinated solvents has been measured.[5] A linear relationship between the energy of the absorption maximum ($h\nu_{CT}$) and the vertical ionization energy of the chloroalkanes was observed. Shoute and Neta performed similar experiments on bromine atoms with brominated alkanes.[6] They found that bromine atoms also form charge transfer complexes with bromoalkanes. Using pulse radiolysis, Shoute and Neta studied the bromine atom complexes with carbon tetrabromide (CBr_4), bromoform ($CHBr_3$), dibromomethane (CH_2Br_2), and ethyl bromide (CH_3CH_2Br). Bromine atoms were produced from pulse radiolysis of cyclohexane solutions of the four bromoalkanes and in neat dibromomethane and bromoform (Scheme 5-1).

$$RBr_n \longrightarrow [RBr_n]^{\bullet +} + e^- \qquad \textbf{Equation 5.3}$$

$$RBr_n \longrightarrow {}^{\bullet}RBr_{n-1} + Br^{\bullet} \qquad \textbf{Equation 5.4}$$

$$RBr_n + Br^{\bullet} \xrightarrow{k_{RBr\bullet Br}} RBr_n \bullet Br \qquad \textbf{Equation 5.5}$$

Scheme 5-1 Bromine atom production and complexation from the pulse radiolysis of bromoalkanes.

In neat solvent, or in the cyclohexane solutions, the bromine atoms were observed to complex with the parent bromo compounds. In Figure 5-2, the maxima of the spectra of the four bromoalkanes are shown to red-shift as the number of geminal bromines is increased. The rate of complexation of Equation 5.5 was beyond the resolution of the instrument and was given a lower-limit of $10^{10}\ M^{-1}s^{-1}$.

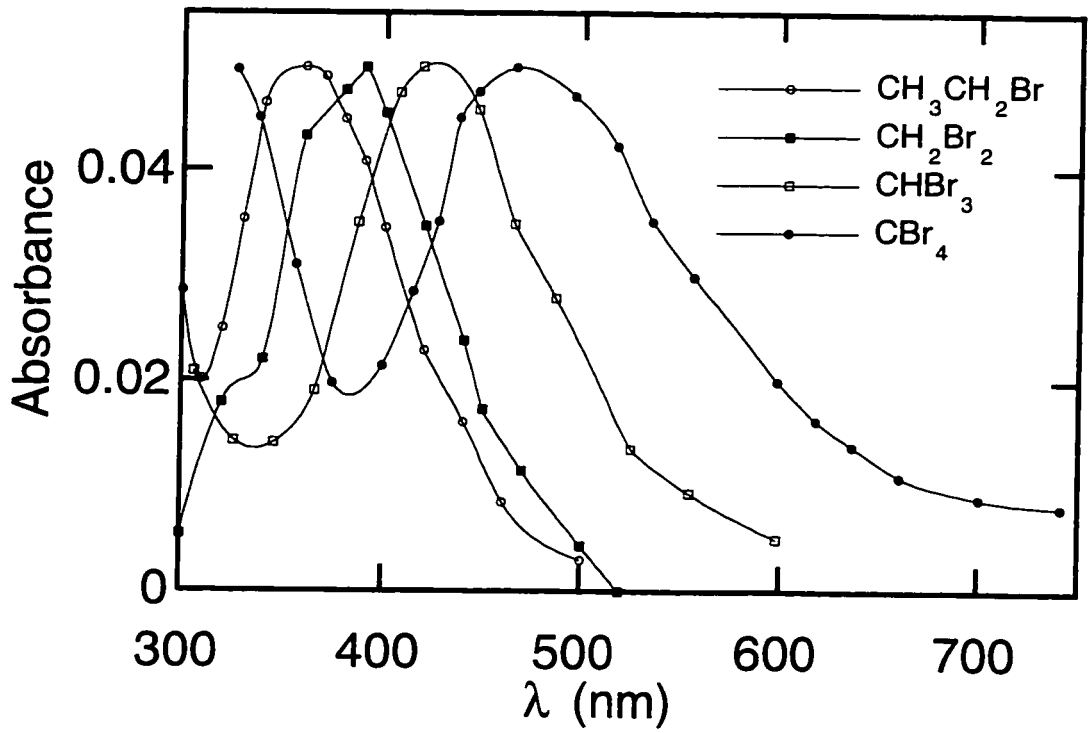

Figure 5-2 **Normalized bromine atom/bromoalkane spectra (RBr_n•Br) in cyclohexane. The spectra were produced from the PR of the bromoalkanes in cyclohexane solution. [CBr_4] = 0.05M, [$CHBr_3$] = 0.23 M, [CH_2Br_2] = 0.29 M, and [CH_3CH_2Br] = 0.54 M.[6]**

In the absence of bromide probe, the LFP of $Si(DBE)_4$ in MeCN shows a weak absorption with a spectrum similar to that of the CH_3CH_2Br•Br complex observed by Shoute and Neta (Figure 5-3). The LFP spectrum of $Si(DBE)_4$ has a maximum around 360 nm (Figure 5-4). The absorption is assumed to be the result of the complexation of the bromine atoms with the parent $Si(DBE)_4$.

There is a striking similarity between the CH_3CH_2Br•Br complex and the spectrum recorded after the 266 nm photolysis of $Si(DBE)_4$ in MeCN in the absence of any halide probe. There is also a remarkable similarity to the $Br_2^{\cdot}$ spectrum in MeCN (including the second weak peak at 700 nm).

Although the complex between bromine atoms and acetonitrile has not been reported, the existence of such a complex is consistent with the studies of other bromine

atom/solvent complexes.[6,7] As mentioned earlier, Shoute and Neta demonstrated that bromine atoms form complexes with bromoalkanes.[6] In a later publication, the study of bromine atom complexes was expanded to include a series of chloroalkanes and alkanes (Table 5-A).[7]

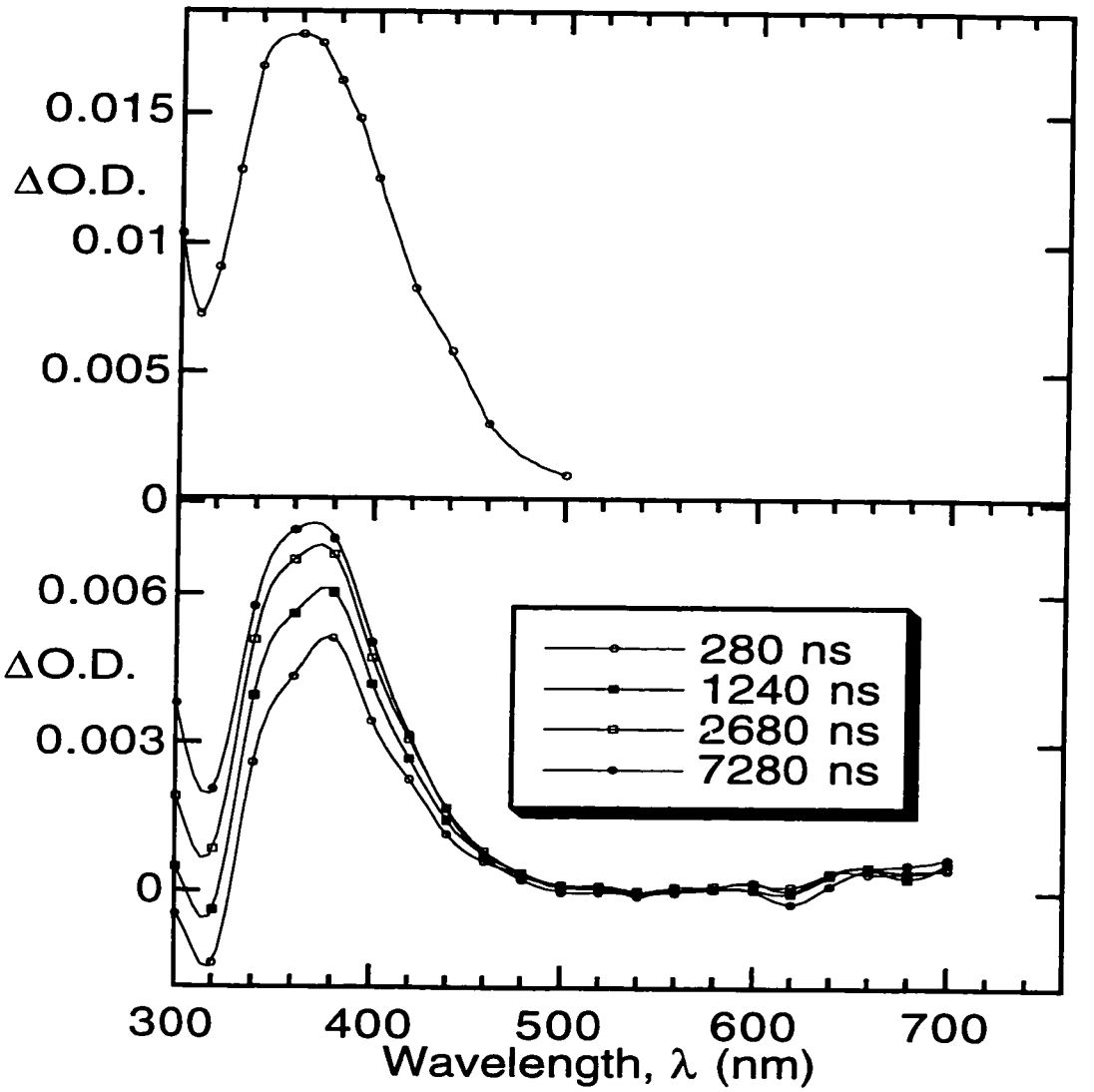

Figure 5-3 (Upper) The spectrum of the complex between bromoethane and a bromine atom in cyclohexane.[6]

Figure 5-4 (Lower) The LFP spectrum of Si(DBE)4 in acetonitrile.

Table 5-A **A compilation of absorption maxima and ionization potentials for various bromine atom complexes (R•Br) with bromoalkanes, chloroalkanes, and alkanes. LFP = Laser Flash Photolysis; PR = Pulse Radiolysis.[7]**

			λ (nm)		
	solvent	complex (R•Br)	LFP	PR	I_p (eV)
1	cyclohexane	CBr_4	480	480	10.31
2	cyclohexane	$CHBr_3$	430	425	10.48
3	cyclohexane	CH_2Br_2	390	390	10.5*
4	cyclohexane	CH_3CH_2Br		365	10.3*
5	cyclohexane	cyclohexane	370		9.86
6	CH_2Br_2	CH_2Br_2		390	10.5*
7	CH_3CH_2Br	CH_3CH_2Br	370	370	10.28
8	$ClCH_2Br$	$ClCH_2Br$	365		10.77
9	CF_2Br_2	CF_2Br_2	360		11.07
10	2-C_4H_9Cl	2-C_4H_9Cl	345		10.53
11	1-C_4H_9Cl	1-C_4H_9Cl	345		10.67
12	2-C_3H_7Cl	2-C_3H_7Cl	350		10.78
13	$ClCH_2CH_2Cl$	$ClCH_2CH_2Cl$	325		11.04
14	CH_2Cl_2	CH_2Cl_2	315		11.32
15	CCl_4	CCl_4	305		11.47
16	decalin	decalin	395		9.25; 9.41
17	n-hexane	n-hexane	350		10.13
18	neohexane	neohexane	340		10.06
19	n-pentane	n-pentane	344		10.35
20	cyclopentane	cyclopentane	335		10.51
21	methanol	methanol	360		10.84
22	benzene	benzene	540		9.25
23	CH_2Br_2	DMSO		425	9.1*

* **From NIST database[8]**

A closer inspection of the $Si(DBE)_4$•Br spectrum reveals that there is more than one transient present. The first spectrum of Figure 5-4 (○) was taken 280 ns after the laser pulse. This spectrum has a maximum at 380 nm. As time progresses, the maxima of the subsequent three other spectra change from the 380 nm of the 280 ns spectrum to 370 nm for the spectrum after 7280 ns (●). Figure 5-5 is an expansion of the 300 - 500 nm range of the spectra of Figure 5-4 obtained after the photolysis of $Si(DBE)_4$ in MeCN. The early spectrum is strongly influenced by the jump region of the reaction and represents the MeCN•Br complex. At later times after the photolysis (> 1 μs), the spectrum is probably completely due to the $Si(DBE)_4$•Br complex.

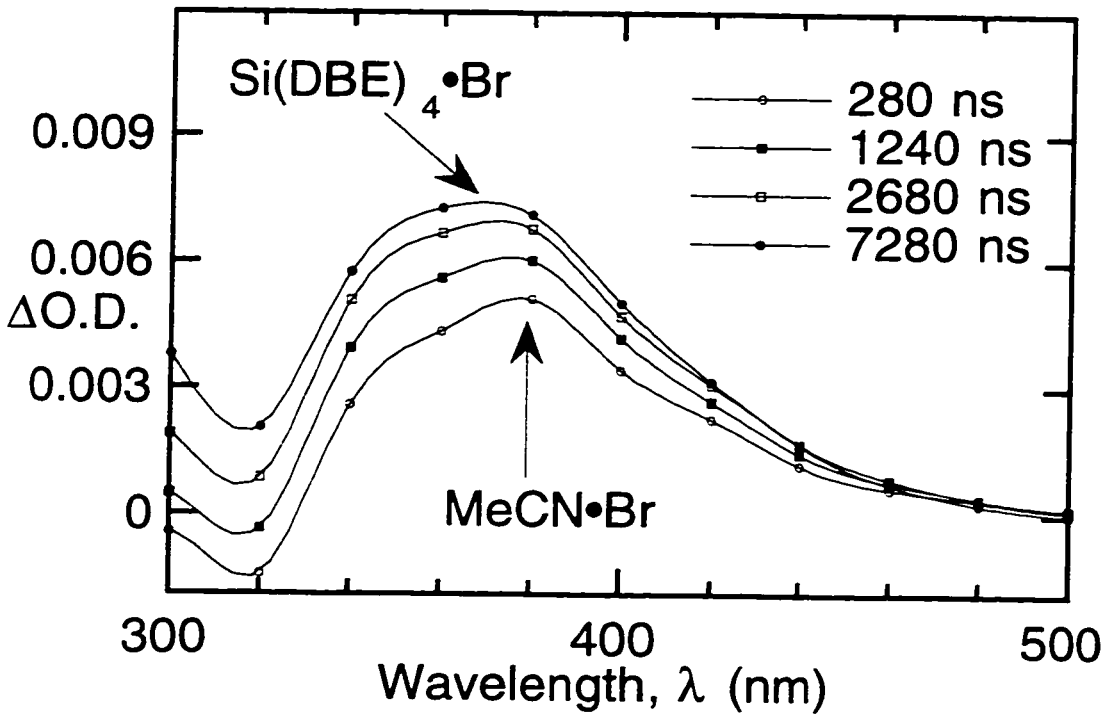

Figure 5-5 **Expansion of Figure 5-4. The spectrum gradually shifts with time from a maximum of 380 nm (after 280 ns) to 370 nm (after 7280 ns). $Si(DBE)_4$ in MeCN.**

The change in these particular spectra are subtle, but for other *vicinal* dibromides the shift is more obvious. Figure 5-6 is one of the more evident examples of the spectrum

shifting away from a 380 nm maximum as time progresses. Figure 5-6 was produced after the LFP of 1,2-dibromo-2-methylpropane (Dibromide **VII**) in MeCN.

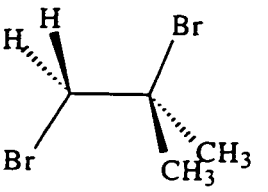

Dibromide VII

1,2-dibromo-2-methylpropane

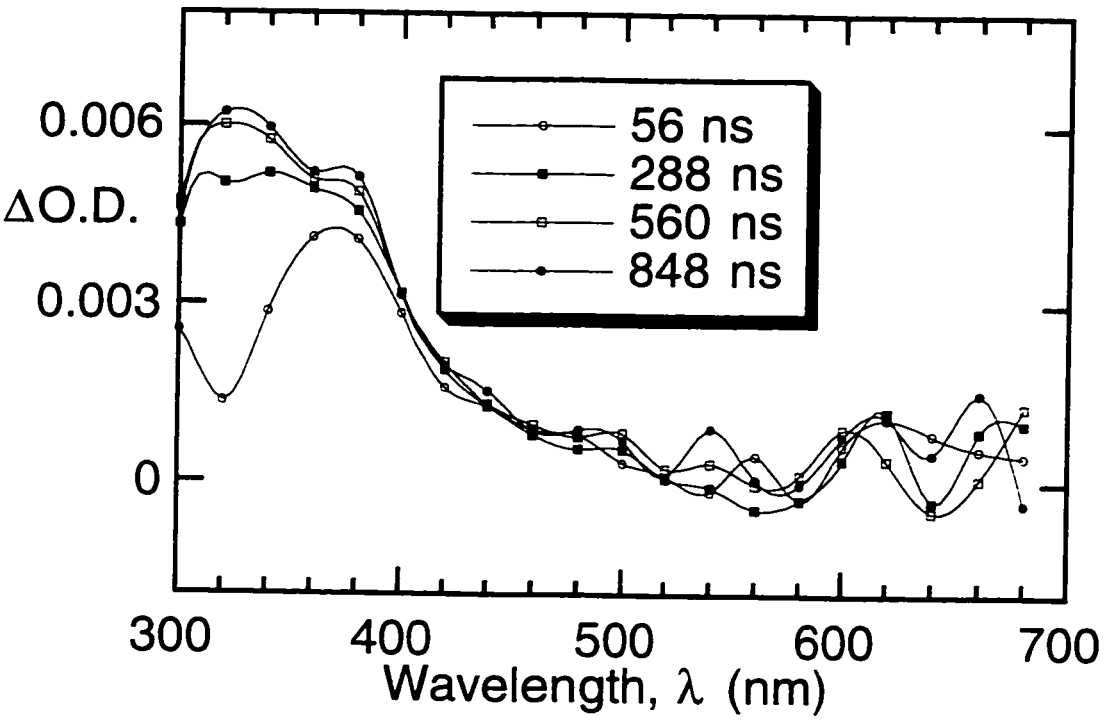

Figure 5-6 **The time evolution of the LFP spectra of 1,2-dibromo-2-methylpropane in MeCN.**

The first spectrum was recorded 56 ns after photolysis and represents the jump in absorption due to the immediate formation MeCN•Br complex. The next spectrum was recorded 288 ns after photolysis and, already, a new lower-wavelength peak almost completely obscures the 380 nm jump. The following two spectra at 560 and 848 ns after

photolysis show the 380 nm peak as a shoulder as it is surpassed by the new 320 nm peak of the 1,2-dibromo-2-methylpropane•Br complex.

Not all of the other *vicinal* dibromide spectra showed this peak shift. The observation of the MeCN•Br peak depends on several factors. The MeCN•Br complex is weak and is quenched by the *vicinal* dibromide precursor. Therefore, the MeCN•Br peak will not be observed if the *vicinal* dibromide precursor is a very fast quencher. The *vicinal* dibromides are also usually in high concentration (> 10 mM) due to their poor absorbances at 266 nm (the excitation wavelength), thus also increasing the quenching rate. Some of the *vicinal* dibromides studied did not have high yields of bromine atoms, therefore the inherently weak MeCN•Br signals would be even weaker.

(i) The Jump

To be an instantaneous jump, the species in question has to be trapped immediately or produced directly. Immediate trapping requires either an extremely fast quencher, or a quencher in high concentration. No substrate is in higher concentration than the solvent. Neat acetonitrile has a concentration of 19.1 M, and the system's rise time is 7 ns, therefore, if MeCN has a rate constant equal to, or greater than 7.5×10^6 M^{-1} s^{-1} , then it would instantly trap the bromine atoms produced.

The majority of our experiments were performed in MeCN. The vertical ionization potential for acetonitrile is 12.3 eV.[8] Based on the trend in Table 5-A, we would expect the maximum for an MeCN•Br complex to be at a wavelength much lower than the 380 nm range postulated from our spectral observations. Treinin and Hayon photolyzed aqueous bromine solutions to study the H_2O•Br system.[1] Water has a vertical ionization potential of 12.6 eV[8], and a maximum absorbance of 275 nm was observed. This is what one would expect for such a high I.E. based on the trend of Table 5-A. However, the authors also noted an instantaneous signal at 360 nm followed by a slow growth. From what we have seen in MeCN and what others have seen in other solvents, we would conclude that Treinin and Hayon's jump and growth is the same as ours. Namely, the jump is the immediate

formation of the $H_2O{\bullet}Br$ complex, and the growth is the slower transfer of the bromine atom from the water to the excess Br_2 in solution (2.5 mM) to form $Br_3^{\bullet}$.

Treinin and Hayon attributed their jump to the presence of trace amounts of Br_3^- in solution. Br_3^- comes from the hydrolysis of Br_2 (Equation 5.6 and Equation 5.7) and has a large extinction coefficient at 266 nm (38 000 M^{-1} cm^{-1}). When Tribromide (Br_3^-) is photolyzed, a bromine atom is ejected, thus producing the $Br_2^{\bullet}$ radical cation directly (Equation 5.8).

$$Br_2 + H_2O \rightleftharpoons Br^- + H^+ + HOBr$$ **Equation 5.6**

$$\left(K_H = \frac{[H^+][Br^-][HOBr]}{[Br_2]} = 7.2 \times 10^{-9}\ M^2 \right)$$

$$Br^- + Br_2 \rightleftharpoons Br_3^-$$ **Equation 5.7**

$$\left(K_3 = \frac{[Br_3^-]}{[Br^-][Br_2]} = 16\ M^{-1} \right)$$

$$Br_3^- \xrightarrow{h\nu} Br^{\bullet} + Br_2^{\bullet-}$$ **Equation 5.8**

The equilibrium constants were taken from Treinin and Hayon's paper and the references within.[1]

Despite working in 0.1 - 1.5 M $HClO_4$ to suppress the Br_2 hydrolysis, there would always be trace amounts of bromide and tribromide in solution. Under their experimental conditions, the maximum equilibrium concentration of tribromide from hydrolysis would be 0.6 μM. This concentration would have an absorbance of 0.0228 at the excitation

wavelength of 266 nm. If every single tribromide ion was photolyzed to $Br_2^{\bullet-}$, then there would only be a corresponding jump in absorbance of 0.006[y] at 360 nm.

1,2-Dibromoethane has been shown to produce a prompt absorbance at 360 nm whether pulse radiolyzed in water[3] or photolyzed in MeCN[2,4]. In both solvents, the prompt absorbance was attributed to the direct formation of $Br_2^{\bullet-}$. It is easier to imagine that pulse radiolysis rather than photolysis might produce $Br_2^{\bullet-}$ directly. Photolysis may result in the direct elimination of Br_2 from a small portion of the 1,2-dibromoethane, but not $Br_2^{\bullet-}$. While the chance of direct $Br_2^{\bullet-}$ production in these two cases may exist, the chance of it happening for Treinin and Hayon's photolysis of aqueous Br_2 solutions is highly unlikely. It is hard to imagine that all three of these examples, with variable techniques, conditions, precursors, and solutions, could produce identical observations. It is more likely that a common mechanism exists for all observations, i.e. the bromine atoms produced initially complex with the solvent.

The production of $H_2O{\bullet}Br$ and $MeCN{\bullet}Br$ complexes have proven to have kinetics and spectra so similar to that of the actual $Br_2^{\bullet-}$ complex that it would be difficult to distinguish one from the other. Experiments were performed in chloroform and the results are much more conclusive than in either of the two previously mentioned solvents. Figure 5-7 is the spectrum produced by the LFP of α-bromoacetophenone in an oxygen purged $CHCl_3$ solution containing 10mM Bu_4NBr. The $Br_2^{\bullet-}$ maximum has shifted to 350 nm from the 360 nm maxima seen in water and MeCN. The smaller peak at 310 nm is assigned to the $CHCl_3{\bullet}Br$ complex. The value of 310 nm for the $CHCl_3{\bullet}Br$ maximum fits perfectly between the values of 315 nm and 305 nm observed for the complexes of CH_2Cl_2 and CCl_4, respectively (Table 5-A).

---

[y] The absorbance of $Br_2^{\bullet-}$ is calculated using the extinction coefficient of 9900 M^{-1} cm^{-1}, the tribromide concentration of 0.6 μM, and a path length of 1 cm.

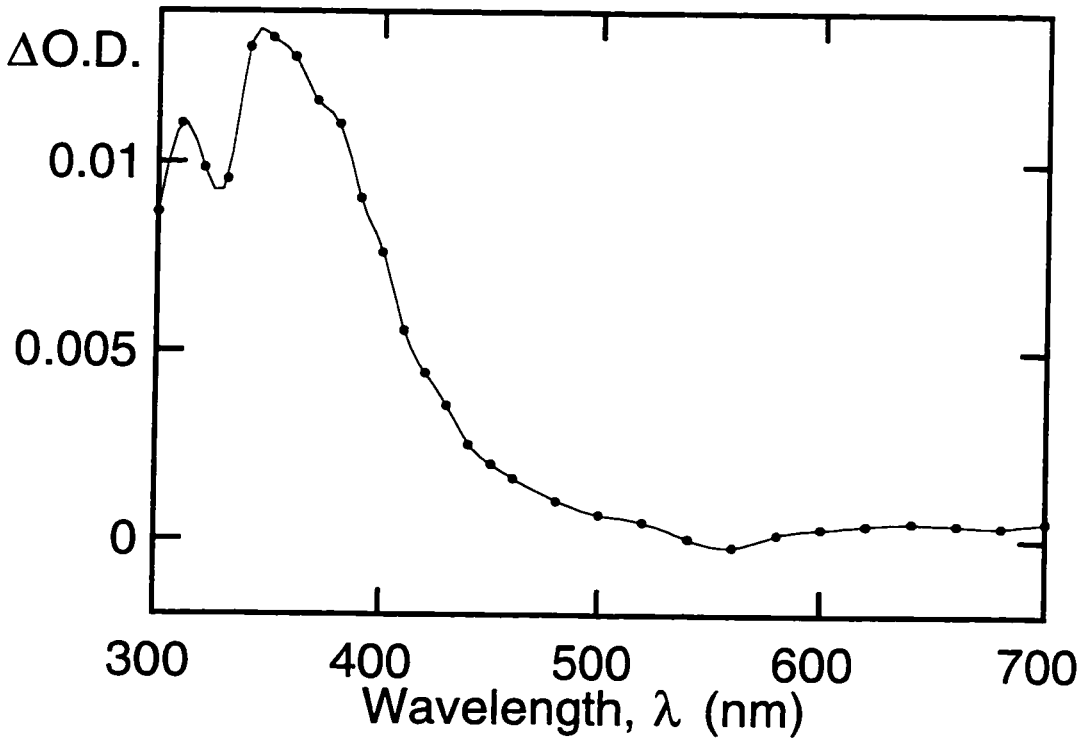

Figure 5-7 **$CHCl_3$•Br (λ_{max} = 310 nm) and $Br_2^{\cdot}$ (λ_{max} = 350 nm) complexes produced by the 337 nm LFP of α-bromoacetophenone in an oxygen purged $CHCl_3$ solution containing 10mM TBAB .**

This time, there is no question that the bromine atoms produced are complexing with the solvent. Based on Table 5-A, one would expect $CHCl_3$ to form a complex. The important lesson to learn from this $CHCl_3$/α-bromoacetophenone experiment is that in the absence of added halide, there can be no $Br_2^{\cdot}$ produced at all, either by direct or indirect formation.

Figure 5-8 is a decay trace of 1,2-dibromoethane/$CHCl_3$ solution recorded at 360 nm in the absence of added halide. The decay trace does not show the typical jump and growth profile that we have come to expect in MeCN. The signal cannot be due to an absorption of a complex with the 1,2-dibromoethane because the 1,2-dibromoethane concentration is too low to generate the instantaneous signal observed. The signal is definitely not due to any direct production of the $Br_2^{\cdot}$ radical anion because the decay is too fast when compared to the signal in the presence of bromide (Figure 5-9).

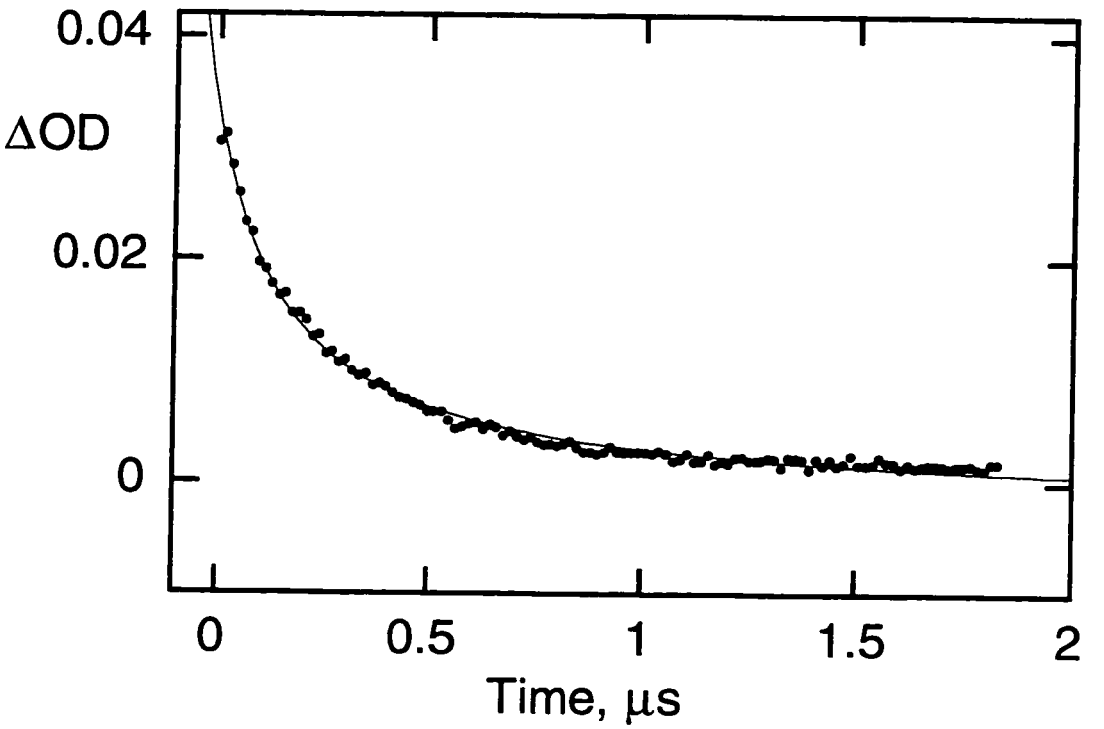

Figure 5-8 **$CHCl_3$•Br second-order decay recorded at 360 nm. The complex was produced by the LFP of 1,2-dibromoethane in an oxygen purged $CHCl_3$ solution containing no TBAB .**

Figure 5-9 shows the decays of the transient with and without the presence of trapping bromide. The time axis for Figure 5-9 has been adjusted so as to show the entire decay of the trace in the presence of 10 mM bromide (○). This long timescale shows the huge disparity between the decays of the transients in $CHCl_3$ when bromide is absent (●) and when it is present (○). Based on this comparison, we can conclude that the decay in $CHCl_3$, when no bromide is added, is not due to $Br_2^{\bullet-}$.

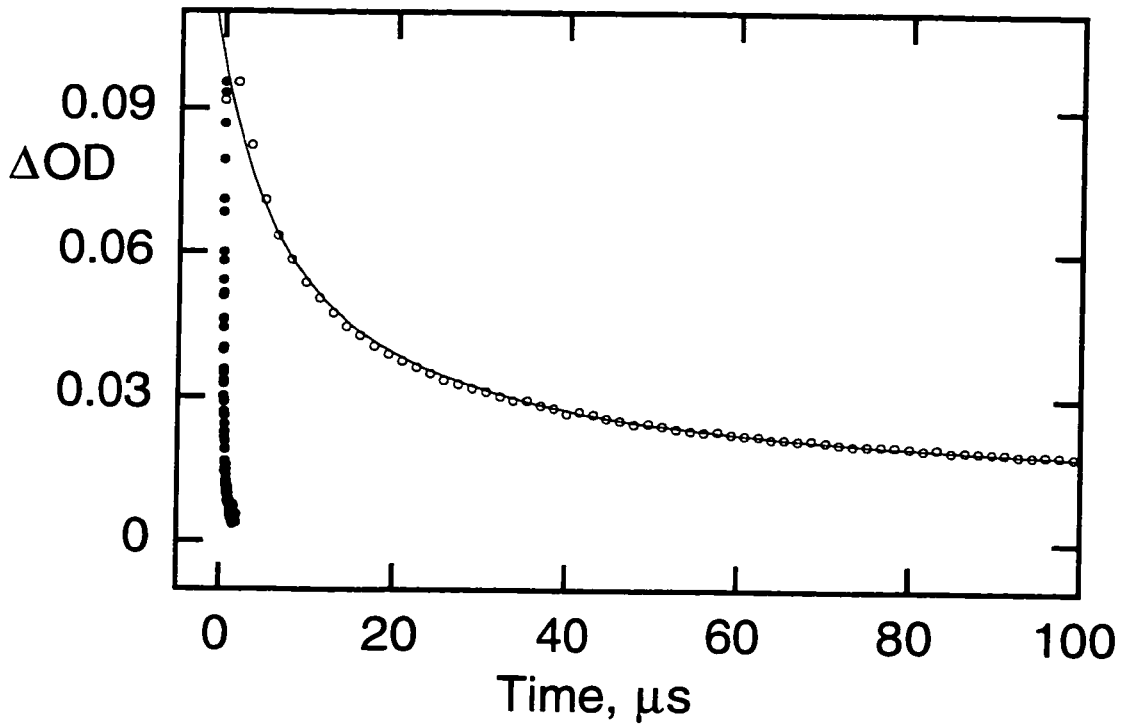

Figure 5-9 **360 nm decay traces in oxygen purged $CHCl_3$: (●) [Br-] = 0.0 mM and (○) [Br-] = 10 mM. From the LFP of 1,2-dibromoethane.**

Figure 5-10 contrasts two decays at 360 nm of the LFP of 1,2-dibromoethane in $CHCl_3$. The fast decay is in the absence of halide and is attributed to the $CHCl_3$•Br complex. The growth and slow decay is observed when 0.16 mM of Bu_4NBr is added to the solution. This trace is assumed to be due to the $Br_2^{\bullet-}$ complex.

The $CHCl_3$•Br complex decays by second-order kinetics or mixed first-order in the absence of halide probe (●, Figure 5-10). When bromide is added (○, Figure 5-10), the 360 nm signal is observed to initially decay rapidly, but then the signal starts to recover and grow. The newly formed transient in the presence of bromide decays on a very long timescale as shown in Figure 5-9. The slow-decaying transient is logically the $Br_2^{\bullet-}$ complex thereby ruling it out as the fast-decaying-transient responsible for the trace in the absence of added bromide (●, Figure 5-10).

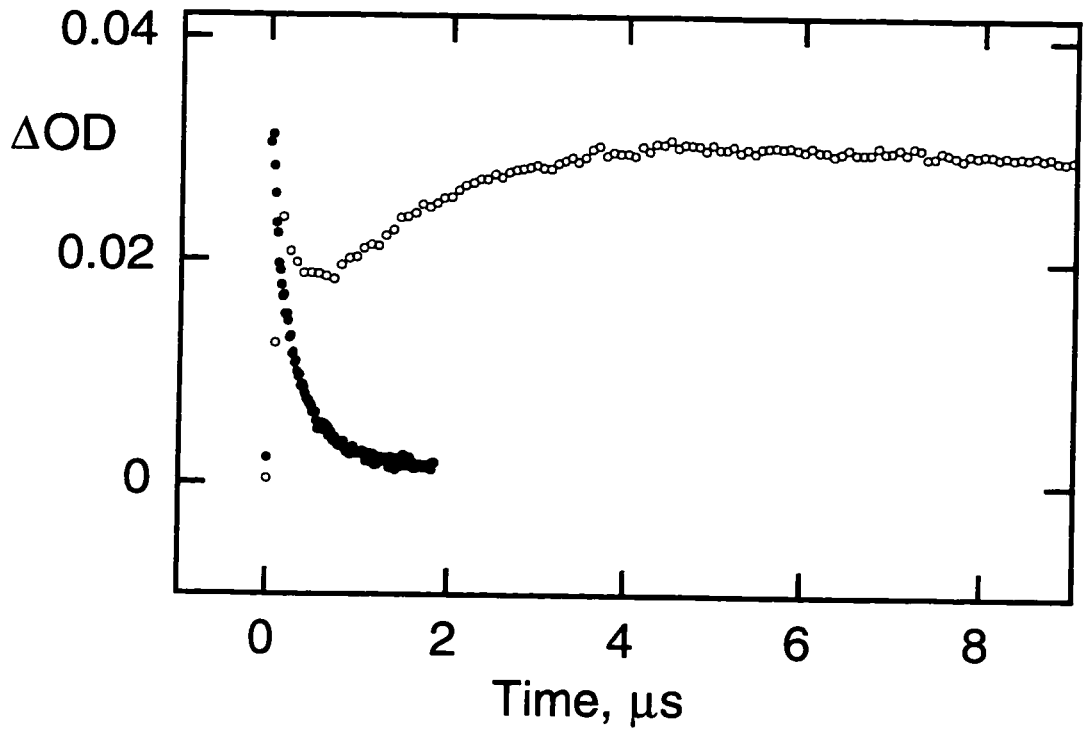

Figure 5-10 **360 nm decay traces in oxygen purged $CHCl_3$: (●) [Br-] = 0.0 mM and (○) [Br-] = 0.16 mM. From the LFP of 1,2-dibromoethane.**

The fast-dip and recovery trace of Figure 5-10 (○) is typical for systems involving one visible transient moving to a second visible transient through an invisible intermediate. It is obvious from the two traces of Figure 5-10 that the decay of the $CHCl_3$•Br complex is not equal to the growth of the $Br_2^{\bullet}$ complex thus confirming that there is an intermediate step between the two transients. This does not mean that bromide does not quench some of the $CHCl_3$•Br complex, just not all of it.

Kinetically, the photolysis of 1,2-dibromoethane in $CHCl_3$ in the presence of 0.16 mM bromide fits our model. The bromine atom is initially complexed by the solvent, then transferred to the 1,2-dibromoethane, and finally to the bromide (Scheme 5-2). For this interpretation to work, the 1,2-dibromoethane•Br complex (DBE•Br) must either absorb weakly or not at all at 360 nm in $CHCl_3$.

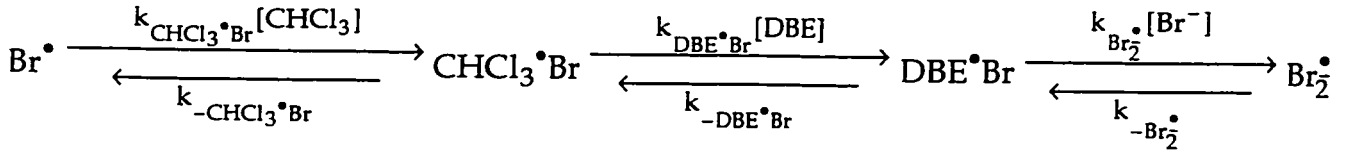

Scheme 5-2 The equilibria of the bromine atom complexes in $CHCl_3$ containing 10 mM 1,2-dibromoethane and 0.16 mM bromide.

The decay and growth profile of Figure 5-10 (○) require that the equilibria of Scheme 5-2 increase going from left to right (Equation 5.9).

$$K_{CHCl_3^{\bullet}Br}[CHCl_3] < K_{DBE^{\bullet}Br}[DBE] < K_{Br_2^{\bullet-}}[Br^-] \qquad \textbf{Equation 5.9}$$

From section 3.4, we know the equilibrium constant for $Br_2^{\bullet-}$ to be $\sim 10^5$ M^{-1} therefore we can estimate the equilibrium constants for the bromine atom complexes with $CHCl_3$ and 1,2-dibromoethane. The solution of Figure 5-10 consisted of 12.5 M $CHCl_3$, 10^{-2} M 1,2-dibromoethane, and 1.6×10^{-4} M Br^-. From these concentrations, we can estimate equilibrium constants of $\sim 10^2$ and $\sim 10^3$ M^{-1} for the $CHCl_3$•Br and DBE•Br complexes, respectively.

Chloroform shows the kinetics that we would argue is also occurring in acetonitrile (and occurred in others' aqueous studies)[1,3,9] in the absence of halide probe. In chloroform, no direct production of $Br_2^{\bullet-}$ is observed from any of the *vicinal* dibromides studied. The bromine atoms produced are immediately complexed by the solvent to produce a jump in the absorption in the 300 to 400 nm range.

(ii) The Growth

In the absence of added bromide, most growth signals at or around 360 nm observed in bromine atom solution studies have been attributed to the $Br_2^{\bullet-}$ radical anion

being formed.[1-3] In aqueous solution, the $Br_2^{\bullet}$ production was attributed to the presence of bromide from the hydrolysis of added Br_2 (Equation 5.6). This explanation is less feasible in acetonitrile although HBr is known to be formed during the course of the LFP of *vicinal* dibromides. Without a doubt, in these examples, there must be some bromide present, but it is not enough to explain the intensity and the kinetics of the observations.

The bromide dependence of the $Br_2^{\bullet}$ growth was studied by photolyzing 2.5 mM Br_2 in 0.12 M $HClO_4$.[1] With this concentration of acid and bromine, there would be a 1.0 x 10^{-5} M concentration of bromide in solution from the hydrolysis of Br_2 according to the well established equilibrium of Equation 5.6. Bromide was shown to trap bromine atoms in water at a rate of 9 x 10^9 M^{-1} s^{-1}, therefore the expected growth rate of the $Br_2^{\bullet}$ radical anion with this concentration of bromide would be 9.2 x 10^4 s^{-1}. The quenching plot obtained has an intercept of 7 x 10^5 s^{-1} suggesting that, in the absence of added bromide, $Br_2^{\bullet}$ grows in approximately 10 times faster than in the presence of the quantity of bromide produced from the hydrolysis. No bromide is better than a trace of bromide?

Merényi and Lind saw the same type of growth for the pulse radiolysis of an Ar purged solution of 1 M H_2SO_4, 10^{-4} M Br_2, and 10^{-2} M MeOH. They observed a rate constant of 5 x 10^5 s^{-1} and also concluded that the equilibrium concentration of bromide would be too low to account for their observations.

In both of the aqueous cases, the growth of the 360 nm signal was observed as being first-order. Since the equilibrium concentration of bromide is in the μM range, it would no longer satisfy the pseudo-first order condition assumed for the formation of the $Br_2^{\bullet}$ complex. In PR or LFP, the concentration of transient Br• usually produced is also in the 10 - 50 μM range.

The observed growths in the absence of added halide are weak enough to be attributed to trace amounts of bromide in solution, but the rate of growth is much faster than any trace amount of bromide could provide. The growths of the weak signals for the LFP of $Si(DBE)_4$ were measured with varying amounts of $Si(DBE)_4$ in MeCN (Figure 5-

11). The concentration of $Si(DBE)_4$ ranged from 0.4 to 1.1 mM. These concentrations are at least one to two orders of magnitude greater than any trace amounts of bromide present, and, of course, one to168

two orders of magnitude greater than the transient concentration of bromide expected. These conditions are sufficient to satisfy a pseudo-first-order reaction if one is occurring between the bromine atoms and the parent *vicinal* dibromide.

Indeed, the first-order growths of the 360 nm signals increased with increasing $Si(DBE)_4$. The slope of Figure 5-11 represents the rate of complexation between $Si(DBE)_4$ and bromine atoms according to Equation 5.10 and Equation 5.11 and was determined to be $4 \times 10^8\ M^{-1}\ s^{-1}$.

$$Si(DBE)_4 + Br^{\bullet} \underset{k_{-RBr2\bullet Br}}{\overset{k_{RBr2\bullet Br}}{\rightleftharpoons}} Si(DBE)_4 \bullet Br \qquad \textbf{Equation 5.10}$$

$$k_{obs} = k_o + k_{RBr2\bullet Br}[Si(DBE)_4] \qquad \textbf{Equation 5.11}$$

The intercept of Figure 5-11 should truly represent the lifetime of a bromine atom in MeCN (k_o, Equation 5.11) in the absence of *vicinal* dibromide. The intercept is equal to $(2 \pm 1) \times 10^5\ s^{-1}$ for a lifetime of $5 \pm 3\ \mu s$. This lifetime, as well as the estimated lifetime of the $Si(DBE)_4 \bullet Br$ complex, is about an order of magnitude shorter than the lifetime of the $Br_2^{\bullet}$ complex in MeCN.

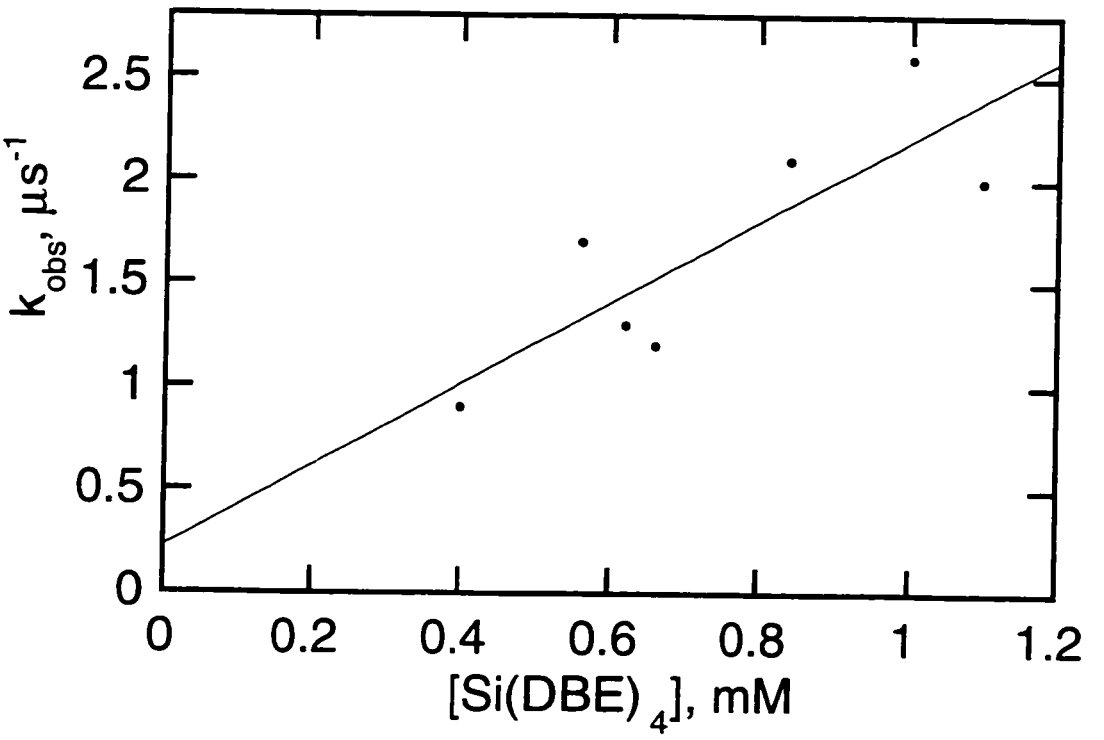

Figure 5-11 **The quenching of bromine atoms by the Si(DBE)$_4$ precursor. The observed growth rate constant, k_{obs} of the Si(DBE)$_4$•Br complex is plotted against the concentration of the Si(DBE)$_4$.**

The linear dependence of the observed growth rate constant with Si(DBE)$_4$ concentration of Figure 5-11 could also be explained if there was a bromide impurity in the Si(DBE)$_4$. A bromide impurity of 2.5% would generate the observed 4 x 10^8 M^{-1} s^{-1} slope of Figure 5-11. If there was 2.5% bromide in the Si(DBE)$_4$ sample, then the bromide concentrations of Figure 5-11 would range from 0.005 to 0.025 mM. In our experience, no $Br_2^{\bullet}$ signal is observed until at least 0.1 mM bromide is added to the solution.

An argument could be made that the signals observed in Figure 5-11 could be due to bromide impurities in the *vicinal* dibromide. However, bromide impurities can never explain decay and recovery traces such as Figure 5-10. For these reasons, we have assigned the zero-added-bromide growths to complexes with the parent *vicinal* dibromides.

Table 5-B **RBr_2•Br Complexes of *vicinal* dibromides in MeCN. The spectra were recorded by the 266 nm LFP of the respective *vicinal* dibromides in MeCN.**

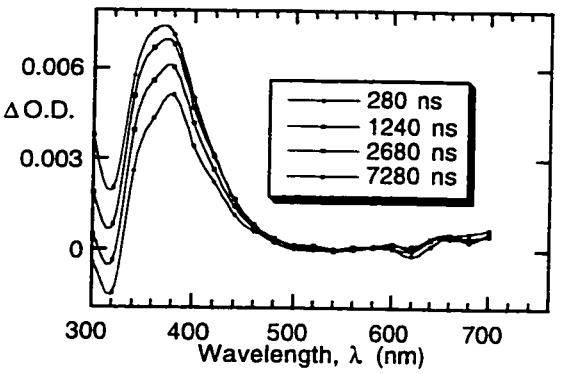

Si(DBE)4•Br

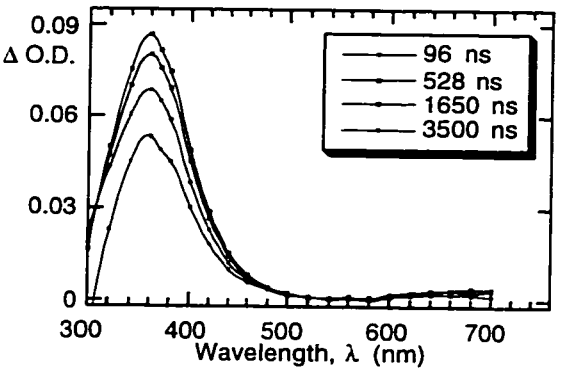

2,3-dibromopropyl-trimethylsilane

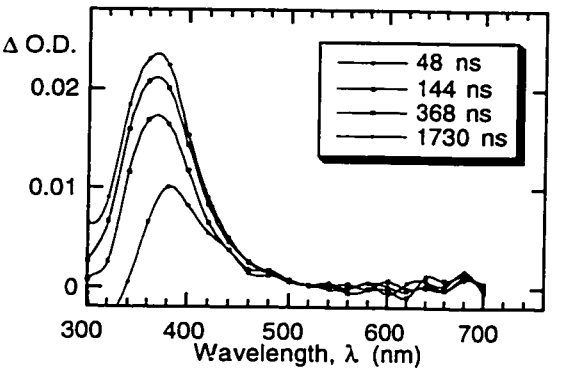

1,2-dibromoethyl-diethylmethylsilane

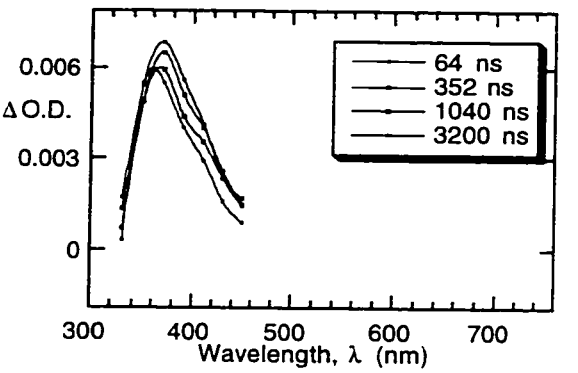

1,2-dibromo-tetrafluoroethane

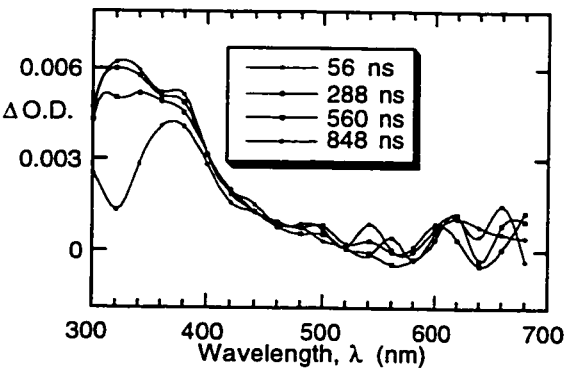

1,2-dibromo-2-methylpropane

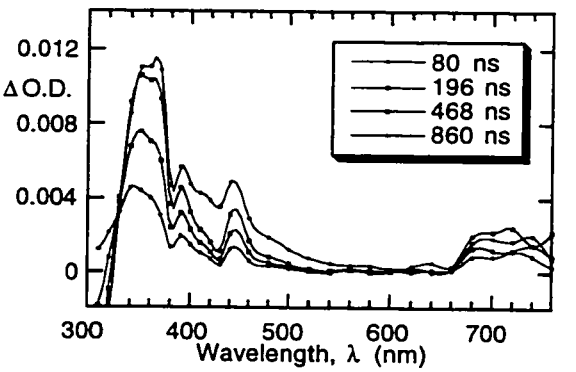

2,3-dibromobutane

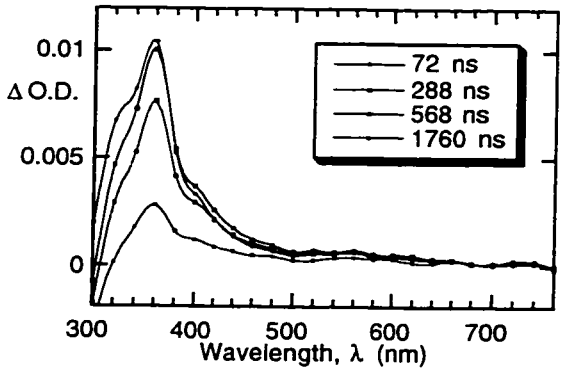

trans-1,2-dibromocycloheptane

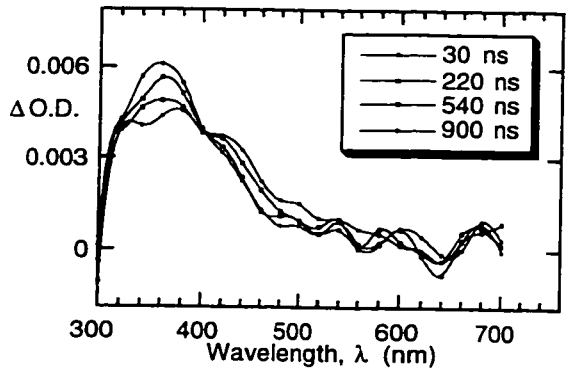

trans-1,2-dibromocyclopentane

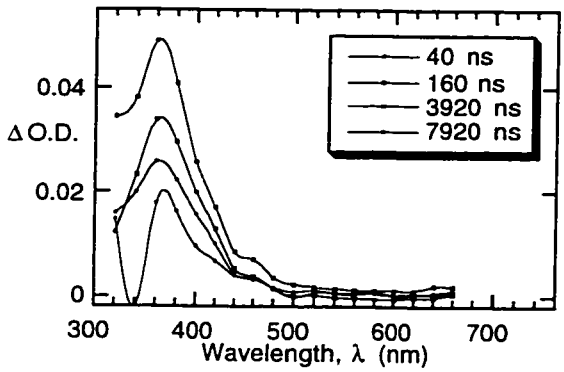

1,2-dibromoindane

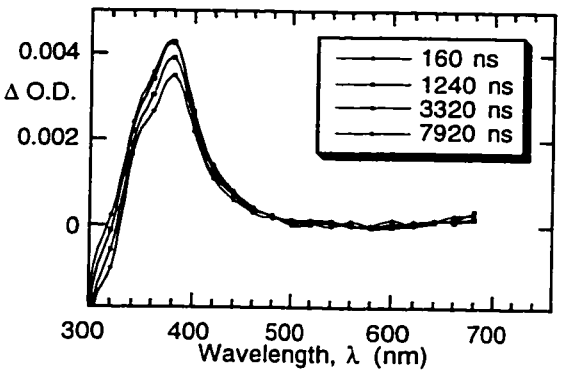

3,4-dibromotetrahydrothiophene-1,1-dioxide

The spectra of many of the *vicinal* dibromide/bromine atom complexes produced via their LFP in MeCN were recorded. In many of the cases, the spectra were recorded on timescales of 1 μs or less so that the spectrum of the MeCN•Br complex at 380 nm is also observed in the earliest spectra.

It appears that the complexes of all the various *vicinal* dibromides, water, and acetonitrile all have spectra that are similar to one another and to the $Br_2^{\bullet}$ radical anion. It is certainly difficult to distinguish between all of them. Unfortunately, in most cases, there is no region in the spectrum where only one of the complexes absorbs without interference

from one or more other complexes. Close inspection of the *trans*-1,2-dibromocyclopentane spectrum in Table 5-B reveals that, along with the growth of the *trans*-1,2-dibromocyclopentane•Br complex at 360 nm, there is also a weak decay that emerges from the spectrum and runs until about 600nm. Both the growth and decay signal are weak, but they are strong enough to be analysed.

Within experimental error, we can conclude that the decay rate constant is equal to the growth rate constant. The first-order rate constants were determined to be $(1.0 \pm 0.4) \times 10^6\ s^{-1}$ and $(2.2 \pm 0.7) \times 10^6 s^{-1}$. It is not surprising that the growth was determined to be slightly slower that the decay because the growth was not corrected for any decay component that surely overlaps the 360 nm signal.

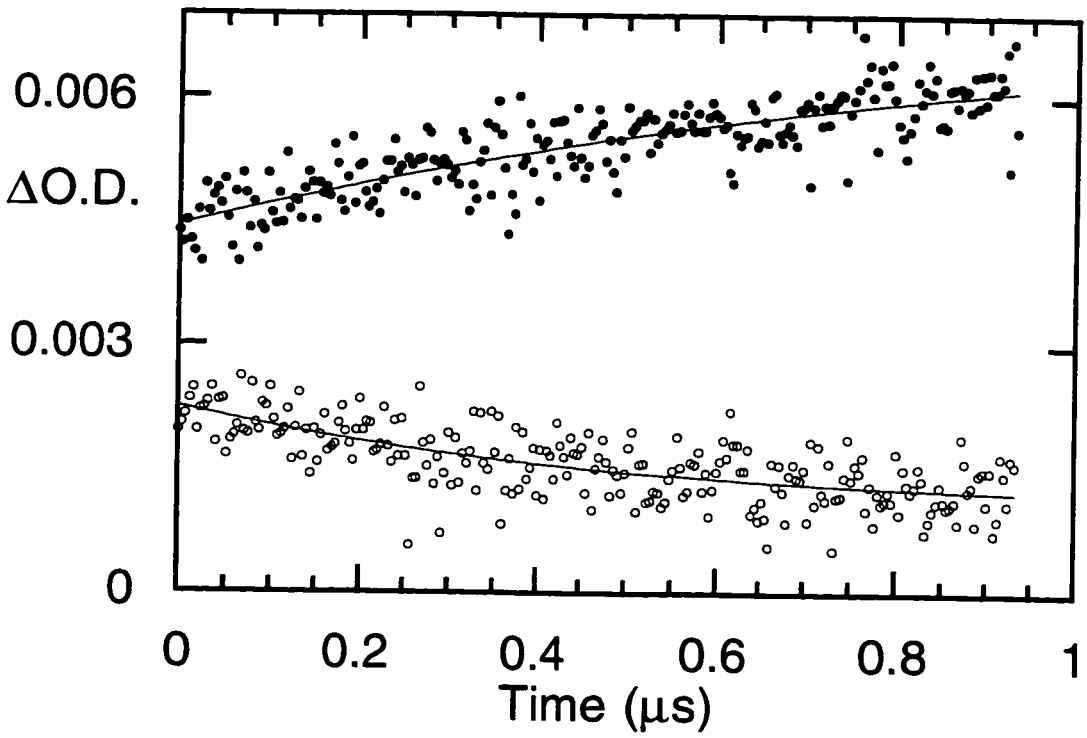

Figure 5-12 **The (●) 360 nm growth and the (○) 460 nm decay traces recorded after the 266 nm LFP of *trans*-1,2-dibromocyclopentane in MeCN.**

Because of the difficulty in separating the signals from one another, this growth and decay matched pair was the only set resolved throughout the study. Despite being weak,

the signals are reliable enough to add proof to the mechanism of solvent complexation of the bromine atoms followed by transfer of the Br• to the parent *vicinal* dibromide.

Table 5-C **The absorption maxima of the *vicinal* dibromide•Br complexes in MeCN and the vertical ionization potentials (I_D) of some of the *vicinal* dibromides studied.**

Vicinal Dibromide	λ_{max} (nm)	I_D (eV)[8]
$Si(DBE)_4$	370	(10.5)*
2,3-dibromopropyl-trimethylsilane	360	(10.38)**
1,2-dibromoethyl-diethylmethylsilane	370	(10.5)*
1,2-dibromo-tetrafluoroethane	370	11.44
1,2-dibromo-2-methylpropane	325	
2,3-dibromobutane	360 (390, 445)	10.14
trans-1,2-dibromocycloheptane	360	
trans-1,2-dibromocyclopentane	360	10.04
1,2-dibromoindan	360	
3,4-dibromotetrahydrothiophene-1,1-dioxide	380	

*** The value for 1,2-dibromoethane.** The value for 1,2-dibromopropane.**

It is difficult to draw any conclusions about the correlation between the absorption maxima of the *vicinal* dibromide•Br complexes and the ionization potentials of the *vicinal*

dibromides of Table 5-C because the majority of the ionization potentials are not known. Alfassi *et al.* concluded that the bromine containing compounds had the worst correlations of the bromine atom complexes that were studied.[6,7,10]

For *vicinal* dibromide studies, it is now obvious that the *vicinal* dibromides are responsible for the initial growths observed, but, in some other situations, the complexing agent is not so obvious. The $[Br^-] = 0$ intercept of the growth rate constant versus bromide concentration was $7 \times 10^5\ s^{-1}$ for Treinin and Hayon's aqueous Br_2 photolysis study.[1] If we assume that the 2.5 mM of Br_2 used in the aqueous study forms a complex with the bromine atoms produced, then a rate constant of $2.2 \times 10^8\ M^{-1}\ s^{-1}$ is obtained for tribromide formation (Equation 5.12).

$$Br_2 + Br^{\bullet} \underset{k_{-Br2\bullet Br}}{\overset{k_{Br2\bullet Br}}{\rightleftharpoons}} Br_2 \bullet Br$$

Equation 5.12

It was observed that the decays of CBr_4•Br and $CHBr_3$•Br complexes were enhanced by the addition of Br_2.[7] From a Br_2 quenching study, the rate constants of $2.2 \times 10^8\ M^{-1}\ s^{-1}$ and $4.0 \times 10^9\ M^{-1}\ s^{-1}$ were measured for the reaction of Br_2 with the CBr_4•Br and $CHBr_3$•Br complexes, respectively. The spectrum of the Br_2•Br complex had an absorption starting from 370 nm and appearing to maximize at 330 nm. Br_2 has a vertical ionization energy of 10.6 eV.[8]

The pulse radiolysis of a 1M H_2SO_4, 0.1 mM Br_2, and 10 mM MeOH solution also produced a growth.[3] The growth this time had a rate constant of $5 \times 10^5\ s^{-1}$. If the reaction of Br_2 with bromine atoms from the previous aqueous example is assumed to be correct ($2.2 \times 10^8\ M^{-1}\ s^{-1}$), then the Br_2 concentration in this second example is too low to produce the observed $5 \times 10^5\ s^{-1}$ rate constant. From our MeCN studies, it would be reasonable to assume that MeOH can also form a complex with bromine atoms. A 10 mM concentration of MeOH would result in the calculation of a $5 \times 10^7\ M^{-1}\ s^{-1}$ second-order rate constant for

the complexation of a bromine atom with MeOH. From our MeCN studies, we never saw a growth because we always worked in neat MeCN. The instantaneous trapping by MeCN in172

our LFP system leads us to estimate a lower limit of 7 x 10^6 M^{-1} s^{-1} for trapping bromine atoms.

5.3 The Nature of the Bromine Atom/Organic Complex

The absorption maxima correlate reasonably well with the ionization potentials of the alkane, I_D. For this reason, the complexes are assumed to be charge-transfer complexes (CTC). The bromine atom complexes with the haloalkanes and DMSO are postulated to be bound by three-electron bonds.[6] The potential CTC complex with acetonitrile could also be bound in this manner.

Table 5-D **The possible three-electron bonds for the charge-transfer complexes (CTC) of a bromine atom with bromoethane, dimethyl sulfoxide (DMSO), acetonitrile (MeCN), and $Si(DBE)_4$.**

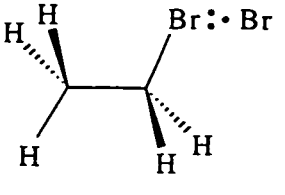

CH_3CH_2Br•Br CTC Complex

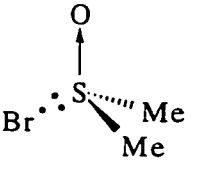

DMSO•Br CTC Complex

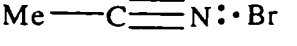

MeCN•Br CTC Complex

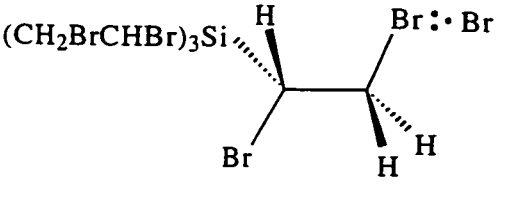

$Si(DBE)_4$•Br CTC Complex

5.4 Conclusions

Bromine atoms have a tendency to complex with other atoms, ions, or molecules. The inorganic $Br_2^{\bullet}$ species, formed from the combination of a bromine atom with a bromide ion, has been well studied in aqueous media.[9,11,12] The π-complex of a bromine atom and a benzene molecule has also been well established.[13] Recently, bromine atoms were shown to form complexes with haloalkanes and other hydrocarbons.[6,7] The complexes are usually based on charge-transfer interactions and have lifetimes of microseconds.

The affinity of bromine atoms to form complexes with almost anything in solution may be a more general phenomenon than we realize. In our group, there have been several photochemical studies of atomic species in solution.[14] In all cases, the use of a complexing agent was employed to make the atoms visible in solution.

Fluorine atoms were possible to study via their complex with freon 113 ($F\bullet CF_2Cl$-$CFCl_2$, λ_{max} = 320 nm, τ = 200 ns).[15] The fluorine atoms were also observed to form complexes with CH_3CN (λ_{max} = 290 and 350 nm), CD_3CN (λ_{max} = 345 nm), $CFCl_3$ (λ_{max} = 310 nm), CCl_4 (λ_{max} = 340 nm), and hexafluorobenzene (λ_{max} = 300 nm). If the transient in MeCN is indeed a fluorine atom complex of MeCN, then its spectrum would have very similar characteristics to the double band (275 and 380 nm) spectrum we propose for the MeCN•Br complex. The spectrum recorded in hexafluorobenzene has a broad band at 600 nm that is reminiscent of the benzene complexes of iodine (450 nm), bromine (490 nm) and chlorine (550 nm). It must be noted that hexafluorobenzene was determined to quench the freon113•F complex with a rate constant of 71 x 10^9 M^{-1} s^{-1}. The spectrum in hexafluorobenzene was recorded after 10 μs, therefore, if the mode of quenching is the formation of the heptafluorocyclohexadienyl radical as the authors suggest, then there is no way that the 600 nm band is a fluorine complex of hexafluorobenzene. However, if the rate of freon•F quenching measured is really the rate at which the fluorine atom is transferred to the hexafluorobenzene, then the 600 nm band could be the hexafluorobenzene•F complex. The hexafluorobenzene•F complex may be the precursor to the heptafluorocyclohexadienyl radical. The similarity with the benzene iodine, bromine,

and chlorine complexes is surely just a coincidence given the extreme reactivity of fluorine atoms.

A recent study on oxygen atoms in solution shows an even closer relationship to the present bromine atom studies.[16] Bucher and Scaiano observed a jump and growth kinetic trace at 325 nm after the photolysis of pyridine N-oxide in MeCN (Equation 5.13).

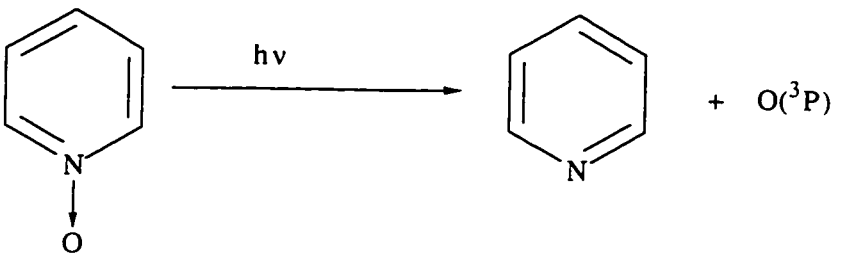

Equation 5.13

The growth was attributed to the reaction of the photogenerated oxygen atoms with MeCN to form acetonitrile oxide. This growth was used as a probe for the reaction of oxygen atoms with added quenchers. For a series of alkyl and aryl substrates, almost all of the rate constants for the reactions with oxygen atoms were measured in the 10^8 to 10^{10} M^{-1} s^{-1} regime. The most notable exception was acetonitrile for which k was estimated as ~ 10^5 M^{-1} s^{-1} based on the observed growth in neat acetonitrile. If the *vicinal* dibromide jump and growth mechanism is applied to this case, we would say that the oxygen atom jump is due to complexation with the MeCN and that the growth is then due to the transfer of the oxygen atom to the parent pyridine N-oxide. The pyridine N-oxide concentration was not included in the paper so, if we assume a concentration of 10 mM, then we calculate a rate constant for complexation of ~2 x 10^9 M^{-1} s^{-1}. This value is in excellent agreement with the rest of the values determined in Bucher and Scaiano's article.

5.5 Chapter 5 References

(1) Treinin, A.; Hayon, E. *J. Am. Chem. Soc.* **1975**, *87*, 1716.

(2) Scaiano, J. C.; Barra, M.; Calabrese, G.; Sinta, R. *J. Chem. Soc., Chem. Commun.* **1992**, 1418.

(3) Merényi, G.; Lind, J. *J. Am. Chem. Soc.* **1994**, *116*, 7872.

(4) Scaiano, J. C.; Barra, M.; Krzywinski, M.; Sinta, R.; Calabrese, G. *J. Am. Chem. Soc.* **1993**, *115*, 8340.

(5) Chateauneuf, J. E. *Chem. Phys Lett.* **1989**, *164*, 577.

(6) Shoute, L. C. T.; Neta, P. *J. Phys. Chem.* **1990**, *94*, 2447.

(7) Alfassi, Z. B.; Huie, R. E.; Mittal, J. P.; Neta, P.; Shoute, L. C. T. *J. Phys. Chem.* **1993**, *97*, 9120.

(8) NIST Chemistry WebBook (NIST Standard Reference Database 69), U.S. Sectretary of Commerce, 1997. (www.webbook.nist.gov)

(9) Zehavi, D.; Rabani, J. *J. Phys. Chem.* **1972**, *76*, 312.

(10) Shoute, L. C. T.; Neta, P. *J. Phys. Chem.* **1990**, *94*, 7181.

(11) Nagarajan, V.; Fessenden, R. W. *J. Phys. Chem.* **1985**, *89*, 2330.

(12) Hug, G. L. *Optical Spectra of Nonmetallic Inorganic Transient Species in Aqueous Solution*; National Bureau of Standards: Washington, 1981; Vol. NSRDS-NBS 69, pp 160.

(13) McGimpsey, W. G.; Scaiano, J. C. *Can. J. Chem.* **1988**, *66*, 1474.

(14) Scaiano, J. C.; Bucher, G.; Barra, M.; Weldon, D.; Sinta, R. *J. Photochem. Photobiol. A: Chem.* **1997**, *102*, 7.

(15) Bucher, G.; Scaiano, J. C. *J. Am. Chem. Soc.* **1994**, *116*, 10076.

(16) Bucher, G.; Scaiano, J. C. *J. Phys. Chem.* **1994**, *98*, 12471.

6. Claims to Original Research

The lifetime and fate of bromine atoms in solution is of particular interest to the photolythographic industry. Nanosecond Laser Flash Photolysis (LFP) is a powerful tool for the study of reactive intermediates in the time domain relevant to the photolythographic industry. Bromine atoms are invisible to the LFP technique, therefore suitable probes must be developed and characterized. The research presented within this thesis contributes to the development and characterization of bromine atom probes.

1. We have measured the rate constants for the complexation of bromine atoms with various halide ions in acetonitrile solution at 296 K. Bromine atoms were found to have near diffusion controlled reaction rate constants of $(1.4 \pm 0.7) \times 10^{10}$ M^{-1} s^{-1} for iodide, $(1.4 \pm 0.1) \times 10^{10}$ M^{-1} s^{-1} for chloride, and $(1.0 \pm 0.1) \times 10^{10}$ M^{-1} s^{-1} for fluoride.

2. The extinction coefficients at 360 nm of the mixed bromine-halogen radical anions were determined in acetonitrile to be $(13 \pm 1) \times 10^3$ M^{-1} cm^{-1} for $BrF^{\cdot}$, $(9 \pm 1) \times 10^3$ M^{-1} cm^{-1} for $BrCl^{\cdot}$, and $(6.9 \pm 0.7) \times 10^3$ M^{-1} cm^{-1} for $BrF^{\cdot}$.

3. The transient absorption spectra of the $BrCl^{\cdot}$ and $BrF^{\cdot}$ radical anions have been measured for the first time in solution. The species were measured in acetonitrile and were found to have absorption maxima at 360 nm.

4. The effect of temperature on the rate of $Br_2^{\cdot}$ formation from a bromine atom and a bromide ion has been measured in acetonitrile. From an Arrhenius plot of our data, a log(A) factor of 11.6 and an activation energy of 1.9 kcal/mol was determined for the reaction of a bromine atom with a bromide anion in acetonitrile.

5. The rate of $Br_2^{\cdot}$ formation from a bromine atom and bromide ion was determined in chloroform to be $(1.0 \pm 0.2) \times 10^{10}$ M^{-1} s^{-1}.

The debate as to whether β-bromo radicals are bridged and whether their lifetimes are measurable has been advanced by the research in this thesis.

1. We give the first reports of β-bromo radicals being reduced by halide ions. The reduction rate constants of a series of transient β-bromo radicals with bromide, chloride, and fluoride were measured. A series of LFP generated β-bromoalkyl radicals were subjected to reduction by the halides in acetonitrile. In all but one case, bromide, chloride, and fluoride were shown to reduce the b-bromoalkyl radicals with rate constants $\geq 10^9$ M^{-1} s^{-1}.

2. By probing the evolution of bromine atoms in solution, we have established the lifetimes of a series of β-bromo-alkyl radicals to be in the 100 to 200 ns range.

3. From temperature dependent halide reduction experiments, the Arrhenius parameters for the β-bromo radicals of 1,2-dibromoethane and *trans*-1,2-dibromocyclopentane were determined. The bromide reduction of the β-bromocyclopentyl radical was found to have a log(A) factor of 11.8 and an activation energy of 3.3 kcal/mol. The fluoride reduction of the β-bromoethyl radical had a log(A) factor of 12.2 and an activation energy of 4.0 kcal/mol. The unimolecular fragmentations of these two radicals were found to have log(A) factors of 7.7 and 9.8 with activation energies of 0.5 and 3.5, respectively.

IMAGE EVALUATION TEST TARGET (QA-3)

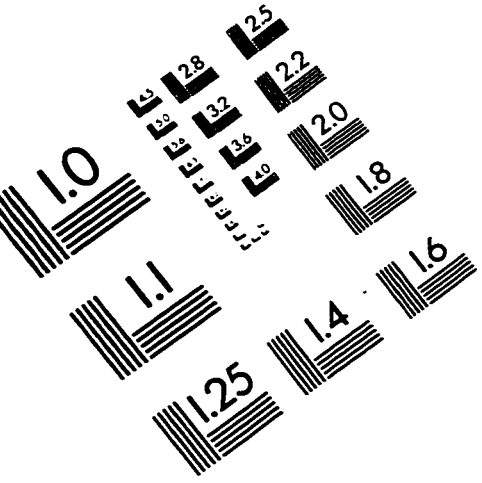

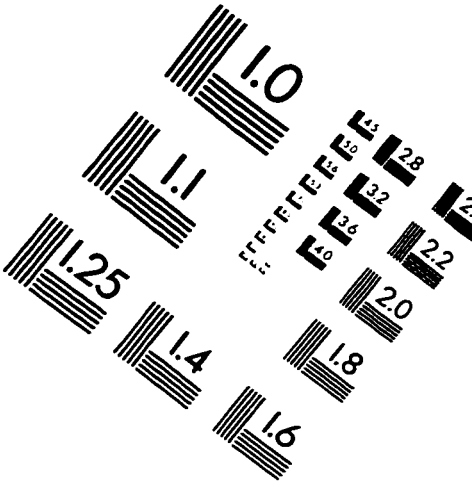

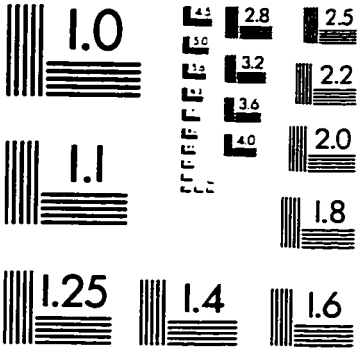

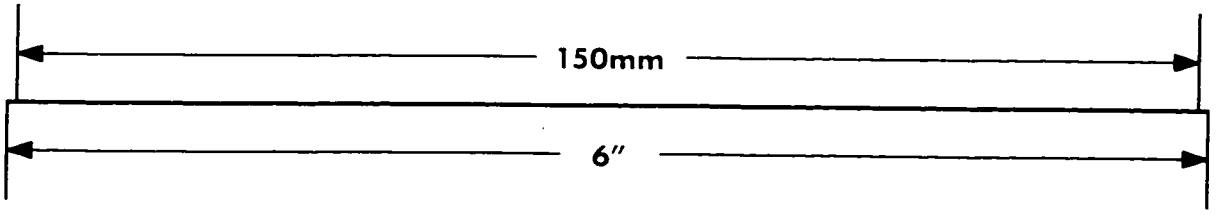

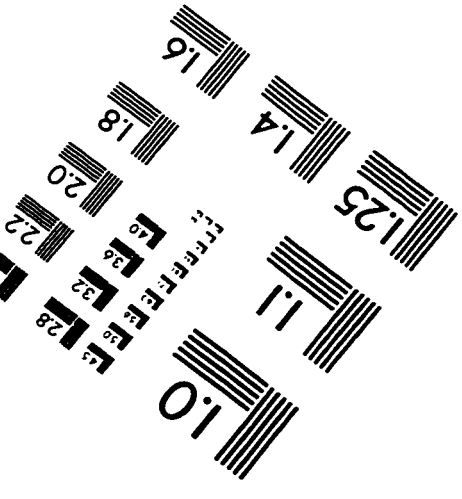

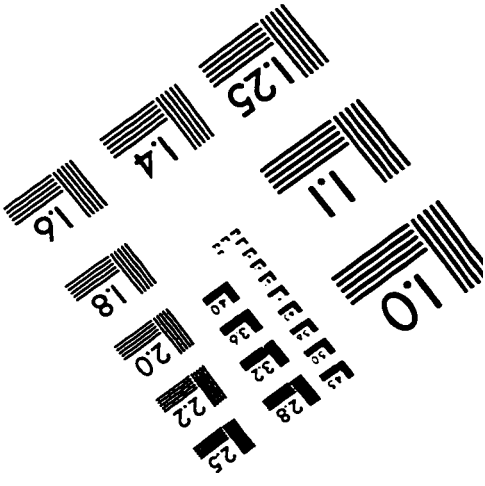

APPLIED IMAGE, Inc
1653 East Main Street
Rochester, NY 14609 USA
Phone: 716/482-0300
Fax: 716/288-5989